

Application of multiple sulfur isotope analysis to Archean ore-forming processes

Elizabeth Ruth Sharman

Department of Earth and Planetary Sciences
McGill University
Montreal, Quebec

June, 2011

A thesis submitted to McGill University in partial fulfillment of the requirements
of the degree of Doctor of Philosophy

© Elizabeth Sharman, 2011

DEDICATION

To my partner in life, John Chapman
and to my parents Angie Harris and David Sharman.
You always believed in me, even at the times when I didn't.

THOUGHTS

“Learn from yesterday, live for today, hope for tomorrow.
The important thing is not to stop questioning.”
Albert Einstein

ACKNOWLEDGEMENTS

First and foremost I would like to acknowledge my supervisor at McGill University, Prof. Boswell Wing, for his enthusiasm, guidance and support throughout my entire thesis. Who knew that the Honours student who gave you a few samples to test an idea way back in 2004 would end up as your first PhD student? This has been quite the journey, and I would like to thank you for all your help in getting through it. Thanks also to my supervisor at the Geological Survey of Canada, Dr. Bruce Taylor, for his patience and encouragement through all my laboratory tribulations. Thank you also for all our scientific discussions.

I have to thank all those who provided scientific guidance. No research should be conducted alone, and this is especially true for a PhD thesis. To Prof. Willy Williams-Jones, thank you for our discussions and for not letting me forget I'm part economic geologist. Thank you also to Dr. William Minarik who always had time to look at my work, and for providing ICP-MS assistance. I would also like to acknowledge Dr. Ian Jonasson, Dr. Patrick Mercier-Langevin and Dr. Benoît Dubé at the Geological Survey of Canada. Ian Jonasson was instrumental in providing samples from the Noranda Camp for this thesis, and this study would not have been possible without all his help and support. Similarly, Patrick Mercier-Langevin facilitated the collection of samples from the Doyon-Bousquet-LaRonde mining camp. As the project leader for TGI-3 Abitibi project Benoît Dubé provided support and funding for this thesis, as well as being an indispensable source of advice. I would also like to acknowledge all those who contributed support and ideas for the work in this thesis on the Platreef – Prof. Sarah Penniston-Dorland, Prof. Judith Kinnaird, Dr. Paul Nex, Prof. Michael Brown and Prof. James Farquhar.

Working on research on ore-forming processes often requires access to ore deposits which are being actively explored or mined and therefore such research is not possible without the support of companies. This thesis would not have been possible without such support. Thank you to Louis Schurmann and Ivanhoe Nickel and Platinum Ltd., Gernot Wober and Hunter Dickinson/Anooraq Resources, and Gordon Chunnett and AngloPlatinum, for providing invaluable access to funding, samples and data for the Platreef component of this research. I would also like to thank Agnico-Eagle Mines Limited and IAMGOLD Corporation (formerly Cambior Inc.) for all their assistance with access to samples, without which the Doyon-Bousquet-LaRonde study would not have been possible.

A PhD thesis also requires financial support, and I would like to acknowledge funding from the Geological Survey of Canada's Targeted Geoscience Initiative-3 Abitibi Project, a Society of Economic Geologists Graduate Student Fellowship, a GEOTOP bourses d'études des cycles supérieurs, and an NSERC Discovery Grant awarded to Boswell Wing.

I would also like to acknowledge all those who assisted me in the numerous analytical aspects of this thesis. Firstly I would like to thank Lang Shi for his sharing extensive knowledge and assistance during my EPMA data collection. Thanks also to Mary McDonough for assistance in acid digestions for ICP-MS analyses. I would also like to thank everyone in the McGill Stable Isotope Lab group, and in particular André Pellerin and Thi Hao Bui, for all their assistance in all that is involved in running sulfur isotope analyses.

For their support in navigating the labyrinth that is the administrative side of any degree I must thank Anne Kosowski, Kristy Thornton and Angela DiNinno for all their help and patience. I would also like to acknowledge Isabelle Girard at the Geological Survey of Canada who assisted in the translation of the abstract for this thesis, merci beaucoup.

Last but no means least I would like to thank my family and friends for all their support. Thank you to John Chapman, for your love and support, scientific discussion and impartial editorial comment. To my parents, thank you for providing the grounding that has let me get this far. Thank you also to all my friends: to Martin, for all your support especially in the early stages of my PhD; to Crystal, Julia, Kent and Dejan for providing me with a home away from home; and to Aleks, Ana, Denis, Jonathan, Kirsten, Michael and Shoshana who along with those already mentioned and the rest of the EPS students made my time at McGill so much fun and introduced me to a lot of very good beer. Finally I would like to thank the music stylings of DJ³ (aka John Jamieson) you provided the soundtrack to the writing of this thesis, UNTZ UNTZ UNTZ.

ABSTRACT

Identification of the sources of sulfur in an ore-forming system is important as it provides a greater understanding of how a mineral deposit forms and how best to explore for that particular type of deposit. It can also aid in the understanding of the ocean and atmosphere chemistry at the time of formation. Mass independent sulfur isotope fractionation ($\Delta^{33}\text{S} = \delta^{33}\text{S}_{\text{measured}} - [(\delta^{34}\text{S}_{\text{measured}}/1000 + 1)^{0.515} - 1] \times 1000 \neq 0$) in the Archean atmosphere provides a fingerprint for identifying non-magmatic sources of sulfur. The chemically conservative nature of $\Delta^{33}\text{S}$ signatures makes sulfur multiple isotope measurements a powerful tool for deconvolving ore-forming processes in the Archean. This thesis presents three applications of multiple sulfur isotope analysis for investigation of ore forming processes in the Archean.

The first study evaluates recently proposed models for formation of volcanogenic massive sulfide (VMS) deposits during the Neo- and Mesoarchean, which demand little to no contribution of seawater sulfate to the ore-forming system. This is in contrast to Phanerozoic and modern VMS systems where evidence for a seawater sulfate component is clear. We re-evaluate these models in the context of the ~2.7 Ga Noranda Camp of the Abitibi subprovince, Québec, using a combination of multiple sulfur isotope and trace element data. Sulfide samples analysed for this study have $\Delta^{33}\text{S}_{\text{V-CDT}}$ values between -0.59 and -0.03 ‰. We interpret these negative $\Delta^{33}\text{S}$ values to reflect a sulfur component that originated in the seawater sulfate reservoir. Incorporation of this component appears to have increased during the collapse and subsequent evolution of the Noranda caldera. Higher concentrations of Se in samples with $\Delta^{33}\text{S}$ values close to 0 ‰, and higher Fe/(Fe + Zn) values in sphalerite, are indicative of higher temperatures of formation. In addition, within Au-rich VMS deposits of the Noranda Camp higher gold grades

are associated with near-zero $\Delta^{33}\text{S}$ values and, by inference, an ore-forming system dominated by igneous-magmatic sulfur sources

The second study is an investigation of sulfur sources that contributed to the formation of Cu- and Au-rich VMS deposits of the ~2.7 Ga Doyon-Bouquet-LaRonde (DBL) mining camp, also within the Abitibi subprovince. This subgroup of deposits has previously been interpreted as having a significant magmatic-hydrothermal source of ore fluids and metals. Multiple sulfur isotope analysis of deposits within the DBL mining camp, with the exception of one minor lens, indicates a very clear igneous-magmatic affinity ($\Delta^{33}\text{S}_{\text{V-CDT}} = -0.14$ to $+0.04 \text{ ‰}$), with little to no contribution from any surficial source of sulfur. In contrast, sulfide that formed at or very near the paleo-seafloor exhibits a distinct component of sulfur from the seawater sulfate reservoir ($\Delta^{33}\text{S}_{\text{V-CDT}} = -1.43$ to -0.34 ‰). This study highlights the isotopic difference between the Noranda VMS deposits and those of the DBL. In addition, a lack of variation in $\Delta^{33}\text{S}$ values between ore lenses which exhibit aluminous alteration and those that do not calls into question the characteristics with which to identify those VMS deposits that required dominant contribution of magmatic fluids.

The final study examines sulfur sources within the Platreef – the main PGE bearing horizon of the Northern Limb of the Bushveld Igneous Complex (BIC), South Africa. The Platreef has a high percentage of sulfides relative to the analogous Merensky Reef in the eastern and western limbs of the BIC. It is in direct contact with underlying Neoarchean to Paleoproterozoic sediments, which are potential local sources of sulfur. However, $\Delta^{33}\text{S}$ analysis of the Platreef sulfides identifies heterogeneous crustal sulfur contribution to the system both prior to and post-emplacement throughout the length of the Platreef.

This thesis clearly demonstrates that multiple sulfur isotope analysis is a powerful tool for the identification of sulfur sources in ore forming processes of the Archean, and those involving Archean rocks, and can be applied to a range of problems and deposit types. It also highlights important issues for future consideration, including the role of seawater sulfate in the formation of Archean VMS deposits, and the characteristics of the parent magma of the Bushveld Igneous Complex.

RESUME

L'identification des sources de soufre d'un système minéralisateur est importante car elle permet une compréhension plus approfondie du processus minéralisateur et de la meilleure méthode pour explorer pour ce type de dépôt. Elle peut aussi aider à la compréhension de la chimie des océans et de l'atmosphère au temps de formation. Le fractionnement indépendant de la masse des isotopes du soufre ($\Delta^{33}\text{S} = \delta^{33}\text{S}_{\text{measured}} - [(\delta^{34}\text{S}_{\text{measured}}/1000 + 1)^{0.515} - 1] \times 1000 \neq 0$) dans l'atmosphère de l'Archéen fournit une emprunte digitale sans équivoque permettant d'identifier les sources de soufre non magmatiques. La nature chimique conservative des signatures du $\Delta^{33}\text{S}$ en fait un outil puissant pour la déconvolution des processus minéralisateurs durant l'Archéen.

Cette thèse présente trois applications de l'analyse multiple des isotopes du soufre pour l'investigation des processus minéralisateurs durant l'Archéen. La première étude teste les modèles de formation des sulfures massifs volcanogènes (SMV) du Néo- et Mésoarchéen récemment proposés, lesquels ne requièrent peu ou pas d'apport de sulfate marin dans le système minéralisateur, contrastant avec les systèmes SMV du Phanérozoïque et contemporains, où le sulfate marin joue un rôle important. Ces modèles sont réévalués en contexte du camp Noranda (~2.7 Ga), situé dans la sous-province de l'Abitibi, Québec, combinant l'utilisation de données multiples provenant de l'analyse des isotopes du soufre et des éléments traces.

Les sulfures analysés pour cette étude ont des valeurs de $\delta^{34}\text{S}_{\text{V-CDT}}$ variant entre -14.90 et +2.49 ‰, et des valeurs de $\Delta^{33}\text{S}_{\text{V-CDT}}$ variant entre -0.59 et -0.03 ‰. Selon notre interprétation, les valeurs négatives de $\Delta^{33}\text{S}$ proviennent de l'incorporation de soufre

ayant l'eau de mer comme origine. La proportion de soufre marin aurait augmenté durant l'affaissement et l'évolution subséquente de la cuvette d'effondrement. Des concentrations plus élevées de Se, combinées à des valeurs près de 0 ‰ et d'un haut ratio Fe/(Fe + Zn) dans les sphalérites sont indicatifs d'une température de formation élevée. De plus, des contenus en or plus élevés sont associés à des valeurs de $\Delta^{33}\text{S}$ approximant zéro, et donc par inférence, associés aux systèmes minéralisateurs dominés par des processus ignés-magmatiques des dépôts riche en or de type SMV du camp Noranda.

La deuxième étude est une investigation des sources de soufre ayant contribué à la formation des dépôts volcanogènes riches en Cu et en Au du camp minier Doyon-Bousquet-LaRonde (DBL) (~2.7 Ga), situé lui aussi à l'intérieur de la sous-province de l'Abitibi. Par le passé, une source magmatique-hydrothermale de fluides minéralisateurs importante était l'interprétation donnée pour ce sous-groupe de dépôt. À l'exception d'une lentille mineure, l'analyse isotopique multiple des dépôts du camp minier DBL indiquent clairement une affinité ignée-magmatique ($\Delta^{33}\text{S}_{\text{V-CDT}} = -0.14$ to $+0.04$ ‰), avec peu ou pas de contribution de soufre provenant de la surface. En contraste, les sulfures s'étant formés sur le plancher océanique ou près de celui-ci exhibe une contribution distinctive des sulfates marins ($\Delta^{33}\text{S}_{\text{V-CDT}} = -1.43$ to -0.34 ‰). D'un autre côté, l'absence de variation des valeurs du $\Delta^{33}\text{S}$ entre des lentilles minéralisées exhibant une altération alumineuse et celles ne démontrant pas cette altération remet en question les caractéristiques permettant l'identification des dépôts de type SMV ayant une contribution importante ou dominante de fluides magmatiques.

La dernière étude examine les sources de soufre du Platreef – horizon principale contenant les éléments du groupe platine (EGP) du flanc nord du Complexe Igné

Bushveld (CIB) en Afrique du Sud. Le Platreef contient un haut pourcentage de sulfures lorsque comparé au dépôt analogue Merensky Reef des flancs est et ouest du CIB. Il est en contact direct avec les couches sous-jacentes de sédiments Néoarchéennes à Paléoprotérozoïque qui sont des sources de soufre locales potentielles. D'un autre côté, les analyses du $\Delta^{33}\text{S}$ des sulfures du Platreef permettent d'identifier une contribution de soufre hétérogène provenant de la croûte terrestre, avant et après la mise en place du gisement sur toute la longueur du Platreef.

Cette thèse démontre clairement que l'analyse multiple des isotopes du soufre est un outil puissant dans l'identification des sources de soufre des processus minéralisateurs durant l'Archéen, ainsi que ceux impliquant des roches archéennes, et cette approche peut être appliquée à un éventail de problèmes et types de dépôt. Aussi, elle met en lumière des questions importantes pour considération future, incluant le rôle du sulfate marin dans la formation des dépôts SMV de l'Archéen et les caractéristiques du magma du Complexe Igné Bushveld.

TABLE OF CONTENTS

DEDICATION.....	i
ACKNOWLEDGEMENTS.....	ii
ABSTRACT.....	v
RESUME.....	viii
CONTRIBUTIONS OF AUTHORS.....	xvi
LIST OF FIGURES.....	xiix
LIST OF TABLES.....	xx
Ch. 1 Overview.....	1
1.1 Introduction.....	1
1.1.1 Isotope effects and fractionation processes.....	1
1.1.2 Multiple sulfur isotope analysis and mass-independent fractionation.....	4
1.1.3 Archean Sulfur Cycle.....	6
1.2 Application of multiple sulfur isotopes to ore-forming processes....	7
1.3 References.....	11
Figures.....	13
Preface to Chapter Two.....	16
Ch. 2 Etiology of VMS mineralization in the Noranda district, Quebec:	
Multiple sulfur isotope and trace element evidence.....	18
2.1 Abstract.....	18

2.2 Introduction.....	19
2.3 Regional Geology.....	23
2.4 Samples.....	26
2.5 Methodology.....	26
2.5.1 Electron Probe Microanalysis (EPMA).....	27
2.5.2 Multiple Sulfur Isotope Analysis.....	27
2.5.3 Inductively Coupled Plasma Mass Spectrometry (ICP-MS)	28
2.6 Results.....	29
2.6.1 Multiple sulfur isotopes.....	30
2.6.2 Trace element geochemistry.....	31
2.6.2.1 EPMA.....	31
2.6.2.2 ICP-MS.....	32
2.7 Discussion.....	33
2.7.1 Sulfur sources in Neoarchean VMS deposits.....	33
2.7.2 Model for hydrothermal circulation, elemental transport, and VMS deposition in the Noranda cauldron.....	35
2.7.2.1 Multiple S isotope constraints.....	35
2.7.2.2 Temperature constraints.....	38
2.7.3 Au-rich deposits in the Noranda camp.....	40
2.7.3.1 Classification of deposits of uncertain affinities...	40
2.7.3.2 Multiple sulfur isotopes and Au-grade predictivity.....	41

2.8 Conclusions.....	42
2.9 Acknowledgements.....	43
2.10 References.....	43
Figures.....	48
Preface to Chapter Three.....	57
Ch. 3 Evidence for a magmatic origin of the Doyon-Bousquet-LaRonde Au-bearing vein and VMS ore deposits: a multiple sulfur isotope study.....	58
3.1 Abstract.....	58
3.2 Introduction.....	59
3.3 Regional Geology.....	62
3.3.1 Mineral Deposits.....	64
3.4 Samples.....	66
3.5 Methodology.....	68
3.6 Results.....	69
3.7 Discussion.....	70
3.7.1 Vein-hosted Deposits.....	70
3.7.2 Au-rich VMS Deposits.....	72
3.7.3 Comparison to the Noranda VMS District.....	75
3.8 Conclusions.....	76
3.9 Acknowledgements.....	77
3.10 References.....	78
Tables and Figures.....	81

Preface to Chapter Four.....	86
Ch. 4 Elucidation of multiple sulfur contamination events in Ni-Cu-(PGE) mineralization: $\Delta^{33}\text{S}$ evidence from the Platreef, Bushveld, South Africa.....	87
4.1 Abstract.....	87
4.2 Multiple sulfur isotopes and Ni-Cu-(PGE) mineralization in the Platreef.....	88
4.3 Regional Geology of the Platreef.....	91
4.4 Sulfur isotope analytical methods.....	93
4.5 Results: Multiple sulfur isotope characteristics of the Platreef and environs.....	94
4.6 Life history of sulfur in Platreef ore sulfides.....	95
4.6.1 Spatial record of sulfur contamination.....	95
4.6.2 Ultimate sources of S contamination.....	96
4.6.3 $\Delta^{33}\text{S}$ constraints on silicate melt:sulfide melt mass ratios...	99
4.7 Conceptual model of Platreef mineralization.....	101
4.8 Implications.....	103
4.9 Acknowledgements.....	104
4.10 References.....	105
Tables and Figures.....	108
Ch. 5 Summary and Discussion.....	114
5.1 Introduction.....	114

5.2 Summary.....	114
5.2.1 Chapter Two: Volcanogenic massive sulfide deposits of the Noranda Camp.....	114
5.2.2 Chapter Three: Au-rich deposits of the Doyon-Bousquet- LaRonde mining camp.....	116
5.2.3 Chapter Four: Ni-Cu-(PGE) Platreef deposit.....	117
5.3 Scientific Contributions and Significance.....	117
5.4 Recommendations for Future Work.....	118
Appendix 1.....	120
Appendix 2.....	169

CONTRIBUTIONS OF AUTHORS

The main body of this thesis comprises three chapters (Chapter 2 to Chapter 4). Chapter 2 utilizes multiple sulfur isotope and trace element data to investigate the sources and evolution of sulfur within the Noranda Camp volcanogenic massive sulfide (VMS) deposits. Chapter 3 focuses on the Au-rich VMS and vein deposits of the Doyon-Bousquet-LaRonde mining camp in the context of their sulfur sources. Chapter 4 investigates the role of crustal sulfur in the formation of the Ni-Cu-(PGE) Platreef deposit, northern limb, Bushveld Igneous Complex. Supplementary data for Chapters 2 and 3 are provided in the Appendices. An introduction and overview is provided in Chapter 1, and conclusions to the work are provided in Chapter 5.

Chapter 2 is the manuscript *Etiology of VMS mineralization in the Noranda district, Quebec: Multiple sulfur isotope and trace element evidence* by Elizabeth Sharman, Boswell Wing, Bruce Taylor and William Minarik. This manuscript has been submitted to the journal *Economic Geology* and is currently in revision. The work presented in this chapter was initiated and performed by the author including all scientific analysis, data processing, interpretation and writing. Boswell Wing assisted in acquiring samples for this study from the Geological Survey of Canada, aided the author in the development of analytical techniques, and contributed to the intellectual development and editing of the manuscript. Bruce Taylor and William Minarik assisted in the application of analytical techniques, and contributed to discussion of the data interpretation, and editing of the manuscript.

Chapter 3 is the manuscript *Evidence for a magmatic origin of the Doyon-Bousquet-LaRonde Au-bearing vein and VMS ore deposits: a multiple sulfur isotope study* by Elizabeth Sharman, Boswell Wing, Patrick Mercier-Langevin and Bruce Taylor. This manuscript will be

submitted to the journal *Mineralium Deposita* and is currently in preparation. The work presented in this chapter was initiated and performed by the author including all sample collection, scientific analysis, data processing, interpretation and writing. Boswell Wing assisted in application of analytical techniques, and contributed to the intellectual ideas and editing of the manuscript. Patrick Mercier-Langevin assisted in the collection of samples and contributed to the intellectual ideas and editing of the manuscript. Bruce Taylor contributed to the intellectual ideas and editing of the manuscript.

Chapter 4 is the manuscript *Elucidation of multiple sulfur contamination events in Ni-Cu-(PGE) mineralization: Δ³³S evidence from the Platreef, Bushveld, South Africa* by Elizabeth Sharman, Sarah Penniston-Dorland, Boswell Wing, Judith Kinnaird, Paul Nex, Michael Brown and James Farquhar. This manuscript will be submitted to the journal *Geology* and is currently in preparation. The work presented in this chapter was initiated and performed by the author including a majority of sample collection and scientific analysis, and all data processing, interpretation and writing. Sarah Penniston-Dorland collected and analysed some of the samples for this study, and contributed to the intellectual ideas and editing of the manuscript. Boswell Wing contributed to the intellectual ideas and editing of the manuscript. Judith Kinnaird and Paul Nex assisted in the collection of samples and contributed to the intellectual ideas and editing of the manuscript. Michael Brown and James Farquhar provided analytical support and contributed to the intellectual ideas and editing of the manuscript.

LIST OF FIGURES

	<u>page</u>
Figure 1.1 Schematic potential energy curve for the interaction of two atoms.....	13
Figure 1.2 Summary plot of compiled $\Delta^{33}\text{S}$ data through geological time	14
Figure 1.3 Conceptual model for the distribution of mass independently fractionated sulfur reservoirs in the Archean.....	15
Figure 2.1 Schematic diagram of volcanogenic massive sulfide formation, with predicted multiple sulfur isotope signatures.....	48
Figure 2.2 Geological map of the Noranda Camp, Abitibi subprovince, Québec, Canada, including sampling locations.....	49
Figure 2.3 Histogram of $\delta^{32}\text{S}_{\text{V}-\text{CDT}}$ values for Noranda Camp samples.....	50
Figure 2.4 Binary plot of $\Delta^{33}\text{S}$ values against $\delta^{34}\text{S}$ values for sulfide samples from the Noranda Camp.....	51
Figure 2.5 Box and whisker diagrams for Noranda Camp $\Delta^{33}\text{S}$ values, by stratigraphic position.....	52
Figure 2.6 Box and whisker diagrams of trace element concentrations for pyrite, chalcopyrite and sphalerite samples from the Noranda Camp.....	53
Figure 2.7 Binary plots of $\Delta^{33}\text{S}$ values against Se and Au concentration.....	54
Figure 2.8 Schematic model for the evolution of the Noranda cauldron and associated hydrothermal circulatory systems.....	55
Figure 2.9 Binary plot of $\Delta^{33}\text{S}$ values against $\delta^{34}\text{S}$ values for Au-rich sulfide deposits of the Noranda Camp.....	56
Figure 3.1 Simplified geological map of the Doyon-Bousquet-LaRonde mining camp, Abitibi subprovince, Québec, Canada.....	82
Figure 3.2 Simplified stratigraphic cross section through the DBL mining camp...	83
Figure 3.3 Binary plots of $\Delta^{33}\text{S}$ values against $\delta^{34}\text{S}$ values for various deposits within the DBL mining camp.....	84
Figure 3.4 Binary plot of $\Delta^{33}\text{S}$ values against $\delta^{34}\text{S}$ values for DBL samples, by stratigraphic position, and comparison to Noranda Camp data.....	85

Figure 4.1 Simplified geological map of the Platreef, northern limb, Bushveld Igneous Complex, South Africa, with sampling locations.....	110
Figure 4.2 Binary plot of $\Delta^{33}\text{S}$ Platreef values against $\Delta^{33}\text{S}$ footwall values for various farms.....	111
Figure 4.3 Binary plot of $\Delta^{33}\text{S}$ values against $\delta^{34}\text{S}$ values for Platreef footwall rocks of the Transvaal Supergroup.....	112
Figure 4.4 Binary plot $\Delta^{33}\text{S}$ values against $\delta^{34}\text{S}$ values for Platreef sulfide samples, showing likely mixing between footwall sulfur sources.....	113
Figure A1.1 Box and whisker plots of trace element EPMA concentration data for pyrite from the Noranda VMS deposits.....	159
Figure A1.2 Box and whisker plots of trace element EPMA concentration data for pyrite from the Noranda Camp, by stratigraphic position.....	160
Figure A1.3 Box and whisker plots of trace element EPMA concentration data for sphalerite from the Noranda VMS deposits.....	161
Figure A1.4 Box and whisker plots of trace element EPMA concentration data for sphalerite from the Noranda Camp, by stratigraphic position.....	162
Figure A1.5 Box and whisker plots of trace element EPMA concentration data for chalcopyrite from the Noranda VMS deposits.....	163
Figure A1.6 Box and whisker plots of trace element EPMA concentration data for chalcopyrite from the Noranda Camp, by stratigraphic position.....	164
Figure A1.7 Box and whisker plots of trace element EPMA concentration data for pyrrhotite from the Noranda VMS deposits.....	165
Figure A1.8 Box and whisker plots of trace element EPMA concentration data for pyrrhotite from the Noranda Camp, by stratigraphic position.....	166
Figure A1.9 Box and whisker plots of trace element EPMA concentration data for galena from the Noranda VMS deposits.....	167
Figure A1.10 Binary plots of $\Delta^{33}\text{S}$ values against trace element concentration data for sulfide samples from the Noranda Camp, by stratigraphic position...	168

LIST OF TABLES

	<u>page</u>
Table 3.1 Sulfur isotope compositions of sulfide samples from the Doyon-Bousquet-LaRonde mining camp.....	81
Table 4.1 Multiple sulfur isotope data for samples from the Northern limb of the Bushveld Igneous Complex.....	108
Table A1.1 Stratigraphic position, deposit and sample numbers for this study, with sample and microprobe descriptions and dominant mineralogy.....	122
Table A1.2 Sulfur isotope compositions and ICP-MS trace element concentrations for sulfides from the Noranda VMS deposits.....	125
Table A1.3 Trace element EPMA data for Noranda VMS sulfide mineral separates.....	128
Table A1.4 Investigation of equilibrium of sulfide mineral pairs and temperature of formation, bold denotes samples that fit both requirements.....	158
Table A2.1 Detailed descriptions of the ore deposits of the Doyon-Bousquet-LaRonde and accompanying samples for each deposit.....	170
Table A2.2 Detailed description of all samples collected from the Doyon-Bousquet-LaRonde mining camp including polished block descriptions.....	172

CHAPTER ONE

Overview

1.1 Introduction

1.1.1 Isotope effects and fractionation processes

Isotopes of a given element have nuclei that contain the same number of protons, but a different number of neutrons. Isotopes are divided into two fundamental kinds, stable and unstable, the distinction between which is dictated by the detection limits of radioactive decay times. As the different isotopes of an element have the same number and arrangement of electrons they exhibit, in general, the same chemical behavior. However, isotopes have a different number of neutrons, and, therefore, different masses, which leads to differences in physicochemical properties, termed “isotope effects” (Hoefs, 2004).

The differences in the physicochemical properties of isotopes are a function of quantum mechanical effects. The energy of a molecule is a function of the distance between the atoms that comprise that molecule (Fig. 1.1) (Bigeleisen, 1965). In accordance with quantum theory, the energy of a molecule is limited to certain discrete energy levels. However, the lowest energy is not at the minimum of the energy curve as shown in Figure 1.1. Rather, it is above it by an amount of $\frac{1}{2} hv$ (termed zero-point energy), where h is Planck’s constant and v is the frequency with which the atoms in the molecule vibrate relative to each other. This vibration is a function of the fundamental frequency of the molecule, which is affected by the mass of the isotopes that make-up the molecule. Therefore, molecules with the same chemical formula, but which contain

different isotopic species, will have different zero-point energies (Hoefs, 2004). Heavy isotope substitution leads to lower vibrational frequencies, and a molecule with a lower zero-point energy compared to the same molecule, but with the lighter isotope (Fig. 1.1). As a result of this, bonds formed by a light isotope are weaker than bonds formed by the heavier isotope, and therefore generally react more readily during a chemical reaction (Hoefs, 2004).

This difference in ease and rate of a reaction among compounds of different isotopic composition can lead to the partitioning of isotopes between two substances or two phases of the same substance. This is termed “isotope fractionation” and is dominantly a result of isotope equilibrium exchange reactions and/or kinetic processes. Isotope exchange reactions are those in which the isotope distribution changes between different chemical substances, phases or individual molecules, but where there is no net (chemical) reaction.

For any specific combination of chemical species and its isotopic composition, a partition function can be constructed to describe the energy distribution among all molecules of that species. This function is referred to as a “partition coefficient”, and is calculated using the equation $Q = \sum_i (g_i e^{(-E_i/kT)})$, where E_i represents each allowed energy level of the molecule, g_i is the statistical weight of that energy level, k is the Boltzmann constant and T is the absolute temperature. Hence, the partition coefficient of a species is strongly dependent on temperature (Chacko et al., 2001). Partition coefficients for any combination of species and isotopic compositions involved in an equilibrium reaction can be combined to produce an isotopic equilibrium constant for that reaction at a specified temperature. Although pressure changes do have a small effect on the distribution of isotopes of an element between different chemical species, the effect is commonly too small to be resolved by current analytical techniques. Hence,

the dominant control on isotope exchange reactions in geological processes is temperature (Hoefs, 2004).

In geochemistry, it is common that the isotope equilibrium constant is substituted by the fractionation factor α , defined as $\alpha_{A-B} = R_A / R_B$, where R_A and R_B are the ratios of two isotopes of an element in compounds A and B, respectively (Hoefs, 2004). The fractionation factor itself can also be expressed as an ϵ -value, where $\epsilon = \alpha - 1$. This latter notation is convenient to employ as $\epsilon \times 1000$ approximates the magnitude of the isotopic contrast in δ -value units (see below).

Fractionation can also be produced by kinetic isotope effects, which are associated with incomplete and unidirectional processes (e.g., evaporation, dissociation reactions, biologically mediated reactions, diffusion). A kinetic isotope effect can also occur when the rate of a chemical reaction is sensitive to atomic mass at a particular position in one of the reacting species (Hoefs, 2004). Simple equilibrium processes can be interpreted to be the result of various isotopic components having different rates of reaction. In the case of isotope measurements taken during unidirectional chemical reactions, the reaction products always show a preferential enrichment in the lighter isotope.

In this thesis, I consider the stable isotopes of sulfur. Sulfur has four stable isotopes, ^{32}S , ^{33}S , ^{34}S and ^{36}S , with relative abundances of 95.02%, 0.75%, 4.21% and 0.02%, respectively. The fractionation of sulfur isotopes occurs through kinetic isotope effects during microbial processes, and through various chemical exchange reactions between different sulfides, and between sulfides and sulfates.

1.1.2 Multiple sulfur isotope analysis and mass-independent fractionation

The analyses of natural samples to investigate their sulfur isotope composition dates back to shortly after the Second World War (MacNamara and Thode, 1950). Traditionally these investigations utilized the ratios of the two most abundant isotopes of sulfur (^{32}S and ^{34}S) within the framework of the $\delta^{34}\text{S}$ notation ($\delta^{34}\text{S} (\text{\textperthousand}) = [(^{34}\text{S}/^{32}\text{S})_{\text{sample}} / (^{34}\text{S}/^{32}\text{S})_{\text{standard}} - 1] \times 1000$). This was in part due to limitations in analytical techniques, but was also based on early observations of a tight correlation between $\delta^{33}\text{S}$, $\delta^{34}\text{S}$ and $\delta^{36}\text{S}$ values (Hulston and Thode, 1965), leading to the assumption that no additional information would be supplied by measuring the less abundant isotopes (Johnston, 2011). However, Farquhar et al. (2000) identified a mass-independently fractionated sulfur isotope signature (expressed as non-zero $\Delta^{33}\text{S}$ and $\Delta^{36}\text{S}$ values, where $\Delta^{33}\text{S} = \delta^{33}\text{S} - [(\delta^{34}\text{S}/1000+1)^{0.515}-1] \times 1000$, and $\Delta^{36}\text{S} = \delta^{36}\text{S} - [(\delta^{34}\text{S}/1000+1)^{1.9}-1] \times 1000$) that appeared to occur exclusively in Archean sedimentary samples. They interpreted this to be the result of one or more gas phase, mass-independent chemical reactions in the sulfur cycle. The recognition that extra data dimensions can be obtained through multiple sulfur isotope analyses has led to renewed interest in the analysis of $\delta^{33}\text{S}$ and $\delta^{36}\text{S}$ values in the last decade.

One of the most important roles that multiple sulfur isotope analyses have played is in the development of our understanding of the Archean sulfur cycle and its place in the evolution of Earth's atmosphere. There are two important observations that have linked mass-independent fractionation of sulfur isotopes to the evolution of Earth's atmosphere. The first observation is that the occurrence of anomalous amounts of ^{33}S in a compound, termed mass-independent fractionation (MIF) of sulfur isotopes, is limited to samples older than ~2.42 Ga (Farquhar et al., 2010) and is prominent prior to 2.450 Ga (Johnston, 2011) (Fig. 1.2). The second was the identification that the anomalous amounts of ^{33}S could be produced by photodissociation of SO_2 .

Photochemical experiments of Farquhar et al. (2001), on the photodissociation of SO₂ by incident radiation, found that wavelengths <220 nm were effective. These wavelengths fall within the spectral window between the Schumann-Runge bands of oxygen and the Hartley bands of ozone which is one of the first spectral windows to open when the column depths of ozone and oxygen decrease because of changes in altitude or atmospheric oxygen content. This link between the UV spectral window, which allows the photodissociation of SO₂, and decreasing atmospheric oxygen content implies a connection between mass-independent fractionation of sulfur isotopes and the oxygen content of the atmosphere (Farquhar et al., 2001). This has led researchers (Farquhar et al., 2001; Farquhar and Wing, 2003; Pavlov and Kasting, 2002) to attribute the mass-independent fractionation of sulfur isotopes to a low partial pressure of oxygen in the Archean atmosphere.

Another implication of the mass-independently fractionated sulfur isotope record is that the chemical environment of the Archean must have allowed for the preservation of this fractionation. Preservation would have necessitated that isotopically distinct reservoirs with different oxidation states remained separate, and did not mix and isotopically homogenize (Johnston, 2011). It has been proposed that the ability to preserve mass-independently fractionated sulfur signatures relies on the *p*O₂ of the atmosphere remaining below 10⁻⁵ present atmospheric levels (Pavlov and Kasting, 2002). Such a low level of oxygen in the Archean atmosphere would be considered anoxic compared to the present day.

Thermochemical sulfate reduction has been proposed as an alternative process to photochemistry (Watanabe et al., 2009). However other researchers (Farquhar et al., 2010; Johnston, 2011) have dismissed this process as it does not account for the tight coupling of Δ³³S and Δ³⁶S in many Archean samples, the production and transfer of the record of anomalous

amounts of ^{33}S through the whole of the Archean rock record, and the apparent coherence of the signal both geographically and temporally. Farquhar et al. (2010) and Johnston (2011) also question the lack of a specific chemical reaction to produce the overall mass-independent fractionation effect (Johnston, 2011). Therefore, for the purposes of this thesis, the generation of mass-independent fractionation of sulfur and its associated preservation is considered to be more readily attributed to photochemical reactions in an anoxic Archean atmosphere.

1.1.3 Archean Sulfur Cycle

The framework presented provides the background to consider a proposed model for the Archean sulfur cycle, along with potential reservoirs of mass-independently fractionated sulfur (Fig. 1.3). The first step to consider is the source of SO_2 in the atmosphere, as well as the processes that govern its atmospheric lifetime (i.e., the longer it remains in the atmosphere the larger the potential for mass-independent fractionation; Halevy et al., 2010). The source of SO_2 to the atmosphere has been identified as volcanogenic (Farquhar and Wing, 2003) and controls on atmospheric lifetime include rate of volcanic supply, photolytic destruction, gas-phase reactions and net deposition to the surface (Halevy et al., 2010). As discussed above, atmospheric oxidation can destroy atmospheric SO_2 at the expense of photolysis (Pavlov and Kasting, 2002), but as long as photolysis rates are significant relative to the other atmospheric SO_2 sinks, mass-independent fractionation of sulfur isotopes is produced (Halevy et al., 2010).

Atmospheric chemistry is also critical in distributing the mass-independently fractionated sulfur isotope signature among different sulfur species (i.e. reduced S_8 aerosols with a positive $\Delta^{33}\text{S}$ and oxidized H_2SO_4 aerosols with a negative $\Delta^{33}\text{S}$) (Farquhar and Wing, 2003). These signatures are then transferred to the surface sub-cycle through at least two channels (Farquhar

and Wing, 2003). Photochemically-produced sulfate is then proposed to accumulate in the oceans (Farquhar et al., 2001; Halevy et al., 2010; Walker and Brimblecombe, 1985), preserving the negative $\Delta^{33}\text{S}$ signature in seawater sulfate. This is supported by measured negative $\Delta^{33}\text{S}$ values in barite deposits (Farquhar et al., 2000; Hoering, 1989), and enhanced by detailed studies from the ~3.47 Ga Dresser Formation in Australia (Golding et al., 2011; Philippot et al., 2007; Shen et al., 2009; Ueno et al., 2008), the ~3.2 Ga Fig Tree Group in the Barberton Greenstone Belt (Bao et al., 2007), and preliminary studies of hydrothermal sulfide sourced from seawater sulfate (Jamieson et al., 2006). It is proposed that the positive $\Delta^{33}\text{S}$ signature is preserved through the formation of sedimentary pyrite (Farquhar and Wing, 2003; Golding et al., 2011; Halevy et al., 2010), likely through the rapid equilibration of the elemental S carrier of the positive $\Delta^{33}\text{S}$ values with the oceanic sulfide pool, and reaction of that free sulfide with dissolved iron to form sedimentary pyrite (Lyons et al., 2009; Ono et al., 2003). Subsequent remobilization of these mass-independently fractionated reservoirs through the processes of the geological S cycle (e.g., metamorphism, recycling of sedimentary crust through subduction) may lead to a dilution of the $\Delta^{33}\text{S}$ signature as the atmospherically derived material is mixed with S that has not acquired a mass-independent signature; this dilution effect cannot change the inherent mass-independent nature of the original atmospheric S, suggesting that $\Delta^{33}\text{S}$ values may act as a unique tracer of the geological S cycle (Farquhar and Wing, 2003).

1.2 Application of multiple sulfur isotopes to ore-forming processes

Due to the nature of the mass-independent fractionation of sulfur isotopes as discussed above multiple sulfur isotope analyses have the potential to provide extra dimensions of understanding in the sources of sulfur in Archean ore deposits. Not only can the identification of

the sources of sulfur in an ore-forming system provide a greater understanding of how a mineral deposit forms and how best to explore for that particular type of deposit, it can also aid in the understanding of the ocean and atmosphere chemistry at the time of formation. The traditional use of $\delta^{34}\text{S}$ in the interpretation of the role of sulfur in these processes, although useful in some cases, is often limited by the one-dimensional nature of $\delta^{34}\text{S}$ data. The inclusion of $\delta^{33}\text{S}$, and by extension $\Delta^{33}\text{S}$, will assist in the interpretation of sulfur sources in Archean ore deposits on a most basic level by adding a second dimension to data analysis.

The identification of crustal sources of sulfur through sulfur isotopes has also proved to be a challenge in a variety of ore-forming environments due to other geological processes affecting $\delta^{34}\text{S}$ values of ore sulfides. For example, the identification of seawater sulfate contributions to ore-forming processes in the Archean is hampered by the $\delta^{34}\text{S}$ value of seawater at that time which is thought to be approximately the same as that of magmatic sulfur (-2 to +2‰) (Huston et al., 2010). It is also possible that sulfur isotope exchange between crustally contaminated sulfide ore accumulation and sulfur of mantle origin which accompanies proposed chalcophile element exchange is capable of masking or limiting the degree of isotopic evidence for an initial stage of ore genesis that involved crustal sulfur (Ripley and Li, 2003). Initial sulfur isotope compositions for sulfide ores can also be affected by metamorphism or later hydrothermal alteration. In contrast, the origin of non-zero $\Delta^{33}\text{S}$ signatures in the Archean atmosphere means that they provide an unequivocal method of identifying non-magmatic sources of sulfur within an ore-forming system. Combining this characteristic with the chemically conservative nature of $\Delta^{33}\text{S}$ signatures makes multiple isotope data an ideal tool for deciphering ore forming processes in the Archean.

Some preliminary studies have utilized multiple sulfur isotopes in the investigation of Archean ore deposits, including the Kidd Creek volcanogenic massive sulfide (VMS) deposit in the Superior Province, Canada (Jamieson et al., 2006). This study utilized $\Delta^{33}\text{S}$ values in ore sulfide pairs to evaluate their state of isotopic equilibrium. Jamieson et al. (2006) also proposed that non-zero $\Delta^{33}\text{S}$ values measured in their samples implied a possible contribution of surface-derived sulfur, but did not quantify this contribution further. A study of the Paleoarchean Panorama VMS deposits of Western Australia identified positive $\Delta^{33}\text{S}$ anomalies within the ore sulfides (Golding et al., 2011). The authors attributed this to mixing between a hydrothermal fluid carrying sulfur leached from volcanic host rocks and connate waters dominated by reduced sulfur, which originated in the marine environment. They also highlighted the lack of negative $\Delta^{33}\text{S}$ values in the ore deposits, which would indicate that seawater sulfate was not a dominant sulfur source in the ore-forming system (Golding et al., 2011). A small-scale study of samples from the Platreef magmatic Ni-Cu-PGE deposit, Bushveld Igneous Complex, South Africa used $\Delta^{33}\text{S}$ data to limit the contribution of crustal sulfur to within 5m of the footwall contact (Penniston-Dorland et al., 2008). However, no detailed deposit- or regional-scale study utilizing multiple sulfur isotope analyses has been undertaken to date.

This thesis presents three studies that apply multiple sulfur isotope analyses to Archean ore deposits. The first (Chapter Two – Manuscript One - *Etiology of VMS mineralization in the Noranda district, Quebec: Multiple sulfur isotope and trace element evidence* by Elizabeth Sharman, Boswell Wing, Bruce Taylor and William Minarik) presents a regional-scale study of the ~2.7 Ga VMS deposits of the Noranda camp, Abitibi subprovince, Superior Province, Canada. The study incorporates multiple sulfur isotope analyses with trace element analyses to propose a model of evolution of sulfur sources coincident with the evolution of Noranda caldera.

The second study (Chapter Three – Manuscript Two – *Evidence for a magmatic origin of the Doyon-Bousquet-LaRonde Au-bearing vein and VMS ore deposits: a multiple sulfur isotope study* by Elizabeth Sharman, Boswell Wing, Patrick Mercier-Langevin and Bruce Taylor) investigates, in detail, the multiple sulfur isotope composition of the Au-rich deposits of the Doyon-Bousquet-LaRonde (DBL) mining camp, which is located ~45 km east of the Noranda VMS camp, the focus of the first study. The DBL mining camp is the same age and located in the same volcanic package as the Noranda VMS deposits, but is unique because the mining camp also includes intrusion-related and shear-hosted Au-rich veins.

The third study presented in this thesis (Chapter Four – Manuscript Three - *Elucidation of multiple sulfur contamination events in Ni-Cu-(PGE) mineralization: $\Delta^{33}S$ evidence from the Platreef, Bushveld, South Africa* by Elizabeth Sharman, Sarah Penniston-Dorland, Boswell Wing, Judith Kinnaird, Paul Nex, Michael Brown and James Farquhar) utilizes multiple sulfur isotope analyses of the younger (~2.05 Ga) magmatic Ni-Cu-PGE Platreef deposit, Bushveld Igneous Complex, South Africa. The Platreef intrudes into Archean granites and Neoarchean sediments, and provides a contrasting mineralization style in which to examine the role of multiple sulfur isotope analyses.

These three studies demonstrate that multiple sulfur isotope analysis is a powerful tool for the investigation of Archean ore-forming processes. They also highlight the wide range of potential applications this analytical technique has in the understanding of sulfur sources in Archean ore deposits.

1.3 References

- Bao, H., Rumble, D., and Lowe, D. R., 2007, The five stable isotope compositions of Fig Tree barites: Implications on sulfur cycle in ca. 3.2 Ga oceans: *Geochimica et Cosmochimica Acta*, v. 71, p. 4868-4879.
- Bigeleisen, J., 1965, Chemistry of Isotopes: *Science*, v. 147, p. 463-471.
- Chacko, T., Cole, D.R., and Horita, J., 2001, Equilibrium Oxygen, Hydrogen and Carbon Isotope Fractionation Factors Applicable to Geologic Systems, in Valley, J.W., and Cole, D.R., eds., *Stable Isotope Geochemistry, Reviews in Mineralogy and Geochemistry*, v. 43, p. 1 – 81.
- Farquhar, J., Bao, H. M., and Thiemens, M., 2000, Atmospheric influence of Earth's earliest sulfur cycle: *Science*, v. 289, p. 756-758.
- Farquhar, J., Savarino, J., Airieau, S., and Thiemens, M., 2001, Observation of wavelength-sensitive mass-independent sulfur isotope effects during SO₂ photolysis: Implications for the early atmosphere: *J Geophys Res-Planet*, v. 106, p. 32829-32839.
- Farquhar, J., and Wing, B. A., 2003, Multiple sulfur isotopes and the evolution of the atmosphere: *Earth and Planetary Science Letters*, v. 213, p. 1 - 13.
- Farquhar, J., Wu, N., Canfield, D. E., and Oduro, H., 2010, Connections between Sulfur Cycle Evolution, Sulfur Isotopes, Sediments, and Base Metal Sulfide Deposits: *Econ Geol*, v. 105, p. 509-533.
- Golding, S. D., Duck, L. J., Young, E., Baublys, K. A., Glikson, M., and Kamber, B. S., 2011, Earliest Seafloor Hydrothermal Systems on Earth: Comparison with Modern Analogues, in Golding, S. D., and Glikson, M., eds., *Earliest Life on Earth: Habitats, Environments and Methods of Detection*, Springer Netherlands, p. 15-49.
- Halevy, I., Johnston, D. T., and Schrag, D. P., 2010, Explaining the Structure of the Archean Mass-Independent Sulfur Isotope Record: *Science*, v. 329, p. 204-207.
- Hoefs, J., 2004, *Stable Isotope Geochemistry*, 5th edition, Springer, 244 p.
- Hoering, T., 1989, Development of the sulfur hexafluoride method for sulfur isotope analysis, Annual Report of the Director, 2200, Geophysical Laboratory, Carnegie Institution, p. 128-131.
- Hulston, J. R., and Thode, H. G., 1965, Variations in the S33, S34, and S36 Contents of Meteorites and Their Relation to Chemical and Nuclear Effects: *J. Geophys. Res.*, v. 70, p. 3475-3484.
- Huston, D. L., Pehrsson, S., Eglington, B. M., and Zaw, K., 2010, The geology and metallogeny of volcanic-hosted massive sulfide deposits: Variations through geologic time and with tectonic setting: *Econ Geol*, v. 105, p. 571.
- Jamieson, J. W., Wing, B. A., Hannington, M. D., and Farquhar, J., 2006, Evaluating isotopic equilibrium among sulfide mineral pairs in Archean ore deposits: Case study from the Kidd Creek VMS deposit, Ontario, Canada: *Econ Geol*, v. 101, p. 1055-1061.
- Johnston, D. T., 2011, Multiple sulfur isotopes and the evolution of Earth's surface sulfur cycle: *Earth-Science Reviews*, v. 106, p. 161-183.
- Lyons, T. W., Anbar, A. D., Severmann, S., Scott, C., and Gill, B. C., 2009, Tracking Euxinia in the Ancient Ocean: A Multiproxy Perspective and Proterozoic Case Study: *Annual Review of Earth and Planetary Sciences*, v. 37, p. 507-534.
- MacNamara, J., and Thode, H. G., 1950, Comparison of the Isotopic Constitution of Terrestrial and Meteoritic Sulfur: *Physical Review*, v. 78, p. 307.

- Ono, S., Eigenbrode, J., Pavlov, A., Kharecha, P., Rumble, D., Kasting, J., and Freeman, K., 2003, New insights into Archean sulfur cycle from mass-independent sulfur isotope records from the Hamersley Basin, Australia: *Earth Planet Sc Lett*, v. 213, p. 15-30.
- Pavlov, A., and Kasting, J., 2002, Mass-independent fractionation of sulfur isotopes in Archean sediments: Strong evidence for an anoxic Archean atmosphere: *Astrobiology*, v. 2, p. 27-41.
- Penniston-Dorland, S. C., Wing, B. A., Nex, P. A. M., Kinnaird, J. A., Farquhar, J., Brown, M., and Sharman, E. R., 2008, Multiple sulfur isotopes reveal a magmatic origin for the Platreef platinum group element deposit, Bushveld Complex, South Africa: *Geology*, v. 36, p. 979-982.
- Philippot, P., Van Zuilen, M., Lepot, K., Thomazo, C., Farquhar, J., and Van Kranendonk, M. J., 2007, Early Archaean Microorganisms Preferred Elemental Sulfur, Not Sulfate: *Science*, v. 317, p. 1534-1537.
- Ripley, E., and Li, C., 2003, Sulfur isotope exchange and metal enrichment in the formation of magmatic Cu-Ni-(PGE) deposits: *Economic Geology*, v. 98, p. 635-641.
- Shen, Y., Farquhar, J., Masterson, A., Kaufman, A. J., and Buick, R., 2009, Evaluating the role of microbial sulfate reduction in the early Archean using quadruple isotope systematics: *Earth Planet Sc Lett*, v. 279, p. 383-391.
- Ueno, Y., Ono, S., Rumble, D., and Maruyama, S., 2008, Quadruple sulfur isotope analysis of ca. 3.5Ga Dresser Formation: New evidence for microbial sulfate reduction in the early Archean: *Geochimica et Cosmochimica Acta*, v. 72, p. 5675-5691.
- Walker, J. C. G., and Brimblecombe, P., 1985, Iron and sulfur in the pre-biologic ocean: *Precambrian Research*, v. 28, p. 205-222.
- Watanabe, Y., Farquhar, J., and Ohmoto, H., 2009, Anomalous fractionations of sulfur isotopes during thermochemical sulfate reduction: *Science*, v. 324, p. 370.

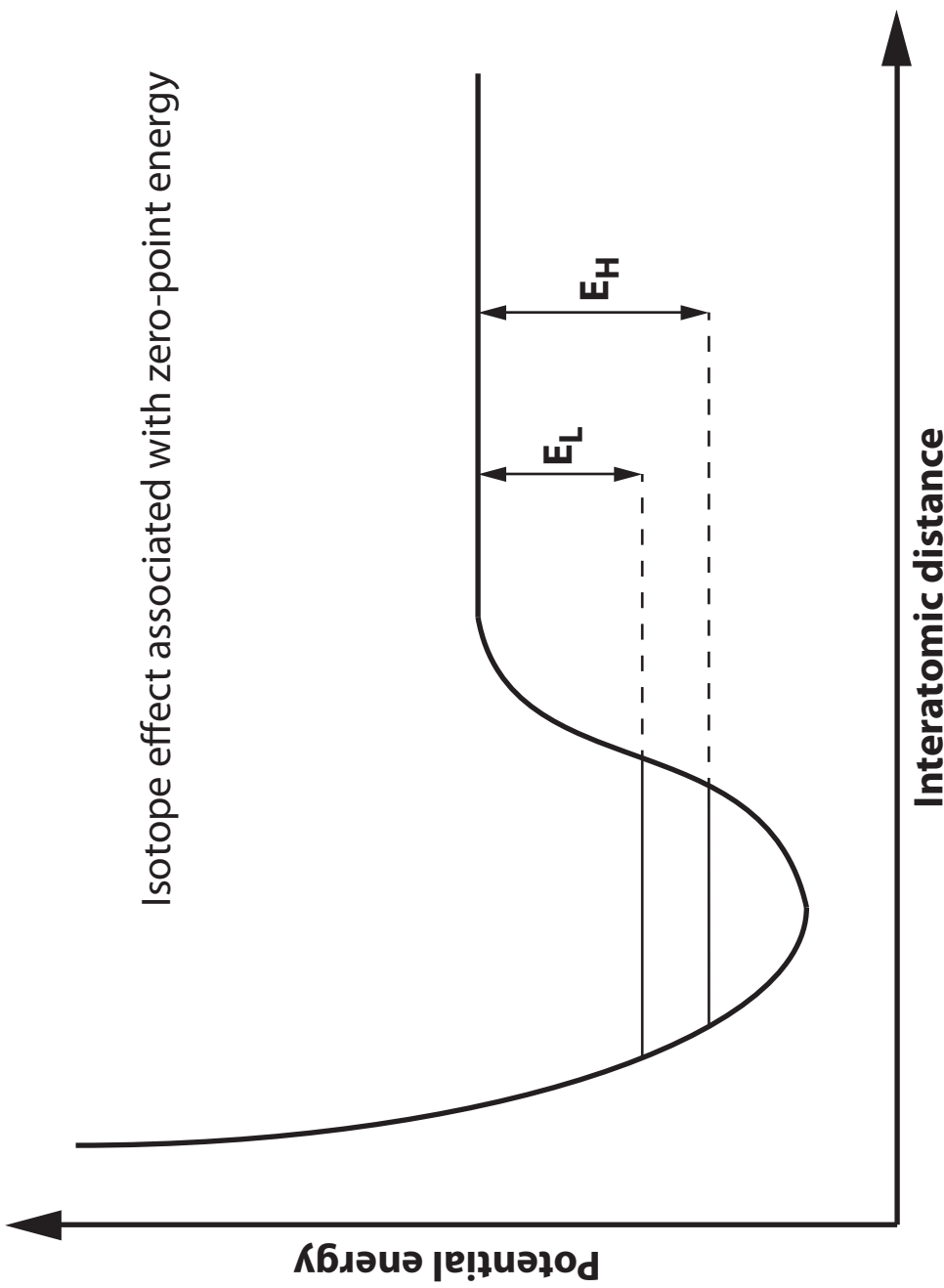


Fig 1.1 Schematic potential energy curve for the interaction of two atoms in a stable molecule or between two molecules in a liquid or solid (after Bigeleisen, 1965). E_L represents the dissociation energy of the light molecule and E_H the dissociation energy of the heavy molecule.

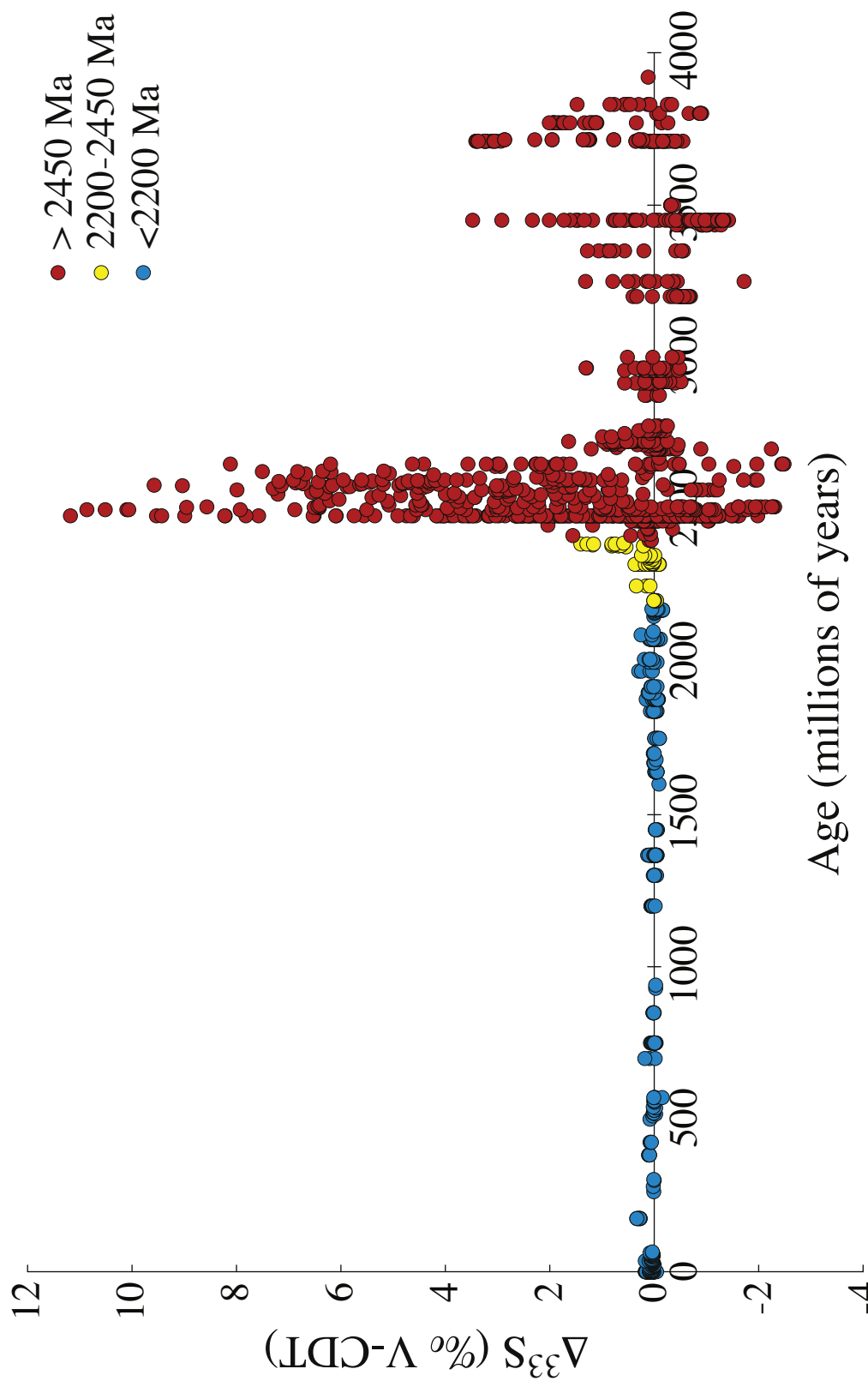


Fig. 1.2: Plot of $\Delta^{33}\text{S}$ versus geological age (in millions of years) highlighting the prominent mass-independent signal prior to 2.45 Ga (modified from Johnston, 2011).

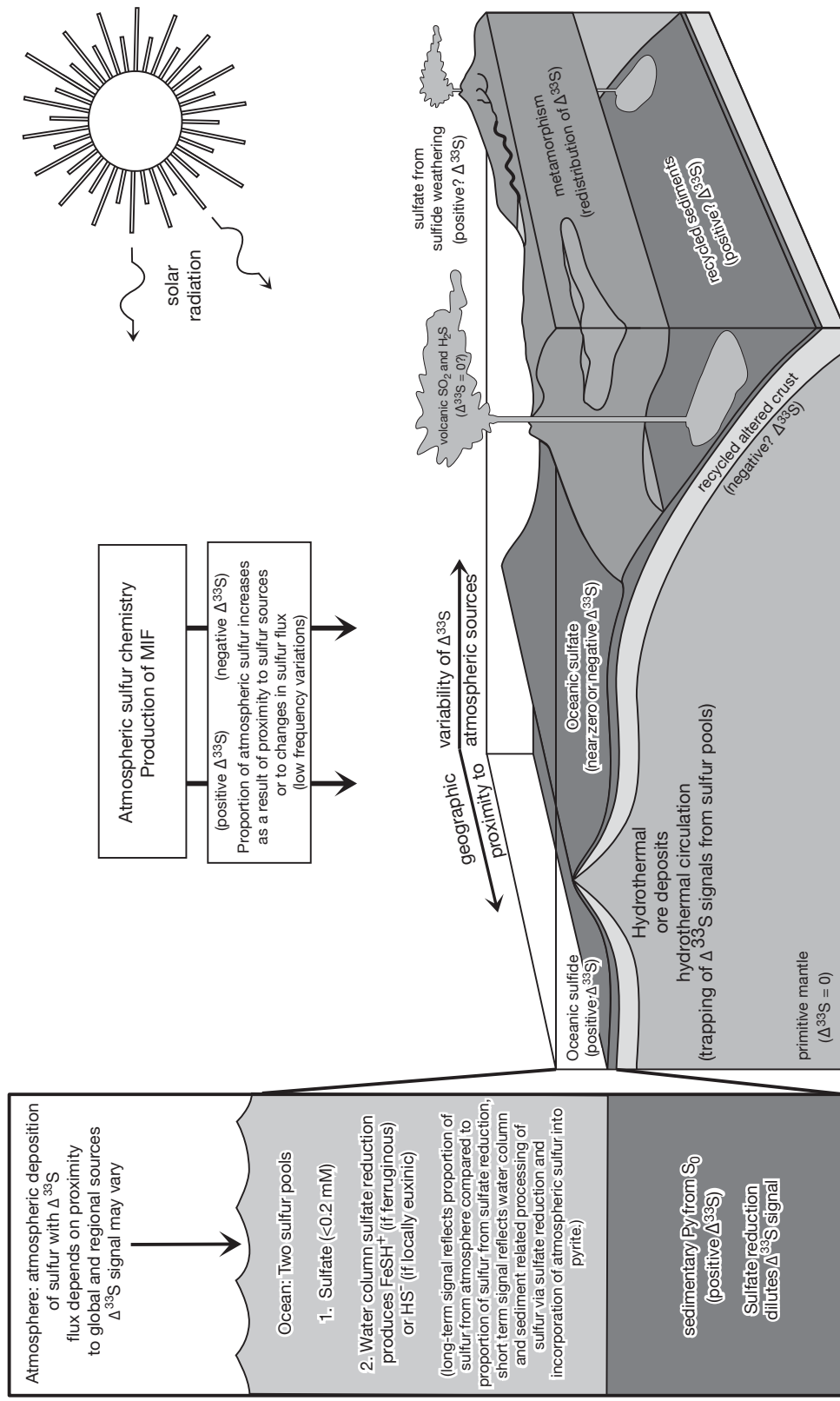


Fig. 1.3: Model of a possible Archean sulfur cycle with associated $\Delta^{33}\text{S}$ signatures at various stages of the cycle including atmospheric, water column and sedimentary processes (modified from Farquhar et al., 2010).

PREFACE TO CHAPTER TWO

The framework for the Archean sulfur cycle and the role of mass-independently fractionated sulfur isotopes presented in the previous chapter provides a structure within which to interpret multiple sulfur isotope data from Archean ore-forming systems. As an initial case study, we consider volcanogenic massive sulfide (VMS) deposits of the Neoarchean (2.5 to 2.8 Ga). In contrast to VMS deposits forming in the Phanerozoic, which have been shown to incorporate a significant amount of seawater sulfate during their formation, Huston et al. (2010) conclude that VMS deposits that formed in the Neo- and Mesoarchean are thought to contain sulfur from solely igneous–magmatic sources. This conclusion is based in part on the $\delta^{34}\text{S}$ values of Neo- and Mesoarchean VMS deposits, which have a limited range of -2 to +2 ‰ that is indistinguishable from the canonical range of mantle $\delta^{34}\text{S}$ values (Seal, 2006). It is also based on the assumption of a relatively small contribution of photochemically produced sulfate in the marine environment under an anoxic atmosphere (Huston and Logan, 2004; Walker and Brimblecombe, 1985), coupled with the relatively rapid consumption of marine sulfate (i.e., by biologic sulfate reduction) by an active Neo- and Mesoarchean microbial biosphere (Huston and Logan, 2004).

In the following chapter, we use multiple sulfur isotope data to reevaluate the recent conclusion of Huston et al. (2010). The ~2.7Ga Rouyn-Noranda district of the Abitibi subprovince, Superior Province, Canada, provides an ideal case study involving the application of multiple sulfur isotopes, as it is one of the best-preserved and most studied, VMS deposit-rich, Archean volcanic terranes in the world (Gibson and Galley, 2007).

- Gibson, H., and Galley, A., 2007, Volcanogenic massive sulfide deposits of the Archean, Noranda district, Quebec, *in* Goodfellow, W. D., ed., Mineral Deposits of Canada: A Synthesis of Major Deposit-types, District Metallogeny, the Evolution of Geological Provinces, and Exploration Methods, Special Publication No. 5, Mineral Deposits Division, Geological Association of Canada, p. 533-552.
- Huston, D. L., and Logan, G. A., 2004, Barite, BIFs and bugs: evidence for the evolution of the Earth's early hydrosphere: *Earth Planet Sc Lett*, v. 220, p. 41-55.
- Huston, D. L., Pehrsson, S., Eglington, B. M., and Zaw, K., 2010, The geology and metallogeny of volcanic-hosted massive sulfide deposits: Variations through geologic time and with tectonic setting: *Econ Geol*, v. 105, p. 571.
- Seal, R. R., II, 2006, Sulfur Isotope Geochemistry of Sulfide Minerals: Reviews in Mineralogy and Geochemistry, v. 61, p. 633-677.
- Walker, J. C. G., and Brimblecombe, P., 1985, Iron and sulfur in the pre-biologic ocean: *Precambrian Research*, v. 28, p. 205-222.

CHAPTER TWO

Etiology of VMS mineralization in the Noranda district, Quebec: Multiple sulfur isotope and trace element evidence

E.R. SHARMAN, B.A. WING, B.E. TAYLOR AND W.G. MINARIK

2.1 Abstract

Recently proposed models for the formation of volcanogenic massive sulfide (VMS) deposits during the Neo- and Mesoarchean assign little to no contribution of seawater sulfate to the ore-forming system. This is in contrast to more modern VMS systems, where seawater sulfate is thought to play an important role. In this chapter, we re-evaluate these models by examining sulfides from the ~2.7 Ga Noranda Camp, Abitibi subprovince, Superior Province, Canada using a combination of multiple sulfur isotope and trace element data. The Noranda camp is a well-preserved, VMS deposit-rich area that is thought to represent a collapsed caldera. Due to its economic value the camp has been studied extensively, providing a robust geological framework within which to assess the new data presented by this study. We also re-examine previously proposed controls on mineralization within the Noranda Camp, as well as exceptional deposits within it (i.e. the Au-rich Horne and Quemont deposits).

This study presents multiple sulfur isotope and trace element compositional data for sulfide separates representing 25 different VMS deposits or “showings” within the Noranda Camp. Multiple sulfur isotope data for this study have $\delta^{34}\text{S}_{\text{V}-\text{CDT}}$ values of between -1.90 ‰ and +2.49 ‰, and $\Delta^{33}\text{S}_{\text{V}-\text{CDT}}$ values of between -0.59 ‰ and -0.03 ‰. We interpret the negative $\Delta^{33}\text{S}$

values to be due to a contribution of sulfur originating in seawater sulfate to the ore sulfides of the Noranda Camp VMS deposits. This contribution increases with the collapse and subsequent evolution of the Noranda caldera; an interpretation supported by selected trace and major element analyses. In particular, higher concentrations of Se occur in samples with $\Delta^{33}\text{S}$ values closer to 0‰, and lower Fe/Zn ratios in sphalerite are indicative of lower temperatures of formation. We also report a direct correlation between Au grade and $\Delta^{33}\text{S}$ values within Au-rich VMS deposits of the Noranda Camp, whereby higher gold-grades are associated with near-zero $\Delta^{33}\text{S}$ values and, by inference, a dominance of an igneous-magmatic sulfur source (i.e., leached from the volcanic pile and/or degassed from an associated intrusive phase).

2.2 Introduction

Volcanogenic massive sulfide (VMS) deposits form on or immediately below the sea floor as a result of mixing between ambient seawater and upwelling hydrothermal fluids. These hydrothermal fluids are primarily generated by the interaction between convectively circulating heated seawater and sub-seafloor rock strata, driven by a cooling magmatic body, which may also contribute fluids to the system (Huston et al., 2010). It has long been assumed that the relative importance of the processes that led to the formation of VMS deposits during the Archean were different to those processes controlling the formation of Phanerozoic deposits. These include “changes in tectonic and volcanic processes, hydrothermal and magmatic processes, atmosphere-hydrosphere conditions, and preservation potential” (Huston et al, 2010).

This conclusion is based in part on a paucity of barite and other sulfate minerals associated with most Archean VMS deposits, in contrast to the abundance of these minerals within Phanerozoic deposits (Huston et al., 2010). Moreover, $\delta^{34}\text{S}$ values measured within VMS

deposits from the Archean are comparatively uniform and unfractionated ($\delta^{34}\text{S} \approx -2$ to $+2\text{\textperthousand}$) as opposed to the significantly broader range of values, and departure from $\delta^{34}\text{S} \approx 0\text{\textperthousand}$, recorded for deposits formed from the Proterozoic onwards (Huston et al., 2010). Although VMS deposits of the Paleoarchean have been shown to contain significant barite mineralization (Huston and Logan, 2004), limited $\delta^{34}\text{S}$ values and the lack of barite have led researchers to conclude that seawater sulfate played little to no role in the formation of Neo- and Mesoarchean VMS deposits. This is thought to reflect a lack of sulfate in Meso- and Neoarchean oceans, as a result either of an overall anoxic water column, or a stratified ocean with reduced bottom waters (Huston and Logan, 2004). In contrast, seawater-derived sulfate plays a significant role in the formation of Phanerozoic and modern seafloor sulfide deposits (Huston et al., 2010 and references therein).

The proposed differences in sulfur sources for Archean VMS mineralization can be sensibly investigated through multiple sulfur isotope analysis. For rocks older than 2.45 Ga, combined $\delta^{33}\text{S}$ and $\delta^{34}\text{S}$ analysis ($\delta^x\text{S} = [({}^x\text{S}/{}^{32}\text{S}_{\text{sample}} / {}^x\text{S}/{}^{32}\text{S}_{\text{standard}}) - 1] \times 1000$) can permit recognition of atmospheric sources of sulfur due to the production of anomalous amounts of ${}^{33}\text{S}$ by mass-independent isotope fractionation. Measured $\delta^{33}\text{S}$ values, in this case, are not solely related to measured $\delta^{34}\text{S}$ values by mass-dependent isotopic fractionation mechanisms ($\delta^{33}\text{S} \neq [(\delta^{34}\text{S}/1000+1)^{0.515}-1] \times 1000$). Most current models attribute anomalous amounts of ${}^{33}\text{S}$ to mass-independent fractionation during photochemical reactions involving SO_2 in an anoxic atmosphere (Farquhar et al., 2000; Farquhar et al., 2010). Such anomalous abundances of ${}^{33}\text{S}$ can be quantified in natural samples by the magnitude and sign of $\Delta^{33}\text{S}$, where $\Delta^{33}\text{S} \equiv \delta^{33}\text{S}_{\text{measured}} - [(\delta^{34}\text{S}_{\text{measured}}/1000+1)^{0.515}-1] \times 1000$. Mass-independent fractionation of sulfur should not be produced in purely magmatic ore-forming processes (Hulston and Thode, 1965), which will result in near-zero $\Delta^{33}\text{S}$ values.

Understanding of the Archean sulfur cycle has been augmented over the past decade by numerous analytical multiple sulfur isotope studies of the sedimentary rock record (Johnston, 2011 and references therein). This work has provided a framework that can now be used to identify contributions from atmospheric and hydrospheric sources for sulfur within Archean VMS deposits (Fig. 2.1). If the only source of sulfur to an Archean deposit was sulfur leached from fresh volcanic host-rocks (e.g. Huston and Logan, 2004), then no mass-independently fractionated sulfur should be observed within ore sulfides. In contrast, if sulfur sources more closely resembled those of modern VMS systems then several variations are possible (Huston and Logan, 2004). If sulfur has been contributed to the system through leaching from the volcanic pile, and atmospherically derived seawater sulfate has been introduced and reduced at or near the discharge zone, the ore sulfides would be expected to have positive $\delta^{34}\text{S}$ and negative $\Delta^{33}\text{S}$ values, reflecting the multiple sulfur isotope signature of contributing seawater sulfate (Fig. 2.1; Farquhar and Wing, 2003). In contrast, if reduced seawater sulfur has been contributed to the ore-forming system it may result in positive $\delta^{34}\text{S}$ and $\Delta^{33}\text{S}$ values (Fig. 2.1; Golding et al., 2011). However, if sulfur has been leached from seafloor sediments as well as the volcanic pile, it may result in variable $\delta^{34}\text{S}$ and $\Delta^{33}\text{S}$ values in the ore sulfides depending on the multiple sulfur isotope composition of the sediments (Fig. 2.1).

It is also possible that seawater sulfate was entrained in the hydrothermal recharge system and precipitated as anhydrite within the reaction zone (e.g. Barker et al., 2010) and would therefore not reflect in the ore-forming fluid. Alternatively, some researchers have suggested that ~0.6 mmol/kg seawater sulfate may remain in the hydrothermal fluid and be reduced, retaining its $\delta^{34}\text{S}_{\text{sulfate}}$ signature (Herzig et al., 1998). However, this scenario is unlikely for Archean ore-forming systems, as the proposed low concentrations of sulfate within Archean

seawater ($\Sigma S < 0.001 \Sigma S_{modern}$, Huston et al., 2004) would not allow for any preservation through the reaction zone.

The chemically conservative nature of the mass-independent fractionation signature – a $\Delta^{33}S$ value cannot be altered by mass-dependent isotope fractionation processes that affect $\delta^{34}S$ values (e.g., inter-mineral equilibrium precipitation) – also means that $\Delta^{33}S$ values provide a robust record of the influence of different sulfur sources during formation of Archean ore deposits.

The ~2.7 Ga Blake River Group volcanic rocks of the Rouyn-Noranda district, within the Abitibi Subprovince of the Superior Province, Canada, comprise one of the best-preserved, VMS deposit-rich, Archean terranes in the world (Gibson and Galley, 2007). A significant volcanic structure of the terrane, the Noranda Cauldron, or caldera, formed during syn-volcanic subsidence, and has previously been described as an “asymmetric volcanic depression filled with effusive basalt and basaltic andesite flows and subordinate rhyolite flow-dome complexes” (Gibson and Galley, 2007). The Rouyn-Noranda district hosts 20 known economic VMS deposits and numerous minor occurrences, as well as orogenic Au and intrusion-related Cu-Mo deposits and occurrences (Gibson and Galley, 2007). Collectively, these are referred to as the Noranda Camp. Due to its extensive mineral wealth, this district has been intensively studied over a period of several decades. Hence, the Noranda Camp provides an ideal case study for the application of multiple sulfur isotope analyses to Archean VMS mineralization.

Herein, we present multiple sulfur isotope and supporting data from 25 VMS deposits or occurrences of the Noranda Camp. A primary objective of this study is to evaluate the potential role of oceanic sulfate in the formation of these Neoarchean deposits. We also evaluate previously proposed controls on VMS mineralization processes. These controls include host

rock lithology (mafic vs. felsic; Gibson and Galley, 2007) as well as temperature-dependent ‘copper’ ($100 \text{ Cu}/(\text{Cu}+\text{Zn})$) and ‘zinc’ ($100 \text{ Zn}/(\text{Zn}+\text{Pb})$) ratios (Huston and Large, 1987; Large, 1992). Lastly, we examine the exceptional Au-rich VMS deposits within the Noranda Camp. We show that, in combination with other data that can fingerprint sources of ore metals (e.g., trace element geochemistry), multiple sulfur isotope analysis is a powerful tool for elucidation of processes that lead to formation of VMS deposits in the Archean.

2.3 Regional Geology

The Rouyn-Noranda district is a geographic area surrounding the town Rouyn-Noranda, Quebec, and is underlain by volcanic rocks of the Blake River Group (BRG). The BRG in this area has a total stratigraphic thickness of ~10 km and ranges in age from 2701 to 2694 Ma (Corfu, 1993), inferred to have formed in a primitive rifting environment (Gibson and Galley, 2007). It comprises andesitic units overlain by bimodal andesite-rhyolite units (Peloquin, 1999; Peloquin et al., 1990) that have been intruded by synvolcanic plutons (the Flavrian and Powell Intrusions) and several other syn- to post-tectonic tonalite-trondjhemite-granodiorite (TTG) suite intrusions (Goldie, 1978; Piercey et al., 2008). The BRG is bounded to the north by the Destor-Porcupine Fault, and to the south by the Cadillac-Larder Lake Fault (Jensen, 1975). The rocks of the BRG are metamorphosed to greenschist assemblages, with some local lower grade prehnite-pumpellyite assemblages (Dimroth et al., 1983).

The BRG itself is separated into six different formations: the Bousquet, Reneault-Dufresnoy (formally Cycle V), Noranda (formally Cycles III and IV), Rouyn-Pelletier, Duprat Montbray (formally cycles I and II) and Hebecourt formations (Peloquin, 2005) (Fig. 2.2). The narrowly constrained age range for the Blake River volcanics, coupled with the absence of

unconformities or thick epiclastic sedimentary successions, indicates that volcanism occurred far from subaerial landmasses (Gibson and Galley, 2007).

The Noranda Cauldron is floored by a large, multiphase subvolcanic intrusive complex: the Flavrian and Powell Intrusions. These synvolcanic intrusions were emplaced into their volcanic equivalents as a series of sill complexes (Galley, 2003; Richard, 1999). The Flavrian pluton, in particular, is considered to be the source of heat that drove hydrothermal circulation within the Noranda district, and also may have contributed directly to the fluids responsible for the formation of the VMS deposits (Gibson and Galley, 2007).

The VMS deposits of the Noranda district belong to the bimodal-mafic (host lithologies are basalt dominated but comprise up to 25% felsic volcanic strata) due to the composition of the strata surrounding the massive sulfide deposits (Franklin et al., 2005), and most deposits occur within the Noranda formation. In general, the massive sulfide deposits of the Noranda district comprise a copper-rich core that grades upwards and outwards to a zinc-rich fringe (Gibson and Galley, 2007). This zoning is thought to be in part due to a zone-refining process whereby early-formed low temperature pyrite and sphalerite are replaced at high temperature by chalcopyrite and pyrrhotite \pm magnetite (Gibson and Galley, 2007). The inferred increase in fluid temperature may reflect a self-sealing process whereby sulfide- and silica-bearing minerals precipitate above hydrothermal upflow zones, thereby preventing hot hydrothermal fluids from interacting with seawater (Gibson and Galley, 2007).

Although the VMS deposits within the Noranda district share some common features, there are critical distinctions that can be made between the various deposits. For example, the deposits can be divided into two subgroups: those that have formed within mafic and felsic flows, and those that have formed within dominantly felsic volcaniclastic lithologies. Although

a larger number of deposits are hosted within flow facies (8 in mafic and 9 in felsic flows), the largest deposits by tonnage are hosted within felsic volcaniclastics (i.e., the Horne, Quemont and Mobrun deposits). Perhaps the clearest controls on the formation of economic deposits, however, seem to be related to periods of quiescence between rifting and subsidence events in the cauldron. As a result, distinguishing characteristics of the VMS deposits within the Noranda Camp appear to correlate with their stratigraphic location within the evolving Noranda Cauldron.

These characteristics, as outlined by Gibson and Watkinson (1990), can be summarized as follows:

Pre-cauldron deposits: These deposits are generally chalcopyrite-pyrrhotite stringer zones and due to the absence of capping massive sulfides are thought to represent the erosional remnants of former VMS deposits.

Cauldron deposits: Typically proximal, these deposits comprise a concordant massive sulfide lens (or series of lenses) with an underlying stringer zone. Some massive sulfide lenses are zoned from a copper-rich core to a zinc- (and lead-) rich fringe. Pyrrhotite-chalcopyrite veins dominate the underlying stringer zones.

Post-cauldron deposits: These deposits are typically zinc-rich as well as more lead-rich, and are locally underlain by a copper-rich stringer zone.

Several of the deposits within the Noranda district are also partially auriferous (Horne, Quemont, Delbridge, Deldona and Mobrun; Dubé et al., 2007). Although these deposits are not confined to one depositional environment, the Horne deposit, which is considered to be a gold deposit with base metal credits, is hosted in felsic volcanoclastics and is two orders-of-magnitude larger in terms of ore tonnage than most other deposits in the area (Kerr and Gibson, 1993). The Horne deposit itself is separated into two main separate lenses: the No. 8 lens, thought to have a

more magmatic origin, and the No. 5 lens, representing an exhalative component of the deposit (Sinclair, 1971). The gold enrichment within certain VMS deposits of the Noranda district is associated with both copper- and zinc-rich deposits and the processes that caused this enrichment are not well understood. Mechanisms that have been proposed for this enrichment include a direct magmatic contribution of gold (Dubé et al., 2007), boiling of the hydrothermal fluid (Dubé et al., 2007; Gibson and Watkinson, 1990), and zone refinement (Dubé et al., 2007; Kerr and Gibson, 1993).

2.4 Samples

Mineral separates for this study were prepared from hand samples taken from a variety of Noranda VMS deposits. Although some of the samples analysed were almost 100% monomineralic, others exhibited compositional variability, not only in the sulfide minerals, but also in the presence of various gangue minerals (see Table A1.1). Inclusions were also commonly observed in individual sulfide grains, typically intergrown sphalerite and chalcopyrite within pyrite, but also sphalerite with pyrite and chalcopyrite inclusions.

2.5 Methodology

Samples for this study comprised nearly 150 sulfide mineral concentrates from 25 different VMS deposits and showings in the Noranda Camp. The sulfide separates came from samples sourced from the Geological Survey of Canada Ore Collection, and were chosen to represent the broadest range of VMS mineralization types within the Noranda area.

2.5.1 Electron Probe Microanalysis (EPMA)

Sample grains were mounted within epoxy resin and polished prior to EPMA analysis, with four samples per mount and hundreds of grains per sample. Each grain mount was then characterized using optical and scanning electron microscopy techniques, to identify the main mineralogical and textural relationships within sulfide mineral grains, as well as to identify any residual gangue mineral grains within the samples. Each mineral identified within the sample was analysed for the concentration of ten elements (S, As, Zn, Cd, Fe, Se, Cu, Ni, Co, Cr), using a JEOL 8900 electron microprobe (JEOL Ltd., Tokyo, Japan), located at McGill University. Approximately 15 individual spot analyses were conducted for each major mineral, with fewer for trace minerals.

2.5.2 Multiple sulfur isotope analysis

Samples for multiple sulfur isotope analyses underwent a three step analytical process. First each sample was ground to a fine powder to allow for more efficient reactions during processing. This was performed by hand, under methanol, using an agate mortar and pestle, each of which was thoroughly cleaned between samples. Secondly, sulfur within the mineral powder was converted to SF₆ gas by laser heating under an F₂ atmosphere, conducted at the Geological Survey of Canada, Ottawa, following the procedure of Beaudoin and Taylor (1994) and Taylor (2004b). The resulting SF₆ gas was purified in a series of cryogenic and variable temperature traps, before being sealed within glass ampoules (Taylor, 2004a; Taylor, 2004b). The final phase involved a secondary purification of the SF₆ gas, using a gas chromatograph procedure as outlined by Hu et al. (2003), prior to introduction to a Thermo Finnigan MAT 253 dual-inlet gas-source mass spectrometer (Thermo Electron Corporation, Bremen, Germany), located at McGill

University. Sulfur isotope abundances were measured by monitoring the $^{32}\text{SF}_5^+$, $^{33}\text{SF}_5^+$, $^{34}\text{SF}_5^+$ ion beams at mass to charge ratios of 127, 128, and 129, respectively. All sulfur isotope ratio data are herein reported relative to the Vienna Cañon Diablo troilite scale (V-CDT), against which the international reference material IAEA-S-1 Ag-sulfide has a defined $\delta^{34}\text{S}$ value of -0.30 ‰ (Robinson, 1995). We take the $\Delta^{33}\text{S}$ value of IAEA-S-1 to be 0.094 ‰ V-CDT. The full analytical uncertainty (1σ) for S isotope analyses is estimated to be ± 0.13 ‰ for $\delta^{34}\text{S}$ values, and ± 0.01 ‰ for $\Delta^{33}\text{S}$ values, based on the long-term standard deviation for repeat analyses of a sphalerite standard (LSI-95-16 BH Sphal) and an internal pyrite sample (A95-16B PY).

2.5.3 Inductively Coupled Plasma Mass Spectrometry (ICP-MS)

Aliquots of the sulfide concentrates used for S isotope analyses were also analysed for their trace element composition using traditional wet chemical methods, in order to compare the trace element geochemistry of samples to their S isotope compositions on similar sampling scales. Approximately 10mg of sample was weighed out into a PTFE reaction vessel designed for this procedure. Each sample was then dissolved in an inverse *aqua regia* solution of 3 ml concentrated trace-metal grade HNO₃ (69%) and 1 ml concentrated trace-metal grade HCl (35%). Each reaction vessel was then sealed with a PTFE stopper and placed on a hot plate at ~75°C within a fume hood for six hours. After this initial reaction the stoppers were removed from the reaction vessels and left for a further six hours, or until the solution had evaporated to dryness, whichever occurred soonest. After being allowed to cool, the samples were then re-dissolved in 2 ml of trace metal grade concentrated HNO₃, and the stoppers placed back into the corresponding reaction vessels. The reaction vessels were again placed on the hot plate at ~75°C for another six hours and then allowed to cool. Each sample was transferred into a 50 ml

centrifuge tube and diluted with 35 ml of $>18.2\text{ M}\Omega\text{ cm}^{-1}$ ultra-pure water. Finally, each sample was diluted in two fractions with 2% OptimaTM grade HNO₃ (SeaStar) forming 1:100 and 1:1000 solutions.

Each resulting solution was analysed for 10 elements (Cu, Zn, Cr, Mn, Co, Ni, Se, Mo, Au, Pb), using a PerkinElmer/SciEx Elan 6100 DRCplus ICP-MS in the Trace Element Analytical Laboratory at McGill University. Standards and calibration solutions were prepared in dilute nitric acid and Rh was used as an internal standard. The ICP-MS was run in standard mode for most elements, but for some elements (e.g. Cr, Mn, Co, Ni, Se) it was necessary to use the Dynamic Reaction Cell (DRC) with ammonia as the reaction gas. Gas flow rate and the DRC quadrupole stability parameters were optimized for each element to remove molecular interferences.

2.6 Results

The large quantity of data produced in this study (>3000 individual electron microprobe analyses, ≈ 150 S isotope analyses, and ≈ 150 ICP-MS analyses), as well as the broad scale of the questions addressed by this study, requires that the data set be grouped into statistical subdivisions. Our strategy was to use exploratory data analysis in order to identify the first-order controls on the variability in the dataset, and then build our interpretations of what influenced VMS mineralization in the Noranda camp around these controls. Owing to the experimental, conceptual, and empirical association of multiple sulfur isotope values with possible sources of sulfur in Archean VMS deposits, the organizing principles behind our exploratory data analysis were to first look for characteristics that explained the variability of our sulfur isotope measurements, and then to interpret the rest of our dataset within the resulting framework.

2.6.1 Multiple sulfur isotopes

$\delta^{34}\text{S}$ data from this study exhibit a relatively narrow range of values (-1.90 to +2.49‰, Table A1.2), as shown in Figure 2.3. This range is the same as has been recorded for other Archean VMS deposits (cf. Fig. 2B in Huston et al., 2010). The range of $\Delta^{33}\text{S}$ values (-0.59 to -0.03 ‰, Table A1.2) includes many samples that have a significant mass-independent fractionation signature. One galena sample (63RF53 GN), which was taken from a late-stage cross cutting vein, has S isotope compositions ($\delta^{34}\text{S} = -27.20\text{\textperthousand}$, $\Delta^{33}\text{S} = +0.09\text{\textperthousand}$) significantly outside the range of the rest of the data. This sample has been excluded from any data interpretation as it is unlikely to be associated with the main ore-forming event, which is supported by an approximate Pb-Pb age of 760 Ma (I. Jonasson pers. comm.).

In order to identify systematic variations within the multiple sulfur isotope dataset, samples were first grouped according to the dominant mineralogy of each sample. Systematic differences between $\delta^{34}\text{S}$ values are observed between mineralogical groups. A slight majority of the sphalerite samples have positive $\delta^{34}\text{S}$ values while most chalcopyrite samples have negative $\delta^{34}\text{S}$ values, as would be expected on the basis of equilibrium S isotope fractionation (Seal, 2006). However, there is no similar association in $\Delta^{33}\text{S}$ values. If the samples are grouped according to host rock lithology (mafic and felsic flows vs. felsic volcanoclastics, from Gibson and Galley, 2007), or by their ‘copper’ or ‘zinc’ ratios (as defined by Large, 1992) there are also no definable correlations. In contrast, when samples are classified by the stratigraphic position within the Noranda Camp of the deposit from which they were taken (pre-cauldron, cauldron and post-cauldron, as defined by Gibson and Watkinson, 1990, along with deposits interpreted to be located at the cauldron margin, Table A1.1), clear relationships emerge (Fig. 2.4; as explained

later, measurements from the Horne mine are included with the pre-cauldron grouping).

Pre-cauldron deposits are characterized by near-zero $\Delta^{33}\text{S}$ values, and decrease to more negative $\Delta^{33}\text{S}$ values in deposits from higher in the stratigraphy (mean $\Delta^{33}\text{S} \approx -0.25\text{\textperthousand}$). These mass-independent sulfur isotope values are greatest in cauldron and post-cauldron deposits (Fig. 2.4). These variations are accentuated if the variation in $\Delta^{33}\text{S}$ values is examined using a box and whisker diagram (Fig. 2.5). This plot highlights two major features of the $\Delta^{33}\text{S}$ dataset: (1) the central tendency of the $\Delta^{33}\text{S}$ population (monitored either as the mean or the mode) within each stratigraphic group becomes progressively more negative up section and; (2) the variability of $\Delta^{33}\text{S}$ values within each stratigraphic group increases from pre-cauldron to cauldron margin and reaches a shared range of values in the main cauldron and post-cauldron deposits. As this classification of samples into stratigraphic position yields a clear order to the multiple sulfur isotope data, we use it as the framework within which we present the rest of our analytical results.

2.6.2 Trace Element Geochemistry

2.6.2.1 EPMA: The trace element EPMA data (see Table A1.3) were assessed for variability relative to their position stratigraphically (Figs. A1.1 – A1.9). This graphical examination revealed that most trace elements have similar concentrations among like sulfide minerals regardless of their associated ore deposit or stratigraphic position. There are, however, some striking exceptions.

Within samples from pre-cauldron deposits, pyrite commonly has elevated average Se concentrations (~0.1 vs. ~0.02 wt% for other deposits), and greater variability (Fig. 2.6A). Similarly, pre-cauldron chalcopyrite exhibits Se concentrations and variability that are far greater

(ave. ~1.5 wt%) than chalcopyrite from the samples taken from other stratigraphic intervals (ave. ~0.04 wt%) (Fig. 2.6B). Sphalerite samples from pre-cauldron deposits have no such relative Se enrichment (Fig. A1.4), however, the measured Fe/(Fe+Zn) ratio of sphalerite taken from post-cauldron deposits is significantly lower (ave. ~0.04) than for sphalerite samples taken from other stratigraphic levels (ave. ~0.1) (Fig. 2.6C). [The apparent contradiction to this statement shown by sphalerite in the pre-cauldron deposits is entirely attributable to samples from Horne No. 5 (Fig. A1.3) and is discussed in a later section]. Neither pyrrhotite nor galena samples show systematic compositional variability with respect to their stratigraphic position (Figs. A1.8 and A1.9).

2.6.2.2 ICP-MS: Trace element compositions of samples determined using ICP-MS techniques are presented in Table A1.2. Trace element concentrations in galena were below the lower limit of detection for our analytical procedure. In order to investigate shared controls on both sulfur and trace metal distributions, we evaluated our trace element measurements with the $\Delta^{33}\text{S}$ values obtained for the same samples using the same stratigraphic classification as outlined above. The $\Delta^{33}\text{S}$ versus trace metal plots appear to fall into one of three general types (Fig. A1.10).

First, some elements display irregular but extreme enrichments (e.g., Cu and Zn; Fig. A1.10) that mask any relationship to the corresponding $\Delta^{33}\text{S}$ values. This is a reflection of the mineralogy of these samples (Table A1.1). Other trace elements (e.g., Co and Ni) have a similar range of concentrations regardless of stratigraphic position (Fig. A1.10), and thus lack any correlation with $\Delta^{33}\text{S}$ values. For some elements, this independence is likely due to the difference between an external control (e.g., $\Delta^{33}\text{S}$ reflects sources) versus an internal control (e.g., temperature-dependent elemental partitioning). For other elements, the lack of a

relationship with $\Delta^{33}\text{S}$ values is most likely a result of slight variations in trace minerals in the sulfide separates (e.g., Mn - gangue minerals; Pb - galena; Table A1.1).

Finally, some trace elements exhibit a distinct correspondence between their compositional range and the magnitude of their paired $\Delta^{33}\text{S}$ values. The most evident of these is Se. Increased variability in concentrations of Se is linked to near-zero $\Delta^{33}\text{S}$ values, and uniformly low Se concentrations are associated with more negative $\Delta^{33}\text{S}$ values (Fig. 2.7A). A similar relationship exists between $\Delta^{33}\text{S}$ values and Au concentrations (Fig. 2.7B).

2.7 Discussion

2.7.1 Sulfur sources in Neoarchean VMS deposits

If $\delta^{34}\text{S}$ data from this study (Fig. 2.3) were to be considered in isolation, a straightforward interpretation might follow established VMS genetic models, reflecting a purely igneous-magmatic source for sulfur (Huston et al., 2010). However, multiple sulfur isotope analysis of the Noranda Camp ore sulfides clearly indicates the presence of atmospherically derived sulfur. Anomalous amounts of ^{33}S , derived from mass independent fractionation, occur within the district VMS deposits. The only mechanisms currently known that can generate significant mass-independent isotopic fractionation (MIF) of sulfur are all limited to surficial processes that occurred in the Archean (Johnston, 2011). Hence, the presence of sulfur with a MIF fingerprint strongly implies that sulfur from the Archean atmosphere and hydrosphere was a significant contributor to the formation of VMS mineralization in the district.

Negative $\Delta^{33}\text{S}$ values observed in many of the samples are most likely due to the incorporation of sulfur derived from the reduction of seawater sulfate during the formation of the sulfides. Oxidized products of laboratory SO_2 photolysis experiments have negative $\Delta^{33}\text{S}_{\text{V}-\text{CDT}}$

values (Farquhar and Wing, 2003). By extension, the oxidized products of SO_2 photolysis reactions in the Archean atmosphere are also expected to have had negative $\Delta^{33}\text{S}_{\text{V}-\text{CDT}}$ values. Such a negative $\Delta^{33}\text{S}$ signature would be preserved in oxidized species (i.e., SO_4^{2-}) within the Archean hydrosphere. This is supported by the observation that barite formed during the Paleoarchean has a ubiquitous negative $\Delta^{33}\text{S}$ signature (Bao et al., 2007; Farquhar et al., 2000; Golding et al., 2011; Mojzsis et al., 2003; Shen et al., 2009; Ueno et al., 2008).

Seawater sulfate plays a major role in the formation of modern VMS deposits (Franklin et al., 2005), and so it is not implausible that any sulfate present in the Archean hydrosphere would play a similar role in VMS deposits forming at that time. Indeed, this role has previously been invoked for both Paleoarchean deposits (Huston et al., 2010) and Neoarchean deposits (Jamieson et al., 2006). This contribution of seawater sulfate to the Noranda VMS deposits is in contrast to the study of Golding et al. (2011) who presented positive $\Delta^{33}\text{S}$ values for the Paleoarchean Panorama VMS deposits, which they attribute to a contribution of reduced seawater sulfur to the ore-forming system.

Sedimentary sulfide formed from the reduction of Neoarchean oceanic sulfate may also preserve a negative $\Delta^{33}\text{S}$ signature (see compilation in Farquhar et al., 2007). However, Archean sedimentary sulfide can exhibit either positive or negative $\delta^{34}\text{S}_{\text{V}-\text{CDT}}$ values, depending on whether sulfate supply was a limiting factor, or not, for microbial sulfate reduction (Farquhar and Wing, 2003). The lack of any significant $\delta^{34}\text{S}$ variation in the sulfide measured for this study would require such a perfect appeal to probability that it is unlikely that sedimentary sulfides are the source of the MIF signature identified by this study. This argument is strengthened considerably by the absence within the Noranda Camp of any significant sedimentary horizons which could have been a source of sedimentary sulfur (Gibson and Watkinson, 1990).

A reduced, sulfur-poor and iron-rich ocean has been proposed for the period during which the Noranda deposits formed (Huston and Logan, 2004; Huston et al., 2010). The lack of observed variability in $\delta^{34}\text{S}$ values of Neoarchean VMS deposits is often taken as support for this model. However, mass balance calculations involving volcanic degassing of SO_2 , followed by photochemical oxidation to sulfate, and reduction of sulfate in hydrothermal sinks, suggest that oceanic sulfate levels could have been maintained at non-negligible levels in the Neoarchean ($\sim 1\text{mM}$; Walker and Brimblecombe, 1985). The multiple sulfur isotope data presented in this study provide strong support to this model. For example, a conservative estimate of the proportion of seawater sulfur in the ore sulfide measured here is $\leq 25\%$, calculated by assuming that the most negative published Neoarchean $\Delta^{33}\text{S}$ value ($\approx -2.4\text{\textperthousand}$; Farquhar et al., 2010) characterizes the Neoarchean sulfate reservoir. The upper end of this range overlaps with that estimated for hydrothermal sulfide deposits on the modern seafloor (e.g., elemental balances on the TAG mound require 20 – 60% seawater S in the sulfide mound; Humphris and Cann, 2000). With the caveat that our study focuses on a single volcanic basin, it seems, then, that models suggesting Neoarchean VMS ore deposition occurred in the absence of an oceanic sulfur reservoir should be re-assessed.

2.7.2 Model for hydrothermal circulation, elemental transport, and VMS deposition in the Noranda cauldron

2.7.2.1 Multiple S isotope constraints: Systematic differences in the magnitude of $\Delta^{33}\text{S}$ values with stratigraphic position (Fig. 2.5) enable the development of a conceptual framework for VMS evolution in the Noranda camp. Samples taken from pre-cauldron deposits exhibit near-zero $\Delta^{33}\text{S}$ values, and therefore are considered to exhibit a dominantly a magmatic-igneous sulfur

isotope signature, which implies that the sulfur in these deposits originated either from the volcanic host rocks, or from the related intrusions. This could be a result of these deposits forming from the first fluids to circulate through the underlying volcanic host rocks, which would provide the ore-forming fluid the most ready access to fresh, reactive sulfur within these rocks, and would result in an igneous-dominated multiple sulfur isotope signature. Another possible interpretation is that there was a large contribution to the ore-forming fluid from devolatilization of the underlying magma chamber; magmatic sulfur-bearing volatiles are also characterized by near zero $\Delta^{33}\text{S}$ values (Mather et al., 2006). However, as both processes would produce the same range of $\Delta^{33}\text{S}$ values ($\approx 0\text{\textperthousand}$) it is not possible to distinguish these two magmatic sources in the Noranda Camp or elsewhere. Similarly, deposits that are interpreted as having formed on the margin of the Noranda cauldron also possess a dominantly magmatic-igneous sulfur isotope signature, with only a small detectable contribution (<5%) from a MIF sulfur source. Their sulfur isotope composition strongly suggests these deposits also primarily incorporated sulfur that was either stripped from volcanic wall rocks or degassed from a magma.

In contrast, the deposits formed within the main Noranda cauldron are characterized by sulfide carrying a MIF sulfur isotope signature. There appears to have been an evolution toward more seawater-dominated sulfur sources within the hydrothermal systems that formed the post-cauldron deposits, when compared to the main cauldron deposits. This pattern is shown by a general increase in $\delta^{34}\text{S}$ values and decrease in $\Delta^{33}\text{S}$ values (Fig. 2.4), with seawater sulfur making up 5–15 % of the sulfur in post-cauldron sulfide. Such a trend is compatible with recently proposed models for the evolution of the hydrothermal system operating within the Noranda cauldron (Stix et al., 2003).

Initial collapse of the Noranda caldera would have initiated the formation of a

hydrothermal system dominated by magmatic volatiles, likely enhanced by degassing during the near-instantaneous decompression of the underlying Flavrian and Powell intrusion magmas (Stix et al., 2003). Near-zero $\Delta^{33}\text{S}$ values should characterize sulfur in ore-forming fluids that were initially tapped during caldera collapse, as shown in the sulfur isotopic composition of the pre-cauldron and cauldron-margin VMS deposits (Fig. 2.8A). Entrainment of seawater into a magmatically-dominated hydrothermal system may account for the slightly more negative $\Delta^{33}\text{S}$ values of ore sulfides interpreted to have formed at the cauldron-margin. Further collapse would subsequently have resulted in the deepening of the water column feeding the hydrothermal system, and created pervasive fracturing in the cauldron rocks allowing enhanced fluid flow (Stix et al., 2003). These fractures would enable seawater to penetrate into the shallow portion of the hydrothermal system more directly, restricting the potential for fluid-rock equilibrium and high-temperature precipitation of sulfate minerals. As a result, the ore-forming fluids would contain a larger contribution of sulfur from reduced seawater sulfate than during the initial stages of caldera collapse. This is in agreement with the observation that VMS deposits within the Noranda cauldron itself are characterized by moderate to large negative $\Delta^{33}\text{S}$ values, which can only be attributed to the presence seawater-derived sulfur (Fig. 2.8B). After collapse, dome resurgence is likely, leading to small-scale development of near-surface hydrothermal systems (Stix et al., 2003). Seawater drawn into these systems would impart a strong seawater sulfate isotopic signature to precipitated ore sulfide (Fig. 2.8C), potentially through direct reduction at the site of mineralization (Shanks, 2001), or through mixing of sulfide sourced from a deeper-seated site of reduction (Herzig and Hannington, 1995).

The conceptual model presented above carries with it some predictive consequences. For example, the deposits here interpreted to form on the cauldron margin should be among the

oldest in the Noranda Camp. In addition, both the pre-cauldron and cauldron-margin deposits should have formed at higher temperatures than those of the cauldron and post-cauldron stages. The cauldron margin deposits were likely underlain by a discrete hydrothermal upflow zone dominated by igneous influences. Lower formation temperatures should characterize the cauldron and post-cauldron deposits, along with upflow and stockwork zones showing more distinct seawater geochemical signatures.

2.7.2.2 Temperature constraints: The above model is supported by trace element and sulfur isotope temperature proxy data. In particular, there are two major observations that we investigate here: (1) greater Se concentrations and variability within sulfides of the pre-cauldron and cauldron margin deposits (Figs. 2.6A, 2.6B, 2.7A); and (2) the distinctive low Fe/(Fe + Zn) ratio measured within sphalerite from post-cauldron deposits (Fig. 2.6C).

Studies of the modern seafloor indicate that Se concentrations in hydrothermal sulfide deposits are highest in those formed at the highest temperatures, and are especially elevated within chalcopyrite and euhedral pyrite (Auclair et al., 1987). Conversely, Se concentrations are at their lowest where mixing between hydrothermal water and seawater is at a maximum (Auclair et al., 1987). Hence, the observed Se enrichment within pre-cauldron sulfide therefore supports our interpretation that the pre-cauldron deposits of the Noranda Camp formed at higher temperatures than the rest of the camp, and with a smaller contribution of seawater.

Greater variability in the Se concentrations of pre-cauldron ore sulfides either reflects varying contributions from two distinct Se sources, both of which are likely to have an igneous affinity, by the sulfur isotope constraints presented above, or variable preservation of early sulfides precipitated at lower temperatures. Both putative igneous sources (leachable volcanic

rocks and magmatic fluids; Huston et al., 1995) have similar Se/S ratios. Hence, even if a variable mixing of both seawater and (magmatic-) hydrothermal fluids occurred during sulfide genesis, no difference should be observed in the Se/S ratios of precipitated sulfides. The presence of significant variation in this ratio, instead, implies that the pre-cauldron deposits retain a record of early low-temperature sulfide precipitation that has been only partially overprinted by subsequent, higher temperature sulfide formation.

Temperatures of equilibration for sulfide mineral pairs can be calculated from differences in paired $\delta^{34}\text{S}$ values (Ohmoto and Rye, 1979). While this approach is straightforward in principle, it is typically difficult in practice due to the complex nature of ore sulfide precipitation (Seal, 2006). As a result, a common approach is to filter calculated temperatures of equilibration on the basis of ‘realistic’ or expected temperatures for the ore-forming environment (here taken as an approximate hydrothermal range of 200 to 400°C; Petersen et al., 1998). In addition, sulfide mineral pairs at thermodynamic equilibrium should have the same $\Delta^{33}\text{S}$ value, within analytical uncertainty ($2\sigma = \pm 0.02\%$ for this study) (Jamieson et al., 2006). Of the 35 paired mineral separates from throughout the Noranda Camp that were analyzed in this study, only eight (63RF31 from Horne No. 5, A95-07B from Amulet A Upper, A95-11A from Vauze, QT4-2 and QT15-4 from Quemont, DELD-F339-999 from Deldona, 98DELB2 from Delbridge, and JH98GLLN-2MS2 from Gallen) met both selection criteria (Table A1.4). The majority of sulfide mineral separates were apparently not formed under equilibrium conditions. This is consistent with the interpretation for the pre-cauldron deposits presented above, and with multiple phases of ore-formation and refinement previously identified for many of these deposits (Gibson and Galley, 2007). The pairs that are consistent with equilibrium occur throughout the stratigraphy (pre-cauldron to post-cauldron), yet all preserve similar temperatures of

equilibration (mean = $287 \pm [32]^\circ\text{C}$; Table A1.4) with no systematic variation between deposit types.

Differences in temperatures of formation are also evident in the relative concentrations of Fe and Zn within sphalerite from deposits within different stratigraphic intervals (Fig. 2.6C). The Fe/(Fe + Zn) ratio remains relatively constant between the majority of deposits (~0.1; Fig. 2.6C), with the exception of the post-cauldron deposits and Horne No. 5 (Fig. A1.3). Here the ratio is closer to 0.03, consistent with a lower temperature of formation (Di Benedetto et al., 2005) and, in the context of the Noranda Camp, would reflect a seawater-dominated rather than a magmatic-hydrothermal system. With the exception of the Horne No. 5 deposit, this observation is consistent with the model described above.

The Horne No. 5 deposit is thought to represent a lower-temperature exhalative part of the Horne VMS system, which formed closer to the sea floor than the Horne No. 8 deposit (Gibson and Galley, 2007; Sinclair, 1971). Hence, the lower (Fe/Fe + Zn) ratio measured within sphalerite from the Horne No. 5 deposit and the exhalative nature of that deposit, when coupled with multiple sulfur isotope data for Horne No. 5 and No. 8, suggests that these two deposits formed at different temperatures, but from the same sulfur source.

2.7.3 Au-rich deposits in the Noranda camp

2.7.3.1 Classification of deposits of uncertain affinity: The gold-rich Horne and Quemont deposits of the Noranda Camp have recently been shown to have similar ages of formation to the pre-cauldron deposits (~2702 Ga, V. McNicoll, pers. comm.). However, both are situated in separate faulted (Fig. 2.2), which makes it difficult to definitively place them within the Noranda Camp stratigraphy. The Horne deposits also have near identical isotopic and trace elemental

characteristics to the pre-cauldron deposits of the main Noranda Camp. We therefore propose that this system can be reliably placed in the pre-cauldron grouping of Gibson and Watkinson (1990), as also suggested by Taylor et al. (2011). In contrast, the Quemont samples exhibit multiple sulfur isotope characteristics that are more akin to those of the Noranda cauldron deposits. Combined with observations that the deposit structure and geochemical characteristics of Quemont are noticeably different from those of the Horne deposits, and are consistent with those of the Noranda cauldron stage (Sinclair, 1973), we propose that the Quemont deposit should be considered a part of the main Noranda cauldron sequence. Alternatively the Quemont deposit may have formed during a cauldron sequence equivalent stage of a caldera that pre-dates the main Noranda caldera (Taylor et al., 2011).

2.7.3.2 Multiple sulfur isotopes and Au-grade predictivity: The correspondence between sulfide Se concentrations, Au concentrations, and $\Delta^{33}\text{S}$ values (Figs. 2.7A, 2.7B) suggests that the grade of gold-rich deposits should correlate with magnitude of their bulk $\Delta^{33}\text{S}$ value. This relationship does, indeed, hold for those gold-rich deposits of the Noranda Camp for which bulk gold assay data have been published (Horne, Quemont, Mobrun, Deldona and Delbridge; Fig. 2.9; Gibson and Galley, 2007). Deposits with higher average gold grades have near-zero $\delta^{34}\text{S}$ and $\Delta^{33}\text{S}$ values (approximately -1.0 to +1.5 ‰ and -0.20 to 0 ‰ respectively), and as gold grade decreases, $\delta^{34}\text{S}$ values increase and $\Delta^{33}\text{S}$ values become more negative. This trend indicates a magmatic-igneous source of gold within the Noranda VMS deposits, possibly from a direct magmatic contribution to the hydrothermal ore-forming fluid, or from a later over-printing event that contributed gold from a magmatic source. The correlations discovered here argue against the second possibility, unless Se, $\Delta^{33}\text{S}$, and Au exhibited equivalent geochemical behavior during the over-printing event.

2.8 Conclusions

Our multiple sulfur isotope and trace element study of the Noranda camp VMS deposits has revealed the following features which may be more generally applicable to Neoarchean VMS deposits in other terranes.

- MIF sulfur isotope compositions in many of the deposits within the Noranda VMS district are a clear indication that seawater sulfur contributed to the formation of those deposits.
- Current models for the formation of Neoarchean VMS deposits postulate that the near-absence of sulfate minerals within these deposits indicates a lack of involvement of seawater sulfur; our estimates of up to 25% seawater sulfur in Noranda VMS deposits suggest these models need revisiting.
- Multiple sulfur isotope and trace element geochemistry data support the following heuristic description of the Noranda camp VMS system. The system was initially dominated by focused hydrothermal upwelling driven by the underlying magma chamber, which stripped sulfur and trace metals from the volcanic host rocks in addition to extracting them from the magmatic system. As the caldera collapsed, fault structures developed which allowed for a more direct incorporation of seawater into the hydrothermal system. As the system evolved, the volcanic pile was stripped of sulfur. Cooling of the system would also have reduced the efficiency of precipitation of sulfate minerals in the reaction zone. This may have allowed a small, but measurable, contribution of seawater sulfate to the formation of ore sulfides. Sealing of the fault structures led to subsidence of the hydrothermal system; hydrothermal fluids then had less access to the volcanic host rocks and their underlying magmatic relatives and resorted to local near-surface mass transfer to precipitate ore sulfides.

- The Au-rich Horne deposits show a strong affinity with other pre-cauldron deposits in the Noranda camp. In contrast, the Quemont deposit should be classified along with other deposits that formed during the main cauldron-forming event.
- Economically relevant Au concentrations can be directly linked to $\Delta^{33}\text{S}$ values of Neoarchean VMS deposits; this discovery has implications in our understanding of how Au-rich VMS deposits form, as well as the potential to direct exploration for such deposits.

2.9 Acknowledgements

ERS was supported by the Geological Survey of Canada's Targeted Geoscience-3 Abitibi Project (B. Dubé – Project Leader), a Society of Economic Geologists Graduate Student Fellowship, a GEOTOP bourses d'études des cycles supérieurs, and an NSERC Discovery Grant to BAW. The McGill Stable Isotope Laboratory is supported by the Canada Research Chairs program, by NSERC through the Research Tools and Infrastructure and Discovery Grant programs, and by GEOTOP. We appreciate the laboratory assistance of André Pellerin, Lang Shi and Mary McDonough. Many thanks also to Ian Jonasson for provision of samples, without which this study would not have been possible, and for numerous productive discussions.

2.10 References

- Auclair, G., Fouquet, Y., and Bohn, M., 1987, Distribution of selenium in high-temperature hydrothermal sulfide deposits at 13 degrees North, East Pacific Rise: Canadian Mineralogy, v. 25, p. 577.
- Barker, A.K., Coogan, L.A., and Gillis, K.M., 2010, Insights into the behaviour of sulphur in mid-ocean ridge axial hydrothermal systems from the composition of the sheeted dyke complex at Pito Deep: Chemical Geology, v. 275, p. 105-115.

- Bao, H., Rumble, D., and Lowe, D. R., 2007, The five stable isotope compositions of Fig Tree barites: Implications on sulfur cycle in ca. 3.2 Ga oceans: *Geochimica et Cosmochimica Acta*, v. 71, p. 4868-4879.
- Beaudoin, G., and Taylor, B. E., 1994, High-precision and spatial-resolution sulfur isotope analysis using MILES laser microprobe: *Geochimica et Cosmochimica Acta*, v. 58, p. 5055-5063.
- Corfu, F., 1993, The evolution of the southern Abitibi greenstone belt in light of precise U-Pb geochronology: *Economic Geology*, v. 88, p. 1323-1340.
- Di Benedetto, F., Bernardini, G. P., Costagliola, P., Plant, D., and Vaughan, D. J., 2005, Compositional zoning in sphalerite crystals: *American Mineralogist*, v. 90, p. 1384-1392.
- Dimroth, E., Imreh, L., Goulet, N., and Rocheleau, M., 1983, Evolution of the south-central segment of the Archean Abitibi Belt, Quebec. Part II: Tectonic evolution and geomechanical model: *Canadian Journal of Earth Sciences*, v. 20, p. 1355 - 1373.
- Dubé, B., Gosselin, P., Mercier-Langevin, P., Hannington, M., and Galley, A., 2007, Gold-Rich Volcanogenic Massive Sulphide Deposits, *in* Goodfellow, W. D., ed., *Mineral Deposits of Canada: A Synthesis of Major Deposit-types, District Metallogeny, the Evolution of Geological Provinces, and Exploration Methods*, Special Publication No. 5, Mineral Deposits Division, Geological Association of Canada, p. 75-94.
- Farquhar, J., Bao, H. M., and Thiemens, M., 2000, Atmospheric influence of Earth's earliest sulfur cycle: *Science*, v. 289, p. 756-758.
- Farquhar, J., Peters, M., Johnston, D. T., Strauss, H., Masterson, A., Wiechert, U., and Kaufman, A. J., 2007, Isotopic evidence for Mesoarchaean anoxia and changing atmospheric sulphur chemistry: *Nature*, v. 449, p. 706-U5.
- Farquhar, J., and Wing, B. A., 2003, Multiple sulfur isotopes and the evolution of the atmosphere: *Earth and Planetary Science Letters*, v. 213, p. 1 - 13.
- Farquhar, J., Wu, N., Canfield, D. E., and Odum, H., 2010, Connections between Sulfur Cycle Evolution, Sulfur Isotopes, Sediments, and Base Metal Sulfide Deposits: *Economic Geology*, v. 105, p. 509-533.
- Franklin, J. M., Gibson, H. L., Jonasson, I. R., and Galley, A. G., 2005, Volcanogenic Massive Sulfide Deposits, *in* Hedenquist, J. W., Thompson, J. F. H., Goldfarb, R. J., and Richards, J. P., eds., *Economic Geology 100th Anniversary Volume*: Littleton, CO, Society of Economic Geologists, Inc., p. 523 - 560.
- Galley, A., 2003, Composite synvolcanic intrusions associated with Precambrian VMS-related hydrothermal systems: *Mineralium Deposita*, v. 38, p. 443-473.
- Gibson, H., and Galley, A., 2007, Volcanogenic massive sulfide deposits of the Archean, Noranda district, Quebec, *in* Goodfellow, W. D., ed., *Mineral Deposits of Canada: A Synthesis of Major Deposit-types, District Metallogeny, the Evolution of Geological Provinces, and Exploration Methods*, Special Publication No. 5, Mineral Deposits Division, Geological Association of Canada, p. 533-552.
- Gibson, H. L., and Watkinson, D. H., 1990, Volcanogenic massive sulphide deposits of the Noranda Cauldron and Shield Volcano, Quebec, *in* Rive, M., Verpaelst, P., Gagnon, Y., Lulin, J. M., Riverin, G., and Simard, A., eds., *The Northwestern Quebec Polymetallic Belt: A summary of 60 years of mining exploration*, Special Volume 43, Canadian Institute of Mining and Metallurgy, p. 119 - 132.
- Goldie, R., 1978, Magma mixing in the Flavrian pluton, Noranda area, Quebec: *Canadian Journal of Earth Sciences*, v. 15, p. 132-144.

- Golding, S.D., Duck, L.J., Young, E., Baublys, K.A., Glikson, M., and Kamber, B.S., Earliest seafloor hydrothermal systems on Earth: Comparisons with modern analogues, *in* Golding, S.D., and Glikson, M., eds., Earliest Life on Earth: Habitats, Environments and Methods of Detection, Springer Netherlands, p. 15-49.
- Herzig, P. M., and Hannington, M. D., 1995, Polymetallic massive sulfides at the modern seafloor a review: *Ore Geology Reviews*, v. 10, p. 95-115.
- Herzig, P.M., Hannington, M.D., and Arribas Jr, A., 1998, Sulfur isotopic composition of hydrothermal precipitates from the Lau back-arc: implications for magmatic contributions to seafloor hydrothermal systems: *Mineralium Deposita*, v. 33, p. 226-237.
- Hu, G., Rumble, D., and Wang, P., 2003, An ultraviolet laser microprobe for the in situ analysis of multisulfur isotopes and its use in measuring Archean sulfur isotope mass-independent anomalies: *Geochimica et Cosmochimica Acta*, v. 67, p. 3101-3118.
- Hulston, J. R., and Thode, H. G., 1965, Variations in the S33, S34, and S36 Contents of Meteorites and Their Relation to Chemical and Nuclear Effects: *Journal of Geophysical Research*, v. 70, p. 3475-3484.
- Humphris, S. E., and Cann, J. R., 2000, Constraints on the energy and chemical balances of the modern TAG and ancient Cyprus seafloor sulfide deposits: *Journal of Geophysical Research*, v. 105, p. 28477-28488.
- Huston, D. L., and Large, R. R., 1987, Genetic and exploration significance of the zinc ratio (100 Zn/(Zn + Pb)) in massive sulfide systems: *Economic Geology*, v. 82, p. 1521-1539.
- Huston, D. L., and Logan, G. A., 2004, Barite, BIFs and bugs: evidence for the evolution of the Earth's early hydrosphere: *Earth and Planetary Science Letters*, v. 220, p. 41-55.
- Huston, D. L., Pehrsson, S., Eglington, B. M., and Zaw, K., 2010, The geology and metallogeny of volcanic-hosted massive sulfide deposits: Variations through geologic time and with tectonic setting: *Economic Geology*, v. 105, p. 571.
- Huston, D. L., Sie, S. H., Suter, G. F., Cooke, D. R., and Both, R. A., 1995, Trace elements in sulfide minerals from eastern Australian volcanic-hosted massive sulfide deposits; Part I, Proton microprobe analyses of pyrite, chalcopyrite, and sphalerite, and Part II, Selenium levels in pyrite; comparison with delta 34 S values and implications for the source of sulfur in volcanogenic hydrothermal systems: *Economic Geology*, v. 90, p. 1167-1196.
- Jamieson, J. W., Wing, B. A., Hannington, M. D., and Farquhar, J., 2006, Evaluating isotopic equilibrium among sulfide mineral pairs in Archean ore deposits: Case study from the Kidd Creek VMS deposit, Ontario, Canada: *Economic Geology*, v. 101, p. 1055-1061.
- Jensen, L. S., 1975, Geology of Clifford and Ben Nevis Townships, District of Cochrane, Ontario Geological Survey Geoscience Report GR132 (accompanied by Map 2283).
- Johnston, D.T., 2011, Multiple sulfur isotopes and the evolution of Earth's surface sulfur cycle: *Earth-Science Reviews*, v. 106, p. 161-183.
- Kerr, D. J., and Gibson, H. L., 1993, A comparison of the Horne volcanogenic massive sulfide deposit and intracauldron deposits of the Mine Sequence, Noranda, Quebec: *Economic Geology*, v. 88, p. 1419-1442.
- Large, R. R., 1992, Australian volcanic-hosted massive sulfide deposits; features, styles, and genetic models: *Economic Geology*, v. 87, p. 471-510.
- Massoth, G. J., Milburn, H. B., Hammond, S. R., Butterfield, D. A., McDuff, R. E., and Lupton, J. E., 1988, The geochemistry of submarine venting fluids at Axial Volcano, Juan de Fuca Ridge; new sampling methods and a vents program rational, *in* Deluca, M. P., and

- Babb, I., eds., Global venting, midwater, and benthic ecological processes(88-4): Rockville, MD, National Undersea Research Program Report., p. 29-59.
- Mather, T. A., McCabe, J. R., Rai, V. K., Thiemens, M. H., Pyle, D. M., Heaton, T. H. E., Sloane, H. J., and Fern, G. R., 2006, Oxygen and sulfur isotopic composition of volcanic sulfate aerosol at the point of emission: *Journal of Geophysical Research*, v. 111, p. D18205.
- Mojzsis, S., Coath, C., Greenwood, J., McKeegan, K., and Harrison, T., 2003, Mass-independent isotope effects in Archean (2.5 to 3.8 Ga) sedimentary sulfides determined by ion microprobe analysis: *Geochimica et Cosmochimica Acta*, v. 67, p. 1635-1658.
- Ohmoto, H., and Rye, R. O., 1979, Isotopes of sulfur and carbon, in Barnes, H. L., ed., *Geochemistry of Hydrothermal Ore Deposits*, Second Edition: New York, John Wiley and Sons, p. 509-567.
- Peloquin, A. S., 1999, Reappraisal of the Blake River Group stratigraphy and its place in the Archean volcanic record Unpub. thèse de doctorat thesis, Université de Montréal, 189 p.
- Peloquin, A. S., 2005, Discover Abitibi project, base metal subproject 3: Geology and base metal mineralization in Ben Nevis, Katrine and Clifford Townships: Sudbury, ON, Ontario Geological Survey Open File Report 6161, p. 86.
- Peloquin, A. S., Potvin, R., Paradis, S., Lafleche, M. R., Verplaelst, P., and Gibson, H. L., 1990, The Blake River Group, Rouyn-Noranda area, Quebec: A stratigraphic synthesis, in Rive, M., P., V., Gagnon, Y., Lulin, L. M., Riverin, G., and Simard, A., eds., *The Northwestern Quebec Polymetallic Belt: A Summary of 60 Years of Mining Exploration*. Special Volume 43, Canadian Institute of Mining and Metallurgy, p. 107 - 118.
- Petersen, S., Herzig, P. M., and Hannington, M. D., 1998, Fluid inclusion studies as a guide to the temperature regime within the TAG hydrothermal mound, 26°N, Mid-Atlantic Ridge, in Herzig, P. M., Humphris, S. E., and Miller, D. J., eds., *Proceedings of the Ocean Drilling Program, Scientific Results*, 158: College Station, TX, U.S.A., Ocean Drilling Program, p. 163-178.
- Piercey, S. J., Chaloux, E. C., Peloquin, A. S., Hamilton, M. A., and Creaser, R. A., 2008, Synvolcanic and Younger Plutonic Rocks from the Blake River Group: Implications for Regional Metallogenesis: *Economic Geology*, v. 103, p. 1243-1268.
- Richard, M. G., 1999, Evolution of the Flavrian Pluton and its association with VHMS deposits and granitoid-hosted gold deposits of the Noranda Cauldron: Rouyn-Noranda, Quebec, Canada: Unpub. Ph.D. thesis, Université de Montreal, 318 p.
- Robinson, B. W., 1995, Sulphur isotope standards, in *Proceedings of a consultants' meeting held in Vienna, 1-3. Dec. 1993*. IAEA-TECDOC-825, p. 39-45.
- Santaguida, F., Gibson, H. L., Watkinson, D. H., and Hannington, M. D., 1998, Semi-conformable epidote-quartz hydrothermal alteration in the Central Noranda Volcanic Complex: Relationship to volcanic activity and VMS mineralization, CAMIRO Project 94E07, Annual Report, *The Use of Regional-Scale Alteration and Subvolcanic Intrusions in the Exploration for Volcanic-Associated Massive Sulphide Deposits*, p. 139-180.
- Seal, R. R., II, 2006, Sulfur Isotope Geochemistry of Sulfide Minerals: *Reviews in Mineralogy and Geochemistry*, v. 61, p. 633-677.
- Shanks, W. C., III, 2001, Stable Isotopes in Seafloor Hydrothermal Systems: Vent fluids, hydrothermal deposits, hydrothermal alteration, and microbial processes: *Reviews in Mineralogy and Geochemistry*, v. 43, p. 469-525.

- Shen, Y., Farquhar, J., Masterson, A., Kaufman, A. J., and Buick, R., 2009, Evaluating the role of microbial sulfate reduction in the early Archean using quadruple isotope systematics: *Earth and Planetary Science Letters*, v. 279, p. 383-391.
- Sinclair, W. D., 1971, A volcanic origin for the No.5 zone of the Horne mine, Noranda, Quebec: *Economic Geology*, v. 66, p. 1225-1231.
- Sinclair, W. D., 1973, A volcanic origin for the No. 5 Zone of the Horne Mine, Noranda, Quebec; reply: *Economic Geology*, v. 68, p. 713-714.
- Stix, J., Kennedy, B., Hannington, M., Gibson, H., Fiske, R., Mueller, W., and Franklin, J., 2003, Caldera-forming processes and the origin of submarine volcanogenic massive sulfide deposits: *Geology*, v. 31, p. 375-378.
- Taylor, B.E., 2004a, Biogenic and thermogenic sulfate reduction in the Sullivan Pb-Zn-Ag deposit, British Columbia (Canada): Evidence from micro-isotopic analysis of carbonate and sulfide in bedded ores: *Chemical Geology*, v. 204, p. 215 – 236.
- Taylor, B.E., 2004b, Fluorination Methods in Stable Isotope Analysis, *in* de Groot, P.A., *Handbook of Stable Isotope Analytical Techniques*, v. 1, Elsevier, p. 400 – 472.
- Taylor, B. E., de Kemp, E. Grunsky, E., Martin, L., Goutier, Lauzière, K., Dubé, B., and Rigg, D., 2011, 3-D Visualization of Multi-Phase Hydrothermal Flow, Silicification, and Hydration: Architecture of the Horne Hydrothermal System, Rouyn-Noranda. Ottawa 2011, GAC-MAC-SEG, Joint Annual Meeting, Geological Association of Canada, Abstracts, v. 34, p. 214-215.
- Ueno, Y., Ono, S., Rumble, D., and Maruyama, S., 2008, Quadruple sulfur isotope analysis of ca. 3.5Ga Dresser Formation: New evidence for microbial sulfate reduction in the early Archean: *Geochimica et Cosmochimica Acta*, v. 72, p. 5675-5691.
- Walker, J. C. G., and Brimblecombe, P., 1985, Iron and sulfur in the pre-biologic ocean: *Precambrian Research*, v. 28, p. 205-222.

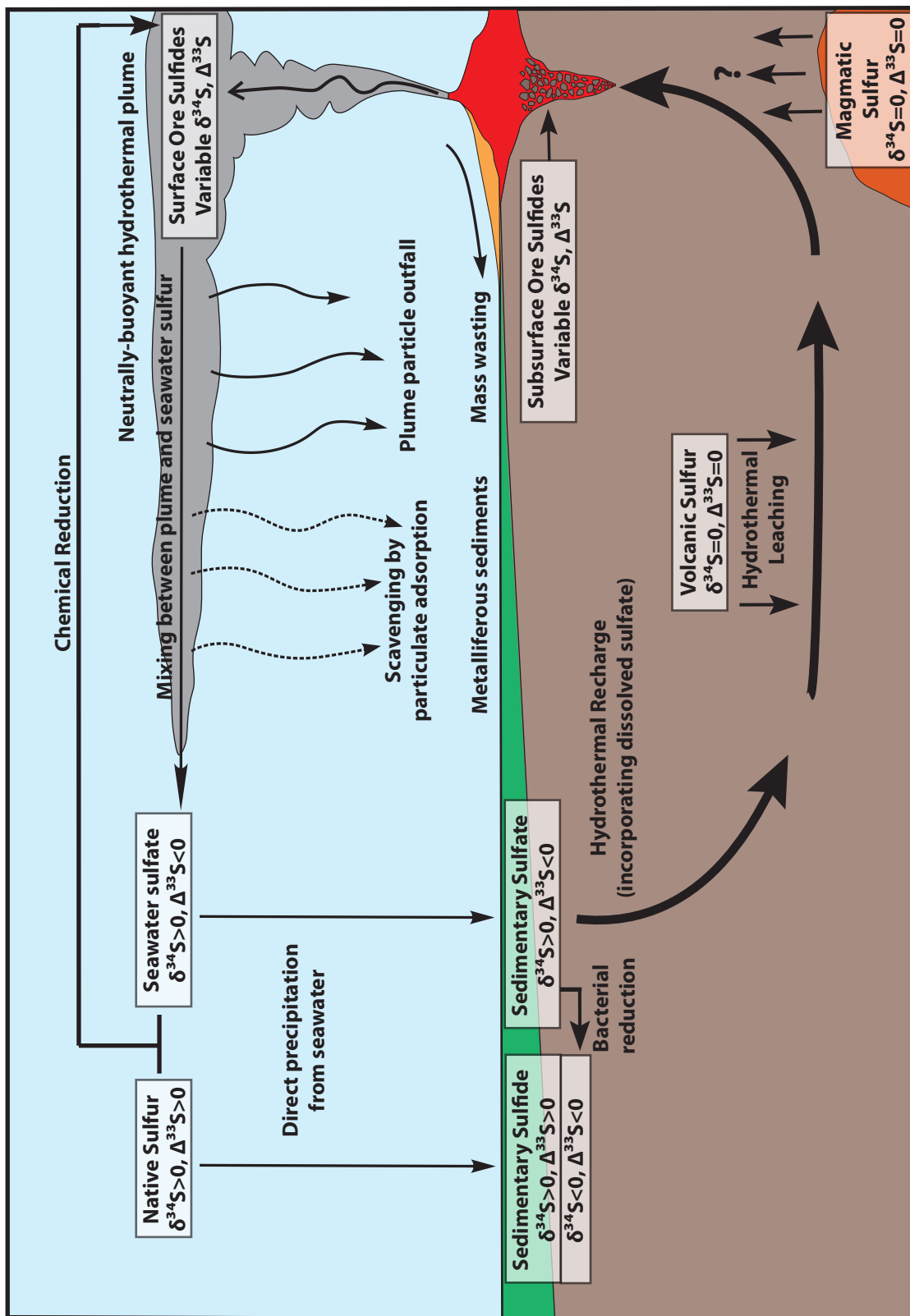


Fig. 2.1: Schematic diagram of an Archean volcanogenic massive sulfide deposit and associated hydrothermal system with predicted multiple sulfur isotope signatures (modified from Farquhar and Wing, 2003; Massoth et al., 1988).

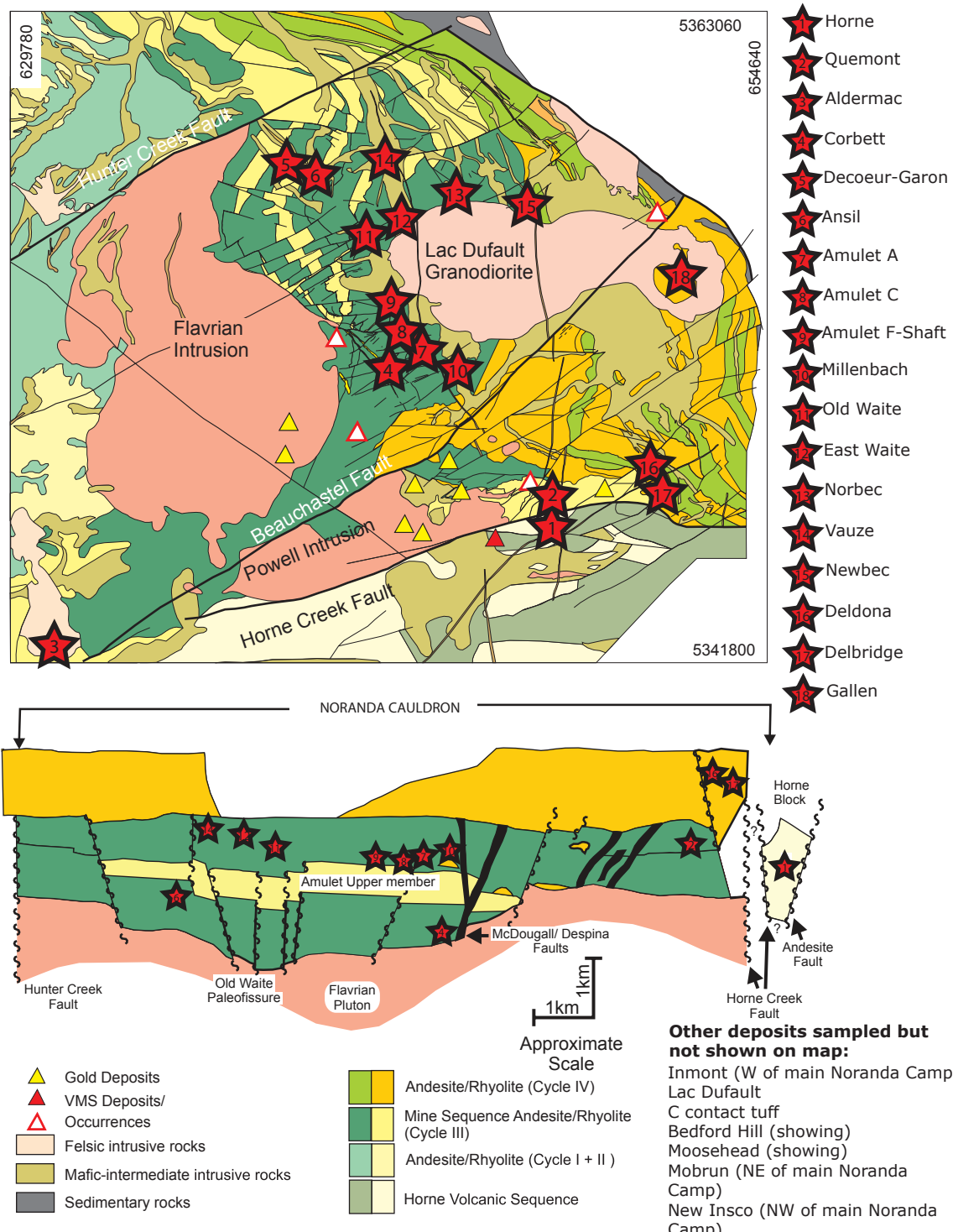


Fig. 2.2: Geological map of the main Noranda Camp and associated cross-section, with red stars indicating locations that have been sampled for this study (modified from Gibson and Galley, 2007; Santaguida et al., 1998).

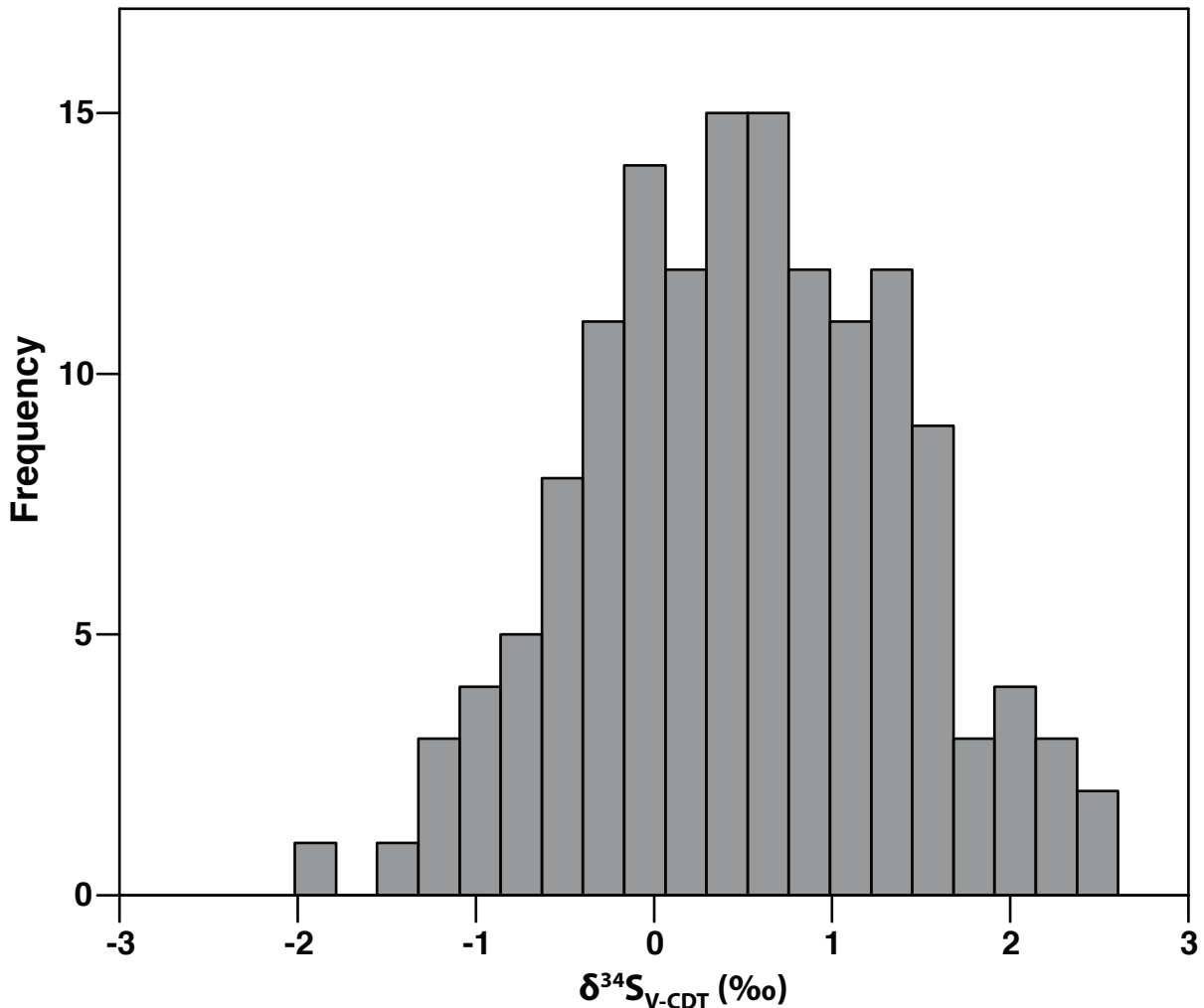


Fig. 2.3: Histogram illustrating the distribution of $\delta^{34}\text{S}$ values for the Noranda Camp sulfides ($n=146$). Both the most common value (~0.5‰) and the overall spread of values (-2 to 2.5‰) are typical for Archean VMS deposits (Huston et al., 2010) and would conventionally be taken to indicate minor fractionation from a dominantly igneous sulfur source.

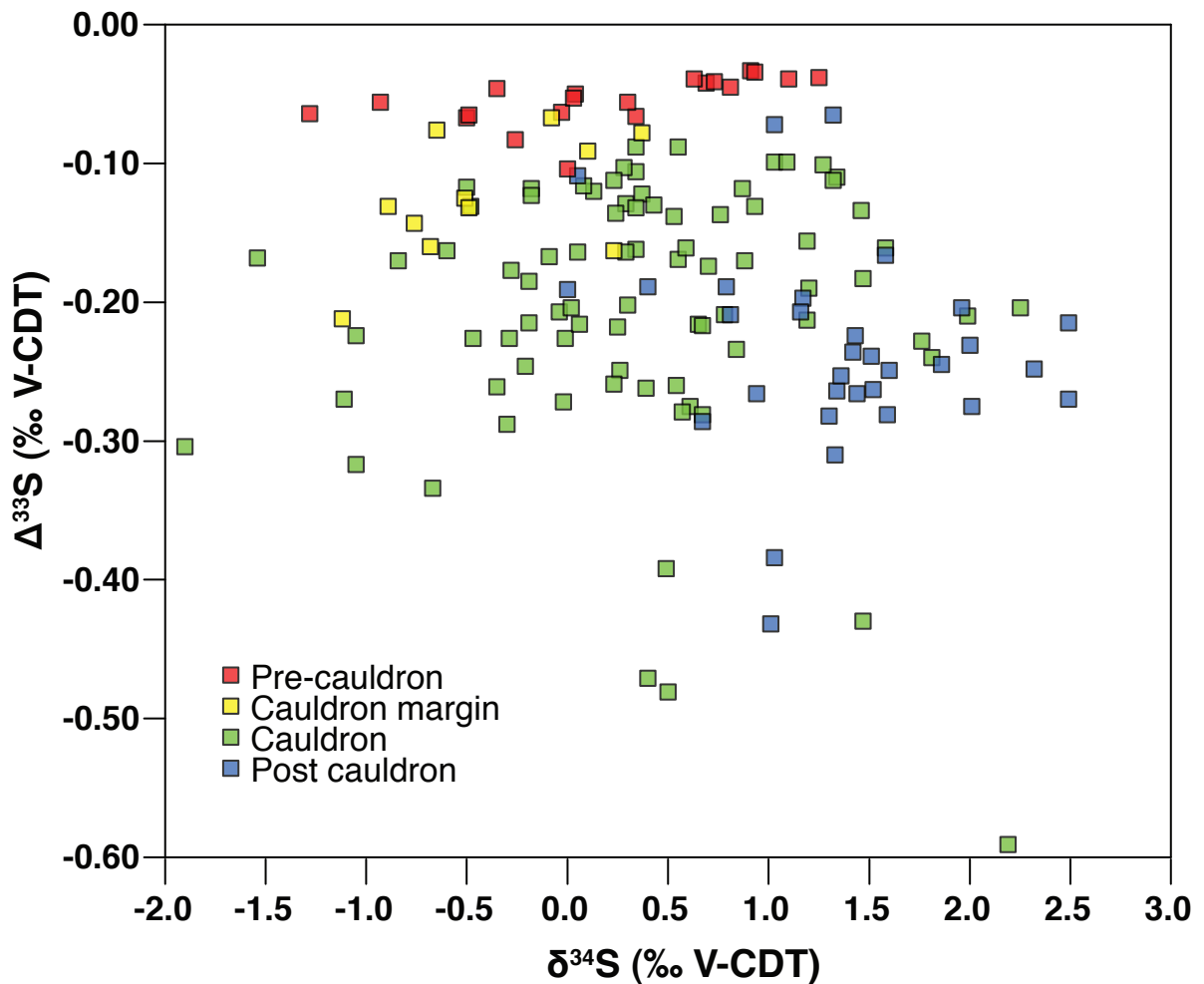


Fig. 2.4: Binary diagram showing $\delta^{34}\text{S}$ values vs. $\Delta^{33}\text{S}$ values for sulfides from the Noranda Camp, divided by stratigraphic location ($\delta^{34}\text{S}$: $1\sigma = \pm 0.13\text{\textperthousand}$, $\Delta^{33}\text{S}$: $1\sigma = \pm 0.01\text{\textperthousand}$). There is a distinct pattern of increasing $\delta^{34}\text{S}$ values and decreasing $\Delta^{33}\text{S}$ values up section.

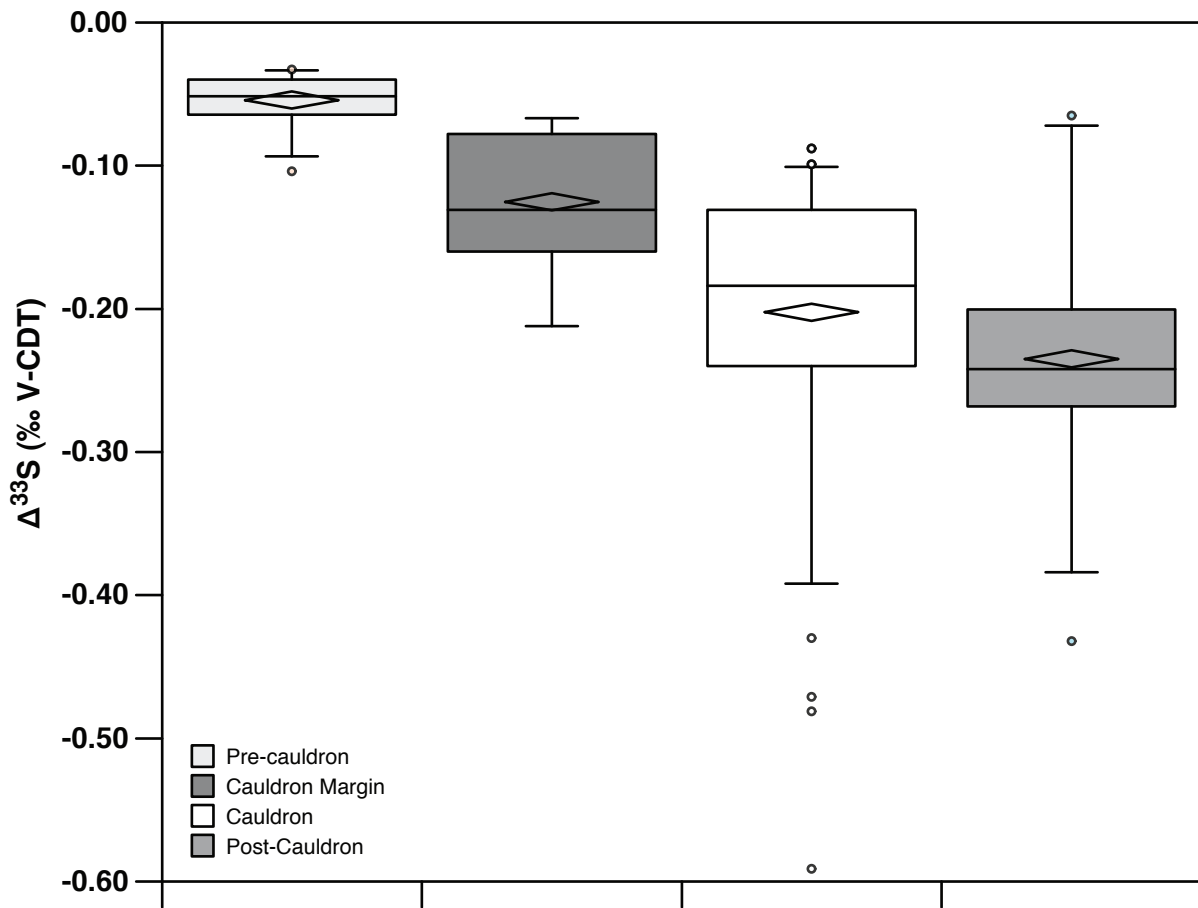


Fig. 2.5: Box and Whisker diagrams for $\Delta^{33}\text{S}$ values for sulfides from the Noranda Camp separated by deposit and stratigraphic position showing the population mean (diamond), mode (horizontal line), first and third quartile (lower and upper ends of the box), 5th and 95th percentile (lower and upper ends of the whisker) and outliers (circles). The most common $\Delta^{33}\text{S}$ values decrease up section, whereas the population variability of the $\Delta^{33}\text{S}$ values increases.

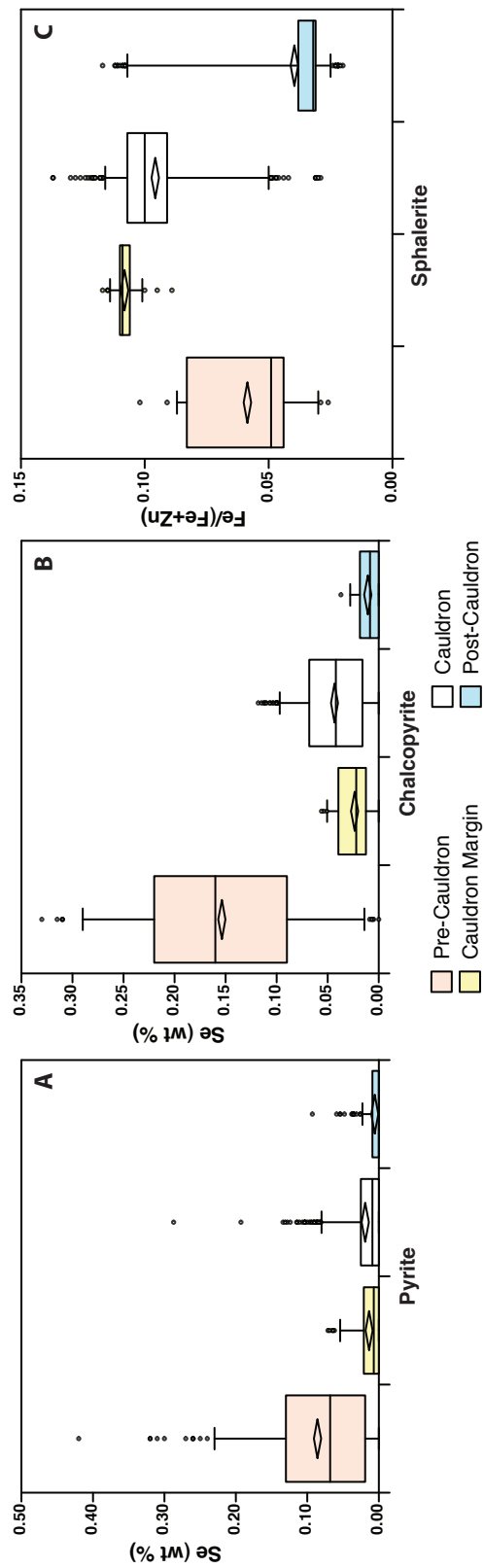


Fig. 2.6: Box and Whisker diagrams of trace element concentrations for different minerals from EMPA data separated by stratigraphic position, showing the population mean (diamond), mode (horizontal line), first and third quartile (lower and upper ends of the box), 5th and 95th percentile (lower and upper ends of the whisker) and outliers. Distinctions among the different stratigraphic types are clear, and largely related to temperature of formation (see text for details). A) Se concentrations in pyrite. B) Se concentrations in chalcopyrite. C) Fe to Fe + Zn ratios in sphalerite.

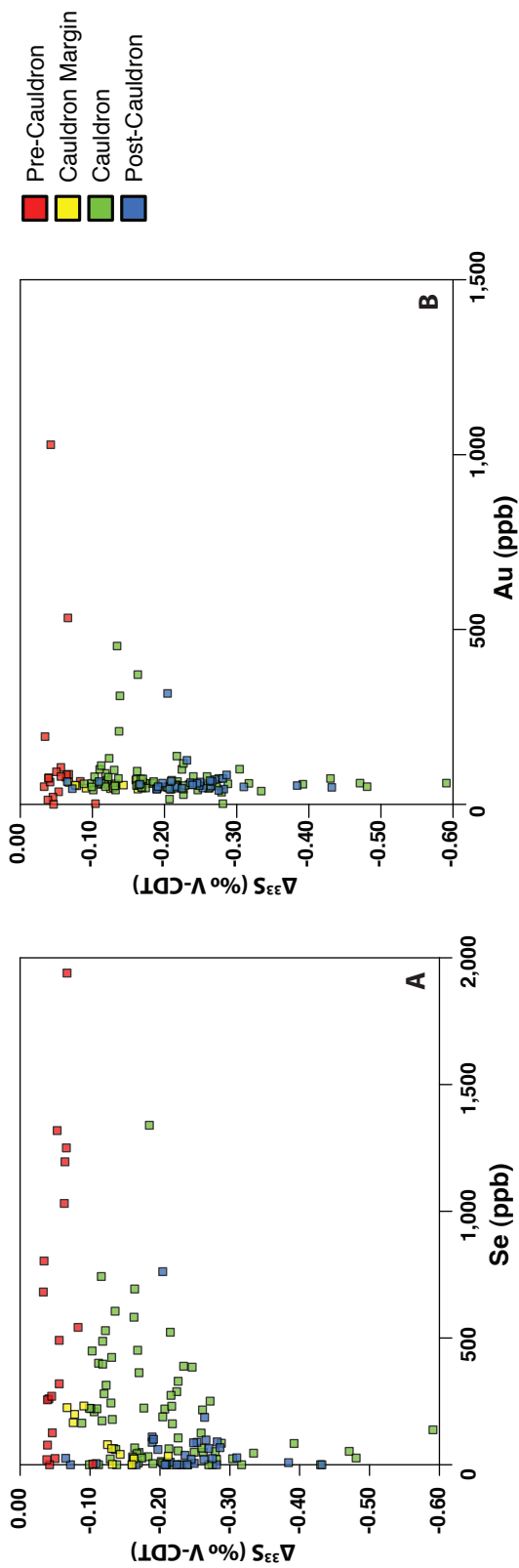


Fig. 2.7: Binary diagram showing bulk trace element concentrations from ICP-MS data vs. $\Delta^{33}\text{S}$ values in sulfide separates for Noranda Camp samples, all separated by stratigraphic position. A broad inverse correlation seems to exist between the range of trace element variability and the magnitude of their paired $\Delta^{33}\text{S}$ values. A) Se concentrations. B) Au concentrations.

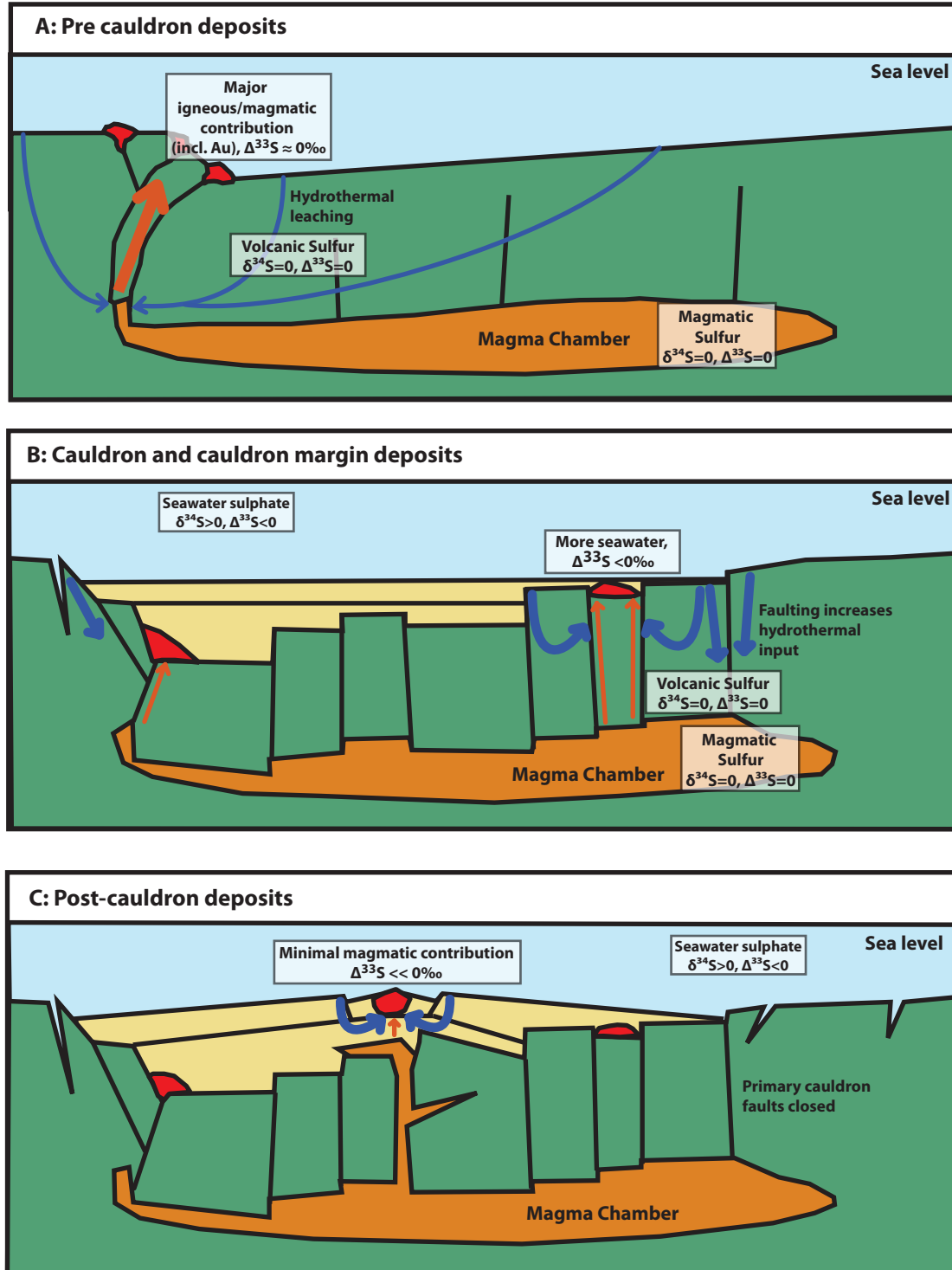


Fig. 2.8: Schematic diagram of the evolution of relative sulfur sources for VMS deposits as associated with the evolution of the Noranda cauldron (modified from Stix et al., 2003). A) Initial stages of collapse accesses magmatic-hydrothermal system, resulting in near-zero $\Delta^{33}\text{S}$ values in ore sulfides in pre-cauldron and cauldron-margin deposits. B) Throughgoing faulting above the magma chamber allows ingress of overlying seawater, introducing sulfur with negative $\Delta^{33}\text{S}$ values into the ore forming system of the cauldron deposits. C) Late-stage resurgence of caldera roof drives shallow, near-surface hydrothermal systems that incorporate largest signature of seawater sulfur in the resulting post-cauldron VMS deposits.

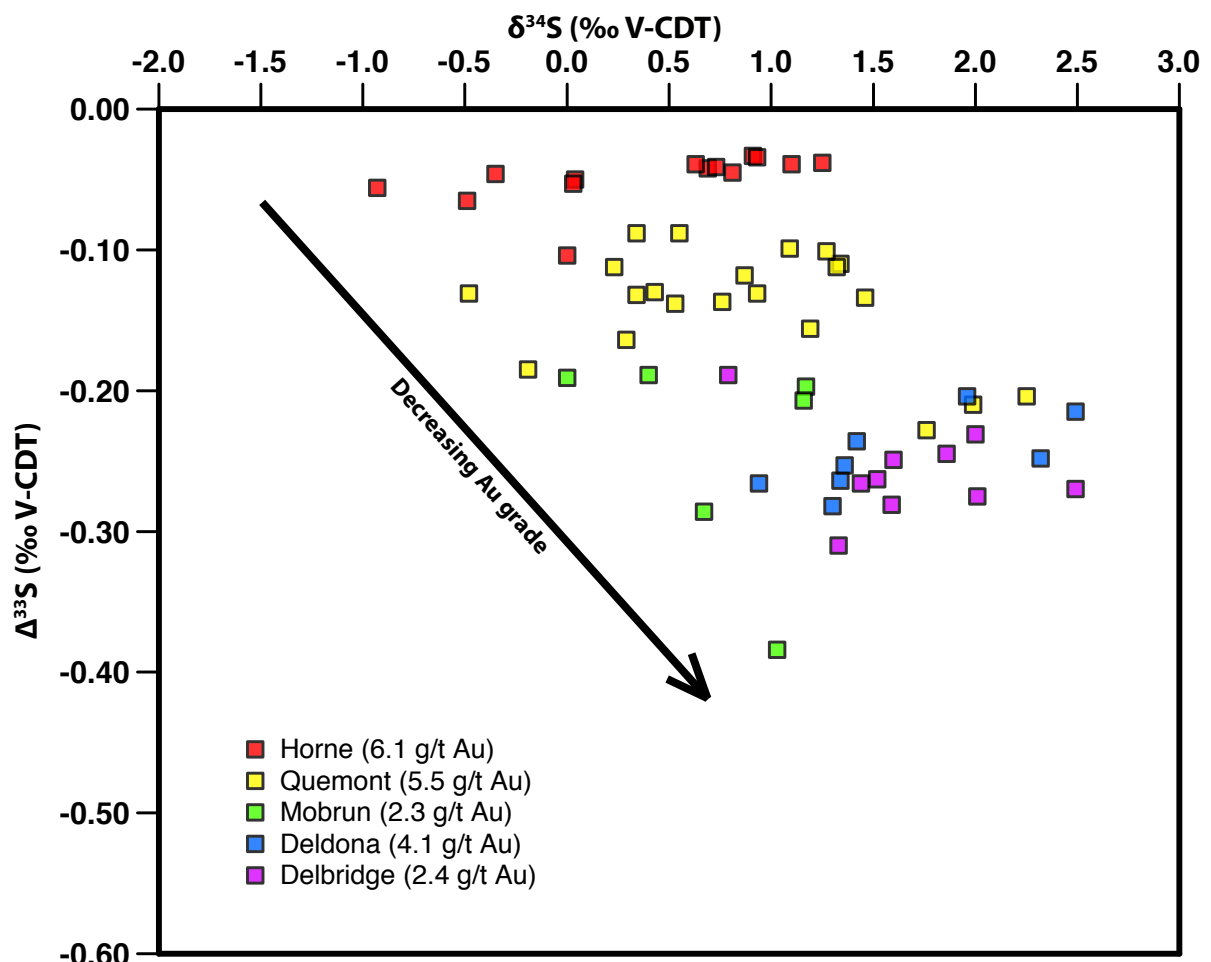


Fig. 2.9: Binary diagram showing $\delta^{34}\text{S}$ values vs. $\Delta^{33}\text{S}$ values for gold-rich sulfide deposits from the Noranda Camp, grouped according to average gold grades for those deposits (Gibson and Galley, 2007). The magnitude of the $\Delta^{33}\text{S}$ values from Mobrun appear to be too small for the reported gold grade, suggesting that there may still be some undiscovered Au potential at this deposit.

PREFACE TO CHAPTER THREE

In the previous chapter we clearly indicate, through multiple sulfur isotope data, the contribution of seawater sulfur during the formation of the Neoarchean Noranda VMS deposits. In combination with trace element geochemistry, we also utilized multiple sulfur isotopes to track the evolution of sulfur sources within the ore forming system, caused by the evolution of the Noranda caldera. We also proposed that economically relevant Au concentrations can be strongly linked to $\Delta^{33}\text{S}$ values of these VMS deposits. These observations clearly illustrate the important role multiple sulfur isotope data can play in interpreting ore forming processes in VMS systems.

In order to expand the dataset obtained from the Noranda VMS camp and test our interpretation of the significance of $\Delta^{33}\text{S}$ variability associated with Au-rich systems, in the following chapter we present multiple sulfur isotope data from the Doyon-Bousquet-LaRonde (DBL) mining camp. The deposits of the DBL are the same age as those of the Noranda camp, and are hosted within the same lithological unit (the Blake River Group of the Abitibi subprovince). The DBL mining camp comprises not only a series of VMS deposits, but also has associated intrusion-related and shear-hosted vein deposits. Its architecture allows for the acquisition and interpretation of multiple sulfur isotope data through a complete spectrum of deep to shallow hydrothermal ore-forming processes within a single system. Lastly, the entire DBL mining camp is considered to be Au-rich, providing an ideal platform to test the link between $\Delta^{33}\text{S}$ values and economic Au mineralization.

Evidence for a magmatic origin of the Doyon-Bousquet-LaRonde mining camp Au-rich VMS
and Au-rich quartz-sulfide veins: a multiple sulfur isotope study

E.R. SHARMAN, B.A. WING, P. MERCIER-LANGEVIN AND B. TAYLOR

3.1 Abstract

The ~2.7 Ga Doyon-Bousquet-LaRonde mining camp comprises three of the largest Au-rich volcanogenic massive sulfide deposits in the world, along with several intrusion-related and shear-zone hosted Au-rich quartz-sulfide vein deposits. The massive sulfide deposits are also proposed to be part of a subgroup of volcanogenic massive sulfide deposits characterized by a Au-Cu association that have a dominant magmatic-hydrothermal contribution to their ore-formation. In this study, we utilize multiple sulfur isotope analysis to investigate the sulfur sources within the different ore deposits of the ~28 Moz Au Doyon-Bousquet-LaRonde mining camp. We also compare and contrast these deposits to the volcanogenic massive sulfide deposits of the Noranda camp, located ~45 km west of the Doyon-Bousquet-LaRonde mining camp and of a similar age, but different metamorphic grade, geochemical characteristics, and metal tenors.

The Au-rich volcanogenic massive sulfide deposits of the Doyon-Bousquet-LaRonde mining camp have $\delta^{34}\text{S}$ values of +0.8 to +3.5 per mil and $\Delta^{33}\text{S}$ values of -0.16 to -0.01 per mil. One sample from the LaRonde Penna mine Zone 7 is an exception, and has a $\Delta^{33}\text{S}$ value of -0.29 per mil. Similarly, other Au-rich, intrusion-related and shear-hosted quartz-sulfide vein deposits have $\delta^{34}\text{S}$ values of +1.7 to +5.1 per mil and $\Delta^{33}\text{S}$ values of -0.14 to +0.00 per mil. We interpret the near-zero $\Delta^{33}\text{S}$ values for these deposits to indicate a primarily igneous-magmatic affinity (i.e. the sulfur in these ore deposits came either from leaching of sulfide in the volcanic pile, or

as a direct contribution of magmatic volatiles). In contrast, the slightly more negative $\Delta^{33}\text{S}$ value of the LaRonde Penna Zone 7 sample can be attributed to a minor contribution (~10 percent) to the ore-forming system of sulfur ultimately sourced as seawater sulfate.

The generally igneous-magmatic dominated sulfur isotope characteristics of the VMS ore sulfides of the Doyon-Bousquet-LaRonde mining camp contrast with those of the Cu-Zn volcanogenic massive sulfide deposits of the Noranda camp, where sulfur originating as seawater sulfate contributed as much as 25 percent of the sulfur currently residing in ore sulfides. In this regard, the Au-rich volcanogenic massive sulfide systems of the Doyon-Bousquet-LaRonde camp share similar characteristics with the giant Horne Au-rich volcanogenic massive sulfide deposit located in the southern part of the Noranda camp.

3.2 Introduction

The Doyon-Bousquet-LaRonde (DBL) mining camp is situated within the Blake River Group, Abitibi Greenstone Belt, and hosts three of the largest Au-rich volcanogenic massive sulfide (VMS) deposits in the world (LaRonde Penna, Bousquet 2-Dumagami, and Bousquet 1; Mercier-Langevin et al., 2007d; 2011a). The DBL mining camp also hosts several Au-rich vein systems including the epizonal intrusion-related Doyon and shear-hosted Mouska deposits (Mercier-Langevin et al., 2007c). The association of ore systems related to synvolcanic intrusions and to volcanic centers represented in the DBL mining camp makes it a unique area in which to examine the origins of sulfur in VMS mineralizing systems. It has also been noted that the VMS deposits of the DBL camp are part of a significant subgroup of VMS deposits characterized by a Au-Cu association, which are proposed to have a major, or dominant,

magmatic-hydrothermal source of ore fluids and metals (Dubé et al., 2007a, b; Huston et al., 2010).

Although the DBL mining camp is located only 45 km east of the Noranda VMS central camp, there are significant differences in metallogeny, alteration assemblages and structural overprinting in deposits of these two camps. Some 20 VMS deposits comprise the Noranda central camp, hosted by cauldron-filling rhyolitic, andesitic and basaltic volcanic rocks that are characterized by greenschist (or lower facies) metamorphism (Kerr and Gibson, 1993; Mercier-Langevin et al., 2011b). The Noranda cauldron is associated with polyphase, trondjhemite-dominated sub-volcanic intrusions (Flavrian and Powell plutons) that are both coeval with, and postdate, the development of the cauldron (Galley, 2003; Goutier et al., this volume; McNicoll et al., this volume). In contrast, the DBL mining camp contains four large VMS deposits in addition to vein-style mineralization (Mercier-Langevin et al., 2007c). The DBL deposits have undergone upper greenschist to lower amphibolite facies metamorphism, higher grades than in the Noranda camp; they are also highly strained. The DBL deposits are characterized in places by aluminous alteration zones interpreted to be metamorphosed submarine advanced argillic-style alteration facies (Dubé et al., 2007b). Rhyolite composition (dominantly transitional to calc-alkaline) further differentiates the DBL mining camp from the Noranda camp (Mercier-Langevin et al., 2007b; 2011b). The DBL camp VMS deposits also tend to be Au-rich and base metal poor, in contrast to most of the base metal-rich deposits of the Noranda camp (Mercier-Langevin et al., 2007c).

In rocks older than 2.45 Ga, combined $\delta^{33}\text{S}$ and $\delta^{34}\text{S}$ analyses permit recognition of mass-independent isotope fractionation (MIF), where measured $\delta^{33}\text{S}$ values are not related to measured $\delta^{34}\text{S}$ values by the conventional mass-dependent fractionation relationship: $\delta^{33}\text{S} =$

$[(\delta^{34}\text{S}/1000+1)^{0.515}-1] \times 1000$. Most current models attribute MIF to atmospheric SO₂ photochemistry in an anoxic atmosphere (Farquhar et al., 2000; Farquhar et al., 2010). It can be quantified in natural samples by non-zero $\Delta^{33}\text{S}$ values, where $\Delta^{33}\text{S} \equiv \delta^{33}\text{S} - [(\delta^{34}\text{S}/1000+1)^{0.515} - 1] \times 1000$. Mass-independet isotope fractionation is not created in purely magmatic ore-forming processes (Hulston and Thode, 1965), which will result in sulfur-bearing compounds with near-zero $\Delta^{33}\text{S}$ values. The general nature of the Archean sulfur cycle has been informed by multiple sulfur isotope analyses of the sedimentary record for nearly a decade, such that a rational multiple sulfur isotope model can now be used to identify contributions of sulfur from atmospheric and hydrospheric sources within Archean deposits (Fig. 2.1). Therefore, a detailed multiple sulfur isotope study of the ore deposits of the DBL mining camp was carried out to evaluate the sulfur sources within that camp, and to provide a basis for comparison to the Noranda VMS camp, and to investigate the link between mass-independent sulfur isotope fractionation signatures and gold grades.

The close temporal and geographical proximity of the DBL mining district to the central Noranda camp, the identified differences noted between the two, plus classification of the DBL camp by Huston et al. (2010) within the Cu-Au rich, magmatic-hydrothermal associated subgroup of VMS deposits, makes for ready comparison with the ore-forming processes that support more conventional Cu-Zn VMS deposits. In this context, we assess the DBL sulfur isotope dataset in terms of some of the hypotheses proposed for the sources and evolution of sulfur within the Noranda camp (Chapter 2, this thesis). Within the Noranda camp, negative $\Delta^{33}\text{S}$ values indicate a contribution of seawater sulfate to the ore-forming system. This contribution increased with the collapse and subsequent evolution of the Noranda cauldron (Chapter 2, this thesis). Further, a direct correlation was found between gold grade and $\Delta^{33}\text{S}$

values within Au-rich VMS deposits of the Noranda camp (Quemont and Horne), whereby higher gold grades are associated with near-zero $\Delta^{33}\text{S}$ values. This implies that igneous-magmatic input (either sulfur leached from the volcanic pile, or by direct magmatic input) of sulfur generally dominated the Au-rich ore-forming systems (Chapter 2, this thesis) at Noranda.

3.3 Regional Geology

The DBL mining camp is an approximately 10 km long, east-west trending succession of volcanic rocks located in the upper part of the ~2.7Ga Blake River Group within the Abitibi greenstone belt, Superior Province (Mercier-Langevin et al., 2007c). The deposits are hosted by the 2701–2696 Ma volcanic and intrusive rocks of the Bousquet Formation, bounded to the north by the Lac Parfouru fault, and to the south by the Cadillac Group and the Cadillac-Larder Lake fault zone (Mercier-Langevin et al., 2007c; Fig. 3.1). The geometry of the area results from regional deformation: D₁ represents a regional folding event throughout the entire Blake River Group; and D₂ within the DBL mining camp resulted in an east-west-trending, steeply south-dipping, penetrative schistosity (Mercier-Langevin et al., 2007a). Two episodes of regional metamorphism, a prograde upper greenschist- to lower amphibolite-facies period related to D₂, and a later, retrograde greenschist-facies event are recognized (Dubé et al., 2007b).

The Bousquet Formation is divided into an upper and lower member (2698-2697 Ma and 2699-2698 Ma, respectively; Fig. 3.2; Mercier-Langevin et al., 2007b, c). The lower member of the Bousquet Formation comprises tholeiitic to transitional mafic to felsic strata which include scoriaceous tuff units interpreted to have been emplaced as high-concentration submarine density currents, possibly of the eruption-fed type (Mercier-Langevin et al., 2008). These tuff units are cut by coeval, cogenetic dikes and sills as well as by felsic feeder dikes associated with the upper

member (Mercier-Langevin et al., 2007c). The scoriaceous tuff units are variably overlain by dacite flows, dacitic to rhyolitic flow breccia, and a heterogeneous unit comprising pillowd basalt and/or andesite with intercalated brecciated flows (Mercier-Langevin et al., 2007c).

The upper member is characterized by transitional to calc-alkaline, intermediate to felsic, effusive and intrusive rocks (Mercier-Langevin et al., 2007a) which are irregularly distributed in the camp. In places, the volcanic rocks are intercalated with thin beds of volcanogenic sedimentary rocks and graphitic argillite that may indicate a period of volcanic quiescence (Mercier-Langevin et al., 2007c).

The Bousquet Formation is underlain by the Hébécourt Formation (Fig. 3.2) which “comprises laterally extensive tholeiitic basalt and basaltic andesitic flows, cogenetic gabbroic sills, and small isolated tholeiitic rhyolite flows” (Mercier-Langevin et al., 2007c). Although the majority of the deposits comprising the DBL mining camp are hosted in the Bousquet Formation, a few of the minor lenses (Mouska zones 07, 08 and 22, and MicMac) are hosted within the underlying Hébécourt Formation.

The lower member of the Bousquet Formation and the Hébécourt Formation were then intruded by a synvolcanic intrusion (Mooshla Pluton) in three differentiated phases (Galley and Lafrance, 2007; Mercier-Langevin et al., 2007c). The intrusion of this pluton is also linked to some of the hydrothermal ore-forming events within the DBL mining camp (Dubé et al., 2007b; Galley and Lafrance, 2007; Mercier-Langevin et al., 2007c).

The Bousquet Formation is overlain by turbidites of the Cadillac Group (Lafrance et al., 2003, Fig. 3.2), an associated thin horizon of semi-massive to massive pyrrhotite and pyrite occurring towards the top of the upper Bousquet Formation (Mercier-Langevin et al., 2007c).

The mineralogical and geochemical compositions of the rocks that comprise the DBL mining camp, characterized as transitional to calc-alkaline, with high concentrations of incompatible elements, low Th/Th* values and low to intermediate Pb/Zn values, have led to the conclusion that the paleotectonic setting of the camp is most likely an intermediate setting between back-arc basin and volcanic-arc environments (Mercier-Langevin et al., 2007b).

3.3.1 Mineral Deposits

Previous studies (Dubé et al., 2007b; Mercier-Langevin et al., 2007a,b,c,d) have classified the mineral deposits of the DBL mining camp into three different deposit types relating to their morphology and mineralogy: (1) gold-rich VMS deposits (LaRonde-Penna, Bousquet 2-Dumagami and Bousquet 1), and ore zones (Westwood, Ellison and Warrenmac); (2) epizonal ‘intrusion-related’ gold-copper veins (Doyon deposit), and (3) shear zone-hosted (‘orogenic’) gold-copper veins (Mouska, Mic-Mac and Mooshla A and B deposits). The main features of each deposit type are presented below and in Table A2.1.

The gold-rich VMS deposits of the DBL mining camp are characterized by semi-massive to massive sulfide lenses and thin zones of transposed veins and veinlets, stacked at different stratigraphic intervals within the Bousquet Formation (Mercier-Langevin et al., 2007c and references therein). All of these lenses plunge steeply to the west, with primary elongation inferred to reflect partial control by synvolcanic faults (Mercier-Langevin et al., 2007c, d).

The epizonal, ‘intrusion-related’ Au±Cu veins comprise sulfide-rich quartz veins and veinlets, sulfide disseminations and quartz-sulfide veins that form slightly discordant ore bodies and intensely transposed vein stockworks hosted within the Mooshla intrusion, as well as in

highly altered schistose volcanic rocks in the upper part of the lower member of the Bousquet Formation (Mercier-Langevin et al., 2007c, d).

The shear-zone hosted deposits are separated further into three main types of mineralization: 1) stringer zones comprising sulfide veins and veinlets in a quartz-dominated matrix, 2) grayish quartz-sulfide veins, and 3) quartz-sulfide veins with associated tourmaline, carbonate and chlorite (Mercier-Langevin et al., 2007c). It should be noted that although these deposits have been classified as a separate group, they share some characteristics with the other types of deposits present in the camp; it has been proposed that some of these “shear zone hosted” deposits may represent transposed and/or remobilized gold-rich VMS lenses or early Au±Cu vein systems (Galley and Lafrance, 2007; Mercier-Langevin et al., 2007d).

The source of the gold in the DBL deposits has been extensively researched and three main models have been proposed. In the first model, gold is considered to be synvolcanic or syngenetic, and a primary component of the hydrothermal fluids involved in formation of the VMS (synvolcanic model) and of the epizonal intrusion-related veins (e.g. Valliant and Barnett, 1982; Valliant et al., 1983; Stone, 1990, 1991; Tourigny et al., 1993). Other authors (e.g., Tourigny et al., 1989a,b; Belkabir and Hubert, 1995; Belkabir et al., 2004) have proposed a multi-stage model, whereby the gold was, in part, structurally introduced within and, in part, remobilized from massive sulfides into high-strain zones. Lastly, a syndeformational model with a metamorphic origin for the gold within the DBL deposits has been proposed (e.g. Marquis et al., 1990a,b; Hoy et al., 1990). In this model the gold was deposited during regional deformation and metamorphism, superimposed onto previously formed alteration and sulfide-rich zones. More recent studies (Dubé et al., 2007; Mercier-Langevin et al., 2007c, d) of the LaRonde Penna deposit and the Mooshla synvolcanic pluton-hosted vein systems, combined with the geological

synthesis and reconstruction of the DBL mining camp geology, have further supported the synvolcanic or syngenetic source of gold in the DB deposits.

3.4 Samples

Samples for this study were collected from drill core and from underground mine workings. They were chosen to ensure a broad coverage of the different deposits present in the DBL mining camp, as well as to represent the different mineralization styles observed (see Table A2.2 for detailed sample descriptions). Many of the Au-rich VMS deposits were sampled, and the LaRonde Penna deposit, in particular, was sampled extensively. A suite of samples representing a stratigraphic section through the LaRonde Penna deposit was collected to investigate the evolution of sulfur sources in this ore-forming environment with depth. From the top of the LaRonde Penna deposit, a disseminated pyrrhotite- and chalcopyrite-bearing sample from the upper contact of the 20 South lens (D167184) was collected along with massive sulfide samples varying in composition from pyrite-dominated (D167177) to massive pyrite, sphalerite and chalcopyrite (D167174) from deeper within the 20 South lens. A sample of argillite with pyrite nodules, possibly representing sedimentation during volcanic quiescence, was also collected from the 20 South lens (D167175). Pyrrhotite stringers that form between the 20 South and 20 North lenses of the LaRonde-Penna deposit were sampled (D167176) to investigate their origin and the potential link between the two ore lenses.

Continuing lower into the LaRonde Penna stratigraphy, we sampled 20N Zn zone of the LaRonde-Penna deposit with a massive sulfide containing subhedral pyrite surrounded by sphalerite and minor galena (D167182). A pyrite-bearing argillite sample was also collected from this part of the deposit (D167181), again, to constrain sulfur cycling during volcanic

quiescence. Two massive sulfide samples were collected from the 20N Au zone, one pyrite dominated (D167179), and one from an anomalously zinc-rich area (D167169). These act as baselines against which to compare samples from the aluminous alteration zone of the 20N Au zone in order to see if sulfur in the fluids leading to aluminous alteration had a different origin than elsewhere in the deposit. Samples from the aluminous alteration zone contained both pyrite- and sphalerite-dominated massive sulfides (D167171 and D167173, respectively), as well as fine-grained (1-2 mm) disseminated pyrite (D167199) and fine-grained disseminated pyrite stringers (D181001). Finally, a sulfide-bearing schist was collected (D167165) at the stratigraphic base of the 20N Au zone to constrain the nature of the sulfur in the environs of the LaRonde Penna deposit prior to ore deposition.

We made similar, but less detailed, transects through other Au-rich VMS deposits. One massive sulfide sample (D181003) was taken from deep in the Bousquet 2 – Dumagami deposit, and is thought to represent the contact between the Bousquet Formation and Cadillac Group. A massive sulfide sample (D18011) at this contact was also collected in the Bousquet 1 area. Several samples (D181013, D181015) comprising fine-grained (1-2 mm) pyrite and/or chalcopyrite within a dominantly felsic host were also collected from the Bousquet 1 deposit. Lastly, two samples were collected from the Ellison deposit, both samples from zone A, one of which (D181009) contains subhedral pyrite with rounded overgrowths that occasionally also have pressure shadows; the other (D181010) comprises semi-massive pyrite.

A selection of different veins sampled from throughout the Doyon deposit to represents the epizonal ‘intrusion-related’ deposits of the DBL camp. These include stockwork veins comprised of pyrite and chalcopyrite, within pink schist alteration envelopes, from Zone 1

(DOPL-2007-001A), and pyrite- and chalcopyrite-bearing quartz-carbonate veins within Zone 2 (DOPL-2007-003) and West Zone (DOPL-2007-005).

Samples were also collected from the Mouska deposit to represent the three main types of mineralization in the shear zone-hosted Au-Cu vein deposit group. Samples with disseminated and stringer sulfides represent type 1 mineralization (MM07B), and those comprising sulfides associated with quartz veins (MM-06, MM-07A) represent type 2 mineralization. Type 3-style mineralization is observed in those samples with sulfides associated with quartz-tourmaline veins (MM-04, MM-10).

3.5 Methodology

Using a microdrill, sulfide powders were collected from whole rock and core samples. Where more than one major sulfide or mineralization style was present, multiple samples were collected. These samples were then reacted with a Cr-reducing solution that allowed the liberation of H₂S (Canfield et al., 1986). This H₂S was subsequently converted to Ag₂S by trapping the H₂S using a zinc acetate solution and reacting it with AgNO₃. The Ag₂S was then reacted in a nickel reaction vessel at 225°C for a minimum of 4 hours in the presence of excess F₂ to produce SF₆. The resulting SF₆ from the above procedure was purified first cryogenically, and then with a gas chromatograph as outlined by Hu et al. (2003). Purified SF₆ was introduced to a ThermoFinnigan MAT 253 dual-inlet, gas-source, isotope ratio mass spectrometer at McGill University, where sulfur isotope abundances were measured by monitoring the ³²SF₅⁺, ³³SF₅⁺, ³⁴SF₅⁺ ion beams at mass to charge ratios of 127, 128, and 129, respectively. All sulfur isotope data are reported on the Vienna-Cañon Diablo Troilite scale (V-CDT), on which the international reference material IAEA-S-1 has a defined $\delta^{34}\text{S}$ value of -0.3‰ (Robinson, 1995). We calculate

IAEA-S-1 to have a $\Delta^{33}\text{S}$ value of 0.094‰. The full analytical uncertainty (1σ) for sulfur isotope analysis is estimated to be $\pm 0.13\text{ ‰}$ for $\delta^{34}\text{S}$ values, and $\pm 0.01\text{ ‰}$ for $\Delta^{33}\text{S}$ values, based on the long-term standard deviation for repeat analyses of in-house standards.

3.6 Results

Multiple sulfur isotope analysis of the DBL mining camp samples indicates a wide range in both $\delta^{34}\text{S}$ and $\Delta^{33}\text{S}$ (Fig. 3.3A-D). Results for both intrusion-related and shear-hosted veins exhibit extremely minor variation in $\Delta^{33}\text{S}$ values (-0.14 to +0.04 ‰), but slightly positive range $\delta^{34}\text{S}$ values (+1.7 to +5.1 ‰) (Fig. 3.3D). Samples from the Au-rich VMS deposits have a similar slightly positive range of $\delta^{34}\text{S}$ values, from +0.83 to +5.23 per mil and a range of $\Delta^{33}\text{S}$ values of -0.27 to -0.01 per mil. Sulfides sampled from mineralized rocks at the top of the Bousquet Formation, close to the contact with the Cadillac Group, have the most positive $\delta^{34}\text{S}$ values (+5.1 to +10.0 ‰) and most negative $\Delta^{33}\text{S}$ values (-1.43 to -1.04 ‰; Fig. 3.3A). These data are markedly different from the bulk of the ore-body sulfides, and the potential for the mixing of more than one source of sulfur is discussed below. Samples from graphitic argillite horizons also exhibit positive $\delta^{34}\text{S}$ values (+2.8 to +8.8 ‰) and negative $\Delta^{33}\text{S}$ values (-0.52 to -0.34 ‰) (Fig. 3.3A). Lastly, two samples from the footwall of the LaRonde Penna 20 South and 20 North lenses have $\delta^{34}\text{S}$ values of +5.89 and +2.83 per mil and $\Delta^{33}\text{S}$ values of -0.82 and -0.03 per mil, respectively (Fig. 3.3B).

3.7 Discussion

3.7.1 Vein-hosted Deposits

Samples from both the intrusion-related veins of the Doyon deposit and the shear-hosted veins of the Mouska deposit have multiple sulfur isotope signatures that are dominantly mass-dependent ($\Delta^{33}\text{S} \approx 0\ \text{\textperthousand}$). The sulfur in these samples therefore likely represents sulfide that was leached from the volcanic pile, or volatiles that were directly input from a magmatic source. However, these vein sulfides exhibit slightly heavier $\delta^{34}\text{S}$ values (approximately +2 to +5 ‰, Fig 3.3C) than would be predicted for uncontaminated magmatic or volcanic sulfur ($\delta^{34}\text{S} \pm 0\ \text{\textperthousand}$; Sakai et al., 1984). However, it should be noted that calc-alkaline rocks formed in back-arc environments are usually characterized by heavier $\delta^{34}\text{S}$ values (average +4 to +5 ‰; Herzig et al., 1998; Ueda and Sakai, 1984; Woodhead et al., 1987) which are attributed to a contribution of sulfur from the subduction of hydrated oceanic crust and sediments containing sulfur originating as seawater sulfate (Woodhead et al., 1987).

As the DBL mining camp is proposed to have formed in a near back-arc paleotectonic environment, it is possible that the Mooshla intrusion and associated volcanics formed from magma that was enriched in ^{34}S and would therefore have positive $\delta^{34}\text{S}$ values. It follows that the vein mineralization formed in association with the Mooshla intrusion might reflect this heavy $\delta^{34}\text{S}$ signature. One flaw in this argument is that the mechanism proposed for the ^{34}S enrichment of back-arc magmas is a contribution of sulfur originating as seawater sulfate from subducted oceanic crust. This seawater sulfate contribution should impart a negative $\Delta^{33}\text{S}$ signature to the magma along with the positive $\delta^{34}\text{S}$ signature; this may be reflected in the decidedly small but uniformly negative $\Delta^{33}\text{S}$ values observed in the vein sulfides of the DBL mining camp.

A second potential mechanism to enrich sulfur in ^{34}S is through the disproportionation of magmatic H_2S and SO_2 (Ohmoto and Rye, 1979; Rye, 1993). In this process magmatic SO_2 becomes enriched in ^{34}S creating positive $\delta^{34}\text{S}$ values, whereas H_2S becomes depleted and acquires negative $\delta^{34}\text{S}$ values. As there are no samples of DBL vein sulfides that exhibit negative $\delta^{34}\text{S}$ values, the following mechanism may be responsible for the enrichment of the ^{34}S within the system:

- 1) Emplacement and crystallization of the various phases of the Mooshla intrusion led to the disproportionation of magmatic H_2S and SO_2 .
- 2) The magmatic H_2S forms sulfides within the intrusion, and will have a slightly negative $\delta^{34}\text{S}$ signature.
- 3) The magmatic SO_2 , with a slightly positive $\delta^{34}\text{S}$ signature, was incorporated in the volatile-rich fluid generated during the cooling of the intrusion.
- 4) These volatile-rich fluids moved out into the surrounding reduced volcanic sequence forming veins, and the reduction of magmatic SO_2 led to the formation of sulfides that preserved the positive $\delta^{34}\text{S}$ signature. The implication would be that the slightly negative $\Delta^{33}\text{S}$ values reflect minor variation of the $\delta^{33}\text{S}$ - $\delta^{34}\text{S}$ fractionation ‘slope’ associated with disproportionation (Farquhar and Wing, 2005).

This process is more complicated than the first proposed mechanism but, has the advantage of providing a testable hypothesis through analysis of samples from the barren portions of the Mooshla intrusion. If the $\delta^{34}\text{S}$ and $\Delta^{33}\text{S}$ values of the intrusion are positive then the first mechanism is most likely, however if the $\delta^{34}\text{S}$ and $\Delta^{33}\text{S}$ values are negative, then the second mechanism may be more plausible.

3.7.2 Au-rich VMS Deposits

The first important thing to note in the multiple sulfur isotope data of the VMS deposits of the DBL mining camp is the near-zero, to slightly positive, $\delta^{34}\text{S}$ values and near-zero $\Delta^{33}\text{S}$ values in the ore lenses (Fig. 3.3A-C). An apparent exception is the Zone 7 lens of the LaRonde Penna deposit, for which a $\Delta^{33}\text{S}$ value of -0.29 per mil was obtained. In general, many of the samples of VMS deposits from the DBL camp have near-zero $\Delta^{33}\text{S}$ values. Within the present understanding of the Archean sulfur cycle, these results indicate an igneous-magmatic source of sulfur (Fig. 3.3B, C). However, approximately 25 percent of the samples analysed bear a clear MIF signal: $\Delta^{33}\text{S} < 0$ per mil (Fig. 3.3A-C).

Samples analysed from the LaRonde Penna 20 North lens Au-rich zone form a very tight cluster. There is no measurable difference in $\delta^{34}\text{S}$ and $\Delta^{33}\text{S}$ between those samples that exhibit aluminous alteration and those where it is absent. This observation is in contrast to the predictions made by Huston et al. (2010) who propose that magmatic-hydrothermal contributions to VMS forming systems can be recognized through argillic alteration and disproportionation of magmatic SO_2 identified by sulfur isotope values ($\delta^{34}\text{S}_{\text{sulfide}} < 0\text{\textperthousand}$, since magmatic $\delta^{34}\text{S}$ values are ~ 0 and the isotopic difference imparted by disproportionation is $\delta^{34}\text{S}_{\text{sulfate}} - \delta^{34}\text{S}_{\text{sulfide}} \sim 20\text{-}30\text{\textperthousand}$). Although the near-zero $\Delta^{33}\text{S}$ values determined for the DBL samples indicate a magmatic origin of sulfur, sulfate minerals are not present in the DBL samples with which to compare $\delta^{34}\text{S}$ values. The slightly positive $\delta^{34}\text{S}$ values for sulfides may be a result of a similar process proposed for the formation of the vein deposits, with a minor contribution of reduced magmatic SO_2 from the underlying rhyodacite-dacite domes to the overlying 20 North lens. Alternatively, slightly positive $\delta^{34}\text{S}$ values may further support the hypothesis that the magma from which the DBL mining camp formed was enriched in ^{34}S from a subducted slab. The lack of variation in

multiple sulfur isotopes between the unaltered and aluminous alteration zones indicates the same sulfur sources for both. This would imply that the mechanism that led to the aluminous alteration either did not contribute any sulfur to the ore forming system, or it was the same isotopic composition as the sulfur from which the ore lens formed initially.

In contrast to samples from within the VMS massive sulfide ore lenses, samples analysed from graphitic argillite horizons within the ore lenses show significant negative $\Delta^{33}\text{S}$ and positive $\delta^{34}\text{S}$ values (Fig. 3.3B). The formation of graphitic argillites and their associated sulfide mineralization occurred on the paleoseafloor during periods of volcanic quiescence (Mercier-Langevin et al., 2007c). The argillite sulfides may have had several potential sources of sulfur: sulfide in seawater, sulfide from vented hydrothermal fluids, sulfide from bacterial reduction of seawater sulfate in the pore-water or water column, and seawater sulfate thermochemically reduced within hydrothermal mounds. The proposed model for the Archean sulfur cycle (Fig. 2.1) indicates that the positive $\delta^{34}\text{S}$ and negative $\Delta^{33}\text{S}$ values of the sulfides within the argillites suggests an ultimate sulfur source from seawater sulfate. This negative $\Delta^{33}\text{S}$ value mostly likely represents a sulfur contribution from seawater sulfate (~20 %, from a simple ratio of $\Delta^{33}\text{S}$ values assuming a maximum $\Delta^{33}\text{S}_{\text{seawater sulfate}} = -2.4 \text{ ‰}$; Johnston, 2011). The process by which the sulfate was reduced to form sulfide may have been either biological or thermochemical. In any case, the positive $\delta^{34}\text{S}$ values suggest that the sulfate supply at the site of reduction was limited.

Sulfides from the contact of the Bousquet Formation and the Cadillac Group have the most positive $\delta^{34}\text{S}$ and most negative $\Delta^{33}\text{S}$ values of all the samples analysed. These sulfides likely formed towards, or after, the cessation of volcanism (Mercier-Langevin et al., 2007a). This would allow for the potential development of shallow, low temperature convection of seawater through the volcanic pile leading to the formation of sulfides, potentially through an

addition of thermochemically reduced seawater sulfate (~40-50 %). This would result in a seawater sulfate signature in the multiple sulfur isotope compositions such as found for the Bousquet Formation – Cadillac Group contact sulfides.

A minor contribution (~10 %) of seawater sulfate would also explain the slight negative $\Delta^{33}\text{S}$ value observed in the Zone 7 lens of the LaRonde Penna deposit. The presence of Au-rich massive sulfide clasts within the surrounding talus and flow breccia deposits and volcanic sedimentary rocks suggest a volcanic hiatus (Mercier-Langevin et al., 2007a), and is consistent with the volcanostratigraphic position of the zone 7 lens at the top of a major volcanic package (the Lower Bousquet Formation, Fig. 3.2). This volcanostratigraphic break may have been associated with a reduction in volcanic activity, allowing for the shallow entrainment of seawater and associated reductive contribution of seawater sulfate within the ore lens.

Fine-grained sulfides from within the schistose footwall of the LaRonde Penna 20 North lens (sample D167165) exhibit $\delta^{34}\text{S}$ and $\Delta^{33}\text{S}$ values that are indistinguishable from the main ore lens (+2.8 and -0.03‰ respectively; Table 3.1). Such results are consistent with a magmatic source of sulfur. In contrast, the footwall sample of pyrrhotite stringers collected in the footwall to the 20 South lens has a greater isotopic affinity with the samples collected from the Cadillac Group – Bousquet Formation contact. The $\delta^{34}\text{S}$ and $\Delta^{33}\text{S}$ values (+5.9 and -0.82 ‰ respectively; Table 3.1) would indicate a contribution of up to 35% sulfur originally from seawater sulfate to this part of the ore-forming system. These characteristics may result from an evolution of the local ore-forming environment, from a deeper-water setting, where sulfate would have less access, to a shallower water setting. They may also simply reflect the ultimate protolith of the 20 North and 20 South lense footwall rocks.

3.7.3 Comparison to the Noranda VMS District

The results of this study can be interpreted within the context of multiple sulfur isotope analyses from the Noranda VMS camp. Although the Noranda camp is slightly older than the DBL mining camp (2702 – 2694 Ma; Corfu, 1993; Mercier-Langevin et al., 2011b), there are significant differences between these two Blake River Group districts. Multiple sulfur isotope results of a camp-wide study of ore sulfides from VMS deposits of the Noranda area yielded $\delta^{34}\text{S}$ values of between -1.9 and +2.5 per mil V-CDT and $\Delta^{33}\text{S}$ values of between -0.59 and -0.03 per mil V-CDT (Chapter 2, this thesis). These negative $\Delta^{33}\text{S}$ values are interpreted to represent a contribution of sulfur ultimately from seawater sulfate to the ore sulfides of the Noranda camp VMS deposits. The contribution increased with the collapse and subsequent evolution of the Noranda cauldron (Chapter 2, this thesis).

Whereas $\Delta^{33}\text{S}$ values for the DBL mining camp sulfides fall within the range of those values for the Noranda camp, the Noranda camp VMS deposits exhibit a wider and more negative range in $\Delta^{33}\text{S}$ values (Fig. 3.4). Also, the samples from the Noranda camp comprise a $\delta^{34}\text{S}$ range of slightly less positive δ -values than the DBL VMS deposits. Furthermore, there is very little overlap in the isotopic compositions of sulfides from the two VMS camps (Fig. 3.4). This observation supports the recognition by Huston et al. (2010) that the DBL VMS deposits are different from those of the Noranda camp. However, it is worth noting that the DBL camp does not exhibit any of the major faulting identified in the Noranda camp, associated with the formation of the caldera. This is an important observation, as this faulting enabled in part, the eventual contribution of seawater sulfate to the ore-forming system.

The Au-rich VMS deposits of the Noranda Camp exhibit a correlation between $\Delta^{33}\text{S}$ values and Au grades, with higher gold grades being correlated with samples with near-zero

$\Delta^{33}\text{S}$, and lower Au-grades with more negative values of $\Delta^{33}\text{S}$ (Chapter 2, this thesis). Similarly, the Au-rich VMS lenses in the DBL camp have near-zero $\Delta^{33}\text{S}$ values, consistent with a magmatic source for the Au in the DBL deposits. However, the apparent negative Au - $\Delta^{33}\text{S}$ correlation of the Noranda Camp cannot be demonstrated in the DBL camp due to the narrow range of $\Delta^{33}\text{S}$ in the DBL sulfides. Nevertheless, our findings support the synvolcanic nature of the gold mineralization proposed for this region (Dubé et al., 2007; Mercier-Langevin et al., 2007c, d).

3.8 Conclusions

The multiple sulfur isotope analysis of the ore deposits within the DBL mining camp indicates a very clear igneous-magmatic affinity. We infer a direct magmatic input, with little contribution from any surficial sources of sulfur. In contrast, sulfides that formed at, or very near to the paleo-seafloor, exhibit a clear contribution of sulfur that ultimately originated from seawater sulfate. This study identifies significant isotopic differences between the Noranda VMS deposits and those of the DBL mining camp. Namely, ore sulfides from the Noranda deposits are characterized by a range of $\delta^{34}\text{S}$ values (~ -2 to $+2\text{\textperthousand}$) and negative $\Delta^{33}\text{S}$ values, whereas those from the DBL mining camp VMS deposits have positive $\delta^{34}\text{S}$ values ($\sim +1$ to $+4\text{\textperthousand}$) and near zero $\Delta^{33}\text{S}$ values. Based on $\delta^{34}\text{S}$ values alone, the DBL ore-forming environment would conventionally be interpreted as having a greater contribution from surficial sulfur. However, the $\Delta^{33}\text{S}$ values indicate that the DBL VMS deposits must have been formed in a dominantly magmatic-hydrothermal environment. Whether this was due to exogenic (i.e., deeper submarine environments for DBL), or endogenic (i.e., a single long-lived hydrothermal system) causes is a question for future work.

This study also demonstrates the ability of multiple sulfur isotope analysis to interpret sulfur sources within ore-forming systems that have undergone relatively high levels of metamorphism. It also supports observations made for the Noranda VMS deposits with respect to their potential for magmatic sources of gold within Archean VMS systems. However, we feel that further, more detailed multiple sulfur isotope analyses are needed. In concert with trace element analyses, isotopic analyses from the DBL mining camp would allow the development of a more coherent model of the evolution of sulfur sources within this complex system.

3.9 Acknowledgements

ERS was supported by the Geological Survey of Canada's Targeted Geoscience-3 Abitibi Project (B. Dubé – Project Leader), a Society of Economic Geologists Graduate Student Fellowship, a GEOTOP bourses d'études des cycles supérieurs, and an NSERC Discovery Grant to BAW. We would also like to thank Agnico-Eagle Mines Limited and IAMGOLD Corporation (formerly Cambior Inc.) for all their assistance, especially with access to samples without which this study would not have been possible. The McGill Stable Isotope Laboratory is supported by the Canada Research Chairs program, by NSERC through the Research Tools and Infrastructure and Discovery Grant programs, and by GEOTOP. We appreciate the laboratory assistance of Thi Hao Bui and André Pellerin.

3.10 References

- Belkabir, A., and Hubert, C., 1995, Geology and structure of a sulfide-rich gold deposit: An example from the Mouska gold mine, Bousquet district, Canada: Economic Geology, v. 90, p. 1064-1079.
- Belkabir, A., Hubert, C., and Hoy, L., 2004, Gold emplacement and hydrothermal alteration in metabasic rocks at the Mouska mine, Bousquet district, Abitibi, Quebec, Canada: The Canadian Mineralogist, v. 42, p. 1079-1096.
- Canfield, D. E., Raiswell, R., Westrich, J. T., Reaves, C. M., and Berner, R. A., 1986, The use of chromium reduction in the analysis of reduced inorganic sulfur in sediments and shales: Chemical Geology, v. 54, p. 149-155.
- Corfu, F., 1993, The evolution of the southern Abitibi greenstone belt in light of precise U-Pb geochronology: Economic Geology, v. 88, p. 1323-1340.
- Dubé, B., Gosselin, P., Mercier-Langevin, P., Hannington, M.D., et Galley, A., 2007a, Gold-rich volcanogenic massive sulphide deposits, *in* Goodfellow, W.D., ed., Mineral Deposits of Canada: A synthesis of Major Deposit-Types, District Metallogeny, the Evolution of Geological Provinces, and Exploration Methods: Geological Association of Canada, Mineral Deposits Division, Special Publication No. 5, p. 75-94.
- Dubé, B., Mercier-Langevin, P., Hannington, M., Lafrance, B., Gosselin, G., and Gosselin, P., 2007b, The LaRonde Penna world-class Au-rich volcanogenic massive sulfide deposit, Abitibi, Quebec: Mineralogy and geochemistry of alteration and implications for genesis and exploration: Economic Geology, v. 102, p. 633-666.
- Farquhar, J., Bao, H. M., and Thiemens, M., 2000, Atmospheric influence of Earth's earliest sulfur cycle: Science, v. 289, p. 756-758.
- Farquhar, J., and Wing, B. A., 2005, The terrestrial record of stable sulphur isotopes: A review of the implications for evolution of Earth's sulphur cycle, *in* McDonald, I., Boyce, A. J., Butler, I. B., Herrington, R. J., and Polya, D. A., eds., Mineral Deposits and Earth Evolution, Geological Society, London, Special Publications, v. 248, p. 167-177.
- Farquhar, J., Wu, N., Canfield, D. E., and Oduro, H., 2010, Connections between Sulfur Cycle Evolution, Sulfur Isotopes, Sediments, and Base Metal Sulfide Deposits: Econ Geol, v. 105, p. 509-533.
- Galley, A., 2003, Composite synvolcanic intrusions associated with Precambrian VMS-related hydrothermal systems: Mineralium Deposita, v. 38, p. 443-473.
- Galley, A.G., and Lafrance, B., 2007, Évolution et métallogénie du pluton de Mooshla: Ministère des Ressources naturelles et de la Faune, ET 2007-02, 32 p.
- Herzig, P. M., Hannington, M. D., and Arribas Jr, A., 1998, Sulfur isotopic composition of hydrothermal precipitates from the Lau back-arc: implications for magmatic contributions to seafloor hydrothermal systems: Mineralium Deposita, v. 33, p. 226-237.
- Hoy, L.D., Trudel, P., Tourigny, G., Kheang, L., Savoir, A., and Crépeau, R., 1990, Isotopic and fluid inclusion constraints on the origin of vein Au mineralization at Bousquet township, Quebec, *in* Rive, M., Verpaelst, P., Gagnon, Y., Lulin, J.-M., Riverin, G., and Simard, A., eds., The Northwestern Quebec Polymetallic Belt: A Summary of 60 Years of Mining Exploration: Canadian Institute of Mining and Metallurgy, Special Volume 43, p. 413-423.

- Hu, G., Rumble, D., and Wang, P., 2003, An ultraviolet laser microprobe for the in situ analysis of multisulfur isotopes and its use in measuring Archean sulfur isotope mass-independent anomalies: *Geochimica et Cosmochimica Acta*, v. 67, p. 3101-3118.
- Hulston, J. R., and Thode, H. G., 1965, Variations in the S33, S34, and S36 Contents of Meteorites and Their Relation to Chemical and Nuclear Effects: *J. Geophys. Res.*, v. 70, p. 3475-3484.
- Huston, D., Relvas, J., Gemmell, J., and Drieberg, S., 2010, The role of granites in volcanic-hosted massive sulphide ore-forming systems: an assessment of magmatic–hydrothermal contributions: *Mineralium Deposita*, p. 1-35.
- Johnston, D. T., 2011, Multiple sulfur isotopes and the evolution of Earth's surface sulfur cycle: *Earth-Science Reviews*, v. 106, p. 161-183.
- Kerr, D. J., and Gibson, H. L., 1993, A comparison of the Horne volcanogenic massive sulfide deposit and intracauldron deposits of the Mine Sequence, Noranda, Quebec: *Economic Geology*, v. 88, p. 1419-1442.
- Marquis, P., Brown, A.C., Hubert, C., and Rigg, D.M., 1990a, Progressive alteration associated with auriferous massive sulfide bodies at the Dumagami mine, Abitibi greenstone belt, Quebec: *Economic Geology*, v. 85, p. 746-764.
- Marquis, P., Hubert, C., Brown, A.C., and Rigg, D.M., 1990b, An evaluation of genetic models for gold deposits of the Bousquet district, Quebec, based on their mineralogic, geochemical, and structural characteristics, in Rive, M., Verpaelst, P., Gagnon, Y., Lulin, J.-M., Riverin, G., and Simard, A., eds., *The Northwestern Quebec Polymetallic Belt: A Summary of 60 Years of Mining Exploration*: Canadian Institute of Mining and Metallurgy, Special Volume 43, p. 383-399.
- Mercier-Langevin, P., Dube, B., Hannington, M. D., Davis, D. W., Lafrance, B., and Gosselin, G., 2007a, The LaRonde penna Au-rich volcanogenic massive sulfide deposit, Abitibi greenstone belt, Quebec: Part I. Geology and geochronology: *Economic Geology*, v. 102, p. 585-609.
- Mercier-Langevin, P., Dube, B., Hannington, M. D., Richer-Lafleche, M., and Gosselin, G., 2007b, The LaRonde penna Au-rich volcanogenic massive sulfide deposit, Abitibi greenstone belt, Quebec: Part II. Lithgeochemistry and paleotectonic setting: *Economic Geology*, v. 102, p. 611-631.
- Mercier-Langevin, P., Dube, B., Lafrance, B., Hannington, M., Galley, A., Moorhead, J., and Gosselin, P., 2007c, Metallogeny of the Doyon-Bousquet-LaRonde Mining Camp, Abitibi Greenstone Belt, Quebec, in Goodfellow, W. D., ed., *Mineral Deposits of Canada: A Synthesis of Major Deposit-Types, District Metallogeny, the Evolution of Geological Provinces and Exploration Methods* Special Publication No. 5, Geological Association of Canada, Mineral Deposits Division, p. 673-701.
- Mercier-Langevin, P., Dube, B., Lafrance, B., Hannington, M. D., Galley, A., Marquis, R., Moorhead, J., and Davis, D. W., 2007d, A group of papers devoted to the LaRonde Penna Au-rich volcanogenic massive sulfide deposit, eastern Blake River Group, Abitibi greenstone belt, Quebec: Preface: *Economic Geology*, v. 102, p. 577-583.
- Mercier-Langevin, P., Ross, P.-S., Lafrance, B., and Dubé, B., 2008, Volcaniclastic rocks of the Bousquet scoriaceous tuff units north of the LaRonde Penna mine, Doyon-Bousquet-LaRonde mining camp, Abitibi Greenstone Belt, Quebec: *Geological Survey of Canada, Current Research* 2008-11, 19p.

- Mercier-Langevin, P., Hannington, M.D., Dubé, B., and Béchu, V., 2011a, The gold content of volcanogenic massive sulphide deposits: Mineralium Deposita, v. 46, p. 509-539.
- Mercier-Langevin, P., Goutier, J., Ross, P.-S., McNicoll, V., Monecke, T., Dion, C., Dubé, B., Thurston, P., Béchu, V., Gibson, H., Hannington, M., and Galley, A., 2011b, The Blake River Group of the Abitibi greenstone belt and its unique VMS and gold-rich VMS endowment. GAC-MAC-SEG-SGA Joint Annual Meeting 2011, Ottawa, Field Trip 02B guidebook; Geological Survey of Canada, Open File report 6869, 61 p.
- Ohmoto, H., and Rye, R. O., 1979, Isotopes of sulfur and carbon, in Barnes, H. L., ed., Geochemistry of Hydrothermal Ore Deposits, Second Edition: New York, John Wiley and Sons, p. 509-567.
- Robinson, B. W., 1995, Sulphur isotope standards: Proceedings of a consultants' meeting held in Vienna, 1-3 Dec. 1993, IAEA-TECDOC-825, p. 39-45.
- Rye, R. O., 1993, The evolution of magmatic fluids in the epithermal environment; the stable isotope perspective: Economic Geology, v. 88, p. 733-752.
- Sakai, H., Marais, D. J. D., Ueda, A., and Moore, J. G., 1984, Concentrations and isotope ratios of carbon, nitrogen and sulfur in ocean-floor basalts: *Geochimica et Cosmochimica Acta*, v. 48, p. 2433-2441.
- Stone, W.E., 1990, Archean volcanism and sedimentation in the Bousquet gold district, Abitibi greenstone belt, Quebec: Implications for stratigraphy and gold concentration: *Geological Society of America Bulletin*, v. 102, p. 147-158.
- Stone, W.E., 1991, Archean volcanism and sedimentation in the Bousquet gold district, Abitibi greenstone belt, Quebec: implications for stratigraphy and gold concentration: Alternative interpretation and reply, Reply: *Geological Society of America Bulletin*, v. 103, p. 1256-1257.
- Tourigny, G., Doucet, D., and Bourget, A., 1993, Geology of the Bousquet 2 mine: An example of a deformed, gold-bearing polymetallic sulfide deposit: *Economic Geology*, v. 88, p. 1578-1597.
- Tourigny, G., Brown, A.C., Hubert, C., and Crépeau, R., 1989a, Synvolcanic and syntectonic gold mineralization at the Bousquet mine, Abitibi greenstone belt, Quebec: *Economic Geology*, v. 84, p. 1875-1890.
- Tourigny, G., Hubert, C., Brown, A.C., and Crépeau, R., 1989b, Structural control on gold mineralization at the Bousquet mine, Abitibi, Quebec: *Canadian Journal of Earth Sciences*, v. 26, p. 157-175.
- Ueda, A., and Sakai, H., 1984, Sulfur isotope study of Quaternary volcanic rocks from the Japanese Islands Arc: *Geochimica et Cosmochimica Acta*, v. 48, p. 1837-1848.
- Valliant, R.I., and Barnett, R.L., 1982, Manganiferous garnet underlying the Bousquet gold orebody, Quebec: Metamorphosed manganese sediment as a guide to gold ore: *Canadian Journal of Earth Sciences*, v. 19, p. 993-1010.
- Valliant, R.I., Barnett, R.L., and Hodder, R.W., 1983, Aluminium silicate-bearing rock and its relation to gold mineralization; Bousquet mine, Bousquet Township, Quebec: *Canadian Institute of Mining and Metallurgy Bulletin*, v. 76, p. 81-90.
- Woodhead, J. D., Harmon, R. S., and Fraser, D. G., 1987, O, S, Sr, and Pb isotope variations in volcanic rocks from the Northern Mariana Islands: implications for crustal recycling in intra-oceanic arcs: *Earth and Planetary Science Letters*, v. 83, p. 39-52.

Table 3.1: Sulfur isotope compositions of sulfide samples from the Doyon-Bousquet-LaRonde mining camp

Sample name	Deposit	Type	$\delta^{33}\text{S}$ (\textperthousand V-CDT)	$\delta^{34}\text{S}$ (\textperthousand V-CDT)	$\Delta^{33}\text{S}$ (\textperthousand V-CDT)
D167165	LaRonde-Penna 20N Au	Au-rich VMS footwall	1.43	2.8	-0.03
D167169B	LaRonde-Penna 20N Au	Au-rich VMS	1.23	2.5	-0.07
D167171	LaRonde-Penna 20N Au Al	Au-rich VMS	1.39	2.7	-0.01
D167173	LaRonde-Penna 20N Au Al	Au-rich VMS	1.37	2.8	-0.06
D167174	LaRonde-Penna 20S	Au-rich VMS	0.84	1.8	-0.08
D167175C	LaRonde-Penna 20S	Graphitic Argillite	4.01	8.8	-0.52
D167176	LaRonde-Penna 20S	Au-rich VMS footwall	2.21	5.9	-0.81
D167177A	LaRonde-Penna 20S	Au-rich VMS	0.41	1.1	-0.16
D167179	LaRonde-Penna 20N Au	Au-rich VMS	1.29	2.6	-0.02
D167181	LaRonde-Penna 20N	Graphitic Argillite	1.10	2.8	-0.34
D167182A	LaRonde-Penna 20N Zn	Au-rich VMS	0.40	0.8	-0.02
D167184	LaRonde-Penna 20S	Cad-BR Contact	1.56	5.1	-1.04
D167185	LaRonde-Penna Zone 7	Au-rich VMS	1.65	3.8	-0.29
D167199	LaRonde-Penna 20N Au Al	Au-rich VMS	1.29	2.6	-0.03
D181001	LaRonde-Penna 20N Au Al	Au-rich VMS	1.36	2.7	-0.04
D181003A	Bousquet 2-Dumagami	Cad-BR Contact	1.26	5.2	-1.43
D181009	Ellison	Au-rich VMS	1.38	2.7	-0.03
D181010	Ellison	Au-rich VMS	1.19	2.4	-0.03
D181011A	Bousquet 1	Cad-BR Contact	2.90	8.2	-1.31
D181011B	Bousquet 1	Cad-BR Contact	4.06	10.0	-1.08
D181013	Bousquet 1	Au-rich VMS	0.47	1.0	-0.03
D181015	Bousquet 1	Au-rich VMS	1.77	3.5	-0.01
DGPL-2007-001A	Doyon Zone 1	Intrusion-related	0.90	1.7	0.00
DGPL-2007-003	Doyon Zone 2	Intrusion-related	1.14	2.2	-0.01
DGPL-2007-005	Doyon West Zone	Intrusion-related	1.61	3.1	0.00
MM04	Mouska Type 3	Shear-hosted	1.74	3.7	-0.14
MM06CP	Mouska Type 2	Shear-hosted	2.36	4.6	0.00
MM07A	Mouska Type 2	Shear-hosted	2.61	5.1	0.00
MM07B	Mouska Type 1	Shear-hosted	1.18	2.3	-0.02
MM10	Mouska Type 3	Shear-hosted	1.00	2.0	-0.02

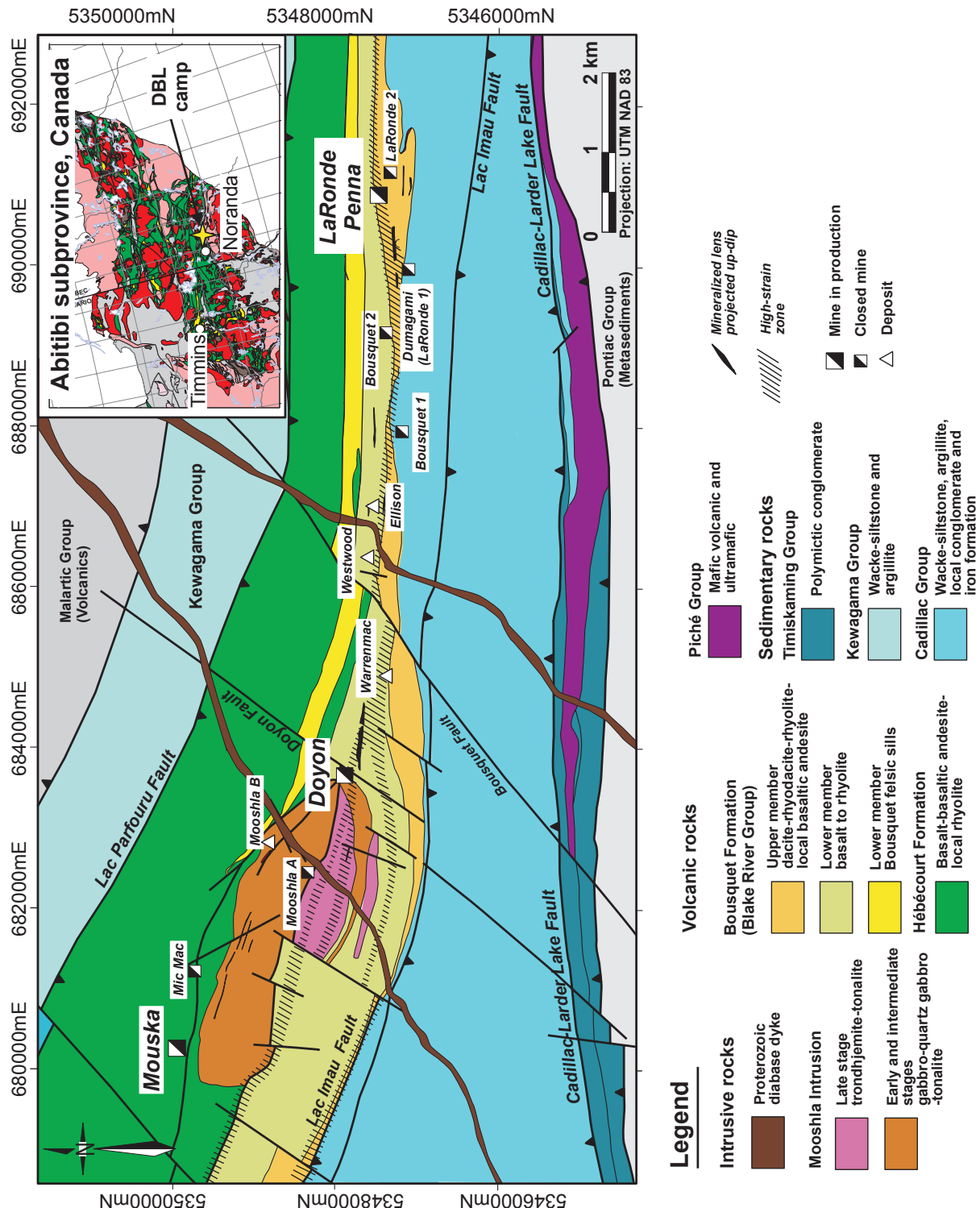


Fig. 3.1: Simplified geological map of the Doyon-Bousquet-LaRonde mining camp, showing its location (inset map) within the Abitibi subprovince (modified from (Mercier-Langevin et al., 2007c).

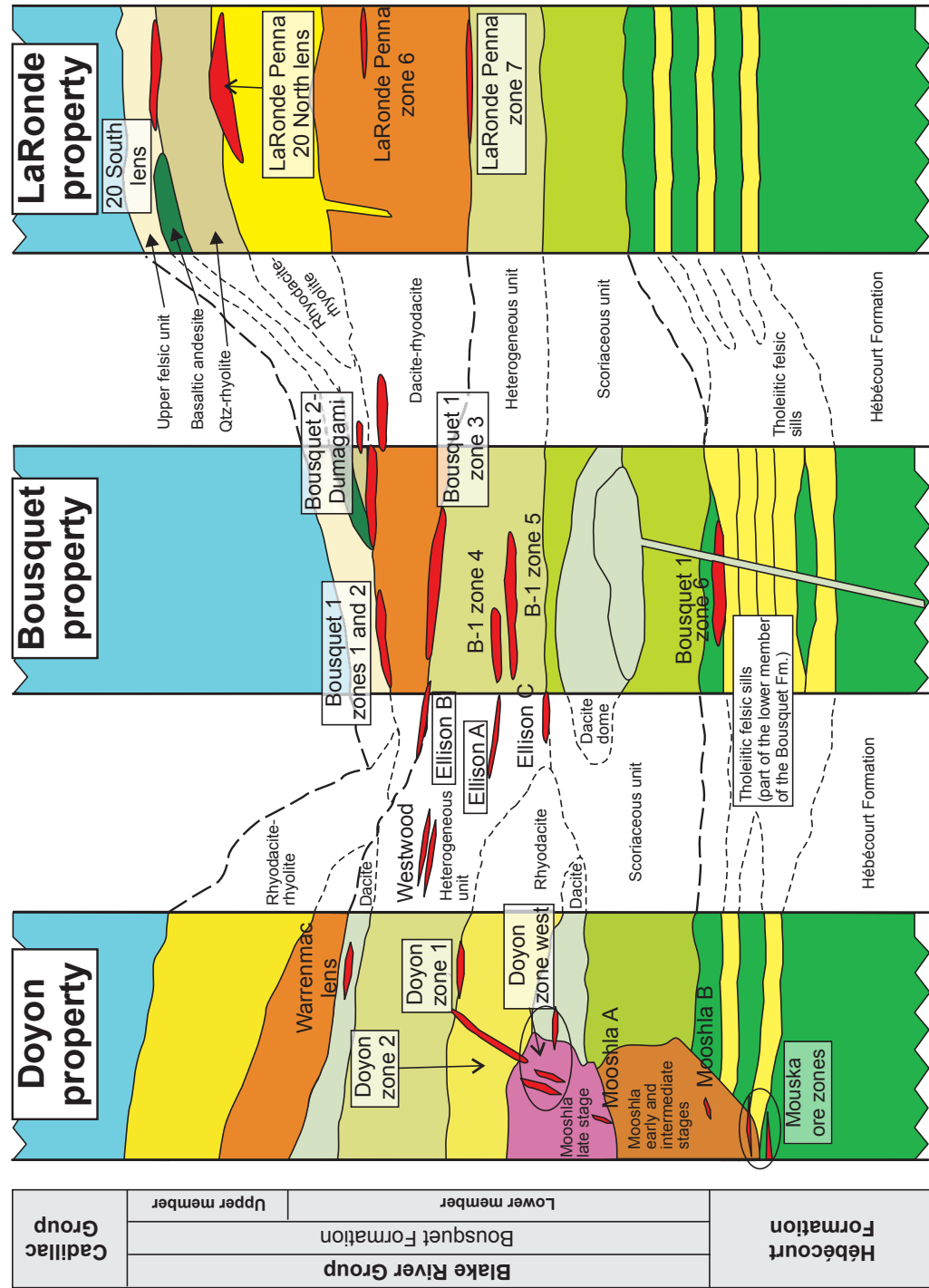


Fig 3.2: Simplified stratigraphic cross sections through the Doyon-Bousquet-LaRonde mining camp, including the stratigraphic setting of the major ore lenses within the camp (modified from (Mercier-Langevin et al., 2007c). The names of sampled deposits are framed.

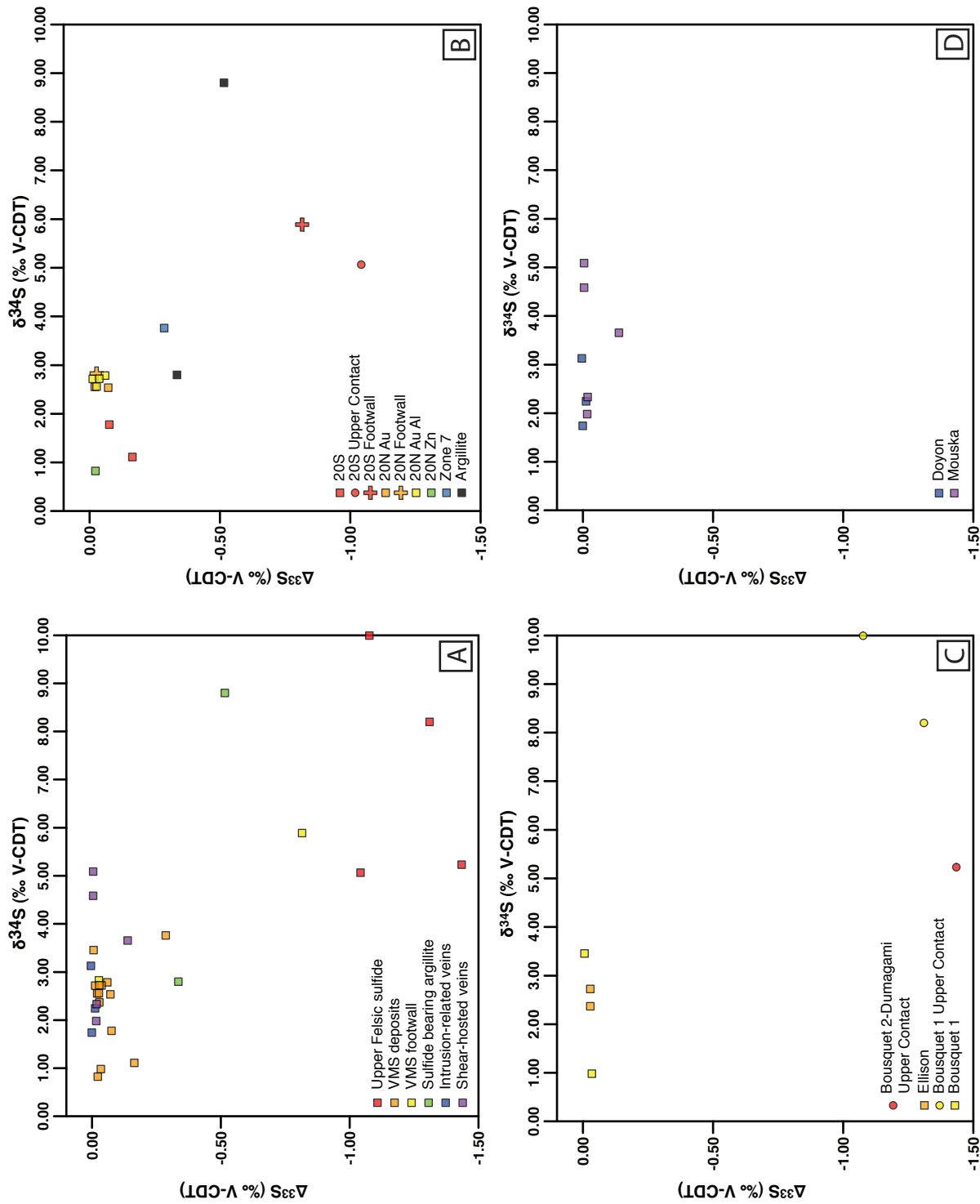


Fig. 3.3: Plots of $\delta^{34}\text{S}$ vs. $\Delta^{33}\text{S}$ for sulfides from the Doyon-Bousquet-LaRonde mining camp represent all samples analyzed. The 1σ uncertainties for $\delta^{34}\text{S}$ and $\Delta^{33}\text{S}$ are 0.13‰ , and $\pm 0.01\text{‰}$, respectively. A) All samples, divided by deposit type or stratigraphic location. B) Samples from the LaRonde-Penna deposits, categorized by major ore lens or stratigraphic location. C) Samples from all Au-rich VMS deposits in the DBL camp, except the LaRonde-Penna deposits, categorized by major ore lens or stratigraphic position. D) Samples represent intrusion-related (Doyon) and shear-hosted vein (Mouska) deposits.

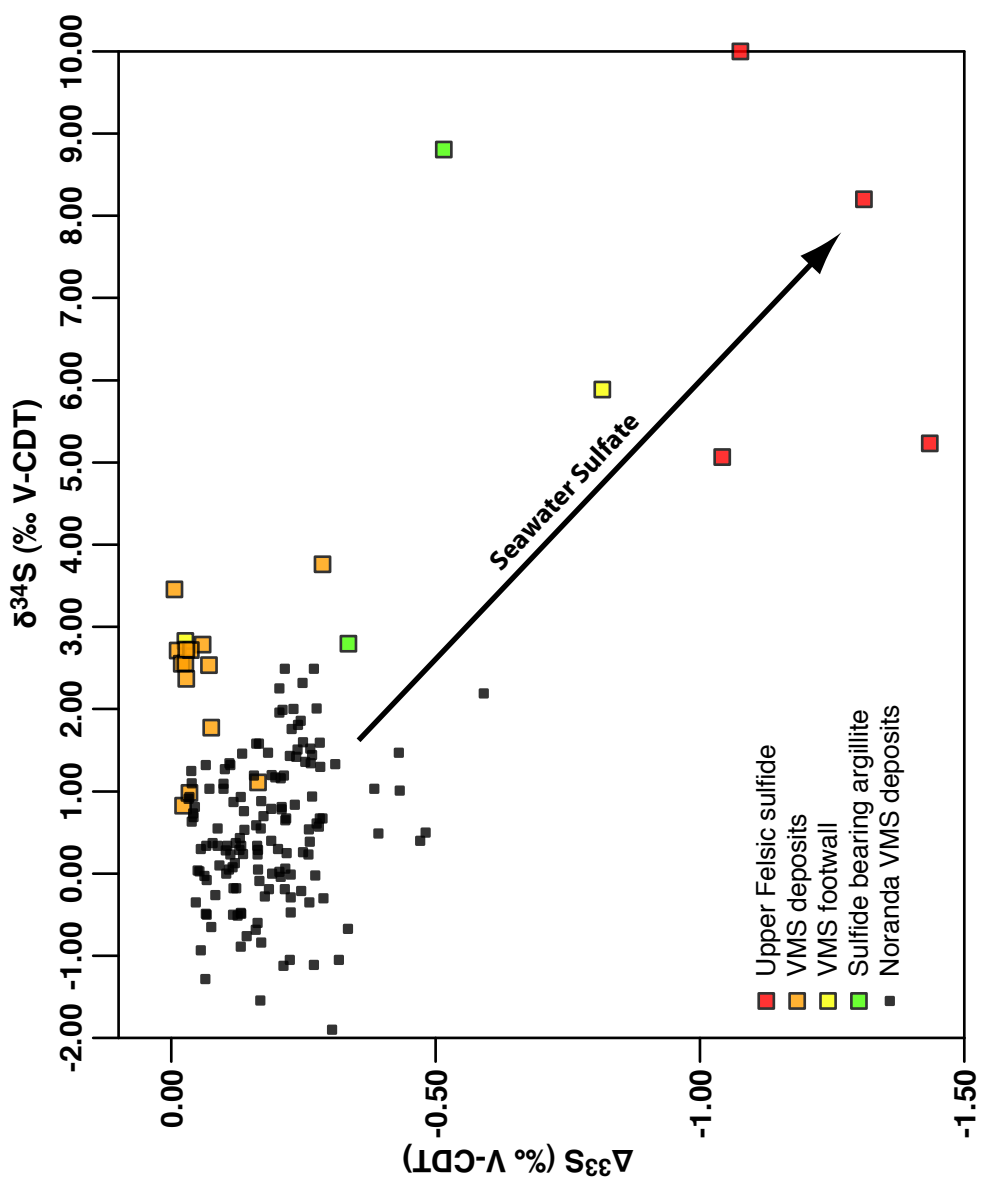


Fig. 3.4: Binary diagram showing $\delta^{34}\text{S}$ values vs. $\Delta^{33}\text{S}$ values for sulfides from the Doyon-Bousquet-LaRonde mining camp divided by deposit type or stratigraphic location as well samples from the Noranda VMS camp (data from Chapter 2, this thesis) ($\delta^{34}\text{S}$: $1\sigma = \pm 0.13\text{‰}$, $\Delta^{33}\text{S}$: $1\sigma = \pm 0.01\text{‰}$).

PREFACE TO CHAPTER FOUR

The previous two chapters have highlighted the application of multiple sulfur isotope data to ore-forming systems in which surficial sulfur has been incorporated through hydrothermal circulation. However, this is not the only method by which surficial sulfur can contribute to an ostensibly magmatic-dominated system. One of the most significant mechanisms for forming immiscible sulfide liquids during the emplacement of magmatic ore deposits is through the addition of sulfur from a crustal source (Naldrett, 2004).

The 2.05 Ga Platreef magmatic Ni-Cu-PGE deposit, in the northern limb of the Bushveld Igneous Complex, is one ore-forming system for which this mechanism has been invoked. This is due to its direct contact with underlying Neoarchean to Paleoproterozoic sediments, as well as its high percentage of sulfide relative to the analogous Merensky Reef in the eastern and western limbs of the Bushveld Igneous Complex. However, this interpretation has been questioned by other workers, who attribute the mineralization of the Platreef to solely magmatic processes. This chapter examines the magnitude, extent and likely origin of the crustal contribution of sulfur to the Platreef.

Naldrett, A.J., 2004, Magmatic Sulfide Deposits Geology, Geochemistry and Exploration. Springer, 727 p.

CHAPTER FOUR

Elucidation of multiple sulfur contamination events in Ni-Cu-(PGE) mineralization: $\Delta^{33}\text{S}$
evidence from the Platreef, Bushveld, South Africa.

E. R. SHARMAN, S. C. PENNISTON-DORLAND, B. A. WING,
J. A. KINNAIRD, P. A. M. NEX, M. BROWN AND J. FARQUHAR

4.1 Abstract

Sulfur isotope analyses have been used by researchers to identify sulfur sources for sulfides within Ni-Cu-(PGE) deposits. However, traditional ($\delta^{34}\text{S}$) sulfur isotope analyses often do not give definitive answers. Mass-independent fractionation (MIF) of sulfur isotopes is a process that is thought to have occurred predominantly in the Archean atmosphere. Isotopic anomalies, expressed as non-zero $\Delta^{33}\text{S}$ values, produced by MIF, indicate the presence of atmosphere- or hydrosphere-derived sulfur. In this study, we test, on a deposit-wide scale, the model proposed by Penniston-Dorland et al. (2008) for formation of sulfides within the Platreef, the main PGE bearing horizon of the Northern Limb of the Bushveld Complex, South Africa. In contrast to this model, which proposes that the only contribution of footwall sulfur in the Platreef occurred post-emplacement, and within 5 meters of the footwall contact, we identify pre-emplacement contamination as the main process that led to formation of sulfides within the Platreef. Multiple sulfur isotope data not only record contributions of non-magmatic sulfur up to 100m from the

footwall contact, but also illustrate that contamination was unlikely to have originated from the immediate footwall.

4.2 Multiple sulfur isotopes and Ni-Cu-(PGE) mineralization in the Platreef

The presence of an immiscible sulfide liquid plays a controlling role in all models for magmatic Ni-Cu-(PGE) deposits, with the sulfide melt partitioning metals from an accompanying silicate melt and thereby forming economic concentrations of Ni, Cu, and Platinum Group Elements (PGEs). Most of the silicate magmas associated with Ni-Cu-(PGE) mineralization appear to have originally been sulfur-undersaturated (Lesher and Burnham, 2001), however. The formation of an immiscible sulfide liquid within a parent silicate melt requires sulfide saturation to be exceeded, with the two main mechanisms for achieving saturation being the addition of either sulfur or silica to a mafic magma from the host country rocks (Naldrett, 2004). Sulfur stable isotope analysis has been promoted as an ideal technique to fingerprint the relative contribution of externally derived sulfur to the saturation processes, as the isotopic variability of primary magmatic S is quite limited relative the sulfur isotope variability of most host rocks (e.g., Ripley and Li, 2003). Conventional sulfur isotope analyses ($\delta^{34}\text{S} = [({}^{34}\text{S}/{}^{32}\text{S})_{\text{sample}} / ({}^{34}\text{S}/{}^{32}\text{S})_{\text{standard}} - 1] \times 1000$), however, has led to conflicting views on the role of crustal sulfur in driving sulfide saturation in the Platreef, a magmatic Ni-Cu-(PGE) deposit in the northern limb of the Bushveld Igneous Complex, South Africa, the world's third largest PGE deposit, after two other PGE horizons within the Bushveld Complex (the Merensky Reef and the UG2; Cawthorn, 1999).

The Platreef is the main platinum group element (PGE)-bearing horizon of the northern limb of the Bushveld Igneous Complex (Fig. 4.1). The northern limb is a slightly sinuous, north-west striking, layered intrusive igneous sequence, with a length of 110 km (Armitage et al, 2002), and is typically divided into southern, central, and northern sectors (Fig. 4.1). The Platreef occurs at the base of the igneous sequence and has an unconformable, transgressive relationship to the underlying footwall rocks: footwall rocks become successively younger to the south (Fig. 4.1).

Various footwall lithologies have been proposed to contribute crustal sulfur to the Platreef magma during post-emplacement contact metamorphic alteration of the country rocks, triggering sulfide saturation within the magma. These putative sources include anhydrite within the Malmani Subgroup in the central sector of the Platreef (Buchanan et al., 1981, Buchanan and Rouse, 1984); crustal sulfur from an unidentified source on the Farm Townlands in the southern sector of the Platreef (Manyeruke et al., 2005); and crustal sulfur contamination associated with footwall xenoliths, having various sulfur sources depending on footwall composition, in both the southern and northern sectors of the Platreef (Sharman-Harris et al., 2005). In contrast, other studies have postulated that no externally derived crustal sulfur was added to the Platreef system and that formation of sulfides was a purely magmatic process (Liebenberg, 1968; Hulbert, 1983; Barton et al., 1986; Holwell and McDonald, 2006). Temporal considerations may reconcile these hypotheses, such that early-formed sulfides have near magmatic $\delta^{34}\text{S}$ values and reflect sulfur saturation of the Platreef magma prior to intrusion, while later-formed sulfides exhibit a wider range of $\delta^{34}\text{S}$ values, suggesting that contamination by footwall material occurred on strictly a local scale, upgrading pre-existing sulfide (Holwell et al., 2007).

In spite of the clear record of crustal contamination in the Platreef parental magmas from oxygen isotopes (Harris and Chaumba, 2001) and Os isotopes (Reisberg et al., 2011), $\delta^{34}\text{S}$ data provide a more equivocal view of the role of crustal contamination during formation of the Platreef. While this is in part due to the complex local geological environment of the Platreef, the susceptibility of $\delta^{34}\text{S}$ values to modification by magmatic (Ripley and Li, 2003) and hydrothermal processes (Penniston-Dorland et al., 2008), and the lack of distinct isotopic contrast between the magma and potential contaminants also play a role. A tracer that could directly document the incorporation of crustal sulfur into a magmatic system of this age, in spite of the processes that might occur after incorporation, has great promise for understanding the Platreef mineralization system.

During the Archean Eon (>2.45 Ga), lack of an oxygenated atmosphere allowed for the MIF of sulfur isotopes during atmospheric photochemical reactions (Farquhar et al., 2001). This isotopic fractionation mechanism can be fingerprinted by measurement of $\delta^{33}\text{S}$ ($\delta^{33}\text{S} = [({}^{33}\text{S}/{}^{32}\text{S})_{\text{sample}} / ({}^{33}\text{S}/{}^{32}\text{S})_{\text{standard}} - 1] \times 1000$) in addition to $\delta^{34}\text{S}$, and is quantified as $\Delta^{33}\text{S}$ ($= \delta^{33}\text{S}_{\text{measured}} - \delta^{33}\text{S}_{\text{predicted}}$, where $\delta^{33}\text{S}_{\text{predicted}} = [\delta^{34}\text{S}_{\text{measured}} + 1]^{0.515} - 1$). Under current working models for the Archean sulfur cycle, mass-independent fractionation ($\Delta^{33}\text{S} \neq 0$) is fundamentally an atmospheric process. A non-zero $\Delta^{33}\text{S}$ value, therefore, indicates the presence of sulfur that cycled through the Archean atmosphere (Farquhar and Wing, 2003). Preservation of non-zero $\Delta^{33}\text{S}$ values through the geological S cycle (e.g., metamorphism, crustal assimilation) should occur with high-fidelity in spite of $\delta^{34}\text{S}$ fractionation, unless mixing processes occur that lead to a dilution of the $\Delta^{33}\text{S}$ signature. This property implies that multiple sulfur isotope analyses may provide a definitive and sensitive tool for identifying crustal sulfur contributions in Archean ore

deposits under certain circumstances.

Previous multiple sulfur isotope investigations on the Platreef focused on evaluating the local transfer of sulfur across the Platreef-footwall contact, as well as on the processes that enabled that transfer (Penniston-Dorland et al., 2008). At least at the locations studied in detail (Farms Tweefontein and Sandsloot), the Platreef magma appeared to be sulfur-saturated prior to emplacement, leading to sulfur transfer, and displacement of $\Delta^{33}\text{S}$ profiles, from the Platreef into the surrounding country rocks. Counter intuitively, however, a small crustal contribution of sulfur to the Platreef sulfides accompanied this process. This enrichment was likely associated with back diffusion against the overall advection of sulfur out of the Platreef, limited to within ~5m of the footwall contact, and not a major mechanism for sulfide mineralization (Penniston-Dorland et al., 2008). In this study, we use $\Delta^{33}\text{S}$ analyses to test this ‘contact source’ model along the full ~100 km strike length of the Platreef, as well as to evaluate the spatial and temporal variability of crustal sulfur incorporated into the immiscible sulfide melt which segregated to form the Platreef sulfide ores.

4.3 Regional Geology of the Platreef

The ca. 2.06 Ga (Buick et al., 2001) Platreef is a highly inhomogeneous body, comprising pyroxenite, feldspathic pyroxenite (pyroxenites with >10% interstitial plagioclase), gabbro-norite, norite; as well as altered versions of these rocks (serpentinite); and physical mixtures of these rocks with highly altered rocks of the Platreef footwall (‘para-pyroxenites’; Kinnaird, 2005). In the north, the footwall comprises Archean granites, followed southward by members of the 2.67 to 2.07 Ga

Transvaal Supergroup sedimentary sequence (Fig. 4.1; Coetzee, 2001, Eriksson et al., 2001). These comprise, from north to south, the Malmani Subgroup (limestone, chert-rich, and chert-poor dolomite), the Penge Formation (predominantly quartz-, magnetite- and hematite-rich rocks interlayered with minor, carbonaceous shale), the Duitschland Formation (dominated by fine-grained, laminated shale and marl with thick dolomite beds more common in the upper part of the formation), and the Timeball Hill Formation (Fig. 4.1). The Platreef also contains xenoliths of a variety of altered footwall rocks, including hornfels derived from shale protoliths, and calc-silicate assemblages, derived from dolomites (Sharman-Harris et al., 2005).

The base- and precious-metal mineralization of the Platreef is unevenly distributed, and occurs over a zone that is up to 400 m thick. Sulfide minerals occur throughout the succession, however, and are generally centimetre- to millimetre-sized blebs and interstitial grains of pentlandite, pyrrhotite and chalcopyrite. A wide range of accessory minerals are also present, including sphalerite, galena, molybdenite, pyrite, chalcocite, and covellite (Hutchinson and Kinnaird, 2005, Holwell et al., 2007). Where present, zones of massive sulfide rich in chalcopyrite may be found close to the footwall contact. Sulfide mineralization also occurs in the metamorphosed footwall of the Platreef. Compositionally complex sulfides are associated with felsic melt phases that pervasively infiltrated the Platreef soon after its partial or complete crystallization (Hutchinson and Kinnaird, 2005). Varied platinum group minerals, including tellurides, bismuthotellurides, antimonides and arsenides, along with sulfides, characterize PGE mineralization. Post-emplacement hydrothermal remobilization of the contained PGEs has been proposed (Hutchinson and McDonald, 2008)

4.4 Sample selection and sulfur isotope analysis

Samples for this study were collected from diamond drill hole cores from the northern and southern sectors of the Platreef (Fig. 4.1), and were chosen to represent as many different footwall lithologies, and varying distances from the footwall contact, as possible. Sulfur isotope analyses were conducted using either whole-rock samples, or sulfide mineral separates. Multiple sulfur isotope analyses were conducted at the University of Maryland. Sulfide mineral separates were converted to SF₆ gas by laser heating of separated sulfides under an F₂ atmosphere, following the methods of Hu et al. (2003). Whole-rock samples were crushed, and then reacted with a Cr-reducing solution that allowed the liberation of H₂S gas (Canfield et al., 1986). This H₂S was subsequently converted to solid Ag₂S by trapping the H₂S in a zinc acetate solution and reacting the ZnS that precipitated with AgNO₃. The Ag₂S precipitate was then rinsed with >18.2 MΩ cm⁻¹ ultra-pure water and 1M NH₄OH and dried, before being reacted in a nickel vessel in the presence of excess F₂ to produce SF₆. The SF₆ resulting from both of the above procedures was purified first cryogenically and then by gas chromatography. Purified SF₆ was introduced to a ThermoFinnigan MAT 253 dual-inlet gas-source mass spectrometer, and sulfur isotope abundances were measured by monitoring the ³²SF₅⁺, ³³SF₅⁺, ³⁴SF₅⁺ ion beams at mass to charge ratios of 127, 128, and 129, respectively. Sulfur isotopic measurements are reported on the Vienna-Cañon Diablo Troilite (V-CDT) scale, on which the isotopic composition of the international reference Ag₂S material IAEA-S-1 has a defined δ³⁴S value of -0.3‰ (Robinson, 1995). We take IAEA-S-1 to have a Δ³³S value of 0.094‰. The analytical precision (1σ) for sulfide mineral separates

is estimated to be $\pm 0.29\text{‰}$ for $\delta^{34}\text{S}$ and $\pm 0.02\text{‰}$ for $\Delta^{33}\text{S}$, based on the standard deviation of multiple analyses of an in-house pyrite standard (P1), conducted over a period of more than five years.

4.5 Results: Multiple sulfur isotope composition of the Platreef and environs

Multiple sulfur isotope compositions of samples from the Platreef and its footwall are listed in Table 4.1. In general, $\delta^{33}\text{S}$ and $\delta^{34}\text{S}$ values throughout the Platreef show similar ranges ($\delta^{34}\text{S}$: approximately +1 to +13‰, $\delta^{33}\text{S}$: approximately +1 to +7‰), although samples from the southern sector have a slightly smaller range than those from the central and northern sectors of the Platreef. In contrast, the footwall and xenolith samples show greater variation. Sulfur from calc-silicate rocks in the northern and central sectors have positive $\delta^{33}\text{S}$ and $\delta^{34}\text{S}$ +0.7 to +8.2‰ and, in the southern sector, have $\delta^{33}\text{S}$ and $\delta^{34}\text{S}$ values ranging from +14.7 to +28.7‰. Hornfels xenoliths record the broadest range, and the only negative, values of $\delta^{33}\text{S}$ and $\delta^{34}\text{S}$, from -10.7 to +9.6‰ and -20.9 to +18.1‰, respectively.

Within the southern, central and northern sectors of the Platreef, $\Delta^{33}\text{S}$ data exhibits some variation, but all within the range of +0.06 to +0.58‰. The range of $\Delta^{33}\text{S}$ in footwall lithologies is very limited, possibly due to the sampling density. However, $\Delta^{33}\text{S}$ values for both hornfels and calc-silicate footwall samples from the central sector show more extensive variation, with $\Delta^{33}\text{S}$ values as high as +5.04‰.

4.6 Life history of sulfur in Platreef ore sulfides

The $\Delta^{33}\text{S}$ and $\delta^{34}\text{S}$ characteristics of the Platreef dataset are consistent with significant contributions of sulfur from Archean crustal sources. In this section we discuss the spatial relationships among $\Delta^{33}\text{S}$ values in Platreef ore sulfides and in the associated footwall, for example, illustrate the scale and original location of the incorporation process. In addition, the covariation of $\Delta^{33}\text{S}$ and $\delta^{34}\text{S}$ values in the ore sulfides fingerprints the ultimate crustal sources of the incorporated sulfur. Finally, the sensitivity of the final $\Delta^{33}\text{S}$ values in the ore sulfides records an integrated history of interaction between the immiscible sulfide melt that concentrated Platreef PGEs and the silicate melt that was the ultimate PGE source.

4.6.1 Spatial record of sulfur contamination

Previous studies on the interaction between the Platreef magmas and their footwall have implied that relatively limited material exchange occurred between the Platreef, the immediate footwall, and footwall-derived xenoliths during emplacement (Sharman-Harris et al., 2005; Holwell et al., 2007; Penniston-Dorland et al., 2008). Direct incorporation of footwall-derived sulfur, for example, seems to have been limited to within 5 m from the footwall contact (Penniston-Dorland et al., 2008). These characteristics suggest a pair of tests for evaluating whether purely local interactions have controlled the sulfur isotopic characteristics of the current dataset. First, $\Delta^{33}\text{S}$ values in ore sulfides far away from any footwall material should be comparable to those from barren Platreef igneous rocks ($\Delta^{33}\text{S} = 0.15 \pm 0.04 \text{ ‰}$; Penniston-Dorland et al., 2008). Second, there should be a limiting relationship between the maximum $\Delta^{33}\text{S}$ values at any location within the Platreef sulfide

deposit and the $\Delta^{33}\text{S}$ values of the immediate footwall to the deposit at that location. On a comparative plot of $\Delta^{33}\text{S}_{\text{Platreef}}$ against $\Delta^{33}\text{S}_{\text{Footwall}}$, no ore sulfide sample should plot above a line with a slope of unity.

While some of the localities in Table 4.1 pass the distance test for localized interaction (mostly previously published analyses from Penniston-Dorland et al., 2008), others do not. For example, the Platreef samples on Farm Turfspruit (core ATS-57) have $\Delta^{33}\text{S}$ values of +0.57‰ occurring approximately 100m from the footwall contact. Similarly, the graphical test indicates localized interaction was the norm at some localities (Sandsloot, Tweefontein North, Rietfontein), whereas it appears not to have been so at others (Turfspruit, Drenthe, Overysel; Fig. 4.2). As Platreef samples taken from these localities exhibit $\Delta^{33}\text{S}$ values that are higher than those of the immediate footwall, incorporation of local footwall sulfur cannot have been the sole mechanism by which the Platreef magma was enriched in sulfur. Sulfur from an additional, allochthonous crustal source must have been incorporated into the Platreef magma at some point during its evolution.

4.6.2 Ultimate sources of S contamination

The identity of additional sulfur sources within the Platreef can be assessed by comparison of the $\Delta^{33}\text{S}$ and $\delta^{34}\text{S}$ values of reasonable sulfur sources within the Platreef district. Country rocks local to the Platreef deposit exhibit a wide range of $\Delta^{33}\text{S}$ and $\delta^{34}\text{S}$ values (Fig. 4.3). The country rock data can be grouped into four distinct categories: 1) ^{34}S -depleted, mass-dependently fractionated sulfur isotope compositions (dominantly Timeball Hill shales and siltstones); 2) ^{34}S -enriched, mass-dependently fractionated

sulfur isotope compositions (Upper Duitschland carbonates); 3) largely $\delta^{34}\text{S}$ -enriched, MIF sulfur isotope compositions (Malmani dolomites and Lower Duitschland shales); and 4) those which we infer to have uniform near-zero $\delta^{34}\text{S}$ and $\Delta^{33}\text{S}$ values (basement granite).

Metamorphic rocks from the immediate footwall to the Platreef show a slightly contracted range in $\delta^{34}\text{S}$ values, but a more extended variability in $\Delta^{33}\text{S}$ values relative to unaltered country rocks (Fig. 4.3). These minor differences are likely a result of original sedimentary heterogeneity. In general, the sulfur isotope compositions of the metamorphosed footwall rocks are comparable with the isotopic compositions of identified unmetamorphosed protoliths. For example, the footwall contains calc-silicate marbles that clearly either originated either as Malmani dolomites or siliceous carbonates from the Upper Duitschland formation (Fig. 4.3). Similarly, footwall hornfels can be divided into those with protoliths from the Lower Duitschland formation, and those with affinities for the Timeball Hill shales (Fig. 4.3). Preservation of the original sedimentary sulfur isotope signatures through the contact metamorphic process suggests that a similar exercise may be able to identify the ultimate sources of the crustal sulfur in the Platreef sulfides.

On a $\Delta^{33}\text{S}$ versus $\delta^{34}\text{S}$ plot, Platreef sulfides occupy only the quadrant with positive $\delta^{34}\text{S}$ and $\Delta^{33}\text{S}$ values (Fig. 4.4). The sulfur isotope compositions of the sedimentary country rock, together with the measured sulfur isotope compositions of unmineralized Platreef magmatic sulfides ($\delta^{34}\text{S} = 2.0 \pm 0.9 \text{ ‰}$, $\Delta^{33}\text{S} = 0.15 \pm 0.04 \text{ ‰}$; Penniston-Dorland et al., 2008), offer a straightforward framework for interpreting this data. There is no preserved evidence for sulfur contributions to the Platreef sulfides from the ^{34}S -depleted Timeball Hill shales and siltstones (Fig. 4.4). Sulfur in the Platreef

sulfides, instead, appears to reflect a mixture of sulfide from the Platreef silicate melt together with sulfur from the lower part of the footwall stratigraphy (Fig. 4.4). When examined in a north to south framework, along strike variation in the apparent proportions of these sources is revealed.

Farm Drenthe, the northernmost property sampled, is underlain by Archean granite footwall. Sulfur isotope analyses of the Platreef reflect dominantly a silicate magmatic source, with some contribution from either the Malmani dolomite or the Lower Duitschland shale. Next to the south, on Farm Overysel, sulfur appears to have been contributed from the same three sources, with perhaps a slightly larger contribution of sulfide from the silicate melt. In the central sector of the Platreef, the main contributors of sulfur in the sulfides sampled on Farm Sandsloot are Upper Duitschland carbonate and Malmani dolomite, with a comparatively smaller silicate magmatic contribution (cf. Penniston-Dorland et al., 2008). Sulfides from Farm Tweefontein North appear to be derived from a dominantly binary mixture of sulfur from silicate magmatic rocks and sulfur from the Upper Duitschland carbonates. Samples analyzed from the southern sector (Farms Turfspruit and Rietfontein) appear to reflect a near binary source mixture as well, with a MIF source of sulfur (most likely Lower Duitschland shales or Malmani carbonates).

When extending the interpretations of the previous section to the deposit scale, there does not appear to be a direct association between proposed sulfur sources for the Platreef sulfides and the underlying footwall (Fig. 4.1). A complication to this interpretation could be sulfur sourced from the abundant footwall xenoliths in the Platreef. However, these come mainly from the local footwall (Sharman-Harris et al,

2005), and so xenolith-sourced sulfur is not a likely explanation for the observations made here. ‘Downstream’ transport of sulfur sourced as the Platreef magma traversed the local footwall during emplacement is also an unlikely explanation for the sulfur isotopic heterogeneity. While there is some hint of a consistent offset between the isotopic compositions of the Platreef sulfides and the footwall rocks to the South (i.e., the inferred ‘downstream’ direction during emplacement; Kinnaird et al., 2005), sulfides from some of the most northerly localities (e.g., farm Drenthe) preserve contributions from some of the most southerly footwall rocks (i.e., the upper Duitschland carbonates, Fig. 4.4).

4.6.3 $\Delta^{33}\text{S}$ constraints on silicate melt:sulfide melt mass ratios

Taken together, the discussions in the two preceding sections suggest that the Platreef magma was exposed to crustal material prior to its final emplacement. Pre-emplacement contamination occurred within sedimentary rocks of the Transvaal Supergroup, and can be pinpointed to strata within the Malmani Dolomite and Duitschland formation specifically (Fig. 4.4). The well-characterized sulfur isotope systematics of these stratigraphic intervals (Guo et al., 2008), as well as the precise estimates available for the final sulfur isotopic composition of the Platreef silicate magma, enable us to use generalized mass balance expressions (Lesher and Burnham, 2001) to constrain the mass ratios of silicate melt to sulfide melt (R factors; Campbell and Naldrett, 1979) responsible for setting the final isotopic distribution of the Platreef sulfides.

We use the following expression to estimate sulfur isotope-based R factors (R_S):

$$R_S = \frac{\Delta^{33}\text{S}_{\text{sul}}^{\text{i}} - \Delta^{33}\text{S}_{\text{sul}}^{\text{f}}}{\Delta^{33}\text{S}_{\text{sil}}^{\text{f}}} \times \frac{C_{S,\text{sul}}}{C_{S,\text{sil}}} \quad (1)$$

where the subscript ‘sul’ refers to the sulfide melt, the subscript ‘sil’ refers to the silicate melt, the subscript ‘S’ refers sulfur, the superscript ‘i’ refers initial quantities, the superscript ‘f’ refers final quantities, and C is concentration. This calculation assumes that an initial sulfide “xenomelt” (see Lesher and Burnham, 2001) forms from interaction between the wall rocks and a silicate magma and the initial silicate magma has a primary $\Delta^{33}\text{S}$ value of 0‰ (Farquhar et al., 2001). It reflects the amount of silicate magma that interacted with the sulfide melt in order to impart the observed $\Delta^{33}\text{S}$ values of the Platreef or sulfides, integrated over entire history of the interaction. Similar expressions can be used for $\delta^{34}\text{S}$ values (Ripley and Li, 2003). We do not attempt a coupled R_S analysis but, instead, assume that all dilution of the initial $\Delta^{33}\text{S}$ value of the sulfide “xenomelt” is due to interaction with the silicate melt. Our estimates are therefore probably maxima. In order to constrain the range of likely R_S values, we use the average $\Delta^{33}\text{S}$ value of the Platreef sulfides from each locality, as well as the average $\Delta^{33}\text{S}$ values from the potential mass-independent contaminants (shales of the Lower Duitschland formation and the Malmani Dolomite). We assume that the average Platreef silicate magma has a sulfur concentration of 300 ppm by mass (Ihlenfeld and Keays, 2011), while the sulfur concentration in the sulfide xenomelt is 38 weight % (Lesher and Burnham, 2001). We note that the first term in equation (1) cannot be less than one as $\Delta^{33}\text{S}$ values are chemically conservative, and cannot be magnified during geological processing.

Estimates of R_S for an initial xenomelt originating from the lower Duitschland shales range from 3400 to 6500 for the different sample localities, with an average of 4900. Assuming that the xenomelt originated from the sulfides associated with Malmani dolomite yields R_S estimates of 11300 to 14400, with an average of 12700. We recognize

that these calculations do not take into account the potential for contact enhancement of the $\Delta^{33}\text{S}$ values in the Platreef (Penniston-Dorland et al., 2008) which would lead to artificially low estimated R_S values. However, R_S estimates for the two localities where this process has been proposed (Sandsloot and Tweefontein North) lie within the middle of the calculated range. We suggest that this range of R_S values, therefore, provides a representative estimate for the Platreef as a whole, as well as a natural explanation for the enigmatic elevated $\Delta^{33}\text{S}$ values found for barren Platreef igneous rocks (Penniston-Dorland et al., 2008). The range of R factors derived here is remarkably consistent with the range of R factors estimated from comparison of Platreef Cu contents, Pd contents, and S to Se ratios (Figs. 6 and 8 of Ihlenfeld and Keays, 2011). This suggests that critical components of the Platreef ore (PGEs and sulfur) must share a common life history.

4.7 Conceptual model of Platreef mineralization

Our interpretations of the new $\Delta^{33}\text{S}$ dataset are most easily explained if the immiscible sulfide melt that is now represented by the Platreef ore sulfides originally formed in a ‘staging chamber’ prior to final emplacement. Numerous lines of evidence have been used to reach similar conclusions in other recent studies of the Platreef (Kinnaird, 2005; Holwell et al., 2007; McDonald et al., 2009; Ihlenfeld and Keays, 2011; Reisberg et al., 2011). Based on detailed geochemical analyses, Kinnaird (2005) suggested that the Platreef intruded into the Upper Transvaal Supergroup as several pulses of magma, rather than one individual event. If local, post-emplacement contamination during these intrusive events were the only external source of sulfur to the Platreef system, or if emplacement of the Platreef were by a single event, sulfur isotope

data should closely reflect the local footwall compositions. However, our observations indicate that contamination by crustal material did not solely occur post-emplacement. Hence, contamination of the Platreef magma by crustal material occurred prior to final emplacement, and heterogeneity in sulfur sources between different intrusive events has been preserved.

Ponding of initial pulses of magma may have led to enhanced melting of surrounding host rocks, thereby contaminating the ponded magma to a greater degree by crustal sulfur. This initial contamination sufficiently enriched the Platreef magma to allow sulfide saturation and the formation of an immiscible sulfide liquid. If the initial contaminant were shales of the lower Duitschland formation, then sulfide saturation may have resulted from the combined effects of sulfur and silica addition. As subsequent pulses of silicate magma traveled past the initial immiscible sulfide xenomelt, sulfur isotope exchange may have caused an evolution of the multiple sulfur isotope, and mass-independent fractionation signature, towards the primary magmatic end member (cf., Ripley and Li, 2003). Once emplaced, the sulfides within the Platreef may have been further enriched by local contamination by footwall material, but this was not a major component to the sulfur within the Platreef sulfides.

This model is supported by previous oxygen isotope data (Harris and Chaumba, 2001) that were interpreted to indicate a staging chamber mechanism, followed by minimal local contamination during evolution of the Platreef silicates. Detailed $\delta^{34}\text{S}$ associated with specific petrographically-classified sulfides also support sulfide saturation occurring within a staging chamber (Holwell et al., 2007). An investigation of the Lower Zone Complex at Zwartfontein by McDonald et al. (2009) indicated that

crustal contamination occurred only on a local scale. Pre-emplacement crustal contamination of the Platreef magma has been identified in Re and Os data (Reisberg et al., 2011), with carbonaceous shales highlighted as a likely contaminant. Similarly, comparison of whole-rock major element data – largely CaO and FeO contents – to PGE tenors and S/Se ratio data support two phases of contamination of the Platreef magma, one prior to emplacement and one post-emplacement (Ihlenfeld and Keays, 2011).

The concordance among the R factors estimated from metal contents, S-Se ratios, and $\Delta^{33}\text{S}$ values is unusual, as decoupling of elemental and isotopic systems appears to be the norm in magmatic sulfide deposits (Lesher and Burnham, 2001). A more complex relationship among the R factors might be expected as there is solid geochemical evidence that the Platreef records intrusion by multiple pulses of silicate magma (Kinnaird et al., 2005). A possible implication is that the PGE and sulfur isotope characteristics of immiscible sulfide melt preserved as Platreef ore were set concurrently through interaction with a separate silicate melt, while the Platreef magmas tapped this reservoir of immiscible sulfide liquid at some later time. The counterintuitive conclusion here is that while coupled metal contents, S-Se ratios, and $\Delta^{33}\text{S}$ values imply shared initial stage of formation, they also imply that this shared common history is decoupled from the final transport and emplacement of the Platreef ore system.

4.8 Implications

Multiple sulfur isotope analysis of the Platreef sulfides has identified crustal sulfur sources as the magma contaminant incorporated prior to emplacement. The heterogenous distribution, and multiple sulfur source contribution, throughout the length

of the Platreef support this interpretation. The identification of this pre-emplacement contamination also raises questions as to the sources of sulfide sulfur in other major ore-bearing horizons of the Bushveld Igneous Complex that have long been interpreted to have a solely magmatic origin. Preliminary $\Delta^{33}\text{S}$ results from sulfides from the Merensky Reef and UG2 exhibit a small but significant crustal sulfur signature ($\Delta^{33}\text{S} = 0.05$ to $0.15\text{\textperthousand}$, Penniston-Dorland et al., 2011) and additional research will allow for this anomaly to be further investigated.

This deposit-wide study proves the power of multiple sulfur isotope analyses as a tool for interpreting the genesis of sulfide ore deposits. The measurement of $\delta^{34}\text{S}$ with $\delta^{33}\text{S}$ to determine $\Delta^{33}\text{S}$ provides, in one analysis, a criterion for the immediate identification of the presence of crustal (previously atmospheric) sulfur with a sulfide system, that can ‘fingerprint’ and potentially quantify those sources. This is in contrast to conventional sulfur isotope ($\delta^{34}\text{S}$) analyses that can be non-conclusive and open to interpretation.

4.9 Acknowledgements

We would like to thank Louis Schurmann and Ivanhoe Nickel and Platinum Ltd.; Gernot Wober and Hunter Dickinson/Anooraq Resources; and Gordon Chunnett and AngloPlatinum for providing access to funding, samples and data for this study. We also acknowledge U.S. Geological Survey MRERP (Mineral Resources External Research Program) grant 05HQGR0158. ERS was supported by a Society of Economic Geologists Graduate Student Fellowship, a GEOTOP bourses d’études des cycles supérieurs, and an NSERC Discovery Grant to BAW. Research costs supported by the Canada Research

Chairs program. Initial funding for this project provided to JAK by the South African Technology and Human Resources for Industry Program.

4.10 References

- Armitage, P.E.B., McDonald, I., Edwards, S.J., and Manby, G.M., 2002, Platinum-group element mineralization in the Platreef and calc-silicate footwall at Sandsloot, Potgietersrus district, South Africa: Transactions of the Institute of Mining and Metallurgy, v. 111, p. B36–B45.
- Bekker, A., Holland, H. D., Wang, P. L., Rumble, D., Stein, H. J., Hannah, J. L., Coetzee, L. L., and Beukes, N. J., 2004, Dating the rise of atmospheric oxygen: Nature, v. 427, p. 117-120.
- Buchanan, D.L., and Rouse, J.E., 1984, Role of contamination in the precipitation of sulfides in the Platreef of the Bushveld Complex, *in* Buchanan, D.L. and Jones, M.J., eds., Sulfide deposits in mafic and ultramafic rocks: London, Institute of Mining and Metallurgy, p. 141–146.
- Buchanan, D.L., Nolan, J., Suddaby, P., Rouse, J.E., Viljoen, M.J., and Davenport, J.W.J., 1981, The genesis of sulfide mineralization in a portion of the Potgietersrus Limb of the Bushveld Complex: Economic Geology, v. 76, p. 568–579.
- Buick, I.S., Maas, R., and Gibson, R., 2001, Precise U-Pb titanite age constraints on the emplacement of the Bushveld Complex, South Africa: Geological Society of London Journal, v. 158, p. 3–6.
- Campbell, I. H., and Naldrett, A. J., 1979, The influence of silicate:sulfide ratios on the geochemistry of magmatic sulfides: Economic Geology, v. 74, p. 1503-1506.
- Canfield, D.E., 1986, The use of chromium reduction in the analysis of reduced inorganic sulfur in sediments and shales: Chemical Geology, v. 54, p. 149–155.
- Cawthorn, R.G., 1999, The platinum and palladium resources of the Bushveld Complex: South African Journal of Science, v. 95, p. 481–489.
- Coetzee, L.L. (2001). Genetic Stratigraphy of the Paleoproterozoic Pretoria Group in the Western Transvaal: Unpublished M.Sc. Thesis, Rand Afrikaans University, 212p.
- Eriksson P.G., Altermann, W., Catuneanu, O., van der Merwe, R., and Bumby, A.J., 2001, Major influences on the evolution of the 2.67 – 2.1 Ga Transvaal basin, Kaapvaal craton: Sedimentary Geology, v. 141-142, p. 205 – 231.
- Farquhar, J. and Wing, B.A., 2003, Multiple sulphur isotopes and the evolution of the atmosphere: Earth and Planetary Science Letters, v. 213, p. 1-13.
- Farquhar, J., Bao, H.M., Thiemens, M., 2000, Atmospheric influence of earth's earliest sulfur cycle: Science, v. 289, p. 756-758.
- Farquhar, J., Wing, B., McKeegan, K., Harris, J., Cartigny, P., and Thiemens, M., 2002, Mass-independent sulfur of inclusions in diamond and sulfur recycling on early earth: Science, v. 298, p. 2369-2372.
- Guo, Q., Strauss, H., Kaufman, A.J., Schroeder, S., Gutzmer, J., Wing, B., Baker, M.A., Bekker, A., Jin, Q., Kim, S. and Farquhar, J., 2009, Reconstructing Earth's surface

- oxidation across the Archean-Proterozoic transition: *Geology*, v. 37, p. 399 – 402.
- Harris, C., and Chaumba, J.B., 2001, Crustal contamination and fluid-rock interaction during the formation of the Platreef, northern limb of the Bushveld Complex, South Africa: *Journal of Petrology*, v. 42, p. 1321–1347.
- Holwell, D.A., and McDonald, I., 2006, Petrology, geochemistry and the mechanisms determining the distribution of platinum group element and base metal sulfide mineralization in the Platreef at Overysel, northern Bushveld Complex, South Africa: *Mineralium Deposita*, v. 41, p. 575–598.
- Holwell, D.A., Boyce, A.J., and McDonald, I., 2007, Sulfur Isotope Variations within the Platreef Ni-Cu-PGE Deposit: Genetic Implications for the Origin of Sulfide Mineralization: *ECONOMIC GEOLOGY*, v. 102, p. 1091 – 1110.
- Hu, G., Rumble, D., and Wang, P., 2003, An ultraviolet laser microprobe for the in situ analysis of multisulfur isotopes and its use in measuring Archean sulfur isotope mass-independent anomalies: *Geochimica et Cosmochimica Acta*. v. 67, p. 3101–3117
- Hulbert, L.J., 1983, A petrographical investigation of the Rustenburg Layered Suite and associated mineralization south of Potgietersrus: Unpublished D.Sc. dissertation, University of Pretoria, 511 p.
- Hutchinson, D., and Kinnaird, J.A., 2005, Complex multi-stage genesis for the Ni-Cu-PGE mineralization in the southern region of the Platreef, Bushveld Complex, South Africa: *Transactions of the Institute of Mining and Metallurgy*, v. 114, p. B208–B224.
- Ihlenfeld, C. and Keays, R.R., 2011, Crustal contamination and PGE mineralization in the Platreef, Bushveld Complex, South Africa: evidence for multiple contamination events and transport of magmatic sulfides: *Mineralium Deposita*.
- Irvine, T.N., 1975, Crystallization sequences of the Muskox intrusion and other layered intrusions—II. Origin of chromitite layers and similar deposits of other magmatic ores: *Geochimica et Cosmochimica Acta*, v. 39, p. 991–1020.
- Keays, R.R., 1995, The role of komatiitic and picritic magmatism and S-saturation in the formation of ore deposits: *Lithos*, v. 34, p. 1–18.
- Kinnaird, J.A., 2005, Geochemical evidence of multiphase emplacement in the southern Platreef: *Transactions of the Institute of Mining and Metallurgy*, v. 114, p. B225–B242.
- Lambert, D.D., Foster, J.G., Frick, L.R., Ripley, E.M., and Zientek, M.L., 1998, Geodynamics of magmatic Cu—Ni-PGE sulfide deposits: New insights from the Re-Os isotopic system: *Economic Geology*, v. 93, p. 121–138.
- Lesher, C. M., and Burnham, O. M., 2001, Multicomponent elemental and isotopic mixing in Ni-Cu-(PGE) ores at Kambaldo, Western Australia: *Canadian Mineralogist*, v. 39, p. 421–446.
- Li, C., and Naldrett, A.J., 1993, Sulfide capacity of magma: A quantitative model and its application to the formation of sulfide ores at Sudbury, Ontario: *Economic Geology*, v. 88, p. 1253–1260.
- Liebenberg L., 1968, The Sulphides in the Layered Sequence of the Bushveld Igneous Complex: Unpublished D.Sc. Thesis, University of Pretoria.
- Manyeruke, T.D., Maier, W.D., and Barnes, S-J., 2005, Major and trace element geochemistry of the Platreef on the farm Townlands, northern Bushveld Complex:

- South African Journal of Geology, v. 108, p. 381–396.
- McDonald, I., Holwell, D.A. and Wesley, B., 2009, Assessing the potential involvement of an early magma staging chamber in the generation of the Platreef Ni-Cu-PGE deposit in the northern limb of the Bushveld Complex: a pilot study of the Lower Zone Complex at Zwartfontein: Transactions of the Institute of Mining and Metallurgy, v. 118, p. 5-20.
- Naldrett, A.J., 2004, Magmatic Sulfide Deposits Geology, Geochemistry and Exploration. Springer, 727 p.
- Penniston-Dorland, S. C., Farquhar, J., Polley, G. J., Mathez, E. A., and Kinnaird, J. A., 2011, Can multiple sulfur isotopes be used as a tracer of sub-continental lithospheric mantle in the Bushveld?, 21st Annual V.M. Goldschmidt Conference: Prague, Czech Republic.
- Penniston-Dorland S.C., Wing, B.A., Nex, P.A.M., Kinnaird, J.A., Farquhar, J., Brown, M., and Sharman, E.R., 2008, Multiple sulfur isotopes reveal a primary magmatic origin for the Platreef PGE deposit, Bushveld Complex, South Africa: Geology, v. 36, p. 979-982.
- Reisberg, L., Tredoux, M., Harris, C., Coftier, A. and Chaumba, J., 2011, Re and Os distribution and Os isotope composition of the Platreef at the Sandsloot-Mogolakwena mine, Bushveld complex, South Africa: Chemical Geology, v. 281, p. 352-363.
- Ripley, E., and Li, C., 2003, Sulfur isotope exchange and metal enrichment in the formation of magmatic Cu-Ni-(PGE) deposits: Economic Geology, v. 98, p. 635-641.
- Robinson, B. W., 1995, Sulphur isotope standards, *in* Proceedings of a consultants' meeting held in Vienna, 1-3. Dec. 1993. IAEA-TECDOC-825, p. 39-45.
- Sharman-Harris, E., Kinnaird, J.A., Harris, C., and Horstmann, U.E., 2005, A new look at sulfide mineralization of the northern limb, Bushveld Complex: A stable isotope study: Transactions of the Institute of Mining and Metallurgy, v. 114, p. B252–B263.

Table 4.1: Multiple sulfur isotope data for samples from the Northern limb of the Bushveld Igneous Complex.

Sample	Farm	Depth (m)	Description	Category	type	$\delta^{33}\text{S}$ ($\text{\textperthousand}_{\text{V-CDT}}$)	$\delta^{34}\text{S}$ ($\text{\textperthousand}_{\text{V-CDT}}$)	$\Delta^{33}\text{S}$ ($\text{\textperthousand}_{\text{V-CDT}}$)
PR174/21.50	Drenthe	21.50	Feldspathic Pyroxenite	Plat	WR	2.19	3.74	0.27
PR174/88.50	Drenthe	88.50	Contaminated Norite	Plat	WR	2.74	4.66	0.34
PR174/106.13	Drenthe	106.13	Serpentinised Pyroxenite	Plat	WR	2.61	4.50	0.29
PR174/207.50	Drenthe	207.50	Granofels	Plat	WR	1.24	1.89	0.27
PR174/240.50	Drenthe	240.50	Serpentinite	Plat	WR	1.48	2.29	0.30
PR175/19.08	Drenthe	19.08	Calc-Silicate	Xeno	WR	3.57	6.30	0.33
PR175/77.18	Drenthe	77.18	Feldspathic Pyroxenite	Plat	WR	3.06	5.24	0.36
PR175/102.50	Drenthe	102.50	Feldspathic Pyroxenite	Plat	WR	5.56	10.53	0.15
PR175/116.81	Drenthe	116.81	Feldspathic Pyroxenite	Plat	WR	2.95	5.14	0.31
OY405/102A	Overysel	404.55	Pyroxenite	Plat	Po/Pnt	2.60	4.64	0.21
OY405/102B	Overysel	404.55	Pyroxenite	Plat	Cp	4.65	8.58	0.24
OY405/102C	Overysel	404.55	Pyroxenite	Plat	Sulf	2.34	4.05	0.26
OY405/189A	Overysel	460.82	Serpentinized pyroxenite	Plat	Cp	2.60	4.71	0.18
OY405/189B	Overysel	460.82	Serpentinized pyroxenite	Plat	Sulf	1.98	3.42	0.23
OY518/14	Overysel	--	Pyroxenite	Plat	Sulf	3.11	5.51	0.27
OY518/51	Overysel	--	Pyroxenite	Plat	Sulf	2.53	4.44	0.25
OY518/126	Overysel	--	Pyroxenite	Plat	Sulf	1.17	2.07	0.10
*ZN259/20	Zwartfontein	49.60	Feldspathic Pyroxenite	Plat	WR	2.32	4.01	0.26
*SS315/5	Sandsloot	102.80	Feldspathic Pyroxenite	Plat	WR	4.66	8.77	0.15
*SS315/11	Sandsloot	131.50	Feldspathic Pyroxenite	Plat	WR	4.96	9.20	0.23
*SS315/14	Sandsloot	144.80	Feldspathic Pyroxenite	Plat	WR	4.04	6.94	0.47
*SS315/6A	Sandsloot	147.10	Feldspathic Pyroxenite	Plat	WR	4.77	8.44	0.44
*SS315/18	Sandsloot	147.10	Feldspathic Pyroxenite	Plat	Po	4.73	8.36	0.43
*SS315/18A	Sandsloot	147.10	Feldspathic Pyroxenite	Plat	Po	4.74	8.36	0.44
*SS315/18B	Sandsloot	147.10	Feldspathic Pyroxenite	Plat	Cp	4.86	8.60	0.44
*SS315/18C	Sandsloot	148.70	Feldspathic Pyroxenite	Plat	WR	4.84	8.34	0.55
*SS315/19	Sandsloot	148.70	Feldspathic Pyroxenite	Plat	Po	4.75	8.39	0.44
*SS315/19A	Sandsloot	148.70	Feldspathic Pyroxenite	Plat	Po	4.86	8.68	0.40
*SS315/19B	Sandsloot	148.70	Feldspathic Pyroxenite	Plat	Cp	3.95	7.19	0.25
*SS315/19C	Sandsloot	149.60	Feldspathic Pyroxenite	Plat	WR	4.79	8.45	0.45
*SS315/20	Sandsloot	150.80	Feldspathic Pyroxenite	Plat	WR	4.73	8.24	0.49
*SS315/21	Sandsloot	151.50	Feldspathic Pyroxenite	Plat	WR	4.52	8.17	0.32
*SS315/22	Sandsloot	159.10	Calc-silicate	FW	WR	1.02	0.72	0.65
*SS315/23	Sandsloot	169.90	Calc-silicate	FW	WR	5.62	8.23	1.39
*SS315/25	Sandsloot	171.60	Calc-silicate	FW	WR	3.73	4.62	1.35
*SS315/25A	Sandsloot	174.80	Calc-silicate	FW	WR	5.08	5.77	2.11
*SS315/25B	Sandsloot	177.30	Calc-silicate	FW	WR	6.11	5.29	3.39
*SS315/25C	Sandsloot	179.30	Calc-silicate	FW	WR	6.92	4.88	4.41
*SS315/26	Sandsloot	185.50	Calc-silicate	FW	WR	8.15	6.07	5.04
*SS315/27	Sandsloot	214.60	Calc-silicate	FW	WR	7.81	6.71	4.36
*SS315/31	Sandsloot	301.90	Calc-silicate	FW	WR	6.23	5.60	3.35
*SS315/38	Sandsloot	130.20	Pyroxenite	Plat	Po	1.93	3.44	0.16
*TN190D1/74	Tweefontein North	196.00	Pyroxenite	Plat	Po	2.18	3.78	0.23
*TN190D1/167	Tweefontein North	206.20	Norite	Plat	Po	1.61	3.07	0.03
*TN190D1/109	Tweefontein North	314.70	Pyroxenite	Plat	Po	1.56	2.74	0.15
*TN190D1/139	Tweefontein North	331.30	Leuconorite	Plat	Po	2.50	4.54	0.16
*TN190D1/22	Tweefontein North	335.00	Pyroxenite	Plat	WR	3.56	6.73	0.09
*TN190D1/2-2	Tweefontein North	336.90	Pyroxenite	Plat	Po	3.14	5.86	0.13
*TN190D1/56A	Tweefontein North	336.90	Pyroxenite	Plat	Cp	3.47	6.59	0.09
*TN190D1/56B	Tweefontein North	338.20	Leuconorite	Plat	WR	5.31	10.14	0.10
*TN190D1/2-1	Tweefontein North	343.90	Serpentinite	Plat	Po	5.97	11.40	0.12
*TN190D1/149	Tweefontein North	345.60	Hornfels	FW	WR	9.62	18.10	0.34
*TN190D1/H1	Tweefontein North	350.10	Calc-silicate	FW	WR	3.29	6.08	0.17
*TN190D1/P2	Tweefontein North	352.80	Hornfels	FW	WR	-0.53	-1.08	0.03
*TN190D1/H2	Tweefontein North	353.60	Hornfels	FW	WR	0.11	0.04	0.09
*TN190D1/H3	Tweefontein North	366.20	Hornfels	FW	WR	-0.02	-0.85	0.41
*TN190D1/H6	Tweefontein North	373.90	Hornfels	FW	WR	0.00	-0.67	0.35
*TN190D1/H7	Tweefontein North	374.90	Hornfels	FW	WR	0.24	-0.26	0.38
*TN190D1/H8	Tweefontein North	381.80	Hornfels	FW	WR	-7.31	-14.47	0.17
*TN190D1/H9A	Tweefontein North	392.50	Hornfels	FW	WR	1.03	0.59	0.72
*TN190D1/H9C	Tweefontein North	395.40	Hornfels	FW	WR	1.73	1.57	0.93
*TN190D1/H10	Tweefontein North	409.40	BIF	FW	WR	8.90	15.83	0.78
*TN190D1/B1	Tweefontein North	414.60	BIF	FW	WR	3.03	4.40	0.77
*TN190D1/B2	Tweefontein North	--	Hornfels	FW	WR	-5.34	-12.05	0.88

Table 4.1 (cont.)

Sample	Farm	Depth (m)	Description	Category	Sample type	$\delta^{33}\text{S}$ ($\text{\textperthousand}_{\text{V-CDT}}$)	$\delta^{34}\text{S}$ ($\text{\textperthousand}_{\text{V-CDT}}$)	$\Delta^{33}\text{S}$ ($\text{\textperthousand}_{\text{V-CDT}}$)
*TN194/7	Tweefontein North	--	Pyroxenite	Plat	Cp	4.23	8.10	0.06
TN92-199A	Tweefontein North	--	Pyroxenite	Plat	Sulf	4.43	8.45	0.08
TN92/199B	Tweefontein North	--	Pyroxenite	Plat	Po/Pnt	6.65	12.70	0.13
TN92/228A	Tweefontein North	--	Pyroxenite	Plat	Cp	5.98	11.44	0.10
TN92/228B	Tweefontein North	--	Main Zone	MZ	WR	1.58	2.86	0.11
*TN31/MZLo	Tweefontein North	--	Main Zone	MZ	WR	0.89	1.32	0.21
*TN31/MZHi	Tweefontein North	--	Calc-silicate	Xeno	Cp	3.11	3.94	1.09
*TN31/134	Tweefontein North	--	Hornfels	Xeno	WR	0.47	-4.08	2.58
*TN31/160	Tweefontein North	221.20	Hornfels	Xeno	WR	-0.08	-0.33	0.09
TN188/H3	Tweefontein North	--	Pyroxenite	Plat	Po	3.12	5.87	0.10
TN192D1/310A	Tweefontein North	--	Pyroxenite	Plat	Po	3.13	5.84	0.12
TN192D1/310B	Tweefontein North	--	Pyroxenite	Plat	Cp	3.24	6.06	0.12
T192D1/310C	Tweefontein North	60.34	Pegmatoidal Norite	Plat	Cp	1.24	2.03	0.19
ATS 46/461.21	Turfspruit	461.21	Feldspathic Pyroxenite	Plat	Po	3.09	5.22	0.41
ATS 57/72.48	Turfspruit	72.48	Pyroxenite	Plat	Po	0.82	1.25	0.17
ATS 57/219.26	Turfspruit	219.26	Pyroxenite	Plat	Po	3.20	5.30	0.47
ATS 57/221.39	Turfspruit	221.39	Massive Sulphide / Pyroxenite	Plat	Cp	3.82	6.32	0.57
ATS 57/221.39	Turfspruit	221.39	Massive Sulphide / Pyroxenite	Plat	Po	3.38	5.49	0.56
ATS 57/325.25	Turfspruit	325.25	Calc-Silicate	FW	Po	14.76	28.72	0.07
ATS 57/335.07	Turfspruit	335.07	Calc-Silicate	FW	Py	10.73	20.62	0.17
ITS054-22	Turfspruit	22.12	Feldspathic Pyroxenite	Plat	WR	0.89	1.43	0.15
ITS054W-198	Turfspruit	197.91	Serpentinite w/interstitial sulfide	Plat	WR	3.07	4.93	0.53
ITS054W-203	Turfspruit	203.4	Hornfels	Xeno	WR	-10.72	-20.92	0.11
ITS054W-223	Turfspruit	223.29	Hornfels	Xeno	WR	-4.44	-8.91	0.16
ITS054W-226a	Turfspruit	225.85	Melanorite w/ massive sulfide	Plat	WR	3.39	5.45	0.58
ITS054W-230	Turfspruit	229.8	Melanorite w/ massive sulfide	Plat	WR	3.73	6.15	0.57
ITS054W-274	Turfspruit	273.88	Feldspathic Pyroxenite	Plat	WR	3.35	5.81	0.37
ITS054W-275	Turfspruit	274.53	Hornfels	Xeno	WR	3.26	5.6	0.38
ITS054W-323	Turfspruit	323.2	Dolomite Footwall	FW	WR	9.28	17.97	0.06
ITS054W-341	Turfspruit	341.33	Dolomite Footwall	FW	WR	7.64	14.7	0.09
ARF 08/49.26	Rietfontein	49.26	Norite	Plat	Po	2.94	4.84	0.45
ARF 08/124.64	Rietfontein	124.64	Massive Sulphide	Plat	Po	3.11	5.17	0.46
ARF 08/124.64	Rietfontein	124.64	Massive Sulphide	Plat	Po	3.83	6.43	0.53
ARF 08/129.78	Rietfontein	129.78	Norite	Plat	Po	3.20	5.30	0.47

Note: Plat - Platreef; Xeno - Xenolith; FW - Footwall; MZ - Main Zone; WR - Whole Rock; Sulf - sulfide; Po - Pyrrhotite; Pnt - Pentlandite; Cp - Chalcopyrite; Py - Pyrite

*data from Penniston-Dorland et al., 2008

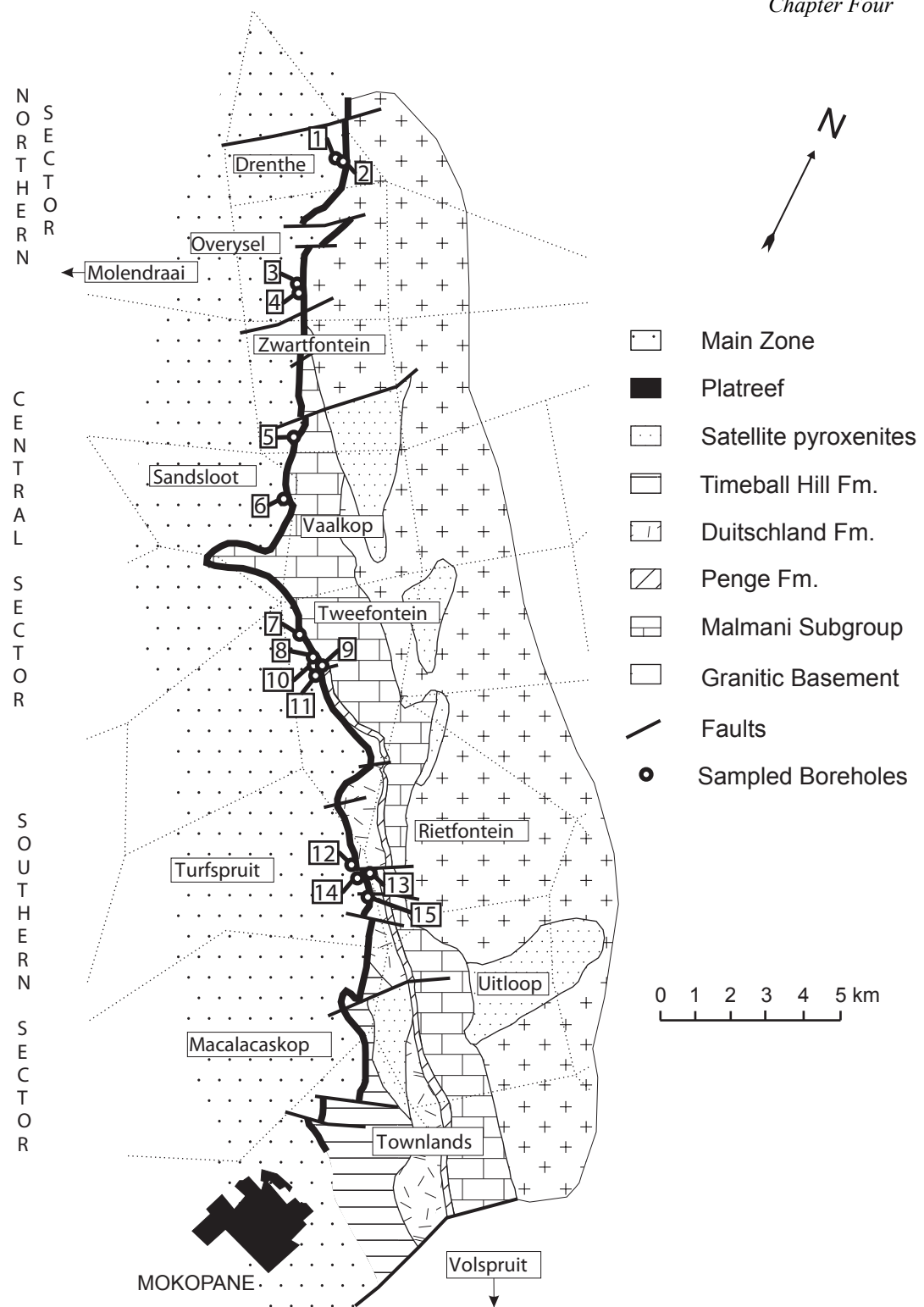


Fig. 4.1: Geological map of the Platreef showing farm boundaries and sampled borehole locations. Boreholes: 1: PR-175, 2: PR-174, 3: OY-405, 4: OY-518, 5: ZN-259*, 6: SS-315*, 7: TN-31*, 8: TN-188, 9: TN-92, 10: TN-190D1*, 11: TN-192D1, TN-194*, 12: ATS-46, 13: ARF-08, 14: ATS-57, 15: ITS054 (* from Penniston-Dorland et al., 2008).

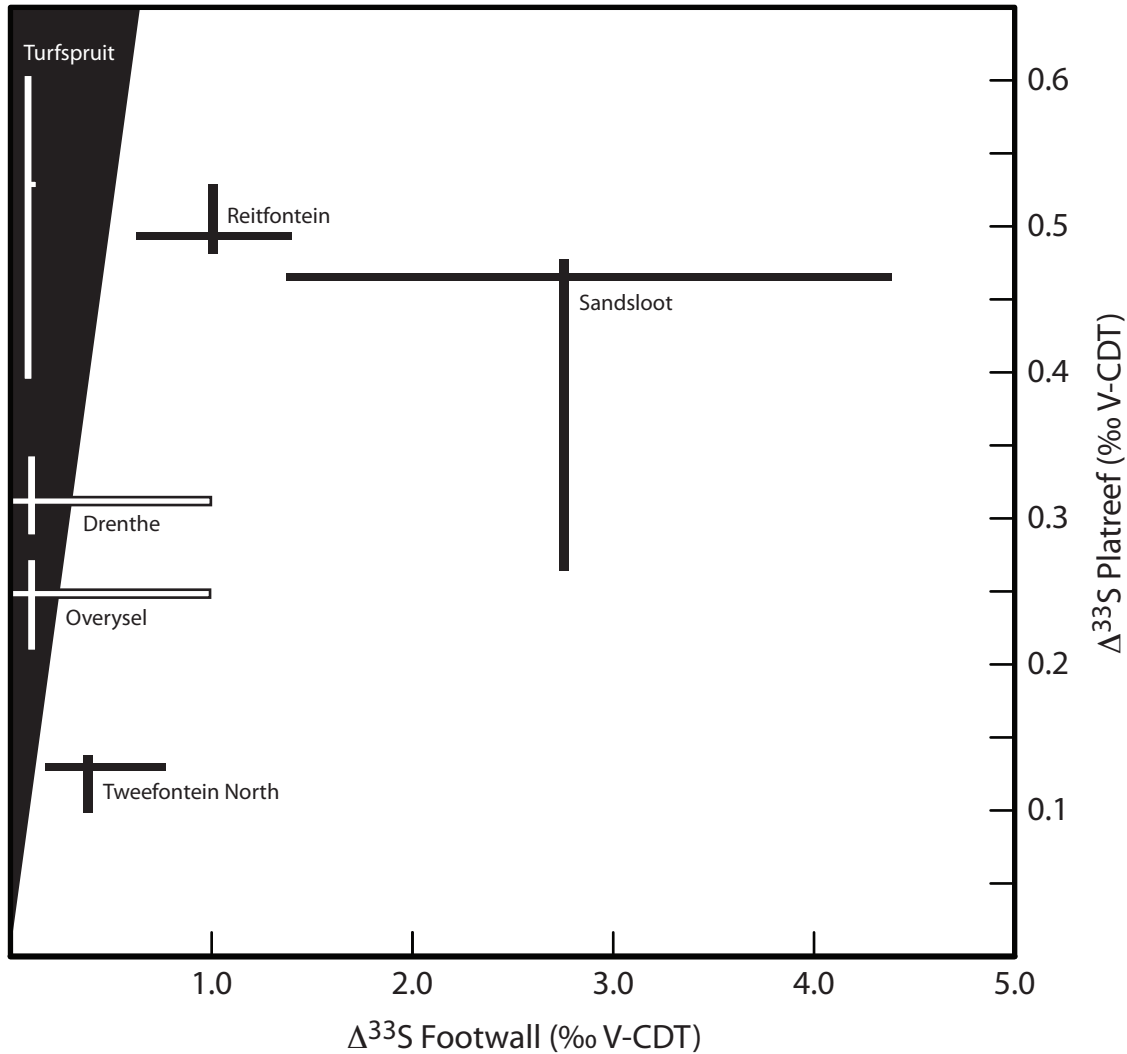


Fig. 4.2: Diagram comparing $\Delta^{33}\text{S}$ values of the Platreef and its direct footwall on different farms. Ranges represent 10th to 90th percentile of each grouping and intersect at the mode. Footwall $\Delta^{33}\text{S}$ values for Overysel and Drenthe are an estimated range from expected primary mantle values (~0‰; Farquhar et al., 2002) to average sedimentary sulfide for Archean (1‰; Johnston, 2011), allowing for the granitic footwall to range from an I- to an S-type granite. Footwall $\Delta^{33}\text{S}$ values for Rietfontein are taken from the range of values measured in the equivalent country rock protolith (Lower Duitschland shales; Guo et al., 2008). Black filled triangle represents region where local contact enrichment of Platreef $\Delta^{33}\text{S}$ values is impossible.

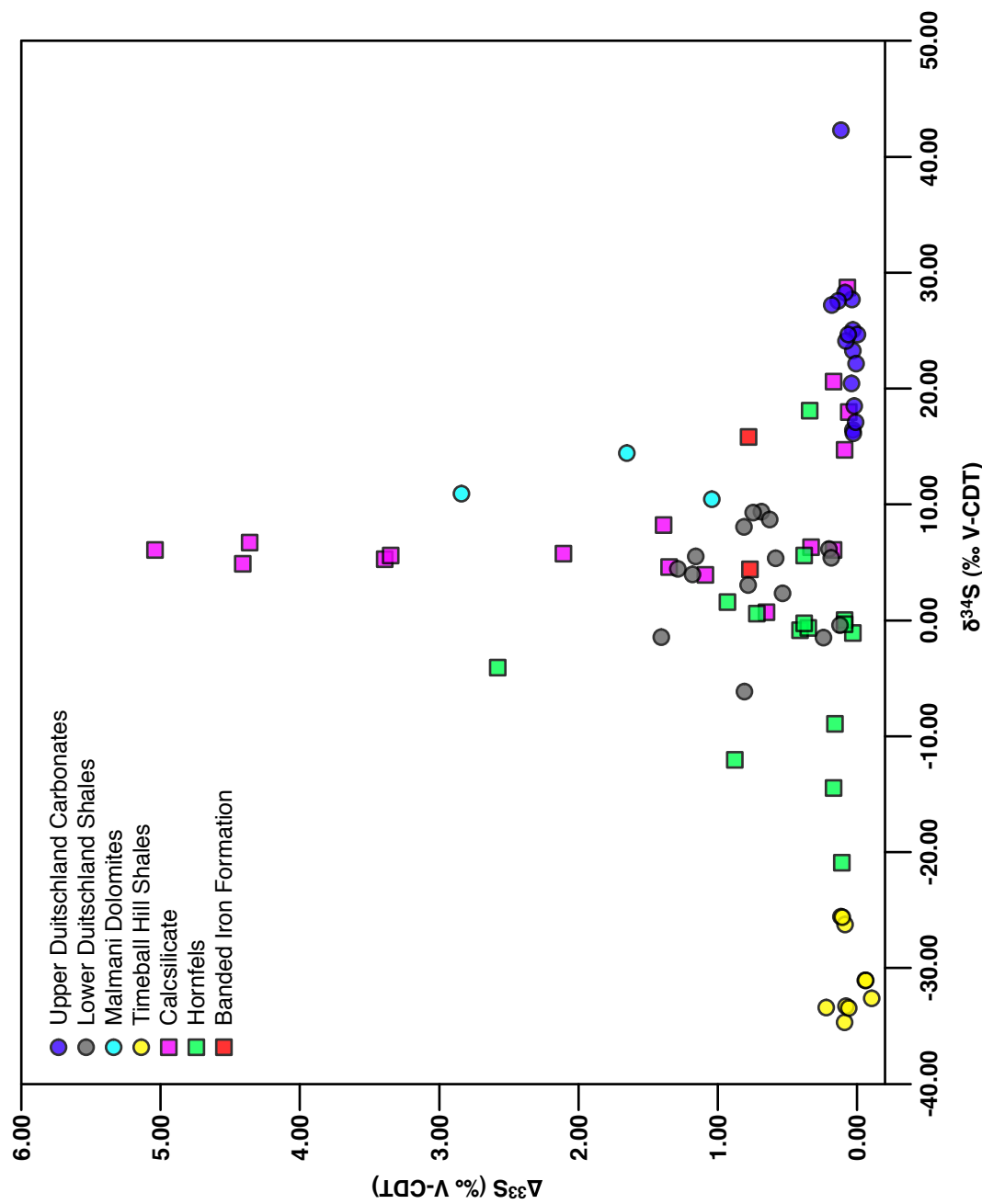


Fig. 4.3: Diagram showing multiple sulfur isotope data for the Transvaal Supergroup and Platreef footwall samples (Data from this study, Bekker et al., 2004, Guo et al., 2009 and Penniston-Dorland et al., 2008).

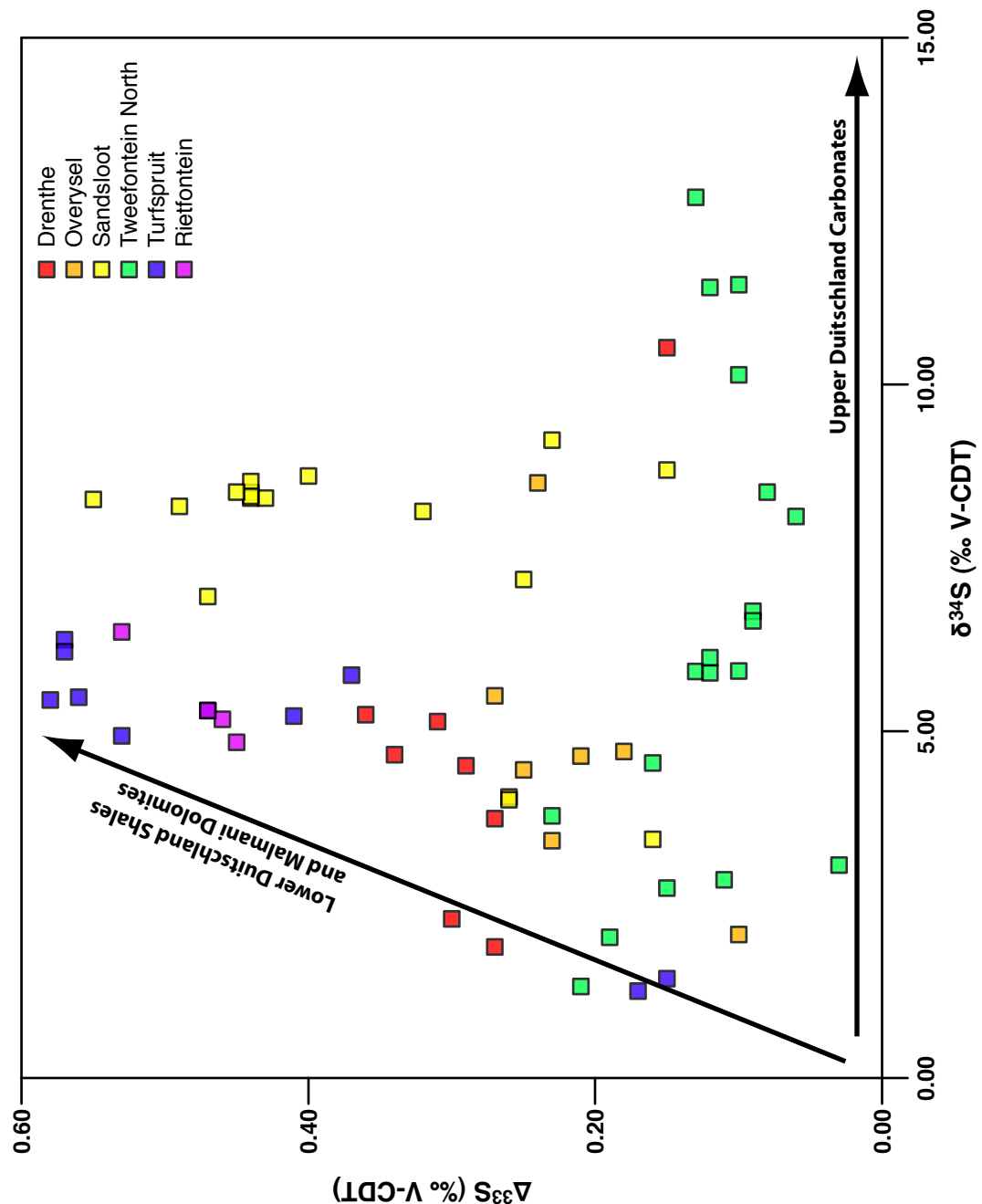


Fig. 4.4: Binary diagram showing multiple sulfur isotope data from the Platreef (data from this study and Penniston-Dorland et al., 2008) and mixing lines with Transvaal Supergroup (Fig. 4.3, data from Guo et al., 2009) multiple sulfur isotope characteristics.

CHAPTER FIVE

Summary and Discussion

5.1 Introduction

Identification of the sources of sulfur in an ore-forming system allows for a greater understanding of how a specific mineral deposit formed, and how best to explore for that particular type of deposit. It can also expand the knowledge of ocean and atmosphere chemistry at the time of formation. The traditional use of $\delta^{34}\text{S}$ to determine the identity and role of sulfur in ore-forming processes, although useful in many cases, is often limited by the one-dimensional nature of $\delta^{34}\text{S}$ data, when it prohibits the unique identification of sulfur reservoirs. Work presented in this thesis has successfully demonstrated how multiple sulfur isotope analysis can provide an extra dimension, which allows deconvolution of multiple, competing genetic influences, to provide a more complete picture of ore formation in the deep past.

5.2 Summary

5.2.1 Chapter Two: Volcanogenic massive sulfide deposits of the Noranda Camp

The application of multiple sulfur isotope analysis to volcanogenic massive sulfide deposits (VMS) of the ~2.7 Ga Noranda Camp, in combination with trace element geochemistry, yields important information on the origins of these orebodies. The mass-independent fractionation of sulfur isotopes resulted in anomalous concentrations of ^{33}S , quantified as negative and positive values of $\Delta^{33}\text{S}$, which have served as a tracer in these studies. In many of

the Noranda VMS deposits, the sign and magnitude of $\Delta^{33}\text{S}$ has indicates that seawater sulfur contributed to their sulfur budgets.

We propose the following evolution of sulfur sources during formation of the Noranda VMS deposits. 1) The system was dominated initially by focused hydrothermal upflow driven by the underlying magma chamber, which stripped sulfur and trace metals from the volcanic host rocks in addition to extracting them from the magmatic system. This is reflected by near-zero $\Delta^{33}\text{S}$ values in pre-cauldron deposits. 2) As the caldera collapsed, steeply dipping normal fault structures developed which allowed for direct entrainment of seawater into the hydrothermal system. As the system evolved, the volcanic pile was stripped of sulfur. 3) Cooling of the system gradually reduced the efficiency of precipitation of sulfate minerals in the reaction zone. This may have allowed a small, but measurable, contribution of seawater sulfate to participate in the formation of ore sulfides. 4) Sealing of the fault structures led to subsidence of the hydrothermal system; hydrothermal fluids then had less access to the volcanic host rocks and their underlying magmatic relatives, and were restricted to local, near-surface mass transfer processes to precipitate ore sulfides. This is supported by $\Delta^{33}\text{S}$ values for post cauldron deposits of ave. -0.24 ‰.

This study also assists in the classification of exceptional deposits within the Noranda camp stratigraphy. The Au-rich Horne deposits show a strong sulfur isotope affinity with other pre-cauldron deposits in the Noranda Camp. In contrast, sulfur isotope analysis suggests that the Quemont deposit – although recently dated to the same age as Horne – should be classified with deposits that formed during the main cauldron-forming event. Finally, economically relevant Au concentrations can be qualitatively linked to near-zero $\Delta^{33}\text{S}$ values within the Neoarchean

Noranda VMS deposits. This discovery has implications for our understanding of how Au-rich VMS deposits form, as well the potential to direct exploration for such deposits.

5.2.2 Chapter Three: Au-rich deposits of the Doyon-Bousquet-LaRonde mining camp

Study of the VMS and vein-hosted Au-rich mineralization of the Doyon-Bousquet-LaRonde (DBL) camp garners further understanding of the sources of sulfur, and potentially Au, in this Neoarchean ore-forming system. Multiple sulfur isotope analysis of ore deposit sulfide from within the DBL mining camp clearly indicates their igneous-magmatic affinity, inferring a direct magmatic or igneous input to the system, with little contribution detected from any surficial source of sulfur. In contrast, sulfides that formed at, or very near to, the paleo-seafloor exhibit $\Delta^{33}\text{S}$ values as low as -1.31 ‰ showing a clear contribution of sulfur from seawater sulfate. This study also identifies significant differences in the dominant sulfur sources in the VMS deposits of the Noranda and DBL mining camps. Based on $\delta^{34}\text{S}$ values alone, the DBL ore-forming environment would conventionally be interpreted to have had the greater contribution from surficial sulfur. However, $\Delta^{33}\text{S}$ values close to zero indicate that the DBL VMS deposits must have been formed from precipitation of dominantly igneous-sourced sulfur. Whether this was due to exogenic (i.e., deeper submarine environments for DBL) or endogenic (i.e., a single long-lived hydrothermal system) mechanisms is a question for future work.

This study also demonstrates the ability of multiple sulfur isotope analysis to interpret sulfur sources within ore-forming systems that have undergone relatively high levels of metamorphism. It further supports interpretations of the origins of the Noranda VMS deposits with respect to potential for magmatic sources of gold within Archean VMS systems.

5.2.3 Chapter Four: Ni-Cu-(PGE) Platreef deposit

Multiple sulfur isotope analysis of Platreef sulfides identified a crustal sulfur contribution to the magmatic system that occurred prior to emplacement. The heterogenous $\Delta^{33}\text{S}$ distribution, and hence, heterogeneous sulfur source contributions, throughout the length of the Platreef support this interpretation. Identification of this pre-emplacement contamination also raises questions as to the sources of sulfur within sulfides in other major ore-bearing horizons of the Bushveld Igneous Complex (BIC), that have long been interpreted to have a solely magmatic origin. This deposit-wide study proves the power of multiple sulfur isotope analysis as a potential tool for interpreting the genesis of sulfide ore deposits, even where sources of sulfur originating in the Archean atmosphere may be cryptic.

5.3 Scientific Contributions and Significance

The studies presented in this thesis have proved the efficacy of multiple sulfur isotope analysis in the interpretation of sulfur source contributions in selected ore-forming processes. This thesis also demonstrated the application of the multiple sulfur isotope technique in a variety of ore-forming environments.

- The study of the Noranda Camp VMS deposits identifies a seawater sulfate contribution of up to 25% in the formation of these ore bodies. This is in contrast to current models for the formation of Neoarchean VMS deposits, which postulate that the near-absence of sulfate minerals within these deposits indicates a lack of involvement of seawater sulfur. Conclusions presented herein suggest that these models need revisiting.
- Multiple sulfur isotope and trace element data from the Noranda Camp suggest a correlation between near-zero $\Delta^{33}\text{S}$ values and higher Au grades in the Au-rich deposits of the study

area. This is supported by ubiquitous near-zero $\Delta^{33}\text{S}$ values observed within the Au-rich VMS deposits in the DBL mining camp. This conclusion leads to the hypothesis that Au-rich VMS deposits are associated with a marked magmatic-hydrothermal contribution to the ore-forming system.

- A number of previous studies have proposed that the presence of advanced argillic alteration is a diagnostic fingerprint of a magmatic-hydrothermal influence within a VMS ore-forming system. However, no differences in multiple sulfur isotope composition were measured between areas of the LaRonde Penna deposit that exhibit aluminous alteration (proposed by others to represent metamorphosed advanced argillic alteration) and those that do not. This observation implies that although magmatic-hydrothermal fluids may cause advanced argillic alteration, it is not a compulsory product of this process.
- The deposit-wide multiple sulfur isotope study of the Platreef, in the northern limb of the Bushveld Igneous Complex, confirms models of pre-emplacement sulfur contamination of the ore-forming magma proposed by previous researchers. In addition, this study positively identifies the sources of sulfur that were incorporated in that magma, which had not previously been shown. In light of this new revelation, the possibility of pre-emplacement contamination of the parent magma of the UG2 and Merensky Reef deposits in the eastern and western limbs of the BIC should be investigated.

5.4 Recommendations for Future Work

There are many questions raised by the studies presented within this thesis. Identification of a seawater sulfate contribution to the Neoarchean VMS deposits of the Noranda Camp will require further investigation. It would be beneficial to investigate the variation in multiple sulfur

isotope signatures of several of the Noranda VMS deposits in more detail, in particular the Au-rich Horne and Quemont deposits. Assessment of variation between sulfur sources within a single ore lens, and to those within the stringer sulfide feeder zone to that same lens, would likely cast light on the relative importance of temperature and localized fluid mixing to the sulfide precipitation process. Detailed investigation may also assist in quantitatively identifying the difference in sulfur sources between two of the world's largest Au-rich VMS deposits. Also of interest would be analogous studies on other VMS deposits of similar age from around the world. These would allow assessment as to whether seawater sulfate contributions recorded in some of the Noranda VMS deposits are the norm, or anomalous, in a global context.

Variations in multiple sulfur isotope compositions within the Au-rich deposits of the DBL mining camp should also be further investigated. This would potentially allow for resolution of the source of enriched $\delta^{34}\text{S}$ values within these deposits. Extensive ongoing exploration and active mining in this area will assist in the collection of samples for a more detailed multiple sulfur isotope study than is presented in this thesis. A trace element geochemical study, similar to that undertaken for the Noranda VMS deposits, would also contribute to the understanding of the ore-forming systems in the DBL mining camp.

Finally, identification of pre-emplacement sulfur contamination of the magma from which the Platreef formed raises the possibility of similar processes affecting the UG2 and Merensky Reef magmas. A study of the variability of multiple sulfur isotope values in the main ore bodies of the eastern and western limbs of the BIC would resolve this question, and may lead to a new understanding of the ore-forming processes associated with emplacement of the world's largest layered mafic intrusion.

Appendix 1

This appendix comprises detailed observations of deposit-scale trace element variability from EMPA. Although there are some variations worth noting, their investigation is more detailed than the main purview of this paper. They are presented here for completeness.

Deposit-scale trace element variability

In general, when comparing samples within a single deposit and also comparing deposits to each other, the trace element composition of a particular mineral can be considered to have little to no compositional variability (see Figures A1.1 – A1.9). However, some variations are worth noting. In the pyrite analyses elevated Co concentrations are observed for the Old Waite, East Waite and Newbec deposits; the Newbec pyrites also exhibit increased Cu and Ni concentrations. Pyrite from the Old Waite deposit not only exhibits a large range in Co, but also Fe concentrations. Lastly, the Se content of pyrite within the Robb-Montbray deposit are clearly elevated when compared to other deposits, and the Horne No. 8, Quemont, New Insco and Vauze deposits also show some elevated Se concentrations (Fig. A1.1). Within the sphalerite analyses one major trend is apparent: Fe concentrations generally show little variation (such as Horne No. 5) with the exception of the Horne No.5 and the post-cauldron deposits (Deldona, Delbridge, Gallen and Mobrun) where the concentration significantly decreases (Fig. A1.3). This trend is seen antithetically in the Zn concentrations. One other notable variation to note is the increased Cd and Co concentrations within the Robb-Montbray sphalerites. Chalcopyrite analyses reveal two observations of interest (Fig. A1.5); the first is the wide-range, and relatively decreased concentrations of Cu, Fe and to a small degree, S within the Corbet deposit. This is coupled with

a large and relatively increased concentration of Zn. Secondly, Se concentrations within chalcopyrite seem to mirror the trend observed with the pyrites analysed, within elevated concentrations recorded within the Robb-Montbray and Horne No. 8 deposits relative to other deposits. Pyrrhotite analyses appear to show a large amount of geochemical variation between different deposits (Fig. A1.7), however concentrations for most elements analysed are considerably lower than that of other minerals, and therefore most variations are negligible. The exception to this is the variations within Se with samples from the Horne No.8 again containing increased concentrations. However in contrast to other minerals analysed this elevated Se signature is also recorded in galena from the Deldona deposit.

Table A.1.1: Stratigraphic position, deposit and sample numbers for this study, with sample and microprobe descriptions and dominant mineralogy

Stratigraphic Position	Deposit	Sample	Sample Description ¹	Microprobe Description	Mineralogy
Pre-cauldron	Robb-Montbrey (Inmont)	A95-16A CP A95-16A PY A95-16B CP A95-16B PY A95-16C PY A95-16D SP	Chalcocite stringer from open cast pit Small V.M.S. from open pit dump Chalcocite stringer from open cast pit	Some minor cp, also qtz ~50-50 mix of cp and py. Essentially clean py with one or two roque grains.	CP CP CP CP CP SD
Horne No.8		H63H10 PO H63H14 PO H63H18 PY H63H20 PY H63H21 PY H63H22 PY H63H23 PY H63RF10 GN H63RF26 CP	Massive monomineralic replacement ores ("likely magmatic") Massive monomineralic replacement ores (likely magmatic) Massive monomineralic replacement ores (likely magmatic) Late vein related to syenite dyke H orebody 8th level	Mostly po with ~30% cp, also quite a lot of magnetite. Occasional intergrown po and cp. Po with some py grains as well (~15%), also a few cp grains. All py with some small minor cp. Mostly py with ~15% cp, quite a lot of which is intergrown with py. Mostly clean py. Mostly py with some cp intergrown/inclusions with py. Mostly fairly clean py although cp inclusions in some grains. Very clean galena Cp with ~25% py, most of which has cp inclusions.	Po Po Py Py Py Py Py Gn CP
Horne No.5		63RF21 CP 63RF31 PY 63RF32(49L) PY 63RF33 SP 64RF23 SP	Likely original exhalative part of the Horne complex Likely original exhalative part of the Horne complex Likely original exhalative part of the Horne complex	So with very clean py. Mostly py, occasionally intergrown with cp and sp. Also some rogue cp and py grains. Mostly sp with occasional cp grains.	CP Py SP
Cauldron Margin	Aldermac	A95-14A PY A95-14A SP	All samples from massive sulfide dump	So with very minor py. Mostly py with some intergrowths.	SD SP
		A95-14B PO A95-14B PY A95-14B SP A95-14C CP A95-14C PY A95-14D CP A95-12A CP1	All samples from massive sulfide dump All samples from massive sulfide dump All samples from massive sulfide dump All samples from massive sulfide dump	~50-50 mix of py and sp, occasional sp with po inclusions, one sp grain with cp. Some complicated grains exhibiting more than one phase of mineralisation, also quite a lot of magnetite. Clean py with very very occasional sp inclusions. Mostly sp but does have some cp, py and even some po intergrown with sp. Relatively clean py, although occasionally intergrown sp and sp inclusions. Very clean cp.	Py (Sp) Py SP
New Inesco		A95-12A CP2 A95-12B PY A95-12C PY		Mostly cp with ~10% py. Mostly cp with 30-40% py. Lots of silicates, mostly in py. Very very occasional py inclusions in cp and visa versa.	CP Py SP
Cauldron	Corbet	CRBT3-15-6 SP	Level 12, lens #3, stope 15	Seems clean py, although not many grains. Quite a lot of silicates	CP
	Decoeur-Garon	A95-13 PO	Level 12, 800N section, lens #3	All py, but seem to be a lot of cp inclusions.	Py
			Disseminated sulfide from trench in vesicular andesite		SD
Bedford Hill	stringer in trenches	A95-10A PY A95-10B CP A95-10C CP	In hyaloclastite / flowtop, brecciated In hyaloclastite / flowtop, brecciated	Py, some of which is heavily included with cp and sp. A few grains have complicated intergrowths between py, cp and sp, also one with galena. Sp seems to have cp all through it. Cp with very minor py.	Py CP CP
Ansil		ANSL11A-247 SP ANSL6A-4140 CP ANSL6C-NW CP ANSL98A-12 SP ANSL983 BX PY ANSL989 SP ANSL98-NMMS PY	Cherty exhalite top orebody Massive sulfide upper lens (4140 drift), Au rich Hanging wall lens Cherty (Cranton tuff) exhalite top of orebody apron Brecciated ore (massive sulfide Cherty (Cranton tuff) exhalite top of orebody apron Magnetite/massive sulfide upper contact	Sp with occasional very small py inclusions. Co. with fair amount of silicate inclusions So with very small inclusions of cp and maybe po. Py with minor po (poor polish) Very clean sp with very very minor py and cp grains and occasional inclusions. ~50-50 po and cp, same intergrowns, no pyrite/thiblue.	CP CP CP Py SP
C contact tuff	near Amulet C	C-TUFF PY2 C-TUFF SP		Py with a few minor cp grains. Clean py with some very minor, very fine grained cp Sp with occasional cp and py inclusions.	Py SP
Lac Dufault		JH70-04 CP LD70-N-127 CP A95-09A PY	Massive sulfide from ore pile Discovery core massive sulfide intersection	Cp with minor associated py. Clean cp separate.	CP CP Py
Moosehead	small deposit in C tuff	A95-09A SP A95-09B PY A95-09B SP	Sulfide tuff, small massive sulfide	Mostly py with some galena (cruddy sample)	SP Py
Amulet F-shaft		AMFT2801 CP AMFT2802 PO AMF6601 CP	Sulfide tuff, small massive sulfide Massive sulfide from dump Massive sulfide from dump	Mixture of sp, py and cp. Get small inclusions of py and po, also sp and py intergrown occasionally. Py with galena Po with large proportion of py. Essentially a clean cp separate.	SP CP Po CD
Millenbach		SP2091 PY	Massive sulfide from underground	Fairly clean py separate.	Py

Table A1.1 (cont.)

Stratigraphic Position Cauldron	Deposit	Sample	Sample Description ¹	Microprobe Description
Amulet A Upper upper mine from wall rocks	A95-07B PY A95-07B SP A95-07C PY A95-07D PY A95-07E CP A95-07F CP	A95-07B PY Open pit massive sulfide Open pit massive sulfide Open pit massive sulfide Open pit massive sulfide Open pit massive sulfide	Py with oxides Mostly sp with some intergrown py. Also get some py and cp grains (one of which is intergrown cp, sp and py). Py with minor sp and very minor cp. Mostly py but also sp and cp, occasionally intergrown. A lot of the py seems to have inclusions of cp and sp. Mostly cp, a few sp grains, intergrown, and have cp inclusions Mostly cp, a few sp grains, intergrown, and have cp inclusions	Py Sp Py CP CP
Amulet C	A95-08A PY A95-08B CP A95-08D SP A95-08E SP A95-08F CP A95-08G PO	A95-08A PY Massive sulfide from dump Massive sulfide from dump Massive sulfide from dump Massive sulfide from dump Massive sulfide from dump	Equal parts py, sp, also some po and cp. Py has a high % of inclusions Sp with very occasional cp and py inclusions and intergrowths. Mostly cp, with very minor cp, also lots of silicates and magnetite (~50%). Clean py Clean py Mix of 70% sp and 30% py. Occasional cp and sp inclusions in py. Mostly cp with ~20% py. Occasional cp and sp inclusions in py. Clean py, gutter a lot of silicate.	Py CP SP Py Po Py CP Po Py CP Po
Old Waite (Waite-Montgomery)	A95-18A PY A95-18A SP A95-18B CP A95-18B PO A95-18B PY	Massive sulfide from dump Massive sulfide from dump Massive sulfide from dump Massive sulfide from dump	Mix of 70% sp and 30% py. Occasional cp and sp inclusions in py. Mostly cp with ~20% py. Occasional cp and sp inclusions in py. Clean py, gutter a lot of silicate.	Py CP Po Py Py
East Waite	A95-17A PO A95-17A PY A95-17A SP A95-17B PY A95-17C PY A95-17D PO	Massive sulfide from dump Massive sulfide from dump	Clean po. Clean py Essentially all sp with occasional very small po inclusions Mostly sp with py and po Py with minor silicate inclusions, also occasional sp and minor cp inclusions Co with a large proportion of silicates. Co and py with some po.	Po Py SP SP Py CP CD
Norbec juxtaposed against Lac Dufault	JH98-03-1 SP JH98-03-2 PY JH98-03-3 SP JH98-03-4 PY	Massive sulfide from underground crown pillar Massive sulfide from underground crown pillar Massive sulfide from underground crown pillar	Sp with associated py and cp. Clean py. Py with minor sp and cp..	SP Py SP
Vauze	A95-11A PY A95-11A SP A95-11B PY A95-11B SP A95-11C CP A95-11F CP A95-11F PO	Stockwork/massive sulfide dump Stockwork/massive sulfide dump Stockwork/massive sulfide dump Stockwork/massive sulfide dump	Very clean py Py with very small sp inclusions ~50:50 mix of sp and py. Very clean cp. Mostly cp with some py and sp, some grains have quite a lot of silicate inclusions. Mostly cp and sp, very occasional py, but no po. Very small grains. Very very fine grained sample seems to be mostly cp with some py. Py, magnetite and cp present.	Py SP Py CP CP (Sp)
Newbec	NEV/B44 CP NEV/B44 PY	Breccia ore	Py with intergrown and included sp and cp. Sp with some minor cp. Mostly po with ~30% sp. Sp with occasional intergrown po. Sp with minor po.	Py SP Po(Sp) Sp
Quemont All samples from East Orebody	Q14-2 SP Q14-2 PY Q17-7 SP Q17-7 SP(Po)	Massive sulfide intersection Massive sulfide intersection Massive sulfide intersection Massive sulfide intersection	Mostly clean cp with some py grains and some cp intergrown with py. One grain has galena intergrown with galena. Mostly po with ~30% cp with some intergrown. Clean py with very occasional small intergrown sp. 70% Py with occasional sp inclusions, 30% cp with occasional intergrown sp, also quite a lot of gangue All py, a few rare cp grains. No po. Clean py, a very few grains have cp inclusions.	CP Py Py Py Py Py
	Q18-6 CP Q18-6 PO(CP) Q19-4 PY	Massive sulfide intersection	Mostly py with ~25% cp, which is occasionally included and intergrown. Also very minor sp.	Py (Cp)
	Q19-4 PY(SP)	Massive sulfide intersection	~65% sp, ~35% py occasionally intergrown. Some very minor po inclusions in sp.	SP
	Q114-1 PO Q114-1 PY	Massive sulfide intersection	Actually no with minor cp. Sp with associated cp and po.	PO (Mt) Po (Cp)
	Q114-1 PY(CP2)	Massive sulfide intersection	Actually py with minor sp.	Py (Gn)
	Q115-4 PY Q115-4 SP	Massive sulfide intersection	Sp with lots of py which has sp inclusions.	SP (Gn)
	Q117-5 PO(MT)	Massive sulfide intersection	Sp with associated po and galena.	PO (Gn)
	Q117-5 PY Q117-5 SP(CP2)	Massive sulfide intersection	Sp with lots of py which has sp inclusions.	Py (Gn)
	Q118-1 PO(SP)	Massive sulfide intersection	Sp with lots of py which has sp inclusions.	SP (Gn)
	Q118-1 PY(GN)	Late galena vein in massive sulfide lower lenses		PO
	Q127-2 PO 63RF53 GN			Gn

Table A.1.1 (cont.)

Stratigraphic Position	Deposit	Sample	Sample Description ¹	Microprobe Description	Mineralogy
Post-Cauldron					
Deidona	All samples from Au rich discovery core	DELD-F339-1004 PY	Semi-massive sulfide	Py with minor sp and very minor galena often occur together. Also some minor silicate/oxide.	Py Py (Gn) Sp
		DELD-F339-985 PY (GN)	Semi-massive sulfide	Py with very minor galena. Get occasional cp inclusions in py.	Sp
		DELD-F339-985 SP	Semi-massive sulfide	Sp with minor associated galena, cp and py.	Sp
		DELD-F339-986 SP	Semi-massive sulfide	Sp with minor associated py and cp.	Sp
		DELD-F339-987 GN(SP)	Semi-massive sulfide	Galena and sp, with lots of py and some minor cp.	Sp
		DELD-F339-987 SP	Semi-massive sulfide	Galena and sp, with lots of py and some minor cp.	Sp
		DELD-F339-999 PY (SP)	Semi-massive sulfide	Py with minor sp. Polish not great so no sp analysed.	Py (Sp)
		DELD-F339-999 SP	Semi-massive sulfide	Sp with minor associated cp and py (too small to do analyses).	Sp
Delbridge		98DELB1 SP	Semi-massive sulfide from orebilles	Sp with some cd.	Sp
		98DELB2 1-PO(SP)	Semi-massive sulfide from orebilles	Equal proportions of py, sp and cp, no po.	Py Py (Sp/Cp)
		98DELB2 SP	Semi-massive sulfide from orebilles	Py with occasional sp.	Py
		98DELB3 SP(GN)	Semi-massive sulfide from orebilles	Sp with py and cp.	Sp (Gn)
		98DELB4 PY	Semi-massive sulfide from orebilles	Py with a significant amount of sp.	Py
		98DELB4 SP	Semi-massive sulfide from orebilles	All py with a lot of sp inclusions. No po.	Sp
		98DELB5 PO	Semi-massive sulfide from orebilles	Py with some minor sp.	Py
		98DELB5 PY	Semi-massive sulfide from orebilles	Py with very minor sp. and very very minor cp. Some of the py has some very small sp inclusions.	Py
		98DELB6 PY(GN)	Semi-massive sulfide from orebilles	No galena.	Py (Gn)
Gallen	Open pit samples from walls	JH98GLN-2HW2 PY	Hanging wall veins	Clean py	Py
		JH98GLN-2M51-1 PY	Massive sulfide	Mostly py with some minor sp.	Py
		JH98GLN-2M51-1 SP	Massive sulfide	Mostly sp with ~30% py.	Sp
		JH98GLN-2M51 SP	Massive sulfide	Sp with minor py.	Sp
		JH98GLN-2M52-1 SP	Massive sulfide	Mostly sp, some py, which is occasionally intergrown.	Sp
		JH98GLN-2M52 PY	Massive sulfide	Mostly py with some sp, and most of the py has sp inclusions.	Py
		JH98GLN-2V2 PY	Crosscut late veins	Mostly py, some sp.	Py
		JH98GLN-3E-FW CP	Football stringer, east end	Co dominated, some grains are intergrown with py.	Co
		SP4860 SP	Massive sulfide	More py than sp	Sp
		86M0BR400 PY	Composite concentrate from mill tailing	Po with occasional sp inclusions.	Py
		86M0BR06 SP	Massive sulfide	Mix of sp and py, some intergrow.	Sp
		86M0BR12 PY	Massive sulfide	Py and minor sp, some intergrow, also occasional sp and cp inclusions.	Py
		86M0BR12 SP	Massive sulfide	Sp dominated with occasional intergrown cp, py and sp.	Sp
		86M0BR2 PY	Massive sulfide	Mix of py and sp, some intergrow.	Py

¹ sample descriptions from Geological Survey of Canada records

Note: py - pyrite; sp - sphalerite; cp - chalcopyrite; po - pyrrhotite; gn - galena

Table A1.2: Sulfur isotope compositions and ICP-MS trace element concentrations for sulfides from the Noranda VMS deposits

Stratigraphic Position	Deposit	Sample	Mineralogy	$\delta^{34}\text{S}_{\text{CFS-CEN}} (\text{\textperthousand})$	$\Delta^{34}\text{S}_{\text{CFS-CEN}} (\text{\textperthousand})$	Cu (wt%)	Zn (wt%)	Cr (ppm)	Mn (ppm)	Co (ppm)	Ni (ppm)	Se (ppb)	Mo (ppb)	Au (ppb)	Pb (ppb)	
Pre-cauldron	Robb-Montbrey (Inmont)	A95-16A CP	Py	-0.08	0.0	-0.06	37.22	0.02	b.d.l.	1113	251	1031	2	533	320	
		A95-16A PY	Py	0.11	0.3	-0.07	0.92	0.00	b.d.l.	2538	51	1250	1	86	1092	
		A95-16B CP	Py	-0.33	-1.5	-0.07	34.09	0.03	b.d.l.	173	134	1939	1	413	413	
		A95-16B PY	Py	-0.72	-1.3	-0.06	12.29	0.15	b.d.l.	2669	134	1195	1	85	1040	
		A95-16C CP	Py	0.10	0.3	-0.06	0.66	0.06	b.d.l.	609	481	491	1	106	94	
		A95-16D SP	Sp	-0.21	-0.3	-0.08	14.80	0.08	b.d.l.	920	8	542	1	66	10140	
Horne No. 8		H6-3110 CP	Py	-0.03	0.0	-0.05	7.90	0.00	b.d.l.	316	100	25	2	93	10	
		H6-2114 CP	Py	0.21	0.7	-0.04	0.82	0.00	b.d.l.	949	222	4	0	1028	25	
		H6-2118 PY	Py	0.43	0.9	-0.03	0.21	0.00	b.d.l.	681	298	0	51	1	320	
		H6-3120 PY	Py	0.45	0.9	-0.03	2.17	0.00	b.d.l.	659	78	804	0	194	7	
		H6-3121 PY	Py	0.33	0.7	-0.04	0.07	0.07	b.d.l.	2310	8	260	1	64	32	
		H6-3122 PY	Py	0.29	0.6	-0.04	0.51	0.00	b.d.l.	3917	2	257	0	76	24	
		H6-3123 PY	Py	0.53	1.1	-0.04	0.13	0.00	b.d.l.	112	4	b.d.l.	78	75	21	
		63R170 GR		-0.32	-0.5	-0.07	0.00	0.00	b.d.l.	920	8	25	2	93	10	
		63R176 CP	CP	-0.04	0.0	-0.05	27.12	0.03	b.d.l.	66	32	b.d.l.	36	16	16	
		63R171 CP	CP	-0.54	-0.9	-0.06	17.96	0.57	b.d.l.	139	28	b.d.l.	30	80	4107	
		63R171 PY	Py	0.37	0.8	-0.05	0.39	0.33	b.d.l.	39	117	b.d.l.	270	21	3491	
		63R173 (99L) PY	Py	0.61	1.3	-0.04	0.04	0.65	b.d.l.	25	37	b.d.l.	126	13	142	
		63R173 SP	Sp	-0.23	-0.4	-0.05	0.77	0.07	b.d.l.	5	382	4	b.d.l.	0	73	73
		64R1623 SP	Sp	-0.10	0.0	-0.10	0.05	0.05	b.d.l.	108	6	b.d.l.	2	41	41	
		A95-14A CP	Py	-0.05	0.2	-0.16	0.05	0.50	b.d.l.	24	54	b.d.l.	2	44	166	
		A95-14A SP	Sp	-0.79	-1.1	-0.21	0.28	0.00	b.d.l.	1319	6	b.d.l.	34	6	353	
		A95-14B SP	Py (Sp)	-0.51	-0.7	-0.16	0.25	14.28	b.d.l.	827	2	b.d.l.	16	70	4399	
Horne No. 5		63R171 CP	Py	-0.54	-0.8	-0.14	0.57	0.03	b.d.l.	879	2	b.d.l.	320	5	285	
		63R171 PY	Py	0.37	0.8	-0.05	0.39	0.33	b.d.l.	39	117	b.d.l.	270	21	3491	
		63R173 (99L) PY	Py	0.61	1.3	-0.04	0.04	0.65	b.d.l.	25	37	b.d.l.	126	13	142	
		64R1623 SP	Sp	-0.23	-0.4	-0.05	0.77	0.07	b.d.l.	5	382	4	b.d.l.	0	73	73
Cauldron Margin	Adermac	A95-14A CP	Py	-0.05	0.2	-0.16	0.05	0.50	b.d.l.	24	54	b.d.l.	2	44	166	
		A95-14A SP	Sp	-0.79	-1.1	-0.21	0.28	0.00	b.d.l.	1319	6	b.d.l.	34	6	353	
		A95-14B PY	Py	-0.51	-0.7	-0.16	0.25	14.28	b.d.l.	827	2	b.d.l.	16	70	4399	
		A95-14B SP	Sp	-0.54	-0.8	-0.14	0.57	0.03	b.d.l.	879	2	b.d.l.	320	5	285	
		A95-14C CP	Py	-0.39	-0.5	-0.13	0.57	0.01	b.d.l.	206	137	b.d.l.	41	3	55	
		A95-14C PY	Py	-0.38	-0.5	-0.13	0.57	0.01	b.d.l.	75	40	b.d.l.	80	31	45	
		A95-14D CP	Py	-0.59	-0.9	-0.13	0.57	0.01	b.d.l.	22	365	b.d.l.	1	2	59	
		A95-14D SP	Sp	-0.04	0.1	-0.10	0.45	0.06	b.d.l.	87	14	b.d.l.	3	37	37	
		A95-12A CP1	CP	-0.11	-0.1	-0.07	0.09	20.48	b.d.l.	724	21	232	0	16	16	
		A95-12A CP2	CP	-0.11	-0.1	-0.07	17.13	0.00	b.d.l.	1156	28	b.d.l.	63	24	24	
		A95-12A CP2	Py	-0.11	-0.4	-0.08	1.42	0.00	b.d.l.	902	41	1999	1	53	25	
		A95-12C PY	Py	-0.41	-0.6	-0.08	0.70	0.04	b.d.l.	1280	2	b.d.l.	320	5	285	
		CRB13-15-5 SP	Sp	0.65	1.6	-0.16	0.68	0.01	b.d.l.	774	2	b.d.l.	320	5	285	
		CRB13-15-5 SP	Py	-0.12	0.3	-0.25	0.08	0.37	b.d.l.	104	2	b.d.l.	320	5	285	
		A95-13 PO	Py	-0.43	1.0	-0.10	0.45	0.06	b.d.l.	181	21	b.d.l.	126	13	142	
		A95-10A PY	Py	-0.05	0.1	-0.10	0.45	0.06	b.d.l.	15	15	b.d.l.	30	2	59	
		A95-10B CP	CP	0.07	0.3	-0.11	29.33	0.00	b.d.l.	234	3	b.d.l.	126	13	142	
		A95-10C CP	Py	0.19	0.8	-0.21	0.14	0.06	b.d.l.	867	7	b.d.l.	209	1	57	
		ANSL11A-247 CP	CP	-0.47	-0.6	-0.16	21.88	0.26	b.d.l.	23	1	b.d.l.	43	27	27	
		ANSL6A-4140 CP	CP	-0.32	-0.3	-0.23	33.51	0.21	b.d.l.	456	11	b.d.l.	582	0	371	
		ANSL6C-HW CP	CP	0.04	0.6	-0.27	0.23	0.23	b.d.l.	75	1	b.d.l.	224	2	16	
		ANSL9B12 SP	Sp	-0.69	1.8	-0.24	0.07	0.94	b.d.l.	91	86	b.d.l.	126	13	142	
		ANSL9B3-BX PY	Py	0.32	1.5	-0.43	0.61	0.02	b.d.l.	762	5	b.d.l.	126	13	142	
		ANSL9B5 SP	Sp	-0.44	-0.4	-0.26	11.00	0.08	b.d.l.	857	12	b.d.l.	209	1	57	
		ANSL9B5MMS PY	Py (CP)	-0.86	-1.0	-0.32	0.11	0.25	b.d.l.	217	0	b.d.l.	46	16	16	
		C-TUFF PY1	Py	-0.68	-0.7	-0.33	0.19	0.26	b.d.l.	36	13	b.d.l.	46	38	801	
		C-TUFF PY2	Py	-0.84	-1.1	-0.27	0.52	0.26	b.d.l.	33.90	3	b.d.l.	46	38	801	
		JH70-04 CP	CP	-0.23	0.0	-0.23	28.39	3.31	b.d.l.	245	3	b.d.l.	55	5	28	
		LDF-N-127 CP	CP	-0.09	0.2	-0.22	34.15	3.00	b.d.l.	206	4	b.d.l.	162	0	65	
		SP2091 PY	Py	0.28	0.9	-0.17	0.19	2.48	b.d.l.	96	33	b.d.l.	49	3	33	
		A95-09A PY	Py	0.11	0.6	-0.17	0.08	0.06	b.d.l.	276	2	b.d.l.	32	2	58	
		A95-09B PY	Py	0.02	0.3	-0.13	0.01	1.19	b.d.l.	105	1	b.d.l.	31	0	54	
		A95-09B SP	Sp	-0.18	0.2	-0.22	0.02	65.00	b.d.l.	769	7	b.d.l.	85	0	4214	
		ANFL28001 CP	CP	-0.01	0.2	-0.14	34.59	2.03	b.d.l.	601	2	b.d.l.	487	14	4942	
		ANFL28001 PO	Py	-0.77	-1.1	-0.22	8.14	0.70	b.d.l.	326	35	b.d.l.	289	215	68	
		ANFL8601 CP	CP	-0.14	0.3	-0.16	17.04	28.87	b.d.l.	201	4	b.d.l.	449	3	46	
		ANFL8601 PY	Py	-0.22	-0.2	-0.12	1.62	10.98	b.d.l.	372	9	b.d.l.	314	7	132	
		A95-07F CP	Py	-0.37	-0.5	-0.17	0.03	0.13	b.d.l.	90	34	b.d.l.	174	1	61	
		A95-07F CP	Py	-0.40	1.2	-0.21	0.93	55.07	b.d.l.	562	6	b.d.l.	63	1	46	
		A95-07B SP	Sp	0.18	0.7	-0.17	1.77	60.55	b.d.l.	811	4	b.d.l.	318	27	342	
		A95-07C PY	Py	-0.45	-0.3	-0.29	0.37	0.35	b.d.l.	23	2	b.d.l.	743	2	58	
		A95-07D PY	Py	0.01	0.3	-0.16	2.85	8.01	b.d.l.	623	14	b.d.l.	95	0	4214	
		A95-07E CP	CP	-0.21	-0.2	-0.29	30.29	4.17	b.d.l.	229	3	b.d.l.	487	7	89	
		A95-07F CP	Py	-0.04	0.3	-0.10	29.35	1.76	b.d.l.	67	26	b.d.l.	449	3	46	
		A95-08A PY	Py	-0.22	-0.2	-0.12	1.62	10.98	b.d.l.	201	4	b.d.l.	372	9	1143	
		A95-08A PY	Py	-0.37	-0.5	-0.17	0.03	0.13	b.d.l.	90	34	b.d.l.	174	1	61	
		A95-08B CP	CP	-0.40	1.2	-0.21	0.93	55.07	b.d.l.	562	6	b.d.l.	63	1	46	
		A95-08B CP	Py	-0.18	0.7	-0.17	1.77	60.55	b.d.l.	811	4	b.d.l.	318	27	342	
		A95-08E SP	Sp	-0.07	0.1	-0.12	35.32	3.75	b.d.l.	23	2	b.d.l.	743	2	58	
		A95-08F CP	Py	0.07	0.4	-0.12	6.12	0.85	b.d.l.	511	6	b.d.l.	529	1	78	

Table A1.2 (cont.)

Stratigraphic Position	Deposit	Sample	Mineralogy	$\delta^{33}\text{S}_{\text{Sulfate}}$ (‰)	$\Delta \delta^{33}\text{S}_{\text{Sulfate}}$ (‰)	Cu (wt‰)	Zn (wt‰)	Cr (ppb)	Mn (ppb)	Co (ppm)	Ni (ppb)	Se (ppb)	Mo (ppb)	Au (ppb)	Pb (ppb)	
Old White (White-Montgomery)	East Waite	A95-16A PY	Py	-0.43	-0.19	0.04	1.16	59.46	50.1	10	13	b.d.l.	13	1	50	
		A95-16A SP	Sp	-0.05	0.3	-0.20	0.27	31.70	3.22	2	37	1909	135	84	21	
		A95-16B CP	CP	-0.14	0.5	-0.39	0.32	4.98	0.33	55	432	1367	546	24	17	
		A95-16B PO	Py	-1.28	-1.9	-0.30	0.08	0.97	0.08	4	11	12497	49	53	15	
		A95-16C PY	Py	-0.27	0.4	-0.47	0.97	0.08	0.08	4	30	110	50	1	101	
		A95-17A PY	Py	-0.14	0.2	-0.26	0.05	0.45	0.45	4	20	5698	15	125	58	
		A95-17A SP	Sp	-0.06	0.4	-0.26	0.02	1.16	1	15	5698	b.d.l.	47	1	5	
		A95-17B PY	Py	-0.02	0.5	-0.26	0.27	56.81	5	8	852	10	13	54	21	
		A95-17C PY	Py	-0.37	-0.3	-0.23	0.51	24.62	1	145	405	21	106	1	13	
		A95-17D CP	CP	-0.54	2.2	-0.59	0.12	0.62	26	38	2171	705	138	0	15	
		A95-17D PO	Py	-0.96	-1.5	-0.17	2.07	0.98	1	60	193	b.d.l.	2	49	21	
		JH98-03-1 SP	Sp	-0.60	-0.8	-0.17	8.05	0.31	4	75	1112	4	363	1	73	
		JH98-03-2 PY	Py	-0.06	0.7	-0.28	0.36	45.94	4	2279	460	b.d.l.	220	2	6513	
		JH98-03-3 SP	Sp	-0.23	0.0	-0.21	0.75	0.28	1	229	1481	7	220	2	15	
		JH98-03-4 PY	Py	-0.19	0.0	-0.20	1.32	53.40	1	2578	416	2	52	0	35	
		A95-11A PY	Py	-0.20	0.8	-0.23	0.03	0.80	0.02	53	320	1465	42	189	1	50
		A95-11A SP	Sp	-0.28	0.0	-0.27	0.19	42.80	1	48	1313	57	389	1	57	
		A95-11B PY	Py	-0.12	0.7	-0.22	0.06	1.64	2	1427	350	5	251	0	53	
		A95-11B SP	Sp	-0.13	0.7	-0.22	0.32	28.04	2	90	2019	25	274	0	56	
		A95-11C CP	CP	-0.31	-0.2	-0.21	35.56	0.29	0	8297	1297	18	231	0	138	
		A95-11F CP	CP (Sp)	-0.35	-0.2	-0.25	26.17	1.54	1	45	402	96	523	2	54	
		A95-11F PO	CP	-0.47	-0.5	-0.23	17.91	19.19	23	283	414	5	385	1	41	
		NEWB44 CP	CP	-0.22	0.5	-0.48	15.42	0.42	2	830	971	320	1	51	154	
		NEWB44 PY	Py	-0.01	0.3	-0.09	2.11	0.07	4	457	3557	957	61	2	50	
		Q14-2 PY(SP)	Py (Sp)	0.58	1.3	-0.11	0.17	6.07	2	25	117	b.d.l.	221	0	39	
		Q14-2 SP	Sp	0.01	0.2	-0.11	1.04	0.06	6	6	164	220	23	100	31	
		Q14-7 PY(SP)	Py (Sp)	0.09	0.4	-0.13	1.64	62.28	2	107	6	401	b.d.l.	60	24	
		Q17-7 SP	Sp	0.33	0.9	-0.12	0.13	10.65	5	2270	4	244	b.d.l.	2	98	
		Q18-6 CP	CP	0.35	0.9	-0.13	0.18	53.29	0	1975	2	30	b.d.l.	397	51	
		Q18-6 PY(CP)	Py	0.08	0.3	-0.09	28.01	2.11	0	271	38	b.d.l.	165	0	59	
		Q19-4 PY(CP)	Py	0.19	0.5	-0.09	0.09	0.09	0.09	3	830	971	347	27	1	
		Q19-4 PY(SP)	Py (Sp)	-0.01	0.3	-0.16	0.13	0.15	1	28	14	4	694	0	56	
		Q19-4 PY(CP)	Py	-0.28	-0.2	-0.18	0.18	2.74	7	1522	19	11	1339	4	65	
		Q114-1 PO	Py	0.57	1.3	-0.11	1.04	0.06	0.06	6	220	23	b.d.l.	2	111	
		Q114-1 PY	Py	0.55	1.3	-0.10	0.14	0.01	0	3	475	13	222	b.d.l.	41	
		Q114-1 PY(CP)	Py (CP)	0.46	1.1	-0.10	2.83	0.14	1	108	310	14	223	0	50	
		Q115-4 PY	Py	0.04	0.3	-0.13	0.13	0.01	50.80	3	107	17	b.d.l.	179	1	41
		Q115-4 SP	Sp	0.44	0.5	-0.14	0.08	0.28	2.61	3	83	216	4	453	4	32
		Q117-5 PO(MT)	Po (Mt)	0.62	1.5	-0.13	0.55	0.38	0.3	4	10	9	64	2	453	
		Q117-5 PY	Py	0.25	0.8	-0.14	1.62	15.93	1	201	40	b.d.l.	61	3	209	
		Q117-5 SP(CP)	Py	0.68	1.8	-0.23	0.17	0.57	2	33	1	54	1	54	2327	
		Q118-1 PO(SP)	Py (Sp)	0.95	2.2	-0.20	0.07	0.79	2	114	12	8	4	49	8096	
		Q118-1 PY(GN)	Py (Gn)	0.82	2.0	-0.21	0.89	47.63	11	484	10	9	69	4	10681	
		Q118-1 SP(GN)	Sp (Gn)	-0.38	-0.5	-0.13	0.10	4.38	4	383	2	424	41	53	90	
		Q172-2 PO	Po	-14.01	-27.2	-0.09	-0.22	0.01	50.80	3	107	17	b.d.l.	179	1	32
		DEL0-1339-1004 PY	Py (Gn)	0.80	2.0	-0.20	0.30	1.17	4	284	6	3	10	0	2827	
		DEL0-1339-985 SP	Sp	0.43	1.3	-0.26	1.42	54.14	0	206	166	6	762	1	1914	
		DEL0-1339-986 SP	Sp	0.39	1.3	-0.28	0.81	52.07	0	229	79	13	187	1	9256	
		DEL0-1339-987 SP	Sp	0.22	0.9	-0.27	0.25	1.20	2	191	97	2	89	0	59	
		DEL0-1339-995 PY(SP)	Py (Sp)	0.45	1.4	-0.25	0.05	56.46	2	265	154	3	87	1	11448	
		DEL0-1339-995 SP	Sp	0.94	2.3	-0.25	0.07	14.10	3	267	34	3	38	0	3102	
		98DELB1 SP	Sp	0.50	1.4	-0.24	0.30	56.73	4	4467	4	539	b.d.l.	110	0	455
		98DELB1 PY(SP)	Py (Sp/Cp)	0.22	0.8	-0.19	4.87	44.67	4	539	91	b.d.l.	110	0	455	
		98DELB2.1 PY	Py	0.54	1.6	-0.28	7.60	26.09	0	126	621	10	9	64	1	1062
		98DELB2 SP	Sp	0.48	1.4	-0.27	0.33	3.89	0	115	57	0	64	2	1736	
		98DELB2.1 SP(GN)	Sp (Gn)	0.52	1.5	-0.26	0.03	29.82	2	270	23	1	71	2	2255	
		98DELB4 SP	Py	0.76	2.0	-0.28	0.05	56.46	2	191	97	2	89	0	2019	
		98DELB4 SP	Sp	0.38	1.3	-0.31	0.02	45.69	1	1154	37	0	28	1	19180	
		98DELB5 SP	Py	0.80	2.0	-0.23	0.07	2.80	0.02	5.80	395	b.d.l.	1	51	215	
		98DELB5 PY	Py	0.57	1.6	-0.25	0.02	0.80	1	459	10	0	64	1	3102	
		98DELB6 PY(GN)	Py (Gn)	0.71	1.9	-0.25	0.02	2.01	4	621	10	9	22	2	14762	
		JH96GLLN-2H2PY	Py	0.65	1.6	-0.17	0.04	0.36	3	17	15	1	58	0	876	
		JH96GLLN-2MSL1 PY	Py	0.54	1.5	-0.24	0.00	4.88	1	72	18	21	b.d.l.	0	223	
		JH96GLLN-2MSL1 SP	Sp	0.51	1.4	-0.22	0.00	47.64	0	299	10	13	b.d.l.	0	395	
		JH96GLLN-2MSL1 SP	Sp	0.21	0.8	-0.21	0.05	53.60	2	327	13	3	b.d.l.	0	292	
		JH96GLLN-2MSL2 PY	Py	-0.08	0.1	-0.11	0.05	61.74	2	34	1	6	b.d.l.	0	344	
		JH96GLLN-2MSL2 PY	Py	0.46	1.0	-0.07	0.00	52.71	0	52	6	1	b.d.l.	0	283	
		JH96GLLN-2V2 PY	Py	0.09	1.0	-0.43	0.00	3.74	4	25	16	10	b.d.l.	49	333	
		JH96GLLN-2E-FV CP	CP	0.61	1.3	-0.07	29.79	0.72	2	38	10	b.d.l.	265	0	164	

Table A1.2 (cont.)

Stratigraphic Position	Deposit	Sample	Mineralogy	$\delta^{34}\text{S}_{\text{CIM}} (\text{\textperthousand})$	$\delta^{34}\text{S}_{\text{CIM}} (\text{\textperthousand})$	$\Delta^{33}\text{S}_{\text{CIM}} (\text{\textperthousand})$	Cu (wt%)	Zn (wt%)	Cr (ppb)	Mn (ppb)	Co (ppm)	Ni (ppb)	Se (ppb)	Mo (ppb)	Au (ppb)	Pb (ppb)
Mobrun		SP4880 SP	Sp	0.02	0.4	-0.19	0.20	13.97	1.26	114	463	34	89	43	297	
		86MBR400 PY	Py	0.40	1.2	-0.20	0.30	1.26	1.3	236	110	10	61	3	1114	
		86MBR06 SP	Sp	0.15	1.0	-0.38	0.14	45.33	1.1	101	10	9	54	1	165	
		86MBR12 PY	Py	0.06	0.7	-0.29	0.24	1.53	1	111	811	30	68	1	125	
		86MBR12 SP	Sp	-0.19	0.0	-0.19	0.79	43.30	1	400	192	6	101	0	84	
		86MBR2 PY	Py	0.39	1.2	-0.21	0.03	12.39	0	85	14	3	b.d.l.	1	86	
															561	

Note: Py - pyrite; Sp - sphalerite; Cp - chalcopyrite; Po - pyrrhotite; Gn - galena; b.d.l. - below detection limit

Table A1.3 Pyrite: EPMA analyses for pyrite separated by sample for sulfide grains from Noranda VMS deposits.

Stratigraphic Position	Deposit	Sample	S (wt%)	As (wt%)	Cu (wt%)	Cd (wt%)	Fe (wt%)	Se (wt%)	Zn (wt%)	Cr (wt%)	Ni (wt%)	Co (wt%)
Pre-cauldron	Robb-Montbray	A95.16A-PY-G1-1	53.3	0.15	0.01	0	46.48	0.13	0	0	0.01	0
		A95.16A-PY-G1-2	52.99	0.14	0	0.01	46.71	0.12	0	0	0	0.01
		A95.16A-PY-G1-3	53.18	0.12	0.03	0.04	46.61	0.13	0.01	0	0.02	0
		A95.16A-PY-G2-1	53.28	0.07	0.07	0	46.36	0.19	0	0	0	0.56
		A95.16A-PY-G2-2	53.41	0.04	0	0	46.53	0.27	0	0	0	0.15
		A95.16A-PY-G2-3	53.09	0.08	0	0.05	46.61	0.24	0.02	0	0.01	0.55
		A95.16A-PY-G3-1	52.3	1	0.02	0.04	46.36	0.16	0.01	0	0	0.02
		A95.16A-PY-G3-2	53.08	0.38	0.02	0.01	46.74	0.26	0	0	0	0.05
		A95.16A-PY-G3-3	53.7	0.01	0.04	0	46.69	0.19	0.01	0	0	0.08
		A95.16A-PY-G4-1	53.38	0.04	0.01	0	46.49	0.06	0	0	0	0.05
		A95.16A-PY-G4-2	53.12	0	0.01	0.02	46.87	0.06	0.02	0	0.01	0.1
		A95.16A-PY-G4-3	53.77	0.04	0	0	46.79	0.13	0.03	0	0	0.1
		A95.16A-PY-G5-1	53.33	0.05	0.01	0.03	46.79	0.11	0	0	0.01	0.02
		A95.16A-PY-G5-2	53.27	0.02	0.01	0.03	46.65	0.11	0	0	0	0
		A95.16A-PY-G5-3	53.39	0.08	0.02	0	46.48	0.08	0.04	0	0	0.01
		A95.16A-PY-G6-1	53.03	0.26	0.04	0	46.66	0.25	0.02	0	0	0.13
		A95.16A-PY-G6-2	53.18	0	0.05	0.01	46.67	0.19	0.02	0	0	0.05
		A95.16A-PY-G6-3	53.23	0.49	0.01	0.02	46.85	0.19	0	0	0	0
		A95.16A-PY-G6-4	51.96	1.3	0.01	0	46.64	0.32	0.02	0	0.01	0
		A95.16A-PY-G7-1	53.53	0.09	0.01	0	46.84	0.1	0.02	0	0	0
		A95.16A-PY-G7-2	53.43	0.01	0.02	0	46.5	0.06	0	0	0	0
		A95.16A-PY-G7-3	53.37	0.06	0.01	0	46.75	0.12	0.02	0	0	0.02
		A95.16A-PY-G7-4	53.29	0.13	0.02	0	46.71	0.15	0.01	0	0.02	0.03
		A95.16A-PY-G8-1	53.26	0.05	0.06	0.01	46.77	0.09	0.01	0	0	0.01
		A95.16A-PY-G8-2	53.63	0.03	0.05	0.04	46.48	0.11	0	0	0	0.01
		A95.16A-PY-G8-3	52.82	0.22	0.28	0.01	45.54	0.07	0.02	0	0	0.58
		A95.16A-PY-G9-1	53.14	0.21	0.04	0	46.59	0.2	0	0	0.01	0
		A95.16A-PY-G9-2	53.35	0.12	0.01	0	46.85	0.15	0	0	0.01	0
		A95.16A-PY-G9-3	53.09	0.13	0.02	0	47	0.16	0	0	0	0
		A95.16A-PY-G9-4	53.32	0.16	0.04	0.02	46.86	0.17	0	0	0	0
		A95.16A-PY-G10-1	52.99	0.05	0	0	46.77	0.04	0.03	0	0	0.11
		A95.16A-PY-G10-2	53.14	0	0.04	0	46.57	0.18	0.02	0	0	0.16
		A95.16A-PY-G10-3	52.63	0	0.01	0	46.53	0.16	0	0	0	0.13
		A95.16A-PY-G10-4	52.69	0	0.03	0.01	46.7	0.17	0	0	0.02	0.16
		A95.16A-PY-G10-5	53.13	0	0	0	46.64	0.02	0	0	0	0.1
		A95.16A-PY-G11-1	52.54	0.82	0.03	0	46.52	0.42	0.01	0	0	0
		A95.16A-PY-G11-2	53.25	0.25	0	0	46.64	0.11	0.02	0	0	0
		A95.16A-PY-G11-3	53.57	0.3	0.07	0	46.16	0.31	0.01	0	0	0
		A95.16A-PY-G11-4	53.61	0.33	0.07	0	46.24	0.26	0	0	0	0
		A95.16A-PY-G11-5	53.59	0.26	0.05	0.01	46.19	0.22	0	0	0.01	0
		A95.16B-PY-1	52.56	0	0.01	0	46.84	0.07	0.02	0	0.01	0.19
		A95.16B-PY-2	52.68	0	0	0	46.43	0.17	0	0	0	0.45
		A95.16B-PY-3	52.59	0	0.32	0.01	46.27	0.15	0	0	0.05	0.24
		A95.16B-PY-4	52.52	0	0.05	0	46.68	0.07	0	0	0	0.2
		A95.16B-PY-5	52.64	0	0.02	0	46.69	0.13	0	0	0	0.11
		A95.16B-PY-6	52.18	0	0	0	46.45	0.3	0	0	0.01	0.3
		A95.16B-PY-7	52.71	0	0.22	0	45.53	0.17	0	0	0.16	0.95
		A95.16B-PY-8	52.11	0	0.02	0	46.73	0.23	0	0	0.01	0.22
		A95.16B-PY-9	52.72	0	0.01	0	46.8	0.23	0	0	0	0.05
		A95.16B-PY-10	52.71	0	0.03	0	46.71	0.12	0.01	0	0.02	0.25
		A95.16C-PY-G1-1	53.6	0.03	0.03	0.01	46.88	0.09	0	0	0.07	0.01
		A95.16C-PY-G1-2	53.89	0	0.01	0	46.97	0.09	0	0	0.03	0
		A95.16C-PY-G1-3	53.45	0	0.03	0	47.08	0.06	0	0	0.04	0
		A95.16C-PY-G1-4	53.56	0.02	0.01	0	46.7	0.11	0	0	0.09	0
		A95.16C-PY-G1-5	53.69	0.02	0.03	0.03	46.99	0.03	0	0	0.04	0
		A95.16C-PY-G2-1	53.73	0.01	0.02	0	46.8	0.14	0	0	0.17	0
		A95.16C-PY-G2-2	53.69	0	0.03	0	46.58	0.07	0	0	0.11	0
		A95.16C-PY-G2-3	53.45	0.02	0.02	0	47	0.08	0	0	0.02	0
		A95.16C-PY-G3-1	53.03	0	0.03	0	47.16	0.15	0	0	0.03	0
		A95.16C-PY-G3-2	53.55	0.04	0.01	0	46.8	0.12	0	0	0.03	0.02
		A95.16C-PY-G3-3	53.1	0.08	0.04	0	46.78	0.14	0.01	0	0.03	0.09
		A95.16C-PY-G3-4	53.69	0.01	0.02	0.01	46.96	0.11	0.02	0	0.02	0
		A95.16C-PY-G4-1	53.82	0.04	0.07	0	47	0	0	0	0.06	0.01
		A95.16C-PY-G4-2	53.55	0.02	0.04	0.02	46.9	0.05	0	0	0.08	0.07
		A95.16C-PY-G4-3rim	53.67	0.06	0.03	0	46.5	0.07	0	0	0.11	0.2
		A95.16C-PY-G4-4	53.3	0.05	0.04	0	46.72	0.04	0	0	0.05	0.2
		A95.16C-PY-G5-1	53.36	0.14	0.06	0	46.34	0.21	0.02	0	0.38	0
		A95.16C-PY-G5-2	53.68	0.17	0.03	0.01	46.33	0.18	0	0	0.39	0
		A95.16C-PY-G5-3	53.63	0	0.03	0	46.87	0.12	0	0.01	0	0
		A95.16C-PY-G5-4	53.66	0.04	0.01	0.03	47.02	0.11	0	0	0	0
		A95.16C-PY-G5-5	53.5	0.04	0.05	0	46.83	0.12	0.01	0	0.24	0
		A95.16C-PY-G6-1	53.67	0.14	0.01	0.03	46.3	0.13	0.03	0	0.35	0
		A95.16C-PY-G6-2	53.66	0.03	0.02	0	46.5	0.17	0.02	0	0.11	0
		A95.16C-PY-G6-3	53.52	0.07	0.04	0	46.49	0.17	0	0	0.33	0
		A95.16C-PY-G7-1	53.66	0.35	0.03	0	46.23	0.12	0	0	0.31	0.15
		A95.16C-PY-G7-2	53.46	0.3	0.02	0	46.25	0.11	0.02	0	0.32	0.16
		A95.16C-PY-G7-3	53.07	0.14	0.03	0	45.9	0.23	0.08	0	0.3	0.19
		A95.16C-PY-G8-1	52.97	0.1	0.01	0	47.11	0.09	0	0	0.11	0.07
		A95.16C-PY-G8-2	52.48	0.18	0	0.04	47.18	0.12	0	0	0.17	0.06
		A95.16C-PY-G8-3	53.42	0.04	0	0	46.98	0.06	0	0	0.14	0.02
		A95.16C-PY-G9-1	52.12	0.06	0.02	0	47.15	0.07	0.02	0	0.02	0.06
		A95.16C-PY-G9-2	53.08	0.02	0	0	47.07	0.32	0.03	0	0	0
		A95.16C-PY-G9-3	53.55	0.01	0.01	0	47.07	0.17	0.02	0	0	0
		A95.16C-PY-G9-4	53.44	0.01	0.01	0	46.83	0.11	0	0	0	0
		A95.16C-PY-G10-1	54.01	0.08	0.02	0	46.59	0.07	0	0.01	0.04	0
		A95.16C-PY-G10-2	53.86	0	0.01	0.01	46.94	0.07	0	0	0.02	0.02
		A95.16C-PY-G10-3	53.56	0	0.01	0	46.91	0.23	0.01	0	0.03	0.01
		A95.16C-PY-G10-4	53.64	0	0.01	0	46.89	0.16	0	0	0	0
		A95.16C-PY-G10-5	53.63	0.06	0.03	0	46.89	0.26	0	0	0.13	0.01
		A95.16C-PY-G10-6	53.62	0	0.03	0.03	46.63	0.08	0	0	0.02	0
		A95.16C-PY-1	53.03	0.08	0	0.01	46.86	0.12	0.01	0	0.05	0
		A95.16C-PY-2	53.46	0	0.01	0	46.81	0.06	0	0	0.04	0
		A95.16C-PY-3	53.07	0.11	0	0.01	46.44	0.18	0.01	0	0.29	0.01
		A95.16C-PY-4	52.85	0.09	0.02	0	46.85	0.09	0	0	0.11	0.01
		A95.16C-PY-5	53.16	0	0	0	46.84	0.06	0	0	0	0
		A95.16C-PY-6	53.27	0	0	0.01	46.58	0.17	0	0	0.17	0.01
		A95.16C-PY-7	53.08	0.17	0.02	0.01	46.55	0.21	0	0	0.08	0.05
		A95.16C-PY-8	53.04	0.12	0.02	0.02	46.56	0.14	0	0	0.3	0.02
		A95.16C-PY-9	53.06	0	0.02	0	46.91	0.16	0	0	0.0	

Table A1.3 Pyrite (cont.)

Stratigraphic Position	Deposit	Sample	S (wt%)	As (wt%)	Cu (wt%)	Cd (wt%)	Fe (wt%)	Se (wt%)	Zn (wt%)	Cr (wt%)	Ni (wt%)	Co (wt%)
Pre-cauldron	Robb-Montbray	A95.16C-PY-G4-2	53.68	0.04	0.04	0	46.79	0.04	0	0	0.05	0.07
		A95.16C-PY-G4-3	52.42	0	0.08	0.01	46.37	0	0.03	0	0.07	0.02
		A95.16C-PY-G5-1	53.66	0.2	0.03	0	46.33	0.15	0	0	0.36	0
		A95.16A-PY-G1-1	53.29	0.13	0.01	0	46.73	0.15	0	0	0	0
		63RF31 PY-1	53.46	0.04	0.03	0	46.72	0.06	0	0	0.01	0.01
Pre-cauldron	Horne No. 5	63RF31 PY-10	53.23	0.04	0.08	0	46.72	0.05	0.02	0	0.01	0.02
		63RF31 PY-11	53.51	0.01	0	0.01	46.77	0.04	0	0	0	0
		63RF31 PY-12	53.44	0.03	0.02	0	46.91	0.01	0	0	0	0
		63RF31 PY-13	53.51	0	0.01	0.02	46.91	0.02	0	0	0.01	0.02
		63RF31 PY-14	53.53	0.04	0	0	46.68	0.04	0	0	0	0
		63RF31 PY-15	53.56	0	0	0	46.86	0.01	0.03	0	0	0
		63RF31 PY-2	53.61	0	0.01	0	46.54	0.02	0	0	0	0
		63RF31 PY-3	53.65	0	0	0	46.7	0.01	0.01	0	0	0.03
		63RF31 PY-4	53.56	0	0.01	0	46.76	0	0.02	0	0	0
		63RF31 PY-5	53.48	0.04	0.03	0	46.79	0.01	0	0	0.01	0
		63RF31 PY-8	53.19	0	0.01	0	46.8	0.07	0.01	0	0	0
		63RF31 PY-9	53.27	0.04	0.02	0	46.7	0.02	0.03	0	0.01	0.02
		63RF32 PY-1	53.58	0.02	0	0	46.79	0	0	0	0	0
		63RF32 PY-10	53.65	0	0	0	46.78	0	0.01	0	0	0
		63RF32 PY-11	53.5	0	0.02	0	46.94	0	0	0	0	0.02
		63RF32 PY-12	53.73	0.02	0	0	46.63	0.01	0	0	0.01	0
		63RF32 PY-13	53.6	0.01	0	0	46.95	0.02	0.03	0	0	0
		63RF32 PY-14	53.4	0.05	0	0	46.76	0	0.1	0	0	0
Horne No. 8	Horne No. 8	63RF32 PY-15	53.5	0.01	0.01	0	46.91	0	0	0	0	0.02
		63RF32 PY-2	53.56	0.02	0	0	47.01	0	0	0	0.01	0
		63RF32 PY-3	53.4	0.03	0.01	0	46.92	0	0.05	0	0.01	0
		63RF32 PY-4	53.72	0.01	0.01	0.02	46.69	0	0.03	0	0	0
		63RF32 PY-5	53.46	0	0.02	0	46.96	0	0	0	0	0
		63RF32 PY-6	53.72	0.02	0	0	46.84	0.01	0.03	0	0	0
		63RF32 PY-7	53.39	0.03	0.07	0	46.84	0	0.04	0	0	0
		63RF32 PY-8	53.7	0.03	0.02	0	46.91	0.01	0	0	0	0
		63RF32 PY-9	53.61	0	0.02	0	46.97	0.01	0	0	0	0
		63RF31 CP-1	53.48	0	0.16	0	46.58	0.2	0	0	0	0
		63RF31 CP-10	53.55	0	0.12	0	46.7	0.02	0	0	0	0.01
		63RF31 CP-2	53.11	0	0.11	0	46.85	0.2	0	0	0	0
		63RF31 CP-3	53.3	0.01	0.16	0	46.79	0.01	0	0	0	0.01
		63RF31 CP-4	53.41	0	0.08	0	46.75	0.09	0	0	0	0.01
		63RF31 CP-5	53.06	0.01	0.12	0	46.55	0	0	0	0.01	0
		63RF31 CP-7	53.72	0	0.29	0	46.75	0.02	0.01	0	0	0.04
		63RF31 CP-8	53.52	0.01	0.1	0	46.76	0.02	0.03	0	0	0
		63RF31 CP-9	53.72	0.02	0.08	0.01	46.7	0.01	0.01	0	0	0.01
Horne No. 18	Horne No. 18	H63H18 PY-1	53.43	0	0.02	0	46.78	0.03	0.02	0	0.02	0.32
		H63H18 PY-10	53.46	0	0.02	0.04	46.75	0	0	0	0	0.22
		H63H18 PY-12	53.31	0	0.03	0	47.11	0.09	0	0	0.01	0
		H63H18 PY-13	53.41	0	0.01	0	46.39	0.1	0.02	0	0.09	0.04
		H63H18 PY-14	53.24	0	0	0	46.87	0.11	0.03	0	0.02	0.04
		H63H18 PY-15	53.57	0	0.02	0.01	47.05	0.05	0	0	0.01	0
		H63H18 PY-16	53.44	0	0.03	0	46.89	0.06	0.01	0	0	0.02
		H63H18 PY-17	53.54	0	0.01	0	46.93	0.05	0	0	0.01	0
		H63H18 PY-18	53.06	0	0.03	0	46.83	0.1	0	0	0.07	0.04
		H63H18 PY-19	53.39	0	0	0.01	46.95	0.04	0	0	0	0
		H63H18 PY-2	53.55	0	0	0	46.95	0.04	0	0	0	0.01
		H63H18 PY-20	53.65	0	0	0.02	46.89	0.07	0	0	0	0.03
		H63H18 PY-3	53.51	0	0.01	0	46.97	0.05	0	0	0	0
		H63H18 PY-4	53.37	0.05	0	0.01	46.67	0.16	0	0	0.27	0.02
		H63H18 PY-5	53.32	0	0.01	0	47.11	0.06	0.02	0	0.01	0.03
		H63H18 PY-7	53.39	0	0.03	0	46.98	0.14	0	0	0.05	0.01
		H63H18 PY-8	53.35	0.03	0	0	47.13	0.1	0	0	0.03	0.04
		H63H18 PY-9	53.88	0.01	0.01	0	46.7	0.03	0	0	0	0.17
		H63H20 PY-10	53.67	0	0.02	0.01	47.12	0.12	0	0	0	0.01
		H63H20 PY-11	53.77	0	0.04	0	47.01	0.05	0.01	0	0	0.01
		H63H20 PY-12	53.3	0	0	0	46.91	0.04	0	0	0	0
		H63H20 PY-13	53.35	0	0.02	0	47.03	0.12	0.01	0	0	0
		H63H20 PY-14	53.26	0.01	0.01	0.01	47.02	0.12	0	0	0.01	0
		H63H20 PY-15	53.58	0	0.09	0.01	46.98	0.09	0	0	0	0.01
		H63H20 PY-16	53.6	0.03	0.01	0.01	46.83	0.06	0.02	0	0	0.04
		H63H20 PY-17	53.3	0	0.01	0.04	46.99	0.11	0	0	0	0
		H63H20 PY-19	53.49	0.02	0.04	0.01	47.01	0.12	0.02	0	0	0
		H63H20 PY-2	53.59	0	0.03	0	47.08	0.19	0	0	0.01	0
		H63H20 PY-20	53.66	0	0.03	0	46.86	0.13	0	0	0.03	0.04
		H63H20 PY-3	52.83	0.03	0.01	0	46.26	0.09	0	0	0	0.05
		H63H20 PY-4	53.69	0	0.03	0	47.03	0.07	0.01	0	0	0.01
		H63H20 PY-5	53.51	0.02	0.08	0	47.07	0.11	0.01	0	0	0.04
		H63H20 PY-7	53.68	0	0.01	0.02	47.17	0.04	0.02	0	0.01	0
		H63H20 PY-8	53.53	0.01	0.07	0.04	46.97	0.06	0.04	0	0	0
		H63H20 PY-9	53.53	0.01	0.02	0	46.86	0.08	0	0	0	0.01
		H63H21 PY-1	53.2	0.01	0.02	0.01	46.92	0.17	0.01	0	0	0
		H63H21 PY-10	53.52	0	0.01	0	46.9	0.02	0	0	0	0.11
		H63H21 PY-11	53.24	0	0.02	0	46.94	0.03	0.01	0	0.01	0
		H63H21 PY-12	53.69	0	0.01	0	46.71	0	0	0	0.01	0.43
		H63H21 PY-13	53.3	0	0	0	46.55	0.01	0	0	0	0.41
		H63H21 PY-14	53.51	0	0.01	0.01	46.97	0.02	0.02	0	0	0
		H63H21 PY-15	53.5	0	0	0.02	46.64	0.02	0	0	0	0.45
		H63H21 PY-2	53.42	0	0.01	0	46.98	0.09	0.01	0	0	0
		H63H21 PY-3	53.43	0	0.02	0.02	46.98	0.04	0	0	0.01	0.02
		H63H21 PY-4	53.47	0	0.05	0	46.95	0.02	0	0	0	0.08
		H63H21 PY-5	53.32	0.02	0.02	0	46.71	0.03	0	0	0	0.19
		H63H21 PY-6	53.61	0	0.02	0	46.46	0.03	0	0	0	0.68
		H63H21 PY-7	53.42	0	0.04	0	46.62	0.01	0.02	0	0	0.22
		H63H21 PY-8	53.51	0.01	0.01	0	46.71	0.02	0	0	0.01	0.22
		H63H21 PY-9	53.47	0	0.01	0	46.87	0.05	0.02	0	0	0.02
		H63H22 PY-1	53.5	0.01	0.01	0	46.68	0.01	0	0	0	0.28
		H63H22 PY-10	53.59	0	0.01	0.02	46.72	0.01	0.01	0	0	0.23
		H63H22 PY-12	53.41	0	0.01	0.02	46.32	0.02	0	0	0	0.61
		H63H22 PY-13	53.46	0	0.01	0.01	46.29	0.02	0	0	0	0.58
		H63H22 PY-14	53.53	0	0.01	0	46.74	0.01	0.02	0	0	0.31

Table A1.3 Pyrite (cont.)

Stratigraphic Position	Deposit	Sample	S (wt%)	As (wt%)	Cu (wt%)	Cd (wt%)	Fe (wt%)	Se (wt%)	Zn (wt%)	Cr (wt%)	Ni (wt%)	Co (wt%)
Pre-cauldron	Horne No. 8	H63H22 PY-9	53.45	0	0.01	0	46.61	0.03	0	0	0	0.47
		H63H23 PY-1	53.39	0.05	0	0.01	46.99	0	0	0	0.01	0
		H63H23 PY-10	53.41	0.03	0	0.01	46.94	0	0	0	0	0.01
		H63H23 PY-11	53.4	0	0	0	47.19	0.01	0	0	0	0.01
		H63H23 PY-12	53.32	0	0	0.01	47.04	0	0.02	0	0	0
		H63H23 PY-13	53.65	0.04	0.02	0.04	47.11	0.01	0.01	0	0	0
		H63H23 PY-14	53.19	0	0.01	0	47.17	0.01	0	0	0	0
		H63H23 PY-15	53.41	0	0	0	46.99	0	0.01	0	0	0
		H63H23 PY-16	53.41	0	0.01	0	46.77	0.01	0	0	0	0.02
		H63H23 PY-17	53.4	0	0.01	0.01	46.81	0.03	0.01	0	0	0.04
		H63H23 PY-18	53.36	0.03	0.03	0.01	47.14	0.05	0	0	0	0
		H63H23 PY-19	53.5	0	0	0	46.94	0	0	0	0.01	0
		H63H23 PY-2	53.7	0	0	0	47.04	0	0	0	0	0
		H63H23 PY-20	53.54	0.03	0	0	46.97	0	0	0	0	0
		H63H23 PY-3	53.75	0	0.03	0.01	47.01	0.01	0	0	0	0.02
		H63H23 PY-4	53.46	0	0	0.01	47.14	0.01	0	0	0.01	0.04
		H63H23 PY-5	53.59	0	0	0	47.01	0.01	0.01	0	0.01	0.01
		H63H23 PY-6	53.28	0.02	0	0	46.97	0.01	0.01	0	0	0.01
		H63H23 PY-7	53.46	0.05	0.01	0.01	46.79	0.01	0	0	0	0.01
		H63H23 PY-8	53.41	0.02	0.01	0	47.19	0	0	0	0.01	0.01
		H63H23 PY-9	53.58	0	0	0	47.06	0.01	0	0	0	0
		H63H14 PO-1	53.48	0	0	0	46.9	0	0	0	0	0
		H63H14 PO-2	53.51	0.06	0.02	0	46.61	0.01	0	0	0	0.19
		H63H14 PO-3	53.28	0	0	0	46.86	0.04	0	0	0.01	0.01
		H63H14 PO-4	53.27	0	0.03	0.01	47.02	0.01	0	0	0	0.03
		H63H14 PO-5	53.36	0.06	0	0	46.71	0	0	0	0	0.19
		63RF36 CP-2	53.61	0	0.22	0.01	46.71	0.03	0	0	0	0.01
		63RF36 CP-3	53.81	0	0.17	0	46.65	0.06	0	0	0	0
		63RF36 CP-4	53.65	0.05	0.14	0	46.51	0.05	0	0	0.02	0.12
		63RF36 CP-5	53.69	0.01	0.1	0	46.69	0.03	0	0	0	0.16
Cauldron margin	Aldermac	A95-14A SP-1	53.1	0.01	0	0	46.72	0	0.09	0	0	0
		A95-14A SP-10	52.54	0	0	0.01	46.67	0.03	0.18	0	0.01	0
		A95-14A SP-2	52.98	0	0	0.03	46.67	0	0.14	0	0	0
		A95-14A SP-3	52.81	0	0	0	46.86	0	0.17	0	0	0
		A95-14A SP-4	52.73	0	0	0.01	46.74	0.03	0.07	0	0	0
		A95-14A SP-5	52.84	0	0.01	0	46.69	0.01	0.09	0	0.01	0
		A95-14A SP-6	52.87	0	0.01	0	46.8	0	0.26	0	0.02	0
		A95-14A SP-7	52.85	0.03	0.04	0.05	46.78	0.01	0.27	0	0	0.01
		A95-14A SP-8	52.57	0.47	0.01	0	46.49	0	0.05	0	0.01	0
		A95-14A SP-9	52.8	0.04	0	0	46.78	0	0	0	0	0
		A95-14A PY-1	52.87	0	0	0	46.68	0	0	0	0	0.01
		A95-14A PY-10	52.91	0.02	0	0	46.6	0.01	0.06	0	0	0
		A95-14A PY-11	52.84	0.03	0.02	0	46.78	0	0	0	0	0.02
		A95-14A PY-12	53.01	0.02	0	0	46.66	0	0	0	0.01	0.01
		A95-14A PY-14	52.99	0	0	0	46.94	0	0	0	0	0.01
		A95-14A PY-15	52.97	0	0	0.03	46.56	0	0.04	0	0	0
		A95-14A PY-16	52.81	0.05	0	0	46.7	0	0.02	0	0.01	0
		A95-14A PY-17	53.01	0	0.02	0.01	46.68	0.02	0.01	0	0.01	0
		A95-14A PY-18	52.68	0	0	0.02	46.9	0	0	0	0	0
		A95-14A PY-19	52.77	0.02	0	0	46.6	0	0	0	0	0
		A95-14A PY-2	53.15	0.03	0	0	46.72	0	0	0	0	0
		A95-14A PY-20	52.93	0.02	0	0.03	47	0.01	0	0	0.02	0
		A95-14A PY-3	52.93	0	0	0	46.81	0	0.02	0	0	0
		A95-14A PY-4	53.2	0.03	0.01	0	46.9	0	0.03	0	0	0.01
		A95-14A PY-5	52.87	0.02	0	0.01	46.52	0.01	0.02	0	0	0
		A95-14A PY-6	52.81	0.02	0	0	46.67	0	0.02	0	0	0.03
		A95-14A PY-7	52.86	0	0	0	46.73	0	0	0	0	0.01
		A95-14A PY-8	53.17	0	0.02	0.01	46.78	0.02	0.02	0	0	0.01
		A95-14A PY-9	53.23	0.06	0	0	46.54	0	0.01	0	0	0
		A95-14B SP-1	52.82	0.08	0	0.01	46.63	0.01	0.01	0	0	0.01
		A95-14B SP-2	52.8	0	0	0	46.39	0.01	0.12	0	0	0.31
		A95-14B SP-3	52.72	0	0	0	46.79	0	0.17	0	0.01	0.03
		A95-14B SP-4	52.22	0.17	0.03	0	46.4	0.01	0.41	0	0	0.14
		A95-14B SP-5	52.81	0	0.01	0	46.7	0.01	0.04	0	0	0.01
		A95-14B PY-1	52.56	0.01	0	0	46.65	0	0.03	0	0	0.02
		A95-14B PY-10	52.98	0	0	0	46.6	0	0.01	0	0	0.02
		A95-14B PY-11	52.7	0	0.01	0.02	46.52	0.02	0	0	0	0.01
		A95-14B PY-12	52.87	0.02	0.01	0.01	46.82	0.03	0	0	0	0.01
		A95-14B PY-13	52.6	0	0.01	0	46.86	0.01	0	0	0	0.02
		A95-14B PY-14	52.57	0.01	0.01	0	46.8	0	0.04	0	0	0
		A95-14B PY-15	53.03	0.01	0.01	0.02	46.79	0	0	0	0	0
		A95-14B PY-16	52.5	0	0.01	0	46.73	0	0.02	0	0	0.04
		A95-14B PY-17	52.74	0	0	0	46.81	0	0	0	0	0.05
		A95-14B PY-18	53.09	0.01	0.01	0	46.79	0	0	0	0.01	0.05
		A95-14B PY-19	52.86	0.01	0.01	0	46.59	0.01	0.01	0	0	0.03
		A95-14B PY-2	53.04	0.02	0.01	0	46.71	0	0.01	0	0	0.13
		A95-14B PY-20	52.74	0.01	0	0	46.64	0.01	0	0	0	0.01
		A95-14B PY-3	52.8	0	0	0	46.69	0	0	0	0.01	0.04
		A95-14B PY-4	52.79	0.01	0	0	46.75	0	0.01	0	0	0.11
		A95-14B PY-5	52.84	0	0	0.01	46.62	0	0	0	0	0.24
		A95-14B PY-6	52.64	0	0.01	0	46.85	0	0	0	0	0.02
		A95-14B PY-7	52.9	0	0	0.02	46.35	0	0	0	0	0.47
		A95-14B PY-8	52.71	0.01	0	0	46.57	0	0.01	0	0	0.01
		A95-14B PY-9	52.89	0.01	0	0	46.62	0	0	0	0	0.03
		A95-14B PO-1	53.56	0	0.01	0	46.96	0.01	0	0	0.01	0.03
		A95-14B PO-10	53.38	0.01	0	0	46.81	0	0.04	0	0	0.03
		A95-14B PO-11	53.66	0.02	0	0	46.63	0	0.1	0	0	0.24
		A95-14B PO-12	53.65	0.03	0	0	46.61	0	0.45	0	0	0.08
		A95-14B PO-13	53.51	0.05	0	0.03	46.87	0.02	0	0	0	0.05
		A95-14B PO-14	53.67	0.03	0	0	46.76	0.01	0.04	0	0.01	0.12
		A95-14B PO-15	53.53	0.02	0.01	0	46.75	0	0.04	0	0	0.17
		A95-14B PO-16	53.69	0.03	0	0.01	46.71	0	0.02	0	0	0.21
		A95-14B PO-17	53.47	0	0	0	46.91	0.01	0.03	0	0	0.02
		A95-14B PO-18	53.57	0.02	0.01	0	46.54	0.01	0.02	0	0	0.26
		A95-14B PO-19	53.46	0	0	0	46.61	0	0	0	0	0.37
		A95-14B PO-2	53.55	0	0	0	46.76	0.01	0.02	0	0	0.07
		A95-14B PO-20	53.41	0	0	0	46.84	0.01	0.03	0	0	0.07
		A95-14B PO-3	53.4	0.01	0	0	46.79	0.02	0.02	0	0	0.18
		A95-14B PO-4	53.58	0.04	0	0	46.6	0	0.02	0	0	0.28
		A95-14B PO-5	53.66	0	0	0.01	46.49	0.01	0	0	0	0.54
		A95-14B PO-6	53.54	0	0	0	46.71	0	0.01	0	0.01	0.11
		A95-14B PO-7	53.67	0	0	0	46.87	0.01	0	0	0.01	0
		A95-14B PO-8	53.75	0	0	0	46.89	0	0.1	0	0	0.01
		A95-14B PO-9	53.55	0	0	0	46.84	0	0.1	0	0	0.08

Table A1.3 Pyrite (cont.)

Stratigraphic Position	Deposit	Sample	S (wt%)	As (wt%)	Cu (wt%)	Cd (wt%)	Fe (wt%)	Se (wt%)	Zn (wt%)	Cr (wt%)	Ni (wt%)	Co (wt%)
Cauldron margin	Aldermac	A95-14C PY-1	53.8	0.03	0	0	47.05	0	0	0	0	0.03
		A95-14C PY-10	53.54	0	0	0.01	46.81	0.01	0.01	0	0	0
		A95-14C PY-11	53.55	0.01	0	0	47.05	0	0.03	0	0.01	0.02
		A95-14C PY-12	53.56	0	0.03	0	46.86	0	0.02	0	0	0.03
		A95-14C PY-13	53.68	0	0	0	47.03	0.01	0	0	0	0
		A95-14C PY-14	53.48	0	0	0.01	46.96	0	0.01	0	0.01	0.07
		A95-14C PY-15	53.48	0	0	0	46.74	0	0.19	0	0	0
		A95-14C PY-16	53.65	0	0	0	46.83	0	0.01	0	0	0.01
		A95-14C PY-18	53.72	0.01	0	0	46.69	0	0	0	0.01	0.09
		A95-14C PY-19	53.13	0	0.03	0.02	46.71	0.01	0	0	0.01	0.03
		A95-14C PY-2	53.83	0	0.01	0	47.07	0	0	0	0	0
		A95-14C PY-20	53.44	0.04	0	0	46.93	0	0.01	0	0	0.08
		A95-14C PY-3	53.67	0.01	0	0.01	46.93	0	0	0	0	0
		A95-14C PY-4	53.86	0	0.02	0	47.05	0.01	0	0	0	0.03
		A95-14C PY-5	53.8	0.04	0	0	46.73	0	0.03	0	0	0
		A95-14C PY-6	53.52	0	0.02	0	47.02	0.01	0	0	0.01	0.04
		A95-14C PY-8	53.57	0.02	0.03	0.02	46.91	0.01	0.01	0	0.01	0.14
		A95-14C PY-9	53.45	0	0.01	0.02	46.58	0	0.02	0	0	0.03
New Inso		A95-12A CP1-1	53.49	0	0.01	0.01	46.82	0.02	0	0	0	0.09
		A95-12A CP1-2	53.57	0.01	0.07	0	46.88	0	0.01	0	0	0.04
		A95-12A CP1-3	53.42	0	0.07	0	46.55	0.05	0	0	0.02	0.21
		A95-12A CP1-4	53.65	0.03	0	0	46.93	0.04	0	0	0	0
		A95-12A CP1-5	53.34	0	0.12	0	46.88	0.01	0	0	0.01	0
		A95-12A CP2-1	53.36	0	0	0.03	46.78	0.03	0.01	0	0	0
		A95-12A CP2-10	53.61	0	0.02	0.02	46.92	0.05	0	0	0	0.15
		A95-12A CP2-2	53.58	0.01	0.05	0.03	46.83	0.05	0	0	0.01	0.15
		A95-12A CP2-3	53.62	0	0.04	0	46.84	0	0.01	0	0	0.03
		A95-12A CP2-4	53.65	0.01	0.01	0	46.82	0.07	0	0	0.03	0.17
		A95-12A CP2-5	53.59	0.01	0.08	0	46.74	0.03	0	0	0	0.06
		A95-12A CP2-6	53.52	0.01	0.11	0.01	46.61	0.03	0	0	0	0.09
		A95-12A CP2-7	53.65	0.01	0	0	46.89	0.01	0	0	0	0.01
		A95-12A CP2-8	53.67	0	0.01	0	46.73	0.06	0	0	0.01	0.07
		A95-12A CP2-9	53.47	0	0.02	0.02	46.78	0.01	0.01	0	0	0.12
		A95-12B PY-1	53.37	0.01	0.02	0.01	46.78	0	0	0	0	0
		A95-12B PY-10	53.57	0	0.05	0.01	46.81	0.01	0.02	0	0	0.03
		A95-12B PY-11	53.11	0	0.01	0	46.78	0.01	0.01	0	0	0.23
		A95-12B PY-12	53.5	0	0.04	0	46.96	0.01	0.02	0	0.01	0.03
		A95-12B PY-13	53.75	0	0.03	0.03	46.84	0	0	0	0	0.06
		A95-12B PY-14	53.8	0	0.03	0	46.55	0.07	0	0	0	0.14
		A95-12B PY-15	53.57	0	0	0	46.87	0.07	0.01	0	0.01	0.01
		A95-12B PY-2	53.5	0	0	0	46.78	0.05	0.03	0	0	0.02
		A95-12B PY-3	53.45	0	0.02	0.02	46.7	0.06	0.01	0	0	0.1
		A95-12B PY-4	53.57	0.01	0.03	0.01	46.85	0.04	0	0	0	0.06
		A95-12B PY-5	53.77	0	0	0	46.92	0.01	0	0	0	0
		A95-12B PY-6	53.22	0	0.02	0.03	46.68	0.03	0	0	0.01	0.05
		A95-12B PY-7	53.76	0	0.01	0	46.42	0.02	0.01	0	0.01	0.53
		A95-12B PY-8	53.52	0.01	0.01	0	46.86	0.01	0.02	0	0.01	0.03
		A95-12B PY-9	53.68	0	0	0	46.91	0.03	0	0	0.01	0
		A95-12C PY-1	53.45	0.06	0.01	0.01	46.73	0.02	0.01	0	0	0
		A95-12C PY-10	53.57	0	0.02	0.01	47	0.02	0	0	0.01	0
		A95-12C PY-11	53.51	0	0	0	46.87	0.04	0.02	0	0	0
		A95-12C PY-12	53.41	0	0.01	0	46.88	0.05	0	0	0.01	0
		A95-12C PY-13	53.18	0	0	0.03	46.63	0.01	0	0	0	0
		A95-12C PY-14	53.47	0.03	0.01	0	46.93	0.05	0	0	0	0.01
		A95-12C PY-15	53.29	0	0.02	0	47.19	0.02	0	0	0.02	0
		A95-12C PY-2	53.65	0.01	0.01	0.02	46.85	0.04	0	0	0	0
		A95-12C PY-3	53.74	0	0	0	46.93	0.05	0	0	0	0
		A95-12C PY-4	53.45	0	0.02	0	47.06	0.03	0.01	0	0	0.01
		A95-12C PY-5	53.45	0	0.03	0	46.65	0.05	0.01	0	0.01	0
		A95-12C PY-6	53.58	0	0.07	0	46.79	0.05	0.02	0	0.03	0
		A95-12C PY-7	53.31	0	0	0	46.71	0.03	0.01	0	0	0.02
		A95-12C PY-8	53.63	0	0.02	0.01	46.85	0.05	0	0	0.01	0
		A95-12C PY-9	53.62	0.04	0.01	0	46.96	0.05	0	0	0	0
Cauldron	Corbet	CRBT3.800N-SP-G7-1	52.84	0.02	0.07	0.03	45.92	0	0.63	0	0.02	0.07
		CRBT3.800N-SP-G7-2	52.76	0	0.04	0	46.13	0.01	0.47	0	0.01	0.02
		CRBT3.800N-SP-G7-3	52.95	0.07	0.09	0	45.74	0	1.1	0	0.02	0.07
		CRBT3.800N-SP-G7-4	53.56	0.03	0.13	0	45.27	0	1.78	0	0.01	0.01
Bedford Hill		A95-10A-PY-1	53.34	0	0.01	0.03	46.96	0	0.02	0	0.01	0
		A95-10A-PY-2	53.29	0.03	0	0	46.91	0.02	0.18	0	0.01	0.05
		A95-10A-PY-3	53.49	0.01	0	0	46.8	0	0	0	0	0.02
		A95-10A-PY-4	53.23	0.02	0.01	0	46.86	0	0	0	0.01	0.04
		A95-10A-PY-5	53.32	0.01	0.01	0	46.86	0	0.01	0	0	0.01
		A95-10A-PY-6	53.54	0.01	0.03	0	46.88	0	0.02	0	0	0
		A95-10A-PY-7	53.31	0.03	0	0.02	46.89	0	0.01	0	0	0
		A95-10A-PY-8	53.35	0	0.01	0.04	47.1	0.01	0.01	0	0	0
		A95-10A-PY-9	53.21	0.06	0.01	0	46.94	0.01	0	0	0	0
		A95-10A-PY-10	53.39	0	0.01	0	46.9	0	0.02	0	0	0
		A95-10A-PY-11	53.14	0.03	0	0	46.84	0.01	0	0	0	0.01
		A95-10A-PY-12	53.53	0.02	0	0	47.03	0	0	0	0.02	0
		A95-10A-PY-13	53.36	0.03	0	0.04	46.83	0	0.02	0	0	0
		A95-10A-PY-14	53.39	0	0.01	0	46.92	0	0.01	0	0.02	0
		A95-10A-PY-15	53.28	0	0	0	46.89	0	0	0	0.01	0
		A95-10A-PY-16	53.49	0.02	0.01	0	46.81	0	0.02	0	0.01	0.01
		A95-10A-PY-17	53.34	0	0	0	46.94	0.01	0	0	0	0.01
		A95-10A-PY-18	53.41	0.01	0	0	47.03	0	0	0	0	0
		A95-10A-PY-19	53.32	0.04	0	0	46.9	0	0.06	0	0	0.1
		A95-10A-PY-20	53.41	0	0	0	46.93	0.02	0	0	0	0
Ansill		ANSL 983-BX-PY-1	52.56	0.04	0	0.01	47.19	0.01	0.02	0	0.01	0.01
		ANSL 983-BX-PY-2	52.42	0.11	0.02	0	47.05	0	0.01	0	0.01	0.01
		ANSL 983-BX-PY-3	52.21	0.05	0.01	0	47.12	0.01	0	0	0	0
		ANSL 983-BX-PY-4	52.76	0.04	0.01	0	47.08	0	0.02	0	0	0.03
		ANSL 983-BX-PY-5	52.36	0.26	0	0	46.94	0	0	0	0	0.01
		ANSL 983-BX-PY-6	52.26	0.02	0	0	47.12	0	0	0	0	0
		ANSL 983-BX-PY-7	52.18	0.07	0	0	47.06	0	0.01	0	0.01	0
		ANSL 983-BX-PY-8	51.93	0.3	0.03	0.01	47.11	0	0	0	0	0.02
		ANSL 983-BX-PY-9	52.22	0.1	0.04	0	47.05	0	0	0	0	0.03
		ANSL 983-BX-PY-10	52.65	0.03	0.04	0	47.02	0.01	0	0	0	0
C-Contact Tuff		C.TUFF PY1-1	53.43	0	0.07	0	46.6	0.01	0.01	0	0	0
		C.TUFF PY1-2	53.03	0	0.04	0	46.53	0.01	0	0	0	0
		C.TUFF PY1-3	53.57	0	0.03	0	46.45	0	0	0	0	0
		C.TUFF PY1-4	53.44	0	0.04	0	46.37	0	0	0	0.02	0
		C.TUFF PY1-5	53.77	0	0.04	0	46.67	0	0	0	0.01	0
		C.TUFF PY1-6	53.52	0.02	0.03	0.01	46.28	0	0.01	0	0	0
		C.TUFF PY1-7</td										

Table A1.3 Pyrite (cont.)

Stratigraphic Position	Deposit	Sample	S (wt%)	As (wt%)	Cu (wt%)	Cd (wt%)	Fe (wt%)	Se (wt%)	Zn (wt%)	Cr (wt%)	Ni (wt%)	Co (wt%)
Cauldron	C-Contact Tuff	C.TUFF PY1-8	53.45	0	0.03	0	46.42	0.01	0	0.01	0	0
		C.TUFF PY1-9	53.71	0	0.09	0	46.46	0	0	0	0.01	0
		C.TUFF PY1-10	53.27	0.01	0.05	0.02	46.46	0	0	0	0	0
		C.TUFF PY1-11	53.27	0	0.02	0	46.41	0.01	0	0	0.01	0.01
		C.TUFF PY1-12	53.54	0	0.01	0	46.59	0.01	0	0	0	0
		C.TUFF PY1-13	53.77	0	0.02	0	46.45	0.01	0	0	0.01	0
		C.TUFF PY1-14	53.89	0	0.02	0	47.14	0	0	0	0	0
		C.TUFF PY1-15	53.3	0.01	0.06	0	46.53	0.01	0	0	0	0.04
		C.TUFF PY1-16	53.59	0.01	0.05	0.02	46.58	0.02	0	0	0.01	0
		C.TUFF PY1-17	53.28	0	0.03	0.01	46.43	0.01	0	0	0	0
		C.TUFF PY1-18	53.65	0	0.04	0	46.44	0	0	0	0	0
		C.TUFF PY1-19	53.62	0	0.03	0.01	46.4	0.03	0	0.01	0.01	0
		C.TUFF PY1-20	53.27	0.01	0.05	0.02	46.48	0.02	0	0	0.01	0
		C.TUFF PY1-21	53.61	0	0.05	0	46.49	0.02	0	0	0.01	0
		C.TUFF PY1-22	53.45	0.01	0.05	0	46.47	0.02	0	0	0	0
		C.TUFF PY1-23	53.58	0	0.04	0	46.31	0.01	0	0	0	0.02
		C.TUFF PY1-24	53.48	0	0.04	0	46.52	0	0	0	0.01	0.01
		C.TUFF PY1-25	53.49	0.01	0.04	0.01	46.44	0	0	0	0	0.01
		C.TUFF PY1-26	53.56	0	0.07	0	46.31	0	0.01	0	0	0.01
		C.TUFF PY1-27	53.45	0	0.05	0	46.34	0.01	0.02	0.01	0.01	0.01
		C.TUFF PY1-28	53.48	0	0.01	0	46.5	0	0	0	0	0
		C.TUFF PY1-29	53.06	0.01	0.06	0	46.38	0	0.02	0	0.01	0
		C.TUFF PY1-30	53.47	0	0.04	0.03	46.41	0.01	0.03	0	0	0
		C.TUFF PY2-1	52.97	0	0	0	46.83	0	0	0	0	0
		C.TUFF PY2-2	53.37	0	0	0	46.64	0.01	0	0	0	0
		C.TUFF PY2-3	52.61	0	0.03	0.03	46.92	0	0	0	0	0.01
		C.TUFF PY2-4	53.14	0	0.03	0.02	46.8	0.01	0	0	0	0
		C.TUFF PY2-5	52.81	0.03	0.02	0.02	46.75	0	0	0	0	0
		C.TUFF PY2-6	52.82	0	0	0	46.62	0.01	0.01	0	0	0
		C.TUFF PY2-8	52.74	0	0.01	0	46.58	0	0.01	0	0	0
		C.TUFF PY2-9	52.84	0	0.01	0	46.74	0	0.02	0	0	0
		C.TUFF PY2-10	53.17	0	0.01	0	46.91	0	0	0	0	0
		C.TUFF PY2-11	52.72	0	0.01	0.01	46.94	0	0	0	0	0
		C.TUFF PY2-12	52.88	0.02	0	0	46.93	0	0	0	0.01	0
		C.TUFF PY2-13	52.92	0.02	0.01	0	47.06	0	0	0	0	0.01
		C.TUFF PY2-14	52.8	0	0	0	47.01	0	0.01	0	0	0
		C.TUFF PY2-16	52.64	0.03	0.02	0	47.08	0	0	0	0	0
Moosehead		A95-09A-SP-1	53.49	0.01	0.04	0	46.67	0	0.06	0	0.01	0
		A95-09A-SP-2	53.22	0.13	0.06	0	46.41	0.01	0.03	0	0	0
		A95-09A-SP-3	53.95	0.02	0.02	0	46.81	0.01	0	0	0.01	0
		A95-09A-SP-4	53.78	0	0.01	0	46.84	0.01	0.01	0	0.01	0
		A95-09A-SP-5	53.32	0.03	0.11	0	46.63	0	0.19	0	0	0
		A95-09A-SP-6	53.29	0.07	0.07	0.01	46.24	0.03	0.12	0	0.01	0
		A95-09A-SP-7	53.15	0.07	0.05	0.03	46.8	0.01	0.25	0	0	0
		A95-09A-SP-8	52.66	0	0.02	0.01	46.47	0	0.2	0	0	0
		A95-09A-SP-9	52.96	0.04	0.04	0	46.34	0	0.16	0	0.01	0.01
		A95-09A-SP-10	53.66	0	0.05	0	46.53	0	0.33	0	0	0
		A95-09A-PY-1	53.06	0.01	0.01	0	47.1	0.01	0.07	0	0	0.01
		A95-09A-PY-2	53.1	0.02	0	0.01	46.83	0	0	0	0.01	0.01
		A95-09A-PY-4	52.9	0	0	0.01	46.84	0	0	0	0	0
		A95-09A-PY-5	51.99	0.01	0.01	0	47.06	0	0.01	0	0	0
		A95-09A-PY-6	53.15	0.02	0.02	0	47.08	0	0.01	0	0.01	0
		A95-09A-PY-9	53.03	0.03	0	0.01	46.92	0.01	0.03	0	0.01	0.01
		A95-09A-PY-11	53.56	0.01	0	0.03	46.82	0	0.03	0	0.01	0
		A95-09A-PY-12	53.15	0	0	0	47.09	0.01	0	0	0	0
		A95-09A-PY-13	52.71	0	0.03	0	46.91	0	0	0	0	0
		A95-09A-PY-14	52.9	0	0	0.01	47	0.01	0.01	0	0	0
		A95-09A-PY-15	52.79	0	0.01	0	47.17	0	0.02	0	0.01	0
		A95-09B-PY-1	52.7	0	0.01	0.02	47.03	0.01	0.01	0	0	0
		A95-09B-PY-2	52.3	0.01	0.04	0	47.21	0.01	0.02	0	0	0
		A95-09B-PY-3	52.66	0	0	0	47.06	0	0	0	0	0
		A95-09B-PY-4	52.83	0	0	0	47.18	0.01	0	0	0.01	0.02
		A95-09B-PY-5	52.78	0	0	0	47.04	0.02	0	0	0.01	0.02
		A95-09B-PY-6	52.43	0.01	0	0	47.12	0	0.01	0	0	0
		A95-09B-PY-7	52.55	0	0	0	47.09	0	0	0	0	0
		A95-09B-PY-8	52.65	0	0	0	47.01	0.02	0	0	0	0
		A95-09B-PY-9	52.76	0	0	0	47	0.01	0.04	0	0	0.01
		A95-09B-PY-10	52.67	0.01	0.01	0	46.98	0	0	0	0.01	0.01
		A95-09B-PY-11	52.65	0	0.02	0	46.9	0.03	0	0	0	0
		A95-09B-PY-12	52.62	0	0.01	0	47.08	0.02	0.04	0	0	0.03
		A95-09B-PY-13	53.19	0	0	0	46.84	0.02	0.01	0	0	0
		A95-09B-PY-14	52.41	0	0.01	0	47.01	0.01	0	0	0	0.04
		A95-09B-PY-15	52.5	0	0	0	47.23	0	0	0	0.01	0
Millenbach		SP2091-PY-1	53.8	0.01	0.03	0	46.21	0	0.01	0	0.01	0
		SP2091-PY-2	53.97	0	0.05	0.01	46.28	0.03	0.03	0	0	0
		SP2091-PY-3	53.75	0.04	0.06	0	46.33	0	0	0	0	0
		SP2091-PY-4	53.78	0	0.01	0	46.25	0	0.01	0	0.01	0.01
		SP2091-PY-5	54.03	0.01	0.04	0	46.34	0	0	0	0.01	0
		SP2091-PY-6	53.76	0	0.02	0.01	46.3	0	0	0	0	0
		SP2091-PY-7	53.6	0.01	0.02	0	46.46	0	0.01	0	0	0
		SP2091-PY-8	53.49	0	0.04	0	46.33	0	0	0	0.01	0
		SP2091-PY-9	53.69	0	0.02	0	46.34	0.02	0.01	0	0.01	0
		SP2091-PY-10	53.61	0	0.02	0.01	46.53	0.02	0	0	0.01	0
		SP2091-PY-11	53.46	0	0.02	0	46.55	0	0	0	0	0
		SP2091-PY-12	53.71	0	0.04	0.02	46.31	0	0	0	0	0
		SP2091-PY-13	53.94	0.03	0.04	0	46.49	0.01	0	0	0	0
		SP2091-PY-14	53.23	0	0.03	0	46.46	0.01	0	0	0	0
		SP2091-PY-15	53.61	0	0.06	0	46.22	0	0	0	0	0.02
		SP2091-PY-16	53.45	0	0.06	0	46.48	0.01	0.01	0	0.01	0
		SP2091-PY-17	53.41	0	0.02	0	46.21	0	0	0	0.01	0
		SP2091-PY-18	53.21	0	0.04	0	46.29	0	0	0	0	0.01
		SP2091-PY-19	53.39	0.01	0.02	0	46.44	0.02	0	0	0.01	0
		SP2091-PY-20	53.2	0	0.06	0	46.42	0.01	0	0	0.01	0.02
		SP2091-PY-21	53.44	0	0.02	0	46.49	0.01	0.02	0.01	0.01	0
		SP2091-PY-22	53.48	0	0.04	0	46.4	0	0	0	0.01	0
		SP2091-PY-23	53.28	0.01	0.05	0	46.5	0.01	0.03	0	0.01	0
		SP2091-PY-24	53.32	0	0.03	0.01	46.5	0	0	0	0	0
		SP2091-PY-25	53.48	0	0.06	0.01	46.36	0	0	0	0.01</	

Table A1.3 Pyrite (cont.)

Stratigraphic Position	Deposit	Sample	S (wt%)	As (wt%)	Cu (wt%)	Cd (wt%)	Fe (wt%)	Se (wt%)	Zn (wt%)	Cr (wt%)	Ni (wt%)	Co (wt%)
Cauldron	Amulet A Upper	A95-07B-PY-1	52.57	0.03	0.01	0	47.05	0	0	0	0	0.07
		A95-07B-PY-10	52.84	0.01	0.02	0	47.04	0	0.01	0	0.01	0
		A95-07B-PY-11	53	0	0.03	0.01	46.69	0	0.04	0	0	0
		A95-07B-PY-12	53.06	0	0.01	0	46.87	0.02	0	0	0	0.05
		A95-07B-PY-13	53.08	0.05	0.03	0.01	47.18	0	0	0	0	0
		A95-07B-PY-14	53.13	0	0.02	0.02	46.93	0	0	0	0.01	0.04
		A95-07B-PY-15	52.81	0.04	0.02	0	46.9	0.01	0.04	0	0	0
		A95-07B-PY-2	52.97	0	0	0	47.1	0.01	0.05	0	0.01	0.04
		A95-07B-PY-4	52.69	0	0.01	0.02	47.02	0.02	0	0	0	0.01
		A95-07B-PY-5	52.79	0.03	0.03	0	47.16	0	0.02	0	0	0.07
		A95-07B-PY-6	52.62	0.01	0	0	47.06	0	0	0	0	0.02
		A95-07B-PY-7	52.69	0.01	0	0	47.2	0.01	0	0	0	0
		A95-07B-PY-8	52.93	0	0	0	47.1	0	0.01	0	0	0.04
		A95-07B-SP-1	53.3	0	0.01	0	46.75	0	0.17	0	0	0.03
		A95-07B-SP-2	53.73	0	0.07	0	46.71	0	0.07	0	0.01	0
		A95-07B-SP-3	50.79	0	0.03	0.02	44.82	0	0.37	0	0	0
Amulet C	Amulet C	A95-07B-SP-4	53.34	0	0.04	0	46.74	0	0.18	0	0	0.02
		A95-07B-SP-5	52.72	0	0.01	0	46.74	0.01	0.27	0	0	0
		A95-07C-PY-1	52.79	0.01	0.01	0.02	46.98	0.02	0.01	0	0	0
		A95-07C-PY-11	53.01	0	0	0	47.1	0.01	0.01	0	0.01	0.03
		A95-07C-PY-12	52.87	0.03	0	0	46.8	0	0.02	0	0	0.07
		A95-07C-PY-13	52.96	0	0.03	0.01	47.08	0	0.06	0	0	0
		A95-07C-PY-14	52.92	0.02	0.01	0	46.87	0.01	0.08	0	0	0
		A95-07C-PY-15	53.03	0	0	0.03	46.98	0.01	0.01	0	0.01	0.06
		A95-07C-PY-2	53.2	0	0	0	46.99	0.02	0	0	0	0.01
		A95-07C-PY-3	52.82	0	0.01	0	47.05	0.01	0.05	0	0	0.1
		A95-07C-PY-4	52.91	0.02	0	0.03	47.17	0	0	0	0.01	0
		A95-07C-PY-5	52.63	0	0	0	46.96	0	0.03	0	0.01	0.02
		A95-07C-PY-6	52.88	0.01	0	0	47.14	0.04	0	0	0.01	0.01
		A95-07C-PY-7	52.88	0.01	0	0	46.95	0	0.02	0	0	0.03
		A95-07C-PY-8	52.7	0	0.01	0	46.95	0	0.01	0	0	0.01
		A95-07C-PY-9	52.65	0	0.02	0	46.98	0.02	0.04	0	0	0.09
Old Waite	Old Waite	A95-07D-PY-1	52.96	0.01	0.01	0	46.76	0.01	0.01	0	0	0.23
		A95-07D-PY-10	52.92	0.02	0.01	0	47.01	0	0	0	0.01	0
		A95-07D-PY-11	52.81	0.02	0	0.01	47.13	0	0	0	0	0
		A95-07D-PY-12	52.83	0	0.02	0	46.78	0.03	0.22	0	0	0.12
		A95-07D-PY-13	52.69	0.02	0	0	47.17	0.02	0	0	0	0.04
		A95-07D-PY-14	53.07	0	0	0	46.92	0.01	0	0	0	0.03
		A95-07D-PY-15	53.02	0.06	0.01	0	46.87	0	0.01	0	0	0.01
		A95-07D-PY-16	53.04	0	0	0	46.84	0	0.02	0	0.02	0
		A95-07D-PY-17	52.94	0.01	0	0	46.61	0	0.02	0	0	0.48
		A95-07D-PY-18	52.96	0.02	0.02	0.02	47.17	0	0.03	0	0	0.08
		A95-07D-PY-19	52.63	0.01	0.03	0	47.13	0	0	0	0	0.01
		A95-07D-PY-20	52.92	0	0.01	0	46.47	0	0.03	0	0	0.64
		A95-07D-PY-21	53.27	0.03	0	0	46.54	0	0.01	0	0	0.4
		A95-07D-PY-3	53.02	0	0	0.01	47.14	0	0	0	0	0.02
		A95-07D-PY-4	53.49	0.04	0.01	0	46.43	0	0	0	0	0.41
Amulet C	Amulet C	A95-08D-SP-1	52.62	0.02	0.06	0	46.52	0.01	0.23	0	0	0.09
		A95-08D-SP-2	52.23	0.03	0.05	0	46.52	0.01	0.23	0	0	0
		A95-08D-SP-3	52.57	0.06	0.04	0.03	46.51	0	0.09	0	0.02	0.04
		A95-08D-SP-4	53.23	0.14	0.04	0	46.69	0	0.12	0	0.01	0.01
		A95-08D-SP-5	53.1	0.15	0.04	0	46.59	0	0.15	0	0	0.18
		A95-08E-SP-1	53.51	0.09	0.04	0	46.53	0	0.02	0	0	0.07
		A95-08E-SP-3	53.54	0.06	0.03	0.02	46.62	0.01	0	0	0.01	0.02
		A95-08A-PY-1	52.45	0.04	0.01	0	47.58	0	0.05	0	0	0
		A95-08A-PY-10	52.87	0.03	0	0.01	46.55	0.01	0.01	0	0	0.31
		A95-08A-PY-11	53.01	0.02	0.01	0	46.9	0.01	0.01	0	0.01	0.21
		A95-08A-PY-2	52.67	0	0.17	0	46.85	0.05	0.16	0	0	0
		A95-08A-PY-3	52.83	0	0.04	0.01	46.85	0.03	0.03	0	0.02	0.01
		A95-08A-PY-4	52.53	0.01	0.03	0	46.58	0	0.06	0	0.01	0.12
		A95-08A-PY-5	52.92	0	0.02	0	46.85	0.03	0.03	0	0.07	0.03
		A95-08A-PY-7	52.98	0.01	0.05	0	46.9	0.03	0.14	0	0	0.01
		A95-08A-PY-8	52.44	0.01	0	0	46.92	0.01	0.02	0	0.05	0
		A95-08A-PY-9	52.64	0	0.02	0	46.64	0.02	0.05	0	0	0
Old Waite	Old Waite	A95-18A-PY-1	53.06	0	0.01	0	46.98	0	0.01	0	0.01	0.11
		A95-18A-PY-10	52.92	0.02	0	0.02	46.93	0	0.04	0	0	0.01
		A95-18A-PY-11	52.73	0.01	0	0.02	46.93	0	0.04	0	0	0
		A95-18A-PY-12	52.63	0	0.01	0	47.25	0.01	0.04	0	0	0
		A95-18A-PY-13	52.5	0	0	0.02	47.35	0.01	0.03	0	0	0
		A95-18A-PY-14	52.66	0	0.01	0	47.16	0	0.02	0	0	0
		A95-18A-PY-15	52.78	0	0.03	0.03	47.07	0.01	0	0	0	0
		A95-18A-PY-2	52.92	0.02	0	0.02	46.91	0	0	0	0.01	0
		A95-18A-PY-3	52.89	0	0.03	0.01	47.08	0	0.01	0	0	0.01
		A95-18A-PY-4	52.86	0.01	0.01	0	46.95	0	0.03	0	0.02	0
		A95-18A-PY-6	52.85	0	0.02	0	47.09	0.01	0.02	0	0	0
		A95-18A-PY-7	52.97	0	0	0	47.11	0	0	0	0	0
		A95-18A-PY-8	53.01	0	0.02	0	47.09	0.01	0.02	0	0	0.02
		A95-18A-PY-9	52.96	0.02	0	0	47.1	0.01	0.02	0	0	0
Old Waite	Old Waite	A95-18A-SP-2	53.03	0	0.03	0	47.08	0	0.02	0	0	0.01
		A95-18A-SP-3	52.85	0	0	0.02	47.41	0.01	0.03	0	0.01	0
		A95-18A-SP-4	52.37	0	0.01	0.03	46.96	0.01	0.14	0	0	0
		A95-18B-CP-1	53.36	0.01	0.32	0	44.83	0.01	0.02	0	0	2.03
		A95-18B-CP-2	53.26	0	0.04	0.01	45.29	0	0	0	0	1.73
		A95-18B-CP-3	53.37	0	0.22	0	45.5	0	0	0	0	1.43
		A95-18B-CP-4	53.29	0.03	0.05	0.01	44.86	0.01	0	0	0.01	1.94
		A95-18B-CP-5	53.48	0	0.07	0	44.94	0	0.01	0	0	2.03
		A95-18B-PY-1	52.67	0	0.03	0.01	44.95	0.01	0.02	0	0	1.91
		A95-18B-PY-10	52.84	0	0.03	0	45.41	0	0	0	0	1.16
		A95-18B-PY-11	52.46	0.01	0.02	0	44.46	0.04	0	0	0	2.56
		A95-18B-PY-12	52.44	0	0	0	45.21	0	0	0	0.01	1.74
		A95-18B-PY-13	53.04	0	0.03	0	44.88	0	0	0	0	1.99
		A95-18B-PY-14	52.87	0	0.01	0.01	46.09	0	0	0	0	0.76
		A95-18B-PY-2	52.83	0	0.02	0	43.87	0.02	0	0	0	2.93
		A95-18B-PY-3	52.87	0	0.04	0	45.11	0.02	0	0	0	1.7

Table A1.3 Pyrite (cont.)

Stratigraphic Position	Deposit	Sample	S (wt%)	As (wt%)	Cu (wt%)	Cd (wt%)	Fe (wt%)	Se (wt%)	Zn (wt%)	Cr (wt%)	Ni (wt%)	Co (wt%)
Cauldron	Old Waite	A95-18B-PY-8	50.98	0.03	0.01	0	43.06	0	0	0	0	1.65
		A95-18B-PY-9	52.92	0	0.02	0.02	45.76	0.01	0	0	0	1.07
	East Waite	A95-17D PO-1	53.54	0	0.04	0	45.7	0.01	0.02	0	0	1.09
		A95-17D PO-2	53.53	0	0	0	45.79	0.03	0	0	0.01	0.98
		A95-17D PO-3	53.49	0.02	0.01	0	45.93	0.03	0	0	0	0.9
		A95-17D PO-4	53.48	0	0.03	0.01	45.88	0.05	0.01	0	0	0.95
		A95-17D PO-5	53.41	0	0.03	0	45.73	0.02	0	0	0.01	1.15
		A95-17A PY-1	52.96	0	0.03	0	46.48	0.01	0	0	0	0.38
		A95-17A PY-10	52.87	0.01	0.01	0.02	46.23	0	0.01	0	0	0.66
		A95-17A PY-11	52.92	0.01	0.06	0	46.22	0	0	0	0	0.45
		A95-17A PY-12	52.78	0	0.01	0.01	46.38	0.02	0	0	0	0.35
		A95-17A PY-13	52.97	0.01	0.01	0.02	46.63	0	0	0	0	0.22
		A95-17A PY-14	52.78	0	0.03	0.04	46.29	0.01	0	0	0	0.59
		A95-17A PY-15	53.05	0.02	0.05	0.03	46.38	0.03	0.03	0	0	0.21
		A95-17A PY-3	52.48	0	0.02	0.01	46.27	0	0.03	0	0	0.39
		A95-17A PY-4	52.66	0	0	0	46.46	0.01	0	0	0.01	0.31
		A95-17A PY-5	52.82	0	0	0	46.17	0	0	0	0.01	0.67
		A95-17A PY-6	52.91	0	0.01	0.01	46.21	0	0	0	0.02	0.55
		A95-17A PY-7	52.5	0	0.01	0	46.77	0	0	0	0	0.25
		A95-17A PY-8	52.76	0.01	0.02	0.01	46.39	0	0	0	0.02	0.42
		A95-17A PY-9	52.86	0	0.03	0	46.07	0.02	0	0	0	0.75
		A95-17B PY-1	53.02	0.02	0.03	0.01	46.9	0.02	0.05	0	0	0.01
		A95-17B PY-2	52.86	0	0.01	0.01	46.79	0.03	0.14	0	0.01	0
		A95-17B PY-4	53.24	0.05	0.03	0.01	46.72	0.02	0.12	0	0	0
		A95-17C PY-1	53.39	0	0	0.04	46.45	0.04	0	0	0.02	0
		A95-17C PY-10	53.43	0	0	0	46.38	0.04	0.03	0	0.11	0
		A95-17C PY-11	53.35	0	0.01	0.01	46.34	0.02	0.01	0	0	0.24
		A95-17C PY-12	53.12	0	0.02	0	46.33	0.02	0	0	0.21	0
		A95-17C PY-14	53.13	0	0	0	46.18	0	0.03	0	0	0.46
		A95-17C PY-15	53.4	0.02	0.02	0.01	46.52	0.03	0	0	0.01	0
		A95-17C PY-16	53.28	0	0.01	0	46.73	0.01	0.01	0	0	0.02
		A95-17C PY-17	52.99	0.02	0.02	0.01	46.47	0.01	0	0	0.02	0.06
		A95-17C PY-18	53.2	0.02	0	0.01	45.86	0	0	0	0	0.8
		A95-17C PY-19	53.16	0.01	0	0	46.13	0	0	0	0.04	0.45
		A95-17C PY-2	52.96	0.05	0.02	0	45.37	0.02	0	0	0	1.33
		A95-17C PY-20	53.08	0	0.01	0.01	45.48	0.02	0.02	0	0.01	1.22
		A95-17C PY-3	52.99	0.03	0.02	0	46.16	0.03	0	0	0.53	0
		A95-17C PY-4	53.1	0.03	0.03	0	46.23	0	0.01	0	0	0.32
		A95-17C PY-5	53.13	0	0.01	0.01	46.64	0.01	0	0	0.1	0.04
		A95-17C PY-6	53.13	0	0.01	0	46.71	0.02	0	0	0	0
		A95-17C PY-7	53.34	0.01	0	0	45.79	0	0	0	0	0.83
		A95-17C PY-8	53.02	0	0.02	0.01	46.59	0.01	0	0	0.2	0.01
		A95-17C PY-9	53.39	0	0	0	46.19	0	0.01	0	0	0.62
Norbec	JH98-03A	JH98-03A PY-1	53.12	0.65	0.07	0	45.07	0	0.03	0	0	1.06
		JH98-03A PY-10	53.88	0.04	0.04	0	46.31	0.02	0.02	0	0.01	0
		JH98-03A PY-11	53.21	0	0.07	0.01	46.54	0.01	0.01	0	0	0
		JH98-03A PY-12	53.21	0.07	0.04	0	46.08	0.01	0.01	0	0	0.53
		JH98-03A PY-13	53.42	0.04	0.06	0	46.03	0	0.02	0	0	0.29
		JH98-03A PY-14	53.41	0	0.12	0	46.41	0.04	0.01	0	0	0.05
		JH98-03A PY-15	53.73	0.32	0.06	0	45.67	0	0.04	0	0	0.58
		JH98-03A PY-16	53.41	0	0.07	0.01	46.27	0	0.03	0.01	0.01	0
		JH98-03A PY-17	53.37	0.09	0.06	0	46.02	0.03	0.03	0	0.02	0.03
		JH98-03A PY-18	53.25	0.03	0.36	0	45.97	0.12	0.05	0.01	0.01	0.07
		JH98-03A PY-19	53.54	0.05	0.06	0	46.23	0.03	0.05	0.01	0.01	0.02
		JH98-03A PY-2	53.84	0.01	0.04	0	46.3	0.04	0.02	0	0	0.05
		JH98-03A PY-20	53.5	0.18	0.01	0.02	46.13	0	0.01	0	0	0.42
		JH98-03A PY-21	53.44	0.05	0.03	0	46.28	0.05	0.01	0	0	0.02
		JH98-03A PY-22	53.27	0.01	0.23	0	46.13	0.05	0.04	0	0	0.1
		JH98-03A PY-23	53.34	0.05	0.05	0	46.51	0.04	0.02	0	0.02	0.02
		JH98-03A PY-24	54.13	0	0.02	0	46.42	0.03	0	0	0	0
		JH98-03A PY-25	52.85	0.1	0.06	0	46.24	0.06	0.05	0	0	0.09
		JH98-03A PY-3	53.5	0.07	0.05	0	46.17	0.05	0	0	0	0.03
		JH98-03A PY-4	53.47	0.07	0.04	0	45.88	0.04	0.03	0	0	0.31
		JH98-03A PY-5	53.73	0	0.05	0.01	46.42	0.04	0.08	0	0.01	0.04
		JH98-03A PY-6	53.33	0.01	0.09	0	46.31	0.01	0.04	0	0	0.02
		JH98-03A PY-7	53.26	0.07	0.06	0	46.27	0.04	0.04	0	0.01	0.05
		JH98-03A PY-8	53.24	0	0.16	0.01	46.01	0.06	0.01	0	0.01	0.13
		JH98-03A PY-9	53.3	0.05	0.06	0	46.4	0.04	0.04	0	0.01	0.02
Vauze	A95-11F	A95-11F CP-1	53.57	0	0.08	0	46.68	0.09	0	0	0.01	0.01
		A95-11F CP-2	53.36	0	0.04	0	46.49	0.04	0.02	0	0	0.26
		A95-11F CP-3	53.46	0.02	0.07	0.01	44.94	0.06	0.01	0	0	1.78
		A95-11F CP-5	53.44	0	0.2	0.03	46.81	0.08	0	0	0.01	0.02
		A95-11A PY-1	53.2	0	0.01	0	46.42	0.02	0.14	0	0.01	0
		A95-11A PY-10	53.05	0	0.01	0	46.56	0.05	0.01	0	0	0.02
		A95-11A PY-11	53.09	0.01	0	0	46.71	0.07	0	0	0	0.01
		A95-11A PY-12	52.9	0.01	0	0	46.75	0	0	0	0	0.05
		A95-11A PY-13	53.15	0	0.01	0.03	46.79	0.07	0	0	0	0
		A95-11A PY-14	53.02	0	0.02	0.02	46.59	0.04	0.02	0	0	0.01
		A95-11A PY-15	53.06	0.01	0	0	46.52	0.02	0.02	0	0.02	0.03
		A95-11A PY-2	53.14	0	0.02	0	46.47	0.08	0.02	0	0.01	0
		A95-11A PY-3	53.21	0.01	0	0.04	46.71	0.07	0.01	0	0	0.01
		A95-11A PY-4	53.05	0	0.01	0	46.68	0.07	0.02	0	0	0
		A95-11A PY-5	52.83	0	0.02	0	46.44	0	0.01	0	0	0.21
		A95-11A PY-6	53.18	0.02	0.02	0	46.55	0.06	0	0	0.01	0
		A95-11A PY-7	53.19	0.04	0	0	46.66	0.05	0	0	0.01	0.03
		A95-11A PY-8	53.01	0	0.01	0	46.61	0.01	0	0	0	0.02
		A95-11A PY-9	52.86	0	0	0	46.57	0.02	0.02	0	0	0
		A95-11B PY-1	53.23	0	0.01	0	46.51	0.04	0.01	0	0	0
		A95-11B PY-10	52.84	0	0.11	0.01	46.56	0.01	0	0	0	0.09
		A95-11B PY-11	52.96	0	0.01	0	46.75	0.01	0.03	0	0	0
		A95-11B PY-12	53.08	0	0.02	0	46.54	0.01	0.01	0	0	0.23
		A95-11B PY-13	53.09	0	0.02	0.04	46.67	0.04	0	0	0.01	0
		A95-11B PY-14	53.13	0	0.01	0	46.8	0.05	0	0	0.02	0
		A95-11B PY-15	52.94	0	0.01	0.02	46.76	0.06	0	0	0	0
		A95-11B PY-16	52.94	0	0.03	0.03	46.52	0.04	0	0	0	0.01
		A95-11B PY-17	52.98	0.01	0.04	0.03	46.57	0.03	0	0	0	0.04
		A95-11B PY-18	52.94	0	0	0.01	46.58	0.02	0	0	0	0
		A95-11B PY-19	52.91	0.01	0.01	0	46.61	0.04	0	0	0.01	0
		A95-11B PY-2	52.84	0	0.03	0.02	46.63	0.03	0	0	0.02	0.08
		A95-11B PY-20	53.08	0.01	0.02	0	46.71	0.06	0	0	0	0
		A95-11B PY-3	53.3	0	0.01	0	46.55	0.04	0	0	0	0
		A										

Table A1.3 Pyrite (cont.)

Stratigraphic Position	Deposit	Sample	S (wt%)	As (wt%)	Cu (wt%)	Cd (wt%)	Fe (wt%)	Se (wt%)	Zn (wt%)	Cr (wt%)	Ni (wt%)	Co (wt%)
Cauldron	Vauze	A95-11B PY-8	53.2	0.02	0.01	0.04	46.39	0.05	0	0	0	0.03
		A95-11B PY-9	53	0	0.01	0	46.17	0	0.02	0	0.01	0.54
		A95-11B SP-1	53.17	0	0.02	0.01	46.72	0.01	0.31	0	0	0
		A95-11B SP-10	52.91	0.02	0	0.01	46.6	0.06	0.29	0	0	0
		A95-11B SP-11	53.28	0	0.01	0.01	46.98	0	0.03	0	0	0.02
		A95-11B SP-12	53.42	0	0.02	0	46.83	0.03	0.15	0	0	0
		A95-11B SP-13	53.21	0	0	0.01	46.77	0.05	0.05	0	0.01	0
		A95-11B SP-14	53.04	0.03	0	0.01	46.85	0.01	0.21	0	0	0.01
		A95-11B SP-15	53.36	0.01	0	0	45.51	0.02	0.09	0	0.02	1.28
		A95-11B SP-2	53.11	0	0.02	0	46.93	0.05	0.12	0	0	0.01
		A95-11B SP-3	53.3	0	0	0	46.69	0.04	0.18	0	0.01	0.01
		A95-11B SP-4	53.1	0	0.02	0	46.76	0.02	0.17	0	0	0.09
		A95-11B SP-5	53.4	0	0.01	0	45.98	0.02	0.28	0	0	0.71
		A95-11B SP-6	53.13	0	0	0.02	46.58	0.01	0.05	0	0	0.29
Newbec	NEWB44	NEWB44 CP-1	53.48	0	0.52	0	45.62	0.01	0.01	0	0.16	1
		NEWB44 CP-2	53.58	0	0.3	0	45.61	0	0.02	0	0.12	0.72
		NEWB44 PY-10	52.82	0.03	0.1	0	46.03	0.03	0.01	0.01	0.03	0.16
		NEWB44 PY-11	53.11	0	0.43	0	44.99	0.01	0.09	0	0.24	0.92
		NEWB44 PY-12	52.81	0	0.07	0	46.13	0.02	0	0	0.1	0.33
		NEWB44 PY-13	53.09	0	0.08	0	45.44	0.02	0	0	0.2	0.68
		NEWB44 PY-15	53.21	0.04	0.07	0	46.09	0.01	0.03	0	0.11	0.38
		NEWB44 PY-16	53.3	0	0.08	0	45.96	0.03	0	0	0.16	0.5
		NEWB44 PY-19	53.66	0.05	0.03	0	46.38	0	0	0	0.03	0.01
		NEWB44 PY-2	53.38	0	0.03	0.01	45.39	0.01	0.03	0	0.18	0.65
		NEWB44 PY-21	53.71	0	0.1	0	46.14	0.01	0	0	0.06	0.3
		NEWB44 PY-23	53.95	0.01	0.38	0.02	45.31	0	0.01	0	0.04	0.3
		NEWB44 PY-24	53.84	0	0.02	0	46.39	0.01	0.02	0	0	0.08
		NEWB44 PY-25	52.91	0	1.28	0	45.91	0.01	0	0	0.01	0.08
Quemont	NEWB44	NEWB44 PY-26	52.91	0	1.3	0	45.94	0.01	0	0	0	0.09
		NEWB44 PY-27	53.3	0	0.07	0	46.31	0	0	0	0.04	0.21
		NEWB44 PY-28	53.11	0	0.56	0	45.99	0.01	0.01	0.02	0.12	0.35
		NEWB44 PY-29	53.66	0	0.07	0.01	45.85	0	0	0	0.02	0.26
		NEWB44 PY-4	53.35	0	0.3	0	46.04	0	0.05	0	0.03	0.29
		NEWB44 PY-5	54.09	0	0.11	0	45.16	0.01	0	0	0.05	0.54
		NEWB44 PY-6	53.11	0.02	0.05	0	46.38	0.01	0	0	0	0.03
		NEWB44 PY-8	53.51	0	0.03	0	46.43	0	0	0	0	0.01
		NEWB44 PY-9	53.15	0	0.06	0.03	44.21	0.01	0	0	0.43	1.65
		QT4-2 PY(SP)-1	54	0.04	0.01	0	46.45	0.02	0	0	0.01	0
		QT4-2 PY(SP)-10	53.71	0.05	0	0	46.47	0.03	0.04	0	0.01	0
		QT4-2 PY(SP)-11	53.65	0.01	0.02	0	46.37	0.03	0.03	0	0	0.01
		QT4-2 PY(SP)-12	53.59	0.04	0.05	0	46.29	0	0.35	0	0	0
		QT4-2 PY(SP)-13	53.52	0.02	0	0	46.41	0.01	0.26	0	0	0
Quemont	QT4-2	QT4-2 PY(SP)-14	53.57	0	0.03	0.01	46.5	0	0.05	0	0	0.02
		QT4-2 PY(SP)-15	53.64	0	0	0	46.21	0.03	0.17	0	0	0
		QT4-2 PY(SP)-16	53.55	0	0.03	0.01	46.6	0	0.01	0	0	0
		QT4-2 PY(SP)-17	53.34	0.03	0.04	0	46.21	0.02	0.04	0	0.01	0.08
		QT4-2 PY(SP)-18	53.59	0.09	0	0	46.41	0.04	0.1	0	0	0
		QT4-2 PY(SP)-19	53.5	0	0.05	0.02	46.26	0.01	0	0	0	0.08
		QT4-2 PY(SP)-2	53.6	0	0.05	0	46.26	0.05	0	0	0.01	0
		QT4-2 PY(SP)-20	53.67	0.01	0.02	0	46.5	0.02	0.01	0	0.01	0
		QT4-2 PY(SP)-21	53.37	0	0.06	0	46.49	0	0	0	0.01	0
		QT4-2 PY(SP)-22	53.71	0	0.02	0.02	46.34	0.01	0.03	0	0	0.03
		QT4-2 PY(SP)-23	53.6	0.02	0.06	0.01	46.32	0.01	0.02	0	0	0.01
		QT4-2 PY(SP)-24	53.56	0	0.04	0.03	46.48	0.01	0	0	0	0.03
		QT4-2 PY(SP)-25	53.36	0.07	0.03	0.01	46.47	0.04	0.21	0	0.02	0
Quemont	QT4-2	QT4-2 PY(SP)-26	53.56	0.03	0.04	0	46.44	0.03	0.01	0	0	0
		QT4-2 PY(SP)-27	53.76	0.04	0.03	0	46.2	0.03	0.09	0	0	0
		QT4-2 PY(SP)-28	53.7	0.05	0.05	0	46.13	0.04	0.03	0	0	0.02
		QT4-2 PY(SP)-29	53.72	0.01	0.07	0	46.45	0.01	0.03	0	0	0.03
		QT4-2 PY(SP)-3	53.51	0	0.03	0.01	46.36	0.03	0.05	0	0	0
		QT4-2 PY(SP)-30	53.26	0	0.04	0.01	46.23	0.01	0	0	0.01	0
		QT4-2 PY(SP)-4	53.44	0.03	0.05	0	46.26	0.02	0	0.01	0	0
		QT4-2 PY(SP)-5	53.44	0.02	0.05	0	46.27	0.02	0.01	0	0.01	0
		QT4-2 PY(SP)-6	53.54	0	0.05	0	46.41	0.01	0	0	0.01	0
		QT4-2 PY(SP)-7	53.86	0	0.05	0	46.37	0.03	0.06	0	0.01	0.01
		QT4-2 PY(SP)-8	54.07	0.07	0.03	0	46.2	0.05	0.03	0	0.01	0
		QT4-2 PY(SP)-9	53.68	0.05	0.07	0	46.43	0.03	0	0	0	0
		QT17-5 PY-1	53.61	0.04	0.04	0	46.61	0.01	0	0	0	0.03
Quemont	QT17-5	QT17-5 PY-10	53.74	0	0.05	0	46.57	0.02	0	0	0.01	0.02
		QT17-5 PY-11	53.53	0	0.06	0	46.18	0	0.01	0	0	0.12
		QT17-5 PY-12	53.9	0.03	0.03	0.02	46.24	0.01	0	0	0.01	0.09
		QT17-5 PY-13	54	0	0.07	0	46.64	0.03	0.02	0	0	0
		QT17-5 PY-14	53.76	0.05	0.05	0.01	46.37	0	0.02	0	0	0.07
		QT17-5 PY-15	53.72	0	0.05	0	46.32	0	0.02	0	0	0.01
		QT17-5 PY-16	53.34	0.01	0.03	0.06	46.53	0.02	0.01	0	0.01	0.01
		QT17-5 PY-17	53.34	0	0.03	0	46.61	0.02	0	0	0	0
		QT17-5 PY-18	53.7	0.04	0.07	0	46.55	0.02	0	0	0	0.04
		QT17-5 PY-2	53.48	0.05	0.01	0.02	46.55	0	0.12	0.01	0	0.09
		QT17-5 PY-20	53.53	0	0.05	0	46.38	0.01	0.02	0	0	0.04
		QT17-5 PY-22	53.52	0	0.06	0	46.55	0.01	0	0	0	0
		QT17-5 PY-23	53.28	0.13	0.03	0	46.52	0	0	0	0	0
		QT17-5 PY-24	53.95	0	0.03	0	46.34	0.03	0	0	0	0.04
		QT17-5 PY-25	53.57	0	0.01	0	46.72	0.01	0.02	0	0	0
		QT17-5 PY-26	53.6	0	0.08	0	46.62	0.01	0	0.01	0.01	0.01
		QT17-5 PY-27	53.26	0.03	0.05	0	46.29	0.01	0.01	0.01	0	0.04
		QT17-5 PY-28	52.76	0.71	0.07	0.02	46.22	0.04	0	0	0	0
		QT17-5 PY-29	53.73	0.01	0.02	0	46.44	0.01	0	0	0	0
		QT17-5 PY-3	53.84	0	0.04	0	46.16	0.01	0	0	0	0.04
		QT17-5 PY-30	53.26	0.06	0.05	0	46.45	0	0	0.02	0	0.14
		QT17-5 PY-4	53.72	0	0.07	0	46.35	0	0	0	0	0.07
		QT17-5 PY-5	53.72	0.03	0.04	0	46.53	0.01	0	0	0	0
		QT17-5 PY-6	53.32	0.06	0.02	0	46.24	0	0	0	0	0.08
		QT17-5 PY-7	53.63	0	0.02	0	46.5	0	0	0	0.01	0
		QT17-5 PY-8	53.52	0	0.07	0	46.39	0	0.03	0	0.01	0.01
		QT17-5 PY-9	53.6	0.03	0.05	0.01	46.					

Table A1.3 Pyrite (cont.)

Stratigraphic Position	Deposit	Sample	S (wt%)	As (wt%)	Cu (wt%)	Cd (wt%)	Fe (wt%)	Se (wt%)	Zn (wt%)	Cr (wt%)	Ni (wt%)	Co (wt%)
Cauldron	Quemont	QT18-1 SP(GN)-22	53.05	0.03	0.04	0	46.64	0	0.02	0	0	0.02
		QT18-1 SP(GN)-23	53.33	0	0.03	0	46.49	0	0.03	0	0.01	0
		QT18-1 SP(GN)-24	53.38	0	0.04	0	46.45	0.01	0.02	0	0	0.03
		QT18-1 SP(GN)-25	53.13	0	0.05	0	46.47	0	0.09	0	0.01	0.02
		QT18-1 SP(GN)-26	53.7	0	0.03	0	46.52	0	0.2	0	0	0
		QT18-1 SP(GN)-27	53.74	0.01	0.04	0	46.73	0	0.11	0	0	0
		QT18-1 SP(GN)-28	53.6	0	0.02	0	46.52	0.01	0.27	0	0.02	0
		QT18-1 SP(GN)-29	53.73	0	0.04	0.01	46.46	0	0.23	0	0	0
		QT18-1 SP(GN)-30	53.7	0	0.04	0	46.55	0	0.18	0	0	0
		QT18-1 SP(GN)-31	53.83	0.01	0.04	0.02	46.63	0	0.2	0	0	0
		QT18-1 SP(GN)-32	53.33	0	0.03	0	46.59	0	0.12	0	0	0.01
		QT18-1 SP(GN)-33	53.57	0	0.03	0.03	46.52	0	0.1	0	0.01	0
		QT18-1 SP(GN)-34	53.51	0.01	0.02	0	46.51	0	0.08	0	0	0.01
		QT18-1 SP(GN)-35	53.5	0.06	0.05	0	46.37	0	0.25	0	0.01	0
		QT18-1 SP(GN)-36	53.61	0.03	0.01	0	46.45	0	0.19	0	0	0
		QT18-1 SP(GN)-37	53.05	0.03	0.03	0	46.52	0	0.1	0	0	0
		QT18-1 SP(GN)-38	54.02	0.01	0.05	0	46.29	0	0.07	0	0.01	0.01
		QT18-1 SP(GN)-39	53.47	0.02	0.05	0	46.56	0.01	0	0.01	0	0
		QT18-1 SP(GN)-40	53.59	0	0.04	0.01	46.47	0	0.07	0	0.01	0.02
		QT18-1 PY(GN)-1	53.19	0.03	0.01	0	46.46	0	0.01	0	0.01	0.01
		QT18-1 PY(GN)-10	53.06	0	0.04	0	46.53	0.01	0.01	0.02	0	0
		QT18-1 PY(GN)-11	53.25	0.02	0.03	0.01	46.37	0	0	0	0	0.01
		QT18-1 PY(GN)-12	53.71	0	0.03	0.01	46.07	0	0	0	0.02	0.01
		QT18-1 PY(GN)-13	53.44	0.01	0.02	0	46.33	0	0	0	0	0.01
		QT18-1 PY(GN)-14	53.09	0	0.01	0.02	46.46	0	0	0	0.01	0
		QT18-1 PY(GN)-15	53.01	0	0.03	0	46.39	0	0	0	0.01	0.01
		QT18-1 PY(GN)-2	53.19	0.02	0.02	0.01	46.49	0	0	0.01	0.01	0.03
		QT18-1 PY(GN)-3	53.35	0	0.05	0	46.45	0	0.02	0	0.01	0
		QT18-1 PY(GN)-4	52.89	0	0.04	0	46.54	0.01	0	0	0	0
		QT18-1 PY(GN)-5	52.83	0	0.05	0	46.54	0.01	0.05	0	0	0.01
		QT18-1 PY(GN)-6	53.34	0.03	0.04	0	46.47	0.01	0.03	0.01	0.01	0
		QT18-1 PY(GN)-7	52.97	0	0.04	0	46.45	0	0.07	0	0.01	0
		QT18-1 PY(GN)-8	53.17	0	0.03	0	46.54	0.01	0	0	0	0
		QT18-1 PY(GN)-9	52.91	0.01	0.05	0	46.55	0	0	0.01	0.01	0
		QT27-2 PO-1	52.87	0.03	0.05	0	46.51	0.13	0.02	0	0.02	0
		QT27-2 PO-2	53.35	0.03	0.05	0	46.31	0.07	0.1	0	0	0
		QT27-2 PO-3	53.42	0.03	0.02	0	46.35	0.04	0	0	0	0.01
		QT27-2 PO-4	52.82	0.01	0.03	0.01	46.29	0.01	0	0	0	0.03
		QT27-2 PO-5	53.53	0.05	0.05	0	46.62	0.02	0.04	0	0.01	0
		QT27-2 PO-6	53.13	0	0.03	0.01	46.73	0.05	0.2	0	0	0
		QT27-2 PO-7	52.89	0.03	0.09	0	46.41	0.01	0.06	0	0.01	0.01
		QT27-2 PO-8	53.32	0	0.02	0	46.33	0.03	0.01	0	0	0
		QT27-2 PO-9	52.96	0	0.06	0	46.33	0.03	0.03	0	0	0
		QT8-6 CP-1	53.05	0	0.43	0	46.76	0	0.01	0	0	0.01
		QT8-6 CP-2	53.44	0	0.2	0.01	46.89	0.02	0.09	0	0	0.02
		QT8-6 CP-3	53.37	0.02	0.21	0	46.82	0	0	0	0	0.02
		QT8-6 CP-4	53.41	0.01	0.12	0	46.96	0.05	0	0	0	0.04
		QT8-6 CP-5	53.45	0	0.33	0.03	46.72	0.03	0.03	0	0	0
		QT8-6 CP-6	53.41	0	0.1	0	46.67	0.04	0	0	0	0
		QT8-6 CP-7	53.06	0	0.21	0	46.58	0.29	0	0	0	0.07
		QT9-4 PY(SP)-1	52.91	0	0.01	0	46.57	0.09	0.02	0	0.01	0.02
		QT9-4 PY(SP)-10	53.05	0	0.02	0.03	46.84	0.11	0.03	0	0	0
		QT9-4 PY(SP)-11	52.87	0	0.02	0	46.75	0.09	0.01	0	0	0
		QT9-4 PY(SP)-12	52.78	0.02	0	0.01	46.84	0.07	0	0	0.01	0
		QT9-4 PY(SP)-13	53.16	0.01	0.01	0	46.44	0.09	0.01	0	0	0
		QT9-4 PY(SP)-14	52.94	0.03	0.04	0.03	46.63	0.08	0.07	0	0	0
		QT9-4 PY(SP)-15	52.7	0.01	0.01	0	46.88	0.07	0.03	0	0	0
		QT9-4 PY(SP)-16	53.02	0	0	0	46.53	0.1	0.03	0	0	0
		QT9-4 PY(SP)-17	53.06	0.05	0.01	0	46.64	0.07	0	0	0	0
		QT9-4 PY(SP)-18	53	0	0	0.01	46.67	0.11	0	0	0	0
		QT9-4 PY(SP)-19	53.02	0.02	0.02	0.02	46.54	0.1	0.03	0	0	0.01
		QT9-4 PY(SP)-2	52.98	0.01	0.01	0.01	46.74	0.09	0	0	0	0
		QT9-4 PY(SP)-20	52.87	0.02	0.01	0	46.68	0.05	0	0	0	0
		QT9-4 PY(SP)-3	52.88	0.03	0	0.03	46.85	0.11	0	0	0	0.02
		QT9-4 PY(SP)-4	52.89	0.04	0.02	0	46.75	0.05	0.04	0	0	0
		QT9-4 PY(SP)-5	52.96	0	0.02	0	46.61	0.05	0.07	0	0	0.01
		QT9-4 PY(SP)-6	53	0	0.03	0.01	46.84	0.08	0	0	0	0.01
		QT9-4 PY(SP)-7	53	0	0.02	0.01	46.7	0.1	0	0	0	0
		QT9-4 PY(SP)-8	52.94	0.01	0	0	46.59	0.19	0	0	0	0
		QT9-4 PY(SP)-9	53.02	0	0.01	0	46.48	0.13	0.01	0	0	0
		QT15-4 SP-1	53.59	0	0	0	46.83	0.01	0.34	0	0	0.02
		QT15-4 SP-10	53.12	0	0.02	0	46.83	0.01	0.1	0	0	0.01
		QT15-4 SP-2	53.41	0.04	0	0.01	46.78	0	0.31	0	0	0.01
		QT15-4 SP-3	53.46	0.01	0	0.02	46.76	0.05	0.09	0	0	0.01
		QT15-4 SP-4	53.36	0	0	0	46.8	0.01	0.39	0	0	0
		QT15-4 SP-5	53.38	0.01	0	0	46.82	0.02	0.24	0	0	0
		QT15-4 SP-6	53.32	0	0	0.01	46.8	0.01	0.09	0	0	0
		QT15-4 SP-7	53.46	0	0	0	46.84	0.02	0.09	0	0	0.01
		QT15-4 SP-8	53.31	0.11	0.02	0	46.6	0	0.64	0	0	0.02
		QT15-4 SP-9	53.52	0.01	0.01	0	46.94	0	0.16	0	0	0.01
		QT14-4 PO-1	53.59	0	0.05	0.01	46.92	0.02	0	0	0	0
		QT14-4 PO-10	53.1	0.04	0.06	0	46.77	0.01	0	0	0	0.12
		QT14-4 PO-11	52.99	0	0.04	0.03	46.97	0.03	0	0	0	0
		QT14-4 PO-12	53.06	0.03	0.08	0	46.81	0.02	0	0	0	0
		QT14-4 PO-13	53.19	0.02	0.09	0.01	46.69	0	0	0	0	0.01
		QT14-4 PO-14	53.14	0.01	0.05	0	46.81	0.03	0	0	0	0.01
		QT14-4 PO-15	53.26	0.02	0.06	0.01	46.76	0.03	0	0	0	0
		QT14-4 PO-2	53.26	0.01	0.04	0	46.89	0.05	0	0	0.01	0
		QT14-4 PO-3	53.14	0	0.06	0	46.74	0	0	0	0	0.06
		QT14-4 PO-5	53.06	0	0.05	0.01	46.79	0.1	0.01	0	0	0
		QT14-4 PO-6	53.16	0.03	0.04	0.01	46.6	0.02	0	0	0	0.09
		QT14-4 PO-7	52.88	0	0.06	0	46.72	0	0	0	0	0.1
		QT14-4 PO-8	53.09	0.04	0.04	0	46.69	0.01	0	0	0.02	0.14
		QT14-4 PO-9	53.1	0.03	0.03	0.02	46.72	0.02	0	0	0	0
		QT9-4 PY-1	53.47	0.02	0.04	0	46.94	0.08	0	0	0	0
		QT9-4 PY-10	53.55	0.03	0.02	0	46.9	0.1	0.01	0	0	0
		QT9-4 PY-11	53.48	0.02	0.05	0	46.86	0.05	0	0	0	0
		QT9-4 PY-12	53.88	0	0.04	0	46.92	0.09	0	0	0	0
		QT9-4 PY-13	53.41	0.01	0.02	0.01	46.76	0.09	0	0	0	0
		QT9-4 PY-14	53.46	0.01	0.02	0	46.71	0.05	0	0	0	0
		QT9-4 PY-15	53.56	0.03	0	0	46.84	0.13	0	0	0	0.01
		QT9-4 PY-2	53.51	0.04	0.02	0	46.83	0.09	0	0	0	0
		QT9-4 PY-3	53.42	0	0.03	0	46.83	0.08	0	0	0	0
		QT9-4 PY-4	53.51	0.03	0.02	0	47.01	0.12	0.01	0	0	

Table A1.3 Pyrite (cont.)

Stratigraphic Position	Deposit	Sample	S (wt%)	As (wt%)	Cu (wt%)	Cd (wt%)	Fe (wt%)	Se (wt%)	Zn (wt%)	Cr (wt%)	Ni (wt%)	Co (wt%)
Cauldron	Quemont	QT9-4 PY-5	53.71	0.01	0.02	0	46.86	0.04	0.03	0	0	0.03
		QT9-4 PY-6	53.6	0.03	0.03	0	46.98	0.1	0	0	0	0
		QT9-4 PY-7	53.65	0.06	0.04	0	46.82	0.06	0.01	0	0	0
		QT9-4 PY-8	53.68	0	0.03	0	46.86	0.09	0	0	0.01	0
		QT9-4 PY-9	53.55	0.02	0.04	0	47.05	0.07	0	0	0.01	0
		QT14-4 PY(CP2)-1	53.67	0	0.02	0	46.92	0.02	0	0	0	0.02
		QT14-4 PY(CP2)-10	53.33	0.02	0.04	0	46.95	0.04	0.01	0	0	0.09
		QT14-4 PY(CP2)-11	53.53	0.04	0.03	0	46.73	0.04	0.01	0	0	0.03
		QT14-4 PY(CP2)-12	53.53	0.05	0.03	0.03	46.91	0.07	0	0	0	0.04
		QT14-4 PY(CP2)-13	53.53	0.02	0.02	0	46.91	0.04	0	0	0.01	0.03
		QT14-4 PY(CP2)-14	53.6	0	0.03	0	46.84	0	0	0	0	0
		QT14-4 PY(CP2)-15	53.61	0	0.04	0	46.84	0.02	0	0	0	0.08
		QT14-4 PY(CP2)-16	53.41	0	0.05	0	46.8	0.04	0	0	0.02	0
		QT14-4 PY(CP2)-17	53.8	0.04	0.03	0	46.93	0.02	0	0	0	0.09
		QT14-4 PY(CP2)-18	53.55	0.02	0.01	0	46.88	0	0	0	0	0.09
		QT14-4 PY(CP2)-19	53.92	0	0.02	0.01	46.92	0	0	0	0.01	0.02
		QT14-4 PY(CP2)-2	53.43	0.01	0.04	0	46.89	0.03	0	0	0	0.02
		QT14-4 PY(CP2)-20	53.47	0.03	0.04	0	46.87	0.01	0	0	0	0
		QT14-4 PY(CP2)-3	53.67	0.02	0.04	0.01	46.81	0.03	0	0	0	0.01
		QT14-4 PY(CP2)-4	53.69	0.01	0.03	0.03	46.73	0.02	0	0	0	0.04
		QT14-4 PY(CP2)-5	53.55	0	0.03	0.03	46.89	0.08	0.02	0	0	0.01
		QT14-4 PY(CP2)-6	53.44	0	0.04	0	46.41	0.02	0.02	0	0	0
		QT14-4 PY(CP2)-7	53.24	0	0.02	0.03	46.96	0.05	0.01	0	0	0
		QT14-4 PY(CP2)-8	53.59	0	0.04	0	46.86	0.01	0	0	0	0
		QT14-4 PY(CP2)-9	53.77	0	0.08	0	46.94	0.06	0	0	0	0.01
		QT14-4 PY-1	53.45	0	0.03	0.01	46.67	0.02	0	0	0	0.06
		QT14-4 PY-10	53.62	0.02	0.01	0.03	46.7	0.02	0.01	0	0	0
		QT14-4 PY-11	53.38	0.01	0.06	0	46.94	0.05	0	0	0	0.03
		QT14-4 PY-12	53.41	0.03	0.04	0	46.84	0.02	0	0	0.01	0.05
		QT14-4 PY-13	53.48	0.02	0.04	0	46.73	0.02	0.01	0	0	0.04
		QT14-4 PY-14	53.45	0.02	0.03	0	46.88	0.01	0	0	0	0.04
		QT14-4 PY-15	53.78	0.04	0.01	0	46.81	0.02	0	0	0	0.01
		QT14-4 PY-2	53.64	0	0.04	0.01	46.78	0	0	0	0	0.07
		QT14-4 PY-3	53.43	0.03	0.03	0.02	46.71	0.02	0	0	0	0.04
		QT14-4 PY-4	53.45	0.06	0.02	0	46.7	0.04	0	0	0	0.02
		QT14-4 PY-5	53.72	0	0.05	0	46.86	0.1	0	0	0	0.01
		QT14-4 PY-6	53.44	0.01	0.02	0.03	46.72	0.01	0	0	0.01	0.13
		QT14-4 PY-7	53.24	0	0.02	0	46.27	0.05	0.01	0	0	0
		QT14-4 PY-8	53.43	0	0.04	0.04	46.95	0	0	0	0.01	0
		QT14-4 PY-9	53.42	0	0.03	0.01	46.89	0.04	0.01	0	0	0.01
		QT17-5 PO(MT)-1	53.55	0.04	0.07	0	46.82	0.01	0.01	0	0.01	0.09
		QT17-5 PO(MT)-2	53.6	0	0.03	0	46.8	0.01	0.01	0	0	0.06
		QT17-5 PO(MT)-3	53.58	0	0.05	0.03	46.71	0	0.06	0	0	0
		QT17-5 PO(MT)-4	53.6	0	0.07	0	46.9	0	0.03	0	0	0
		QT17-5 PO(MT)-6	53.64	0.01	0.08	0	46.76	0.02	0	0	0	0
		QT17-5 PO(MT)-7	53.44	0	0.06	0.02	46.95	0.01	0.01	0	0	0
Post-cauldron	Deldona	DELD-F339-986 SP-1	52.48	0.06	0.04	0.01	45.88	0	0.66	0	0.01	0.01
		DELD-F339-986 SP-2	52.66	0.08	0.07	0	45.98	0	0.52	0	0	0.01
		DELD-F339-985 SP-2	52.51	0	0.4	0	45.84	0.05	0.24	0	0.01	0
		DELD-F339-985 SP-3	52.66	0	0.09	0	46.26	0	0.07	0	0	0.01
		DELD-F339-985 SP-4	52.55	0.02	0.03	0	46	0.01	0.59	0	0	0.02
		DELD-F339-999 PY/SP-1	53.37	0	0.04	0.01	46.28	0	0.48	0	0.01	0.01
		DELD-F339-999 PY/SP-11	53.09	0.78	0.03	0.01	46.26	0	0.05	0	0	0.01
		DELD-F339-999 PY/SP-13	53.29	0.03	0.02	0	46.48	0	0	0	0	0
		DELD-F339-999 PY/SP-14	53.22	0	0.02	0	46.55	0	0.1	0	0.01	0.03
		DELD-F339-999 PY/SP-15	52.97	0.03	0.06	0	46.13	0	0.25	0	0	0
		DELD-F339-999 PY/SP-3	52.99	0.03	0.03	0	46.11	0.01	0.35	0	0.01	0.02
		DELD-F339-999 PY/SP-4	53.43	0.08	0.03	0	46.41	0	0.05	0	0.01	0
		DELD-F339-999 PY/SP-5	53.06	0.06	0.03	0.02	46.46	0	0.06	0	0	0.01
		DELD-F339-999 PY/SP-6	53.42	0	0.03	0	46.67	0.01	0.08	0	0	0
		DELD-F339-999 PY/SP-8	53.79	0.01	0.02	0.03	46.38	0	0.31	0	0	0
		DELD-F339-999 PY/SP-9	53.36	0	0	0	46.67	0	0.07	0	0	0
		DELD-F339-1004 PY-1	53.38	0.03	0.03	0.01	46.71	0	0.12	0	0	0.02
		DELD-F339-1004 PY-10	52.73	0.16	0.43	0	46.36	0.02	0.02	0	0	0.02
		DELD-F339-1004 PY-11	53.57	0	0.05	0	46.7	0	0	0	0	0
		DELD-F339-1004 PY-12	53.48	0	0.03	0.01	46.79	0.01	0.01	0	0.01	0.01
		DELD-F339-1004 PY-13	52.86	0	0.03	0	46.72	0	0.01	0	0	0
		DELD-F339-1004 PY-14	53.64	0.1	0.11	0	46.22	0.01	0.03	0	0.02	0
		DELD-F339-1004 PY-15	53.1	0	0.02	0.01	46.79	0	0.01	0	0	0.01
		DELD-F339-1004 PY-16	53.11	0	0.02	0	46.58	0.02	0.03	0	0	0
		DELD-F339-1004 PY-17	53.47	0	0.01	0	46.78	0	0	0	0	0
		DELD-F339-1004 PY-18	53.25	0	0.04	0	46.82	0.02	0	0	0	0.01
		DELD-F339-1004 PY-19	53.27	0	0.04	0.01	46.78	0.01	0.12	0	0	0
		DELD-F339-1004 PY-2	53.4	0.01	0.05	0.01	46.65	0	0.06	0	0	0.01
		DELD-F339-1004 PY-20	53.34	0.01	0.03	0	46.82	0	0	0	0.01	0
		DELD-F339-1004 PY-3	52.72	0.01	0.03	0	46.72	0	0	0	0.01	0
		DELD-F339-1004 PY-4	53.04	0	0.02	0	46.5	0.02	0.03	0	0	0
		DELD-F339-1004 PY-5	53.55	0.04	0.03	0.02	46.74	0	0	0	0	0
		DELD-F339-1004 PY-6	53.66	0	0.01	0	46.91	0	0.01	0	0	0
		DELD-F339-1004 PY-7	53.45	0	0.03	0	46.84	0.01	0.01	0	0	0
		DELD-F339-1004 PY-8	53.26	0.02	0.03	0	46.61	0.01	0.04	0	0	0
		DELD-F339-1004 PY-9	53.25	0.01	0.03	0.02	46.84	0	0.03	0	0	0
		DELD-F339-985 PY/GN-1	53.29	0.03	0.06	0.01	46.1	0.09	0.39	0	0	0.26
		DELD-F339-985 PY/GN-10	52.91	0.06	0.57	0	46.16	0	0	0	0	0.02
		DELD-F339-985 PY/GN-11	52.98	0.01	0.07	0	46.68	0	0	0	0.01	0
		DELD-F339-985 PY/GN-12	53.05	0.03	0.05	0	46.73	0	0	0	0.02	0
		DELD-F339-985 PY/GN-13	53.24	0	0.05	0	46.5	0	0.13	0	0.01	0.02
		DELD-F339-985 PY/GN-14	53.41	0.01	0.03	0.03	46.49	0	0	0	0.01	0
		DELD-F339-985 PY/GN-15	53.31	0.09	0.03	0.01	46.37	0.01	0.07	0	0.02	0.08
		DELD-F339-985 PY/GN-16	53.63	0	0.02	0.01	46.79	0.02	0.02	0	0.01	0
		DELD-F339-985 PY/GN-18	53.44	0.04	0.15	0	46.54	0.01	0.01	0	0	0.01
		DELD-F339-985 PY/GN-19	53.24	0	0.03	0	46.65	0	0.01	0	0	0.02
		DELD-F339-985 PY/GN-2	53.44	0	0.04	0	46.72	0	0.06	0	0	0.02
		DELD-F339-985 PY/GN-21	53.47	0.05	0.04	0	46.48	0	0	0	0	0.04
		DELD-F339-985 PY/GN-3	53.5	0	0.01	0.01	46.6	0	0.02	0	0.01	0.01
		DELD-F339-985 PY/GN-4	53.26	0	0.03	0	46.41	0	0	0	0	0.02
		DELD-F339-985 PY/GN-5	53.48	0.05	0.04	0.01	46.57	0	0.01	0	0.02	0
		DELD-F339-985 PY/GN-6	53.5	0.03	0.03	0	46.68	0.01	0	0	0	0
		DELD-F339-985 PY/GN-7	53.27	0.01	0.02	0.01	46.65	0	0.09	0	0	0
		DELD-F339-985 PY/GN-9	53.5	0.03	0.02	0	46.53	0</				

Table A1.3 Pyrite (cont.)

Stratigraphic Position	Deposit	Sample	S (wt%)	As (wt%)	Cu (wt%)	Cd (wt%)	Fe (wt%)	Se (wt%)	Zn (wt%)	Cr (wt%)	Ni (wt%)	Co (wt%)
Post-cauldron	Deldona	DELD-F339-987 GN/SP-13	53.11	0.33	0.05	0.03	46.44	0.01	0.01	0	0	0
		DELD-F339-987 GN/SP-14	53.63	0.01	0.06	0	46.71	0	0.1	0	0	0
		DELD-F339-987 GN/SP-15	52.8	0.13	0.06	0	46.41	0	0.22	0	0	0.02
		DELD-F339-987 GN/SP-2	51.1	0.24	0.03	0.01	43.88	0.06	0.09	0	0	0
		DELD-F339-987 GN/SP-3	53.26	0.06	0.04	0.02	46.62	0	0.03	0	0.01	0.02
		DELD-F339-987 GN/SP-4	53.53	0.01	0.04	0	46.62	0.05	0.25	0	0	0
		DELD-F339-987 GN/SP-5	53.57	0.01	0.04	0.01	46.64	0.01	0.22	0	0.01	0.02
		DELD-F339-987 GN/SP-6	53.33	0.02	0.04	0	46.5	0	0.22	0	0	0
		DELD-F339-987 GN/SP-8	53.4	0.02	0.04	0	46.46	0.01	0.03	0	0	0
		DELD-F339-987 GN/SP-9	53.32	0.03	0.03	0.03	46.58	0	0.17	0	0.01	0.05
Delbridge		98DELB-2 SP-1	53.18	0.01	0.03	0	46.47	0	0.13	0	0.01	0
		98DELB-2 SP-10	53.02	0.03	0.1	0.01	46.65	0	0.12	0	0	0
		98DELB-2 SP-11	53.04	0.01	0.06	0	46.59	0	0.05	0	0	0
		98DELB-2 SP-12	53.3	0	0.04	0	46.31	0	0.73	0	0	0
		98DELB-2 SP-13	53.08	0.03	0.05	0	46.41	0.01	0.32	0	0	0
		98DELB-2 SP-14	52.97	0.02	0.05	0	46.58	0	0.55	0	0	0
		98DELB-2 SP-15	53.21	0	0.04	0	46.51	0	0.28	0	0.01	0
		98DELB-2 SP-17	52.77	0.12	0.07	0.01	46.36	0	0.63	0	0.02	0
		98DELB-2 SP-18	53.11	0	0.04	0.03	46.81	0.01	0.31	0	0	0
		98DELB-2 SP-19	52.64	0.03	0.07	0	46.37	0.02	0.44	0	0.01	0
		98DELB-2 SP-2	53.33	0	0.06	0	46.85	0.01	0.05	0	0.02	0.01
		98DELB-2 SP-20	53.12	0	0.11	0.02	46.54	0	0.35	0	0	0
		98DELB-2 SP-3	53.37	0.01	0.01	0	46.79	0	0.04	0	0	0
		98DELB-2 SP-4	53.37	0	0.01	0	46.7	0.01	0.08	0	0	0
		98DELB-2 SP-5	52.91	0.02	0.05	0.02	46.53	0.01	0.04	0	0.01	0.01
		98DELB-2 SP-7	52.91	0.03	0.78	0.01	45.97	0.04	0.28	0	0	0.01
		98DELB-2 SP-8	53.05	0.02	0.06	0.01	46.8	0.01	0.13	0	0.01	0
		98DELB-2 PY-1	53.36	0	0.05	0.03	46.69	0	0.19	0	0.01	0
		98DELB-2 PY-10	53.33	0.04	0.03	0	46.7	0	0.04	0	0	0
		98DELB-2 PY-11	53.29	0.01	0.03	0	46.72	0	0.01	0	0	0
		98DELB-2 PY-12	53.46	0.01	0.01	0	46.89	0.01	0.01	0	0	0
		98DELB-2 PY-13	53.12	0	0.05	0	46.65	0	0.02	0	0.01	0
		98DELB-2 PY-14	53.29	0.03	0.03	0.01	46.64	0.05	0.06	0	0.01	0.01
		98DELB-2 PY-15	53.25	0	0.06	0	46.6	0	0.01	0	0	0
		98DELB-2 PY-16	53.35	0	0.03	0.02	46.76	0.01	0.04	0	0	0
		98DELB-2 PY-17	53.07	0	0.07	0	46.35	0.02	0.02	0	0	0
		98DELB-2 PY-18	53.02	0	0.01	0	46.72	0.01	0.13	0	0	0.01
		98DELB-2 PY-2	53.32	0.01	0.05	0	46.54	0	0	0	0.01	0.02
		98DELB-2 PY-20	53.03	0.05	0.04	0	46.65	0.02	0	0	0	0
		98DELB-2 PY-3	53.18	0.02	0.03	0	46.74	0.03	0	0	0	0
		98DELB-2 PY-4	53.15	0.01	0.05	0	46.7	0.01	0.01	0	0.01	0.01
		98DELB-2 PY-5	53.26	0	0.02	0	46.74	0	0	0	0	0.01
		98DELB-2 PY-6	53.25	0.01	0.01	0	46.67	0.02	0.01	0	0	0
		98DELB-2 PY-7	53.23	0.02	0.06	0.01	46.82	0.01	0	0	0	0
		98DELB-2 PY-9	53.44	0	0.05	0.02	46.69	0.01	0.02	0	0	0.02
		98DELB-2-1 PO(SP)-1	53.24	0.01	0.06	0.02	46.49	0	0.43	0	0	0
		98DELB-2-1 PO(SP)-10	53.11	0	0.07	0	46.65	0.01	0.05	0	0	0
		98DELB-2-1 PO(SP)-11	53.04	0.03	0.11	0	46.78	0	0.08	0	0	0
		98DELB-2-1 PO(SP)-12	53.05	0.02	0.1	0.02	46.45	0	0.7	0	0	0
		98DELB-2-1 PO(SP)-13	52.66	0	1.41	0	44.72	0.02	1.19	0	0	0
		98DELB-2-1 PO(SP)-14	52.85	0	0.04	0	46.84	0.01	0.14	0	0	0
		98DELB-2-1 PO(SP)-15	53.23	0.04	0.08	0	46.56	0.02	0.17	0	0.02	0
		98DELB-2-1 PO(SP)-16	53.13	0.06	0.1	0	46.46	0	0.42	0	0	0
		98DELB-2-1 PO(SP)-17	53.33	0	0.08	0	46.5	0	0.22	0	0.01	0.02
		98DELB-2-1 PO(SP)-18	52.98	0.06	0.09	0	46.52	0	0.12	0	0	0.01
		98DELB-2-1 PO(SP)-19	52.92	0.01	0.07	0	46.56	0	0.33	0	0	0.03
		98DELB-2-1 PO(SP)-2	53.14	0	0.05	0	46.59	0	0.3	0	0	0
		98DELB-2-1 PO(SP)-20	53.33	0	0.06	0	46.85	0	0.12	0	0	0
		98DELB-2-1 PO(SP)-3	53.16	0.01	0.06	0	46.59	0.01	0.21	0	0.01	0
		98DELB-2-1 PO(SP)-4	53.09	0	0.14	0	46.45	0	0.31	0	0	0
		98DELB-2-1 PO(SP)-5	53.19	0.04	0.08	0	46.71	0	0.08	0	0.01	0.01
		98DELB-2-1 PO(SP)-6	52.94	0.01	0.1	0	46.51	0.01	0.12	0	0	0
		98DELB-2-1 PO(SP)-7	53.38	0.02	0.07	0.01	46.59	0.02	0.11	0	0	0.01
		98DELB-2-1 PO(SP)-8	53.14	0.01	0.09	0.01	46.76	0	0.25	0	0	0
		98DELB-2-1 PO(SP)-9	52.97	0.07	0.07	0.02	46.36	0	0.12	0	0	0
		98DELB-4 SP-1	52.71	0	0.03	0	46.52	0.01	0.36	0	0	0
		98DELB-4 SP-2	52.38	0.02	0.03	0	46.47	0	0.17	0	0	0.02
		98DELB-4 SP-3	52.31	0	0.04	0.01	46.44	0	0.28	0	0.01	0
		98DELB-4 SP-4	52.63	0.15	0.05	0.03	46.3	0.01	0.28	0	0	0
		98DELB-4 SP-5	52.67	0	0.08	0.04	46.21	0.01	0.16	0	0	0.03
		98DELB-4 SP-6	52.47	0.02	0.05	0	46.51	0	0.05	0	0	0
		98DELB-4 SP-7	52.56	0.01	0.06	0.01	46.47	0	0.23	0	0	0
		98DELB-4 PY-1	53.01	0	0.04	0	46.86	0	0.01	0	0	0
		98DELB-4 PY-10	52.81	0.2	0.04	0.03	46.8	0	0.05	0	0	0
		98DELB-4 PY-11	52.65	0.02	0.07	0.01	47.08	0.01	0.01	0	0	0
		98DELB-4 PY-13	52.99	0	0.02	0.01	46.88	0	0.06	0	0	0
		98DELB-4 PY-14	53.46	0.03	0	0.02	46.82	0.01	0.22	0	0	0
		98DELB-4 PY-15	53.11	0	0.04	0	46.72	0	0.13	0	0	0
		98DELB-4 PY-16	52.82	0	0.02	0.02	46.59	0	0.25	0	0	0.03
		98DELB-4 PY-17	52.92	0	0.02	0	47.22	0	0.11	0	0	0
		98DELB-4 PY-19	52.82	0	0.05	0	46.55	0	0.08	0	0	0
		98DELB-4 PY-2	52.95	0.01	0.02	0	46.86	0	0	0	0.01	0.01
		98DELB-4 PY-4	52.69	0.03	0.02	0.01	46.89	0	0.02	0	0	0.02
		98DELB-4 PY-5	53.22	0.01	0.02	0	46.78	0	0.06	0	0	0
		98DELB-4 PY-6	52.64	0	0.03	0	46.71	0	0.15	0	0	0.01
		98DELB-4 PY-7	52.86	0.02	0.02	0	46.68	0.02	0.05	0	0	0
		98DELB-4 PY-8	52.9	0	0.03	0	46.95	0.01	0.03	0	0	0.01
		98DELB-4 PY-9	52.86	0	0.04	0	46.82	0.01	0.03	0	0.01	0
		98DELB-5 PY-1	52.78	0.02	0.04	0	46.87	0.02	0	0	0	0
		98DELB-5 PY-10	53.16	0	0.03	0	46.68	0.01	0.01	0	0	0.01
		98DELB-5 PY-11	53.3	0	0.05	0	46.72	0.01	0	0	0	0
		98DELB-5 PY-15	52.68	0.03	0.06	0.01	46.47	0	0	0	0	0
		98DELB-5 PY-16	53.03	0.05	0.05	0	46.93	0	0.02	0	0	0
		98DELB-5 PY-17	53.15	0	0.06	0	47.05	0	0.01	0	0	0
		98DELB-5 PY-18	53	0.01	0.05	0.03	46.92	0.01	0	0	0.02	0.02
		98DELB-5 PY-19	52.69	0.01	0.03	0	46.42	0	0	0	0	0
		98DELB-5 PY-3	53.45	0	0.03	0.01	46.73	0.01	0.02	0	0	0
		98DELB-5 PY-4	52.92	0.02	0.04	0	46.8	0	0.01	0	0	0
		98DELB-5 PY-5	52.65	0.03	0.05	0	46.71	0.01	0	0	0	0.01
		98DELB-5 PY-6	52.89	0.02	0.04	0.01	46.72	0.01	0	0	0	0
		98DELB-5 PY-7	53.09	0	0.03	0.01	46.81	0	0	0	0	0
		98DELB-5 PY-8	52.99	0	0.04	0	46.81</					

Table A1.3 Pyrite (cont.)

Stratigraphic Position	Deposit	Sample	S (wt%)	As (wt%)	Cu (wt%)	Cd (wt%)	Fe (wt%)	Se (wt%)	Zn (wt%)	Cr (wt%)	Ni (wt%)	Co (wt%)
Post-cauldron	Delbridge	98DELB-5 PO-12	52.57	0	0.02	0.01	46.58	0	0.01	0	0	0
		98DELB-5 PO-13	52.41	0	0.03	0	46.67	0	0.01	0	0.01	0
		98DELB-5 PO-14	52.86	0.04	0.03	0	46.06	0	0.01	0	0	0
		98DELB-5 PO-15	52.59	0.02	0.02	0.02	46.67	0	0	0	0	0
		98DELB-5 PO-16	52.51	0	0.04	0.03	46.6	0	0.02	0	0	0.01
		98DELB-5 PO-17	52.84	0.03	0.02	0	46.7	0.01	0.01	0	0.02	0
		98DELB-5 PO-18	52.32	0	0.05	0.01	46.61	0	0.06	0	0.01	0.01
		98DELB-5 PO-19	53.22	0	0.02	0	46.67	0.01	0	0	0	0
		98DELB-5 PO-2	52.63	0	0.02	0	46.9	0	0.03	0	0	0
		98DELB-5 PO-3	52.49	0	0.02	0	46.78	0	0	0	0	0
		98DELB-5 PO-4	52.34	0.76	0.02	0	46.38	0.01	0	0	0	0
		98DELB-5 PO-6	52.98	0.01	0.05	0	46.92	0.02	0.01	0	0	0
		98DELB-5 PO-9	52.31	0.17	0.04	0	46.53	0	0.01	0	0	0
		98DELB-6 PY(GN)-10	52.88	0.01	0.03	0	46.53	0	0	0	0.01	0
		98DELB-6 PY(GN)-11	52.87	0	0.04	0	46.46	0	0	0	0.01	0
		98DELB-6 PY(GN)-12	52.72	0	0.03	0.03	46.61	0.01	0	0	0	0
		98DELB-6 PY(GN)-13	52.7	0.02	0.04	0.02	46.76	0	0	0	0	0
		98DELB-6 PY(GN)-16	52.79	0.04	0.04	0	46.62	0.01	0	0	0	0
		98DELB-6 PY(GN)-17	53.11	0	0	0	46.72	0	0.03	0	0	0
		98DELB-6 PY(GN)-18	52.67	0	0.03	0.04	46.67	0.02	0	0	0	0
		98DELB-6 PY(GN)-19	52.83	0	0.04	0	46.72	0	0.01	0	0	0
		98DELB-6 PY(GN)-20	53.04	0.01	0.01	0	46.7	0	0	0	0	0
		98DELB-6 PY(GN)-3	52.72	0.03	0.02	0	46.54	0	0.01	0	0	0
		98DELB-6 PY(GN)-4	52.96	0	0.04	0.02	46.62	0	0	0	0	0
		98DELB-6 PY(GN)-6	52.74	0.18	0.03	0.02	46.14	0.01	0	0	0	0
		98DELB-6 PY(GN)-7	53.31	0	0.02	0	46.72	0.01	0	0	0	0.02
		98DELB-6 PY(GN)-8	52.32	0	0.04	0	46.71	0	0.03	0	0	0
		98DELB-6 PY(GN)-9	52.99	0.07	0.02	0.03	46.57	0.02	0	0	0	0
Gallen		JH98GLLN-2MS1 SP-1	53.31	0.01	0.06	0	46.66	0	0.2	0	0	0
		JH98GLLN-2MS1 SP-1	53.1	0.03	0	0	46.45	0.01	0.32	0	0	0
		JH98GLLN-2MS1 SP-2	52.83	0	0.02	0	46.46	0	0.4	0	0.01	0
		JH98GLLN-2MS1 SP-3	53.6	0.04	0.01	0	46.34	0	0.13	0	0.01	0.01
		JH98GLLN-2MS1 SP-5	52.89	0.02	0.04	0.03	46.5	0.01	0.11	0	0	0
		JH98GLLN-2MS1 SP-7	53.1	0.11	0.04	0	46.58	0	0.19	0	0.01	0
		JH98GLLN-2MS1 PY-1	53.15	0	0.02	0.01	46.61	0.01	0.01	0	0	0
		JH98GLLN-2MS1 PY-10	53.04	0.02	0.05	0	46.66	0.01	0.01	0	0.02	0
		JH98GLLN-2MS1 PY-11	53.18	0.02	0.04	0.02	46.78	0	0.04	0	0	0
		JH98GLLN-2MS1 PY-12	53.07	0.01	0.04	0	46.79	0.01	0	0	0	0
		JH98GLLN-2MS1 PY-13	53.06	0.03	0.02	0	46.55	0	0.01	0	0	0
		JH98GLLN-2MS1 PY-14	53.01	0.01	0.03	0	46.8	0.01	0.06	0	0.01	0
		JH98GLLN-2MS1 PY-15	52.52	0.1	0.04	0	46.35	0	0.03	0	0	0
		JH98GLLN-2MS1 PY-16	52.94	0	0.04	0	46.48	0	0.05	0	0	0
		JH98GLLN-2MS1 PY-17	53.1	0.04	0.04	0.03	46.74	0	0.06	0	0	0
		JH98GLLN-2MS1 PY-18	53.1	0	0.04	0.02	46.66	0	0.07	0	0	0.01
		JH98GLLN-2MS1 PY-19	53.28	0.03	0.03	0	46.8	0.01	0.05	0	0	0.01
		JH98GLLN-2MS1 PY-20	53	0	0.04	0	46.78	0	0.03	0	0	0
		JH98GLLN-2MS1 PY-3	53.07	0	0.04	0.02	46.86	0	0	0	0	0
		JH98GLLN-2MS1 PY-4	53.08	0.04	0.05	0.02	46.84	0.02	0.05	0	0	0
		JH98GLLN-2MS1 PY-5	52.9	0.28	0.05	0	46.48	0	0.04	0	0.15	0.01
		JH98GLLN-2MS1 PY-6	53.19	0.01	0.07	0	46.61	0	0.07	0	0	0.01
		JH98GLLN-2MS1 PY-7	53.08	0.02	0.03	0	46.63	0	0.07	0	0	0
		JH98GLLN-2MS1 PY-8	53.07	0.01	0.04	0.02	46.73	0	0.11	0	0.01	0
		JH98GLLN-2MS1 PY-9	53.26	0	0.05	0	46.88	0	0	0	0.02	0
		JH98GLLN-2MS2 PY-10	53.16	0.01	0.01	0	46.75	0	0	0	0	0
		JH98GLLN-2MS2 PY-11	53.18	0	0.01	0	47.01	0	0.02	0	0	0
		JH98GLLN-2MS2 PY-12	53.1	0	0.03	0.01	46.93	0.01	0.11	0	0	0
		JH98GLLN-2MS2 PY-13	53.1	0	0.02	0	46.87	0	0.01	0	0	0
		JH98GLLN-2MS2 PY-14	53.38	0	0.01	0	46.85	0	0	0	0.01	0
		JH98GLLN-2MS2 PY-15	53.28	0.02	0.02	0.01	46.71	0	0.07	0	0	0
		JH98GLLN-2MS2 PY-16	53.05	0	0.03	0	46.83	0.01	0.02	0	0	0
		JH98GLLN-2MS2 PY-17	53.2	0	0.03	0	46.83	0	0.02	0	0	0
		JH98GLLN-2MS2 PY-18	52.98	0.01	0.04	0.01	46.78	0	0.08	0	0	0
		JH98GLLN-2MS2 PY-19	53.32	0	0.04	0	46.79	0	0.02	0	0	0
		JH98GLLN-2MS2 PY-2	53.02	0	0.05	0.02	46.9	0.02	0	0	0.01	0
		JH98GLLN-2MS2 PY-20	53.05	0	0.02	0.03	46.77	0.02	0.01	0	0	0
		JH98GLLN-2MS2 PY-3	52.96	0.01	0.03	0	46.84	0	0	0	0.01	0
		JH98GLLN-2MS2 PY-4	53.21	0	0.05	0.02	46.76	0	0	0	0	0.02
		JH98GLLN-2MS2 PY-6	53.14	0.08	0.06	0	46.79	0.01	0.03	0	0	0
		JH98GLLN-2MS2 PY-7	53.06	0.05	0.04	0	47	0	0	0	0	0
		JH98GLLN-2MS2 PY-8	53.36	0.01	0.03	0	46.81	0.01	0.09	0	0	0
		JH98GLLN-2MS2 PY-9	53.07	0.02	0.03	0.01	46.88	0	0.03	0	0	0
		JH98GLLN-2MS2 SP-1	53.53	0.07	0.04	0	46.42	0	0.51	0	0	0
		JH98GLLN-2MS2 SP-2	53.22	0	0.03	0	46.38	0	1.08	0	0	0
		JH98GLLN-2MS2 SP-3	53.34	0.01	0.08	0.01	46.61	0	0.41	0	0	0
		JH98GLLN-2MS2 SP-4	53.46	0.02	0.04	0	46.45	0	0.62	0	0	0
		JH98GLLN-2MS2 SP-5	53.32	0.03	0.01	0.02	46.68	0	0.33	0	0.01	0
		JH98GLLN-ZV2 PY-1	53.12	0.05	0.03	0	46.73	0	0	0	0	0.01
		JH98GLLN-ZV2 PY-10	53.11	0.02	0.05	0.03	46.94	0	0	0	0	0.01
		JH98GLLN-ZV2 PY-11	53.43	0	0.04	0	46.54	0	0	0	0	0
		JH98GLLN-ZV2 PY-12	53.14	0.02	0.01	0	46.59	0.01	0.04	0	0	0.01
		JH98GLLN-ZV2 PY-14	52.85	0	0.04	0	46.84	0	0	0	0.02	0.01
		JH98GLLN-ZV2 PY-15	52.68	0.02	0.06	0	46.82	0	0	0	0	0
		JH98GLLN-ZV2 PY-16	53.26	0.02	0.02	0	46.78	0	0.01	0	0	0
		JH98GLLN-ZV2 PY-17	52.9	0.03	0.04	0	46.85	0	0	0	0	0
		JH98GLLN-ZV2 PY-18	52.7	0.03	0.02	0	46.64	0	0.01	0	0	0.02
		JH98GLLN-ZV2 PY-19	52.81	0	0.02	0.04	46.94	0	0.03	0	0.01	0
		JH98GLLN-ZV2 PY-2	53.04	0.04	0.03	0	46.69	0	0.01	0	0.01	0
		JH98GLLN-ZV2 PY-20	52.86	0	0.04	0	46.93	0	0.07	0	0	0.02
		JH98GLLN-ZV2 PY-3	53.13	0	0	0	46.74	0	0	0	0	0
		JH98GLLN-ZV2 PY-4	53.27	0.01	0.05	0	46.76	0	0	0	0.01	0
		JH98GLLN-ZV2 PY-5	52.95	0.02	0	0.01	46.78	0	0.01	0	0	0
		JH98GLLN-ZV2 PY-6	53.28	0.04	0.02	0	46.65	0	0.05	0	0.01	0
		JH98GLLN-ZV2 PY-7	53.16	0	0.04	0	46.61	0	0.01	0	0	0
		JH98GLLN-ZV2 PY-8	52.96	0	0.04	0	46.86	0	0.06	0	0	0
		JH98GLLN-ZV2 PY-9	53.2	0.06	0.03	0.02	46.82	0	0.04	0	0	0
		JH98GLLN-ZV2 PY-10	53.25	0	0.02	0	46.64	0	0.01	0	0	0
		JH98GLLN-ZV2 PY-12	52.87	0.1	0.05	0	46.7	0	0.02	0	0	0
		JH98GLLN-ZV2 PY-13	52.9	0	0.03	0	46.7	0.01	0.01	0	0	0
		JH98GLLN-ZV2 PY-14	53.25	0	0	0	46.74	0	0	0	0.01	0
		JH98GLLN-ZV2 PY-15	53.07	0	0.02	0	46.73	0.02	0.02	0	0	0
		JH98GLLN-ZV2 PY-2	53.27	0.03	0.02	0	45.68	0	0	0	0.01	0.02
		JH98GLLN-ZV2 PY-3	52.77	0.05	0.04	0	46.65	0.01	0.02	0	0.02	0
		JH98GLLN-ZV2 PY-4	53.08	0.01	0.							

Table A1.3 Pyrite (cont.)

Stratigraphic Position	Deposit	Sample	S (wt%)	As (wt%)	Cu (wt%)	Cd (wt%)	Fe (wt%)	Se (wt%)	Zn (wt%)	Cr (wt%)	Ni (wt%)	Co (wt%)
Post-cauldron	Gallen	JH98GLLN-2HW2 PY-5	53.45	0.04	0.02	0	46.78	0	0	0	0	0
		JH98GLLN-2HW2 PY-6	53.17	0.03	0.05	0	46.95	0.01	0	0	0	0.02
		JH98GLLN-2HW2 PY-7	53	0	0.02	0	46.79	0.01	0	0	0	0
		JH98GLLN-2HW2 PY-8	53.18	0.04	0.07	0	46.67	0.01	0	0	0	0
		JH98GLLN-2HW2 PY-9	52.99	0.04	0.04	0	46.73	0	0.01	0	0	0
		JH98GLLN-3EFN CP-1	53.08	0	0.16	0.01	46.49	0.01	0.02	0	0.01	0.01
		JH98GLLN-3EFN CP-2	53.14	0.03	0.2	0	46.56	0	0.01	0	0	0
		JH98GLLN-3EFN CP-3	52.95	0.04	0.12	0.02	46.88	0.01	0	0	0	0
		JH98GLLN-3EFN CP-4	52.81	0	0.18	0.01	46.67	0.03	0.01	0	0	0
		JH98GLLN-3EFN CP-5	53.04	0.01	0.15	0.02	46.71	0	0	0	0	0
Mobrun		SP4880 SP-1	53.66	0.07	0.01	0	46.25	0.01	0.43	0	0.01	0.14
		SP4880 SP-4	52.77	0.07	0.03	0	46.47	0.04	0.11	0	0	0.11
		86MOBR12 SP-1	52.46	0.03	0.03	0.02	46.41	0	0.18	0	0	0.01
		86MOBR12 SP-2	52.61	0.05	0.08	0	46	0.04	0.21	0	0	0.19
		86MOBR12 SP-4	51.72	0.01	1.48	0.02	45.6	0	0.28	0	0	0.03
		86MOBR2 PY-1	53.42	0.03	0.09	0	46.36	0	0.03	0	0.02	0
		86MOBR2 PY-12	53.68	0	0.07	0	46.8	0	0.09	0	0	0
		86MOBR2 PY-14	53.63	0.01	0.09	0	46.76	0	0.22	0	0	0.01
		86MOBR2 PY-15	53.65	0.04	0.08	0	46.79	0	0.14	0	0	0.01
		86MOBR2 PY-16	53.55	0.03	0.03	0	46.49	0.01	0.11	0	0	0
		86MOBR2 PY-19	53.03	0.01	0.07	0	46.4	0.01	0.17	0	0.01	0
		86MOBR2 PY-2	53.48	0.04	0.07	0.01	46.91	0	0.04	0	0	0
		86MOBR2 PY-20	53.26	0	0.08	0.04	46.82	0.01	0.12	0	0	0.02
		86MOBR2 PY-3	53.48	0	0.12	0	46.65	0	0.12	0	0	0
		86MOBR2 PY-4	53.57	0	0.04	0.01	46.69	0	0.14	0	0	0
		86MOBR2 PY-5	53.66	0.04	0.04	0	46.84	0	0.05	0	0	0.02
		86MOBR2 PY-6	53.34	0.01	0.05	0	46.63	0.01	0.15	0	0	0
		86MOBR2 PY-7	53.49	0	0.07	0	46.85	0	0.09	0	0	0
		86MOBR2 PY-8	52.84	0	0.06	0.03	46.52	0	0.04	0	0	0
		86MOBR12 PY-1	53.56	0.01	0.07	0	46.67	0.02	0	0	0	0.03
		86MOBR12 PY-10	53.22	0.08	0.02	0	46.07	0	0.1	0	0	0.07
		86MOBR12 PY-11	53.36	0.08	0.04	0	46.62	0	0	0	0	0.11
		86MOBR12 PY-12	53.67	0	0.04	0.03	46.82	0	0.01	0	0	0.01
		86MOBR12 PY-14	53.01	0	0.01	0.01	46.38	0.01	0.06	0	0	0.08
		86MOBR12 PY-15	52.9	0.03	0.05	0	46.4	0.02	0.13	0	0	0.05
		86MOBR12 PY-17	53.65	0.04	0.06	0	46.7	0.02	0.03	0	0	0.11
		86MOBR12 PY-18	53.44	0.09	0.04	0	46.72	0.01	0.01	0	0	0.01
		86MOBR12 PY-2	53.64	0.03	0.04	0	46.77	0.01	0	0	0	0.02
		86MOBR12 PY-20	53.47	0.04	0.04	0	46.75	0.04	0	0	0.01	0.07
		86MOBR12 PY-3	53.6	0.05	0.04	0	46.82	0.04	0	0	0.01	0.03
		86MOBR12 PY-4	53.66	0	0.05	0	46.81	0.01	0	0	0.01	0.05
		86MOBR12 PY-5	53.67	0.03	0.04	0	46.56	0.02	0.11	0	0	0.06
		86MOBR12 PY-6	53.5	0	0.03	0	46.42	0	0.05	0	0	0.01
		86MOBR12 PY-7	53.65	0.05	0.06	0	46.82	0.01	0.01	0	0	0.06
		86MOBR12 PY-8	53.75	0.02	0.04	0	46.67	0.01	0	0	0.01	0.16
		86MOBR12 PY-9	53.49	0	0.03	0	46.68	0	0.03	0	0.01	0.11
		86MOBR-400 PYT-1	53.84	0.02	0.12	0	46.68	0	0.02	0	0	0
		86MOBR-400 PYT-10	53.99	0	0.02	0.02	46.66	0.01	0.02	0	0.04	0
		86MOBR-400 PYT-11	53.77	0.01	0.02	0.01	46.74	0	0.03	0	0	0
		86MOBR-400 PYT-12	53.54	0.01	0.04	0	46.49	0.02	0	0	0	0
		86MOBR-400 PYT-13	53.43	0.04	0.05	0	46.16	0	0	0	0	0
		86MOBR-400 PYT-14	53.47	0.07	0.02	0.03	46.74	0	0.02	0	0	0
		86MOBR-400 PYT-15	53.47	0	0.1	0.01	46.75	0	0	0	0	0
		86MOBR-400 PYT-3	53.72	0.02	0.33	0	46.69	0.01	0.01	0	0	0
		86MOBR-400 PYT-4	53.19	0.02	0.01	0	46.44	0	0	0	0	0.05
		86MOBR-400 PYT-5	52.7	0	0.01	0	46.66	0	0	0	0	0
		86MOBR-400 PYT-6	52.73	0.01	0.01	0	46.4	0.03	0	0	0	0.08
		86MOBR-400 PYT-7	53.78	0	0.01	0	46.37	0.01	0	0	0	0
		86MOBR-400 PYT-9	53.62	0.07	0.01	0	46.52	0.01	0.02	0	0.01	0.11

Note: Those data shown as 0 are below detection limit

Table A1.3 Sphalerite: EPMA analyses for sphalerite separated by sample for sulfide grains from Noranda VMS deposits.

Stratigraphic position	Deposit	Sample	S (wt%)	As (wt%)	Zn (wt%)	Cd (wt%)	Fe (wt%)	Se (wt%)	Cu (wt%)	Cr (wt%)	Ni (wt%)	Co (wt%)
Pre-cauldron	Robb-Montbray	A95-16D-SP-G1-1	33.59	0.06	59.96	0.5	5.47	0.02	0.08	0	0	0.14
		A95-16D-SP-G1-2	33.23	0.02	59.73	0.48	5.45	0	0.09	0	0	0.17
		A95-16D-SP-G1-3	33.5	0	59.29	0.5	5.38	0.02	0.08	0	0	0.16
		A95-16D-SP-G2-1	33.31	0.01	59.85	0.5	5.7	0	0.09	0	0	0.18
		A95-16D-SP-G2-2	33.16	0	59.81	0.53	5.66	0.01	0.08	0	0	0.17
		A95-16D-SP-G2-3	33.41	0	59.68	0.56	5.63	0.06	0.11	0	0.02	0.18
		A95-16D-SP-G3-1	33.56	0	59.89	0.58	5.4	0.02	0.05	0	0	0.14
		A95-16D-SP-G3-2	33.77	0	59.97	0.52	5.38	0.02	0.07	0	0	0.15
		A95-16D-SP-G3-3	33.29	0	59.74	0.59	5.49	0	0.23	0	0	0.15
		A95-16D-SP-G4-1	33.91	0	59.17	0.53	5.51	0.01	0.06	0	0	0.14
		A95-16D-SP-G4-2	33.96	0	59.42	0.49	5.53	0	0.05	0	0	0.15
		A95-16D-SP-G4-3	33.86	0.01	59.32	0.57	5.48	0.03	0.08	0	0	0.15
		A95-16D-SP-G5-1	33.79	0.01	59.57	0.55	5.41	0	0.04	0	0	0.16
		A95-16D-SP-G5-2	33.79	0	59.55	0.58	5.44	0.06	0.05	0	0.02	0.16
		A95-16D-SP-G5-3	34.1	0.04	59.42	0.49	5.37	0.04	0.05	0	0.02	0.14
		A95-16D-SP-G6-1	33.5	0	58.49	0.53	5.88	0	0.5	0	0	0.14
		A95-16D-SP-G6-3	33.7	0.07	59.34	0.51	5.28	0.01	0.06	0	0.03	0.13
Horne No. 5	63RF3 SP-1	63RF3 SP-1	33.03	0	63.42	0.22	3.27	0.02	0.04	0	0	0
		63RF3 SP-10	33.12	0.04	63.27	0.22	3.33	0.03	0.05	0	0	0
		63RF3 SP-11	33.35	0	63.56	0.2	3.25	0.01	0.06	0	0	0.01
		63RF3 SP-12	33.08	0.02	63.06	0.25	3.4	0	0.01	0	0	0
		63RF3 SP-13	33.11	0.05	63.38	0.14	3.27	0.03	0.04	0	0	0.01
		63RF3 SP-14	33.15	0	63.55	0.23	3.21	0.02	0.04	0	0.01	0
		63RF3 SP-15	33.17	0.07	63.27	0.23	3.36	0	0.03	0	0	0
		63RF3 SP-2	33.34	0	63.61	0.23	3.38	0.03	0.03	0	0.01	0
		63RF3 SP-4	33.2	0	63.28	0.18	3.22	0.01	0	0	0	0
		63RF3 SP-5	33.28	0	63.46	0.23	3.28	0	0.03	0	0	0.01
		63RF3 SP-6	33	0.04	63.32	0.2	3.16	0.01	0.03	0	0.01	0
		63RF3 SP-7	32.99	0.05	63.26	0.23	3.27	0.01	0.05	0	0	0.01
		63RF3 SP-8	32.74	0.02	63.17	0.25	3.53	0.03	0.02	0	0.01	0
		63RF3 SP-9	33.15	0	63.47	0.23	3.36	0.01	0.03	0	0	0
		63RF3 PY-1	33.17	0.03	64.62	0.15	2.03	0.01	0.04	0	0	0.02
		63RF3 PY-2	33.14	0	63.87	0.17	2.91	0.01	0.01	0	0	0
		63RF3 PY-3	33.09	0.02	64.38	0.19	1.92	0	0.01	0	0	0
		63RF3 PY-4	33.17	0.03	64.85	0.22	1.73	0	0.01	0	0.01	0
		63RF3 PY-5	33.35	0	64.37	0.18	2.13	0	0.03	0	0.01	0
Cauldron margin	Aldermac	64RF623 SP-1	33.32	0.03	63.74	0.24	2.87	0	0.01	0	0.01	0
		64RF623 SP-10	33.27	0	63.6	0.2	2.86	0.01	0.04	0	0	0.01
		64RF623 SP-11	33.21	0.03	63.6	0.25	2.95	0	0.01	0	0.01	0
		64RF623 SP-12	33.3	0.03	63.62	0.22	2.72	0.02	0.06	0	0	0.01
		64RF623 SP-13	33.09	0.02	63.32	0.24	2.88	0.02	0.02	0	0.01	0.03
		64RF623 SP-14	33.22	0	63.47	0.24	3.09	0	0.01	0	0.01	0
		64RF623 SP-15	33.09	0	64.1	0.27	2.81	0.01	0.03	0	0	0
		64RF623 SP-2	33.47	0	63.32	0.28	2.89	0	0.03	0	0	0.02
		64RF623 SP-3	33.06	0.04	63.9	0.23	2.73	0	0.01	0	0.01	0
		64RF623 SP-4	33.14	0.01	63.73	0.23	2.87	0.01	0.03	0	0.01	0
		64RF623 SP-5	33.61	0.07	64.1	0.17	2.74	0	0.03	0	0	0
		64RF623 SP-6	33.14	0	63.48	0.21	2.89	0	0.03	0	0	0
		64RF623 SP-7	33.56	0.03	64.05	0.28	2.92	0	0.03	0	0	0
		64RF623 SP-8	33.25	0.09	63.07	0.28	3.18	0.02	0.01	0	0	0
		64RF623 SP-9	33.33	0	63.28	0.31	2.85	0	0	0	0	0.01
		A95-14A SP-1	33.19	0	59.78	0.2	6.77	0.01	0	0	0	0.01
		A95-14A SP-10	33.49	0	59.48	0.23	7.14	0	0.03	0	0	0.01
		A95-14A SP-12	33.23	0	59.72	0.21	6.9	0	0.02	0	0.01	0
		A95-14A SP-13	33.24	0.03	59.38	0.23	7.35	0.02	0.01	0	0	0
		A95-14A SP-14	33.69	0	59.34	0.24	7.32	0.04	0.02	0	0	0
		A95-14A SP-15	33.52	0	59.17	0.2	7.21	0	0.01	0	0	0
		A95-14A SP-16	33.37	0	59.28	0.21	7.23	0	0	0	0	0
		A95-14A SP-17	33.58	0	59.23	0.21	7.36	0	0.01	0	0	0
		A95-14A SP-18	33.44	0	59.55	0.17	7.36	0.03	0.01	0	0	0.02
		A95-14A SP-19	32.94	0.02	59.2	0.2	7.16	0	0	0	0	0.01
		A95-14A SP-2	33.49	0.01	58.85	0.24	7.48	0	0.04	0	0.01	0
		A95-14A SP-20	33.44	0.04	59.36	0.17	6.81	0	0	0	0.01	0
		A95-14A SP-3	33.01	0	58.92	0.18	6.94	0	0.04	0	0	0
		A95-14A SP-4	33.11	0.03	59.39	0.16	6.87	0.01	0.07	0	0	0
		A95-14A SP-5	33.83	0	59.63	0.2	7.08	0.03	0.01	0	0	0
		A95-14A SP-6	33.11	0.02	59.44	0.19	7.29	0	0.01	0	0.01	0
		A95-14A SP-7	33.11	0	59.08	0.24	7.28	0.03	0.01	0	0	0
		A95-14A SP-8	33.39	0	59.25	0.26	7.28	0.01	0.02	0	0.01	0
		A95-14A SP-9	33.48	0	59.42	0.2	7.27	0.03	0.01	0	0.01	0
		A95-14A PY-1	33.01	0	59.55	0.27	6.62	0	0.26	0	0.01	0
		A95-14A PY-2	33.27	0.03	59.2	0.2	7.09	0	0.02	0	0	0.01
		A95-14A PY-3	33.38	0	59.82	0.17	6.71	0.01	0.02	0	0.01	0
		A95-14A PY-4	33.57	0.01	58.84	0.23	7.45	0.01	0	0	0	0
		A95-14A PY-5	33.34	0	59.64	0.24	7.05	0.02	0.01	0	0	0
		A95-14B SP-1	33.26	0.05	59.53	0.16	7.1	0.03	0.03	0	0	0.01
		A95-14B SP-10	33.23	0	58.91	0.24	6.65	0	0.03	0	0.03	0
		A95-14B SP-11	33.26	0.02	60.52	0.21	5.9	0	0.03	0	0	0.02
		A95-14B SP-12	33.19	0	59.52	0.23	7.19	0.01	0	0	0	0
		A95-14B SP-13	33.43	0	58.33	0.22	7.54	0.02	0.03	0	0	0
		A95-14B SP-14	33.27	0.08	59.04	0.21	7.21	0.01	0.04	0	0	0
		A95-14B SP-15	35.53	0	59.07	0.22	7.23	0.03	0.01	0	0	0.01
		A95-14B SP-16	33.42	0	58.64	0.22	7.16	0	0	0	0	0
		A95-14B SP-17	33.34	0.04	59.28	0.2	7.31	0	0.04	0	0	0.01
		A95-14B SP-18	33.25	0.03	59.22	0.23	7.34	0	0.02	0	0	0.01
		A95-14B SP-19	33.42	0	59.22	0.18	7.14	0.02	0.02	0	0.01	0
		A95-14B SP-2	33.28	0.01	58.81	0.21	7.22	0	0.03	0	0.01	0
		A95-14B SP-20	33.38	0.01	59.34	0.17	7.22	0.02	0.03	0	0.01	0.01
		A95-14B SP-3	33.34	0.03	58.84	0.19	7.3	0.01	0.02	0	0	0
		A95-14B SP-4	33.54	0	59.53	0.2	7.05	0	0.01	0	0	0
		A95-14B SP-5	33.39	0.03	59.17	0.2	7.24	0	0.02	0	0	0.01
		A95-14B SP-6	33.26	0	58.36	0.19	6.92	0	0.01	0	0.01	0
		A95-14B SP-7	33.44	0	58.39	0.12	7.62	0	0			

Table A1.3 Sphalerite (cont.)

Stratigraphic position	Deposit	Sample	S (wt%)	As (wt%)	Zn (wt%)	Cd (wt%)	Fe (wt%)	Se (wt%)	Cu (wt%)	Cr (wt%)	Ni (wt%)	Co (wt%)
Cauldron	Corbet	CRB3.15.6-SP-G1-1	32.98	0.06	59.99	0.13	7.02	0.02	0.07	0	0	0.01
		CRB3.15.6-SP-G1-2	32.98	0	59.16	0.12	7.05	0.01	0.07	0	0	0
		CRB3.15.6-SP-G1-3	32.99	0	59.09	0.11	7.01	0.02	0.09	0	0.01	0.01
		CRB3.15.6-SP-G1-4	32.91	0	59.48	0.14	6.78	0	0.14	0	0	0.01
		CRB3.15.6-SP-G2-1	33.4	0.01	58.69	0.11	7.17	0.02	0.03	0	0.01	0.02
		CRB3.15.6-SP-G2-2	33.54	0.01	58.68	0.12	7.19	0	0.05	0	0.01	0
		CRB3.15.6-SP-G2-3	33.53	0	58.71	0.12	7.12	0	0.09	0	0	0.01
		CRB3.15.6-SP-G3-1	33.4	0.05	58.68	0.11	7.07	0	0.02	0	0	0.02
		CRB3.15.6-SP-G3-2	33.52	0	58.7	0.15	7.23	0	0.01	0	0	0.01
		CRB3.15.6-SP-G4-1	33.53	0.01	58.45	0.14	7.17	0	0.02	0.02	0	0.02
		CRB3.15.6-SP-G4-2	33.64	0	58.44	0.15	7.14	0.01	0.02	0	0	0.01
		CRB3.15.6-SP-G4-3	33.64	0.03	58.66	0.14	7.25	0.02	0.02	0	0	0
		CRB3.15.6-SP-G5-1	33.14	0	58.92	0.12	6.96	0.02	0.04	0	0	0.01
		CRB3.15.6-SP-G5-2	33.37	0	58.75	0.13	6.95	0	0.03	0	0	0
		CRB3.15.6-SP-G5-3	33.56	0	59.23	0.1	7.02	0	0.03	0	0	0.02
		CRB3.15.6-SP-G5-4	33.28	0	59.04	0.13	7.05	0	0.02	0	0	0
		CRB3.15.6-SP-G5-5	33.19	0.02	59.02	0.11	6.93	0	0.02	0	0	0
		CRB3.15.6-SP-G5-6	33.12	0.04	59.64	0.11	6.43	0.01	0.02	0	0.01	0
		CRB3.15.6-SP-G6-1	33.26	0.01	59.49	0.1	6.57	0	0.02	0	0.01	0.04
		CRB3.15.6-SP-G6-2	33.26	0.04	59.69	0.1	6.34	0	0.01	0	0	0.01
		CRB3.15.6-SP-G6-3	33.54	0	59.82	0.1	5.53	0	0.03	0.01	0.01	0.01
		CRB3.15.6-SP-G7-1	33.16	0	59.11	0.09	6.98	0	0.03	0	0.01	0
		CRB3.15.6-SP-G7-2	33.21	0	59.18	0.13	6.95	0.03	0.04	0	0	0.02
		CRB3.15.6-SP-G7-3	33.43	0	57.76	0.11	7.03	0	0.03	0.02	0	0
		CRB3.15.6-SP-G8-1	33.56	0.04	58.56	0.12	7.13	0.01	0.05	0	0	0.01
		CRB3.15.6-SP-G8-2	33.38	0.02	58.55	0.15	7.12	0	0.05	0.02	0.02	0.01
		CRB3.15.6-SP-G8-3	33.41	0	58.73	0.1	7.09	0	0.05	0	0	0
		CRB3.15.6-SP-G8-4	33.41	0	59.29	0.13	6.93	0.02	0.05	0	0	0
		CRB3.15.6-SP-G9-1	33.45	0	58.35	0.13	7.09	0.02	0.03	0	0	0.02
		CRB3.15.6-SP-G9-2	33.18	0.05	58.9	0.09	7.12	0.01	0.03	0	0.01	0.02
		CRB3.15.6-SP-G9-3	33.44	0.04	58.26	0.15	7.09	0	0.04	0	0	0.02
		CRB3.15.6-SP-G9-4	33.45	0.03	58.35	0.11	7.08	0	0.03	0	0	0.02
		CRB3.15.6-SP-G10-1	33.52	0	58.83	0.13	7.06	0	0.01	0	0.01	0
		CRB3.15.6-SP-G10-2	33.71	0	58.67	0.12	7.04	0	0.02	0.01	0.01	0.02
		CRB3.15.6-SP-G10-3	33.44	0	58.86	0.17	6.89	0	0.02	0	0	0
		CRB3.800N-SP-G1-1	33.61	0.04	60.35	0.13	5.34	0.04	0.43	0	0.03	0
		CRB3.800N-SP-G1-2	33.42	0	60.66	0.14	5.41	0	0.43	0	0	0
		CRB3.800N-SP-G1-3	33.3	0.03	60.55	0.14	5.36	0	0.23	0	0	0
		CRB3.800N-SP-G2-1	33.53	0	60.58	0.15	5.31	0.02	0.61	0	0.01	0.02
		CRB3.800N-SP-G2-2	33.46	0	60.15	0.13	5.3	0.03	0.34	0.01	0.02	0
		CRB3.800N-SP-G2-3	33.17	0	60.44	0.14	5.32	0.03	0.17	0	0	0
		CRB3.800N-SP-G2-4	33.45	0	60.2	0.14	5.28	0.01	0.29	0	0	0.02
		CRB3.800N-SP-G3-1	33.83	0	60.8	0.12	5.38	0.02	0.07	0	0	0.01
		CRB3.800N-SP-G3-2	34	0.02	60.83	0.15	5.44	0.04	0.06	0	0	0
		CRB3.800N-SP-G3-3	33.75	0	60.56	0.14	5.34	0.02	0.07	0.01	0	0
		CRB3.800N-SP-G4-1	33.58	0.04	60.39	0.12	5.45	0.01	0.29	0	0	0
		CRB3.800N-SP-G4-2	33.4	0	60.49	0.14	5.51	0	0.22	0.02	0	0
		CRB3.800N-SP-G4-3	33.26	0.03	59.98	0.12	5.7	0.01	0.47	0	0	0
		CRB3.800N-SP-G5-1	33.45	0.02	60.45	0.12	5.54	0.03	0.34	0	0.02	0
		CRB3.800N-SP-G5-2	33.45	0.01	60.29	0.11	5.42	0.01	0.26	0	0.01	0.02
		CRB3.800N-SP-G6-1	33.59	0.04	60.87	0.16	5.46	0.02	0.05	0	0.03	0
		CRB3.800N-SP-G6-2	33.47	0	60.86	0.13	5.43	0.03	0.04	0	0.01	0
		CRB3.800N-SP-G6-3	33.55	0	61.05	0.14	5.42	0.02	0.03	0	0	0
		CRB3.800N-SP-G7-1	33.64	0	60.99	0.14	5.35	0.03	0.05	0	0.01	0
		CRB3.800N-SP-G7-2	33.17	0.02	60.9	0.17	5.21	0.01	0.05	0	0	0
		CRB3.800N-SP-G7-3	33.42	0	60.54	0.14	5.33	0.02	0.05	0.02	0.01	0
		CRB3.800N-SP-G8-1	33.35	0.01	60.8	0.12	5.26	0	0.04	0	0.01	0.01
		CRB3.800N-SP-G8-2	33.47	0.02	60.62	0.13	5.39	0.04	0.03	0	0	0
		CRB3.800N-SP-G8-3	33.41	0.02	60.76	0.15	5.34	0.01	0.03	0	0	0.01
		CRB3.800N-SP-G9-1	33.4	0.02	60.44	0.14	5.39	0.03	0.04	0	0	0
		CRB3.800N-SP-G9-2	33.69	0.01	60.31	0.14	5.31	0.02	0.03	0	0	0.02
		CRB3.800N-SP-G9-3	33.59	0.02	60.69	0.1	5.34	0.04	0.03	0	0	0.01
		CRB3.800N-SP-G10-1	33.86	0.01	60.65	0.11	5.21	0.01	0.06	0	0	0
		CRB3.800N-SP-G10-2	33.56	0	60.59	0.13	5.28	0	0.04	0	0	0.02
		CRB3.800N-SP-G10-3	33.54	0	60.66	0.17	5.16	0.02	0.07	0	0	0
Bedford Hill	Ansill	A95-10A-PY-1	33.07	0.04	62.39	0.16	3.84	0.03	0.14	0	0	0.01
		A95-10A-PY-2	33.09	0	61.8	0.15	4.87	0	0.04	0	0	0
		A95-10A-PY-3	33.08	0.02	62.35	0.11	4.26	0.01	0.13	0	0	0.02
		A95-10A-PY-4	33.12	0	62.48	0.16	4.45	0.02	0.03	0	0.02	0
		A95-10A-PY-6	33.18	0	62.04	0.17	4.58	0.04	0.01	0	0	0
		A95-10A-PY-7	33.07	0	62.2	0.12	4.73	0.01	0.01	0	0.01	0.04
		A95-10A-PY-9	32.97	0	62.3	0.14	4.43	0	0.02	0	0	0.01
		A95-10A-PY-9	33.07	0	62.18	0.16	4.46	0	0.03	0	0	0
		A95-10A-PY-10	33.35	0	62.8	0.12	4.45	0.03	0	0	0.01	0
		ANSL 989-SP-1	33.47	0	59.38	0.19	6.7	0	0.05	0	0.01	0
		ANSL 989-SP-2	33.43	0	58.47	0.18	6.91	0.01	0.07	0	0.01	0
		ANSL 989-SP-3	33.35	0.03	59.81	0.16	6.11	0	0.06	0	0.01	0
		ANSL 989-SP-5	33.54	0.02	58.86	0.17	6.99	0	0.06	0	0.01	0
		ANSL 989-SP-6	33.62	0.01	59.77	0.19	6.59	0.01	0.07	0	0	0
		ANSL 989-SP-7	33.37	0	58.9	0.17	7.27	0.01	0.04	0	0	0
		ANSL 989-SP-8	33.45	0	59.47	0.22	6.97	0	0.06	0	0	0
		ANSL 989-SP-9	33.21	0	59.65	0.15	6.7	0	0.1	0	0	0
		ANSL 989-SP-10	33.5	0	59.35	0.17	6.87	0.01	0.05	0	0	0.03
		ANSL 989-SP-11	33.43	0	60.15	0.2	6.45	0	0.07	0	0	0
		ANSL 989-SP-12	33.72	0	59.79	0.17	6.48	0	0.04	0	0.01	0.02
		ANSL 989-SP-13	33.65	0	59.74	0.19	6.45	0	0.05	0	0	0
		ANSL 989-SP-14	33.5	0.02	59.16	0.17	7	0	0.06	0	0	0
		ANSL 989-SP-15	33.27	0.03	59.33	0.19	6.93	0	0.02	0	0.01	0.01
		ANSL 989-SP-16	33.24	0	59.29	0.2	6.9	0.01	0.05	0	0.01	0.01
		ANSL 989-SP-18	33.36	0	59.04	0.19	7.07	0.01	0.04	0	0	0.02</td

Table A1.3 Sphalerite (cont.)

Stratigraphic position	Deposit	Sample	S (wt%)	As (wt%)	Zn (wt%)	Cd (wt%)	Fe (wt%)	Se (wt%)	Cu (wt%)	Cr (wt%)	Ni (wt%)	Co (wt%)
Cauldron	Ansil	ANSL 98-12-SP-9	33.55	0.04	59.21	0.15	7.07	0	0.09	0	0	0
		ANSL 98-12-SP-10	33.45	0.01	59.1	0.14	7.01	0	0.05	0	0	0.01
		ANSL 98-12-SP-11	33.41	0.01	59.52	0.22	6.83	0	0.06	0	0	0
		ANSL 98-12-SP-12	33.41	0.02	59.37	0.16	7.07	0.01	0.12	0	0	0.03
		ANSL 98-12-SP-13	33.53	0	59.96	0.21	6.46	0.01	0.1	0	0.01	0.03
		ANSL 98-12-SP-14	33.46	0	59.53	0.19	6.84	0	0.05	0	0	0.01
		ANSL 98-12-SP-15	33.17	0.02	59.86	0.16	6.77	0	0.03	0	0.01	0.02
		ANSL 98-12-SP-16	33.6	0.01	59.5	0.18	6.83	0	0.06	0	0.01	0
		ANSL 98-12-SP-17	33.27	0	59.31	0.15	6.85	0	0.08	0	0	0.02
		ANSL 98-12-SP-18	33.2	0.01	59.34	0.19	7.07	0.02	0.04	0	0.01	0.01
		ANSL 98-12-SP-19	33.67	0	59.29	0.17	7.04	0	0.08	0	0.01	0.03
		ANSL 98-12-SP-20	33.37	0.03	59.19	0.16	6.84	0	0.06	0	0	0.03
C Contact Tuff	C.TUFF1 SP-1	33.71	0	60.32	0.13	6.13	0	0.07	0	0.01	0	0
	C.TUFF1 SP-2	33.33	0	60.27	0.14	6.47	0	0.1	0	0.02	0	0
	C.TUFF1 SP-3	33.33	0	59.9	0.14	6.67	0	0.06	0	0.01	0	0
	C.TUFF1 SP-4	33.43	0	59.87	0.16	6.59	0.02	0.03	0.01	0.01	0	0
	C.TUFF1 SP-5	33.35	0	60.09	0.15	6.49	0	0.09	0	0	0	0
	C.TUFF1 SP-6	33.54	0	59.84	0.16	6.51	0.01	0.05	0	0	0	0
	C.TUFF1 SP-7	33.36	0	59.75	0.14	6.7	0.04	0.06	0	0.01	0.01	0.01
	C.TUFF1 SP-8	33.77	0.01	59.79	0.18	6.71	0.01	0.05	0	0	0.01	0
	C.TUFF1 SP-9	33.56	0.03	60.08	0.15	6.29	0	0.09	0	0.01	0	0
	C.TUFF1 SP-10	33.47	0	59.53	0.14	6.75	0	0.08	0	0	0	0
	C.TUFF1 SP-11	33.26	0	59.99	0.11	6.75	0.02	0.07	0.01	0.01	0	0
	C.TUFF1 SP-12	33.21	0	60.21	0.14	6.35	0.01	0.1	0.02	0	0.02	0
	C.TUFF1 SP-13	33.29	0.04	59.48	0.15	6.6	0.02	0.09	0	0.01	0	0
	C.TUFF1 SP-14	33.5	0.06	60.27	0.13	6.17	0	0.07	0.01	0	0.03	0
	C.TUFF1 SP-15	33.53	0	60.08	0.11	6.73	0.02	0.04	0	0	0	0
	C.TUFF1 SP-16	33.38	0	60.28	0.19	6.14	0.02	0.17	0	0.01	0	0
	C.TUFF1 SP-17	33.26	0	59.68	0.15	6.58	0	0.05	0	0	0	0
	C.TUFF1 SP-18	33.29	0	59.66	0.12	6.6	0.02	0.07	0	0	0	0
	C.TUFF1 SP-19	33.31	0.02	59.56	0.17	6.66	0.01	0.06	0	0	0	0
	C.TUFF1 SP-20	33.36	0	60.7	0.16	5.85	0	0.07	0.01	0	0	0
	C.TUFF1 SP-22	33.16	0.02	59.38	0.17	6.8	0.01	0.07	0	0	0	0
	C.TUFF1 SP-23	33.43	0.01	60.09	0.12	6.51	0.01	0.19	0	0.01	0	0
	C.TUFF1 SP-24	33.38	0	59.9	0.17	6.55	0	0.07	0.03	0	0.02	0
	C.TUFF1 SP-25	33.7	0	59.73	0.18	6.71	0.03	0.04	0	0	0	0
	C.TUFF1 SP-26	33.41	0	59.95	0.14	6.54	0	0.05	0	0.01	0.01	0
Moosehead	A95-09A-SP-1	33.6	0.06	58.94	0.12	7.59	0.01	0.05	0	0.01	0.01	0.01
	A95-09A-SP-2	33.7	0.01	58.87	0.13	7.67	0	0.04	0	0	0	0
	A95-09A-SP-3	33.44	0	60.66	0.04	6.31	0.01	0	0	0.02	0	0
	A95-09A-SP-4	33.34	0.06	61.41	0.1	5.16	0	0.06	0	0.03	0	0
	A95-09A-SP-5	33.41	0	58.97	0.1	7.73	0	0.03	0	0.04	0.03	0
	A95-09A-SP-7	33.28	0	61.33	0.1	5.11	0	0.05	0	0.03	0	0
	A95-09A-SP-8	33.32	0	60.44	0.05	6.29	0	0.05	0	0.03	0	0
	A95-09A-SP-9	33.54	0	59.26	0.06	7.37	0	0.06	0	0.02	0	0
	A95-09A-SP-10	33.41	0.04	61.77	0.08	4.76	0	0.06	0	0	0	0
	A95-09A-SP-11	33.52	0	58.82	0.04	7.68	0.01	0.06	0	0	0	0
	A95-09A-SP-12	33.56	0	58.42	0.07	7.39	0	0.08	0	0	0	0
	A95-09A-SP-13	33.55	0	60.79	0	6.23	0	0.03	0	0	0	0
	A95-09A-SP-14	33.48	0	60.71	0.04	6.24	0	0.09	0	0	0.01	0
	A95-09A-SP-15	33.86	0	58.59	0.1	7.68	0.01	0.04	0	0.01	0	0
	A95-09A-SP-16	33.34	0	59.14	0.12	7.35	0	0.07	0	0	0	0
	A95-09A-SP-17	33.27	0	61.65	0.08	4.94	0.01	0.03	0	0	0	0
	A95-09A-SP-18	33.66	0	61.96	0.04	4.9	0	0.07	0	0.02	0	0
	A95-09A-SP-19	33.25	0.01	62.03	0.12	4.9	0.01	0.05	0	0.01	0	0
	A95-09A-SP-20	33.35	0.02	58.46	0.09	7.61	0	0.03	0	0.02	0	0
	A95-09B-SP-1	33.08	0.06	59.49	0.14	6.85	0.01	0.04	0	0	0.02	0
	A95-09B-SP-2	33.59	0	59.37	0.2	7.08	0	0.06	0	0.01	0.02	0
	A95-09B-SP-4	33.16	0	58.76	0.12	7.42	0	0.05	0	0.02	0	0
	A95-09B-SP-5	33.71	0	59.76	0.16	6.65	0	0.03	0	0	0.01	0
	A95-09B-SP-6	33.47	0.01	58.97	0.13	7.22	0.02	0.06	0	0	0	0
	A95-09B-SP-7	33.22	0	60.2	0.17	6.47	0.01	0.05	0	0	0.01	0
	A95-09B-SP-8	33.4	0.01	60.26	0.16	6.42	0	0.03	0	0	0	0
	A95-09B-SP-9	33.53	0.01	60.2	0.17	6.39	0.01	0.06	0	0.01	0.02	0
	A95-09B-SP-10	33.34	0	59.56	0.17	7.02	0.01	0.06	0	0	0	0
	A95-09B-SP-11	33.41	0	59.18	0.11	7.41	0	0.05	0	0	0	0
	A95-09B-SP-12	33.41	0	59.23	0.19	7.46	0	0.07	0	0.01	0.01	0
	A95-09B-SP-13	33.52	0.06	60.08	0.15	6.61	0	0.07	0	0	0	0
	A95-09B-SP-14	33.41	0.01	59.04	0.13	7.18	0	0.07	0	0.01	0	0
	A95-09B-SP-15	35.3	0.02	57.87	0.12	7.21	0	0.1	0	0.01	0.01	0
Amulet F-Shaft	AMLF8601-CP-31	33.54	0.01	59.54	0.16	7.01	0	0.13	0	0	0	0.03
	AMLF8601-CP-32	33.74	0.01	59.79	0.17	6.49	0.02	0.16	0	0.01	0.04	0
	AMLF8601-CP-33	33.35	0.01	59.36	0.16	7.22	0	0.23	0	0	0.05	0
	AMLF8601-CP-34	33.53	0	59.3	0.14	7.07	0.01	0.09	0	0	0.04	0
	AMLF8601-CP-35	33.37	0.03	59.22	0.15	7.03	0.04	0.07	0	0	0.04	0
	A95-07B-SP-1	33.62	0	58.33	0.18	7.69	0	0.09	0	0	0	0
	A95-07B-SP-10	33.46	0.01	58.48	0.19	7.42	0	0.07	0	0	0	0
	A95-07B-SP-11	31.89	0	53.51	0.17	7.42	0	0.06	0	0.01	0	0
	A95-07B-SP-12	33.31	0	58.24	0.18	7.68	0	0.07	0	0.01	0.02	0
	A95-07B-SP-13	33.47	0.06	58.58	0.17	7.58	0	0.11	0	0.01	0	0
	A95-07B-SP-14	33.65	0	58.33	0.16	7.65	0.02	0.07	0	0	0.01	0
	A95-07B-SP-15	33.03	0	57.62	0.18	7.66	0	0.06	0	0	0	0
	A95-07B-SP-2	33.98	0	58.12	0.17	7.76	0	0.06	0	0.01	0	0
	A95-07B-SP-3	33.3	0	58.08	0.14	7.76	0.02	0.09	0	0	0.01	0
	A95-07B-SP-4	33.72	0.01	58.52	0.19	7.56	0	0.07	0	0	0	0
	A95-07B-SP-5	33.64	0	58.65	0.19	7.75	0	0.05	0	0	0	0
	A95-07B-SP-6	33.58	0	58.93	0.21	7.17	0.02	0.06	0	0.01	0	0
	A95-07B-SP-7	33.72	0.01	58.74	0.19	7.6	0	0.08	0	0.01	0	0
	A95-07B-SP-8	33.6	0.06	59.03	0.17	6.92	0.03	0.08	0	0	0	0
	A95-07B-SP-9	33.88	0	58.33	0.18	7.35	0	0.07	0	0	0	0
	A95-07C-PY-1	33.14	0	58.49	0.27	7.7	0	0.5	0	0	0	0
	A95-07C-PY-2	33.05	0	59.27	0.26	7.44	0	0	0	0	0.01	0
	A95-07C-PY-3	33.11	0	58.72	0.25	7.72	0.02	0	0	0	0.01	0
	A95-07E-CP-1	33.3	0.01	59.21	0.35	7.08	0.07	0.19	0	0.01	0.01	0
	A95-07E-CP-2	33.52	0	58.85	0.14	7.4	0.04	0.08	0	0.01	0.03	0

Table A1.3 Sphalerite (cont.)

Stratigraphic position	Deposit	Sample	S (wt%)	As (wt%)	Zn (wt%)	Cd (wt%)	Fe (wt%)	Se (wt%)	Cu (wt%)	Cr (wt%)	Ni (wt%)	Co (wt%)
Cauldron	Amulet C	A95-08A-PY-3	32.92	0	59.86	0.18	6.91	0.07	0.01	0	0	0
		A95-08A-PY-4	33.33	0	59.11	0.21	7.34	0.03	0.02	0	0.01	0
		A95-08A-PY-5	33.19	0.05	59.25	0.21	7.25	0.01	0.07	0	0	0
		A95-08F-CP-1	33.22	0	59.35	0.13	7.11	0.1	0.11	0	0	0.04
Old Waite		A95-18A-SP-1	33.22	0.04	60.18	0.13	6.58	0	0.04	0	0	0
		A95-18A-SP-10	33.25	0.03	60.61	0.13	6.26	0	0.04	0	0	0.01
		A95-18A-SP-2	32.95	0.03	60.42	0.15	6.47	0	0.03	0	0	0.02
		A95-18A-SP-3	33.25	0.06	60.66	0.13	6.3	0.02	0.04	0	0.01	0
		A95-18A-SP-4	33.28	0	60.56	0.13	6.27	0	0.06	0	0.01	0.03
		A95-18A-SP-5	33.41	0.01	60.74	0.11	6.23	0	0.03	0	0	0.01
		A95-18A-SP-6	33.08	0	59.59	0.17	7.29	0.01	0.07	0	0.01	0
		A95-18A-SP-7	33.08	0	60.23	0.12	6.25	0	0.03	0	0	0.01
		A95-18A-SP-8	33.38	0.01	60.57	0.17	6.22	0	0.07	0	0.01	0
		A95-18A-SP-9	33.53	0	60.27	0.17	6.7	0	0.05	0	0	0
East Waite		A95-17A-SP-1	33.33	0	59.29	0.12	7.32	0.01	0.06	0	0.01	0
		A95-17A-SP-10	33.29	0	58.84	0.14	7.52	0.02	0.04	0	0	0.01
		A95-17A-SP-11	33.13	0	59.43	0.17	6.89	0	0.07	0	0	0.02
		A95-17A-SP-12	33.37	0	59.38	0.11	7.42	0	0.11	0	0	0.02
		A95-17A-SP-13	33.15	0	59.38	0.16	7.16	0.02	0.08	0	0.01	0.01
		A95-17A-SP-14	33.45	0.03	59.17	0.14	7.45	0	0.04	0	0	0
		A95-17A-SP-15	33.42	0.02	59.23	0.15	7.43	0	0.07	0	0	0.02
		A95-17A-SP-3	33.32	0	59.6	0.12	7.2	0.01	0.05	0	0	0
		A95-17A-SP-4	33.33	0	59.07	0.16	7.47	0	0.05	0	0	0
		A95-17A-SP-5	33.43	0.05	59.03	0.15	7.49	0	0.07	0	0	0
		A95-17A-SP-6	33.18	0.04	59.1	0.13	7.6	0.02	0.08	0	0.01	0.02
		A95-17A-SP-7	33.25	0	59.83	0.13	6.7	0	0.07	0	0	0.01
		A95-17A-SP-8	33.71	0.01	59.07	0.14	7.57	0.02	0.09	0	0.01	0.03
		A95-17A-SP-9	33.18	0.01	59.45	0.12	7.12	0.01	0.07	0	0	0
		A95-17B-PY-1	33.41	0	60.75	0.15	6.16	0.03	0.14	0	0	0.01
		A95-17B-PY-2	33.03	0	59.02	0.17	7.49	0	0.08	0	0	0
		A95-17B-PY-5	33.29	0	58.98	0.16	7.41	0	0.07	0	0	0
Norbec		JH98-03A-PY-26	33.49	0	57.1	0.2	7.84	0	0.09	0	0.01	0.02
		JH98-03A-PY-27	33.26	0.02	56.45	0.14	8.45	0.01	0.33	0	0	0.02
		JH98-03A-PY-28	33.53	0.03	63.77	0.16	2.95	0	0.09	0	0.02	0.01
		JH98-03A-PY-29	33.8	0.05	57	0.12	8.19	0.01	0.14	0	0	0
		JH98-03A-PY-30	33.68	0	58.04	0.14	8.17	0.03	0.11	0	0	0.03
		JH98-03A-SP-10	32.98	0	57.91	0.16	7.99	0	0.09	0.02	0.02	0.02
		JH98-03A-SP-13	34.38	0.04	56.95	0.15	7.73	0	0.08	0	0.01	0
		JH98-03A-SP-18	34.42	0.01	56.89	0.15	7.63	0.01	0.17	0	0	0.01
		JH98-03A-SP-28	33.08	0	57.43	0.17	7.72	0	0.05	0	0.01	0.03
		JH98-03A-SP-29	33.26	0	58.42	0.15	7.49	0	0.18	0	0.01	0.02
		JH98-03A-SP-3	33.12	0.02	58.03	0.08	7.97	0.02	0.09	0.01	0	0
		JH98-03A-SP-4	33.28	0	58.13	0.12	7.94	0.01	0.08	0	0.01	0.04
		JH98-03A-SP-5	33.43	0	58.09	0.16	7.51	0	0.08	0	0	0.01
		JH98-03A-SP-3	34.11	0	56.87	0.12	8.33	0.02	0.13	0.01	0.01	0.04
Vauze		A95-11F-CP-1	33.44	0.01	59.49	0.18	6.7	0.05	0.43	0	0	0.06
		A95-11F-CP-2	33.71	0	59.4	0.18	6.69	0.08	0.43	0	0	0.08
		A95-11F-CP-3	33.44	0	59.15	0.16	6.83	0.07	0.31	0	0.01	0.08
		A95-11B-SP-1	33.56	0	59.65	0.14	6.85	0.01	0.01	0	0.01	0
		A95-11B-SP-10	33.19	0	60.68	0.12	6.28	0.03	0.06	0	0	0.01
		A95-11B-SP-11	33.49	0	59.39	0.09	6.88	0.04	0.02	0	0.01	0
		A95-11B-SP-12	32.74	0.01	59.85	0.15	6.55	0.01	0.11	0	0	0.04
		A95-11B-SP-13	33.43	0.03	59.43	0.12	6.8	0.03	0.06	0	0.02	0.07
		A95-11B-SP-14	33.52	0.03	58.51	0.17	7.26	0.03	0.04	0	0.01	0
		A95-11B-SP-15	33.65	0	59.42	0.11	6.4	0	0.04	0	0.01	0.01
		A95-11B-SP-2	33.36	0	59.7	0.14	6.82	0.04	0.02	0	0.01	0
		A95-11B-SP-3	33.36	0.02	59.42	0.11	6.36	0	0.05	0	0	0.01
		A95-11B-SP-4	33.58	0.06	59.1	0.14	7.03	0.02	0.05	0	0	0.01
		A95-11B-SP-5	33.03	0.05	59.63	0.13	6.73	0.04	0.03	0	0.01	0.01
		A95-11B-SP-6	33.43	0.06	59.7	0.11	6.75	0.05	0.03	0	0	0
		A95-11B-SP-7	33.41	0	58.59	0.14	7.33	0.04	0.03	0	0.01	0.01
		A95-11B-SP-8	33.26	0.03	59.75	0.12	6.48	0.01	0.05	0	0.01	0.01
		A95-11B-SP-9	33.23	0	60.22	0.14	6.23	0.03	0.06	0	0	0.01
		A95-11F-PO-1	33.54	0	58.52	0.14	7.19	0.02	0.41	0	0	0.13
		A95-11F-PO-10	33.7	0.01	59.22	0.2	7.21	0	0.2	0	0	0.11
		A95-11F-PO-2	33.42	0.03	58.67	0.13	7.07	0.02	0.23	0	0.01	0.09
		A95-11F-PO-3	33.25	0	59.46	0.16	6.71	0.01	0.3	0	0	0.08
		A95-11F-PO-4	33.49	0.01	58.95	0.14	7.1	0.05	0.27	0	0	0.05
		A95-11F-PO-5	33.26	0	59.52	0.17	6.6	0.08	0.39	0	0	0.06
		A95-11F-PO-6	33.5	0.01	58.95	0.17	7.35	0.04	0.32	0	0	0.11
		A95-11F-PO-7	33.3	0.04	59.7	0.18	6.78	0.06	0.44	0	0	0.06
		A95-11F-PO-8	33.04	0	59.23	0.14	7.01	0.08	0.28	0	0.01	0.06
		A95-11F-PO-9	33.19	0	59.41	0.18	6.99	0.06	0.34	0	0	0.06
Quemont		QT4-2-SP-11	33.31	0.02	62.54	0.22	3.21	0.05	0.04	0	0.01	0
		QT4-2-SP-12	33.08	0	63.13	0.25	3.24	0.06	0.16	0	0	0
		QT4-2-SP-13	33.27	0	62.66	0.21	3.26	0.05	0.11	0	0	0
		QT4-2-SP-14	33.28	0	62.89	0.21	3.23	0.07	0.09	0	0	0
		QT4-2-SP-15	33.39	0.03	63	0.19	3.33	0.02	0.03	0	0	0
		QT4-2-SP-16	33.17	0	63.1	0.23	3.4	0.02	0.06	0	0	0.01
		QT4-2-SP-17	33.6	0	63.47	0.2	3.33	0.06	0.08	0	0	0
		QT4-2-SP-18	33.75	0	62.82	0.21	3.17	0.02	0.09	0	0.01	0.01
		QT4-2-SP-19	33.54	0.08	63.72	0.14	3.1	0.07	0.05	0	0	0.01
		QT4-2-SP-2	33.09	0.01	62.54	0.21	3.29	0.02	0.21	0	0	0
		QT4-2-SP-20	33.41	0	63.32	0.18	3.31	0.05	0.05	0	0	0
		QT4-2-SP-21	33.47	0	63.39	0.26	3.31	0.05	0.11	0	0.01	0
		QT4-2-SP-22	33.4	0.05	63.81	0.17	2.83	0.08	0.25	0	0	0.01
		QT4-2-SP-23	33.04	0	63.47	0.2	3.31	0.04	0.07	0	0	0.01
		QT4-2-SP-24	33.17	0	63.05	0.22	3.33	0.05	0.05	0	0	0
		QT4-2-SP-25	33.25	0	63.18	0.23	3.29	0.05	0.01	0	0	0
		QT4-2-SP-26	33.53	0.01	63.78	0.2	3.15	0.04	0.07	0	0.01	0.01
		QT4-2-SP-28	33.94	0.06	62.77	0.21	3.28	0.05	0.09	0	0	0
		QT4-2-SP-29	33.12	0.02	63.09	0.19	3.34	0.08	0.07	0	0.01	0.01
		QT4-2-SP-30	33.15	0.03	63.06	0.2	3.22	0.01	0.02	0	0	0
		QT4-2-SP-4	33.16	0.02	63.15	0.22	3.12	0.04	0.12	0	0.01	0.01
		QT4-2-SP-5	33.49	0	62.66	0.19	3.34	0.06	0.09	0.01	0.01	0
		QT4-2-SP-6	33	0	62.61	0.2	3.43	0.04	0.51	0	0	0
		QT4-2-SP-7	33.19	0	63.02	0.25	3.27	0.04	0.06	0	0.01	0
		QT4-2-SP-8	33.77	0	62.45	0.17	3.21	0.05	0.72	0	0	0
		QT4-2-SP-9	33.64	0	63							

Table A1.3 Sphalerite (cont.)

Stratigraphic position	Deposit	Sample	S (wt%)	As (wt%)	Zn (wt%)	Cd (wt%)	Fe (wt%)	Se (wt%)	Cu (wt%)	Cr (wt%)	Ni (wt%)	Co (wt%)
Cauldron	Quemont	QT17-5 SP(CP2)-4	34.23	0.02	58.25	0.32	6.34	0	0.12	0	0	0.01
		QT17-5 SP(CP2)-5	33.51	0.02	59.6	0.17	5.62	0.05	0.17	0	0	0
		QT17-5 SP(CP2)-7	33.64	0.01	59.25	0.29	6.27	0.03	0.3	0	0	0
		QT17-5 SP(CP2)-8	33.27	0.02	59.28	0.31	6.42	0	0.32	0	0	0.02
		QT17-5 SP(CP2)-9	33.65	0	59.8	0.37	6.62	0	0.12	0	0	0.01
		QT18-1 SP(GN)-1	33.58	0	59.47	0.14	5.76	0.01	0.05	0	0	0
		QT18-1 SP(GN)-10	33.66	0.03	57.73	0.2	8.16	0	0.09	0	0.01	0
		QT18-1 SP(GN)-11	33.45	0.06	61.01	0.17	5.75	0	0.11	0	0	0
		QT18-1 SP(GN)-12	33.53	0.02	58.45	0.72	6.91	0	0.15	0	0.01	0.02
		QT18-1 SP(GN)-13	33.53	0	60.41	0.49	5.01	0	0.15	0	0.01	0
		QT18-1 SP(GN)-14	33.57	0	60.69	0.19	5.99	0.02	0.15	0	0	0
		QT18-1 SP(GN)-15	33.37	0	60.73	0.17	6.06	0	0.09	0	0	0
		QT18-1 SP(GN)-16	33.36	0.01	60.21	0.19	6.53	0.01	0.1	0	0	0
		QT18-1 SP(GN)-17	33.46	0	59.46	0.17	7.09	0	0.07	0	0	0
		QT18-1 SP(GN)-18	33.61	0	59.66	0.22	6.82	0.01	0.05	0	0	0
		QT18-1 SP(GN)-19	33.49	0	60.54	0.17	5.9	0	0.17	0	0.01	0
		QT18-1 SP(GN)-20	33.42	0.07	59.39	0.18	6.86	0.01	0.06	0	0	0
		QT18-1 SP(GN)-3	33.08	0	60.62	0.18	5.98	0.01	0.1	0	0	0
		QT18-1 SP(GN)-4	33.34	0	60.67	0.59	5.34	0	0.14	0	0	0.01
		QT18-1 SP(GN)-6	33.3	0	59.07	0.14	7.22	0	0.08	0	0	0
		QT18-1 SP(GN)-7	33.55	0	60.67	0.17	6.13	0.01	0.1	0	0.01	0
		QT18-1 SP(GN)-8	33.56	0.01	59.02	0.32	7.61	0.01	0.13	0	0	0
		QT18-1 SP(GN)-9	33.44	0	61.23	0.18	5.64	0.02	0.07	0	0.01	0
		QT7-7 SP(PO)-1	33.1	0	60.34	0.19	6.17	0.04	0.07	0	0.02	0.01
		QT7-7 SP(PO)-10	32.95	0	59.87	0.21	6.26	0.05	0.54	0	0.02	0
		QT7-7 SP(PO)-11	32.95	0	60.53	0.24	5.9	0.05	0.1	0	0.01	0
		QT7-7 SP(PO)-12	32.9	0	60.68	0.19	5.98	0.04	0.1	0	0	0
		QT7-7 SP(PO)-13	33.13	0.02	60.43	0.21	6.39	0.02	0.03	0	0	0
		QT7-7 SP(PO)-14	33.01	0.02	60.43	0.22	6.45	0.08	0.1	0.01	0	0
		QT7-7 SP(PO)-15	32.93	0	60.94	0.19	5.96	0.03	0.06	0	0	0
		QT7-7 SP(PO)-16	33.24	0	60.22	0.22	6.47	0.03	0.03	0	0	0
		QT7-7 SP(PO)-17	33.04	0	59.87	0.21	6.56	0.02	0.07	0	0	0
		QT7-7 SP(PO)-18	33.94	0	59.53	0.22	6.16	0.03	0.15	0.01	0	0
		QT7-7 SP(PO)-19	32.92	0	59.91	0.21	6.28	0.03	0.14	0	0	0
		QT7-7 SP(PO)-2	33	0	60.62	0.17	6.05	0.03	0.07	0	0	0
		QT7-7 SP(PO)-20	32.75	0	59.54	0.23	5.87	0	0.09	0	0	0
		QT7-7 SP(PO)-21	33.04	0.01	60.69	0.23	6.04	0.04	0.05	0	0	0
		QT7-7 SP(PO)-22	32.88	0	59.88	0.21	6.49	0.04	0.18	0	0	0
		QT7-7 SP(PO)-23	32.96	0	60.25	0.23	6.45	0.06	0.07	0.01	0.01	0
		QT7-7 SP(PO)-24	32.89	0.03	59.92	0.22	6.34	0.05	0.06	0	0.01	0
		QT7-7 SP(PO)-25	33.27	0.03	59.39	0.18	6.47	0.07	0.06	0	0.01	0
		QT7-7 SP(PO)-26	33.06	0.03	60.22	0.19	6.11	0.03	0	0	0.01	0
		QT7-7 SP(PO)-27	32.98	0.04	61.01	0.2	5.56	0.04	0.07	0	0.01	0
		QT7-7 SP(PO)-28	33.17	0	59.89	0.2	6.1	0.04	0.07	0	0.01	0
		QT7-7 SP(PO)-3	32.96	0.03	60.66	0.21	6.1	0.05	0.05	0	0.01	0
		QT7-7 SP(PO)-4	32.97	0.04	59.41	0.21	6.52	0.05	0.06	0	0.01	0.01
		QT7-7 SP(PO)-5	32.9	0.03	60.73	0.16	5.93	0.03	0.03	0	0	0
		QT7-7 SP(PO)-6	32.97	0.01	60.31	0.14	6.15	0.03	0.07	0	0.01	0
		QT7-7 SP(PO)-7	33.04	0.03	60.84	0.21	5.49	0.07	0.11	0	0	0
		QT7-7 SP(PO)-8	32.95	0.06	60.28	0.2	6.26	0.04	0.06	0	0.01	0
		QT7-7 SP(PO)-9	33.11	0	60.49	0.2	5.94	0.04	0.03	0	0	0
		QT8-6 CP-1	33.27	0	59.82	0.23	6.01	0.03	0.27	0	0	0
		QT9-4 PY(SP)-1	33.04	0	60.81	0.19	5.29	0.01	0.68	0	0	0.02
		QT7-7 SP-1	33.38	0.04	59.6	0.22	6.45	0.01	0.02	0	0	0
		QT7-7 SP-10	33.46	0	59.81	0.22	6.5	0.04	0.02	0	0.01	0
		QT7-7 SP-11	33.32	0.04	59.67	0.18	6.36	0	0	0	0	0.01
		QT7-7 SP-12	33.47	0	59.63	0.2	6.49	0.04	0.03	0	0	0
		QT7-7 SP-14	33.54	0.02	59.95	0.23	6.31	0.04	0.06	0	0.01	0
		QT7-7 SP-2	33.25	0.05	59.5	0.21	6.53	0.04	0.03	0	0	0
		QT7-7 SP-3	33.53	0	59.67	0.16	6.79	0.04	0.02	0	0	0
		QT7-7 SP-4	33.44	0	59.81	0.21	6.3	0.04	0.02	0	0.01	0.03
		QT7-7 SP-5	33.51	0	59.61	0.22	6.44	0.06	0.03	0	0.01	0
		QT7-7 SP-6	33.36	0	60.23	0.22	6.02	0.05	0	0	0	0
		QT7-7 SP-7	33.44	0.01	59.84	0.24	6.76	0.03	0.05	0	0	0
		QT7-7 SP-8	33.36	0	59.57	0.24	6.23	0.06	0.01	0	0	0.01
		QT7-7 SP-9	33.36	0.04	60.3	0.18	6.19	0.03	0.08	0	0	0.01
		QT15-4 SP-1	33.54	0.09	59.26	0.23	6.94	0.05	0.02	0	0	0
		QT15-4 SP-10	33.33	0	59.34	0.19	7.04	0.05	0.02	0	0.02	0
		QT15-4 SP-11	33.44	0.04	58.67	0.19	7.26	0.02	0.02	0	0	0
		QT15-4 SP-12	33.33	0	59.69	0.2	7.03	0.02	0.02	0	0	0
		QT15-4 SP-13	33.36	0	59.94	0.2	6.71	0.03	0.02	0	0	0
		QT15-4 SP-14	33.57	0.01	59.96	0.15	6.88	0.03	0.02	0	0.01	0
		QT15-4 SP-15	33.61	0	61.01	0.16	5.62	0.02	0	0	0	0
		QT15-4 SP-2	33.63	0.01	58.95	0.2	6.98	0.02	0	0	0.02	0
		QT15-4 SP-3	33.48	0.03	59.57	0.21	6.93	0.07	0.04	0	0	0
		QT15-4 SP-4	33.45	0	59.06	0.21	7.22	0.03	0.01	0	0	0
		QT15-4 SP-5	33.39	0	59.39	0.19	7.14	0.06	0.04	0	0	0
		QT15-4 SP-6	33.49	0	59.26	0.17	7.28	0.03	0.01	0	0	0
		QT15-4 SP-7	33.37	0	59.43	0.21	6.79	0.02	0.03	0	0	0.01
		QT15-4 SP-8	33.57	0	58.96	0.2	7.28	0.05	0.02	0	0.02	0.03
		QT15-4 SP-9	33.51	0	59.46	0.18	7.19	0.01	0.02	0	0	0
		QT7-7 PO(SP)-1	33.39	0	59.95	0.17	6.42	0.01	0.09	0	0.01	0
		QT7-7 PO(SP)-2	33.24	0	60.74	0.19	5.99	0.06	0.2	0	0.02	0
		QT7-7 PO(SP)-3	33.51	0.04	59.85	0.19	6.57	0.03	0.26	0	0.01	0
		QT7-7 PO(SP)-4	33.24	0	54.43	0.21	8.67	0.06	3.95	0	0	0.01
		QT7-7 PO(SP)-5	33.59	0	59.83	0.21	6.51	0.03	0.13	0	0	0
		QT7-7 PO(SP)-6	33.3	0	60.34	0.17	6.25	0.04	0.09	0	0	0
		QT7-7 PO(SP)-7	33.33	0	60.34	0.21	6.28	0.05	0.12	0	0	0
		QT7-7 PO(SP)-8	33.48	0	60.06	0.18	6.44	0.03	0.23	0	0	0
		QT17-5 PO(MT)-1	33.47	0	58.95	0.38	7.27	0	0.1	0	0	0
		QT17-5 PO(MT)-3	33.61	0	59.19	0.35	7.08	0	0.12	0	0	0
Post cauldron	Deldona	DEL-D339-999 SP-1	32.87	0	64.44	0.17	2.05	0.01	0.01	0	0.01	0
		DEL-D339-999 SP-13	32.45	0	64.53	0.1	2.08	0.03	0.05	0	0	0
		DEL										

Table A1.3 Sphalerite (cont.)

Stratigraphic position	Deposit	Sample	S (wt%)	As (wt%)	Zn (wt%)	Cd (wt%)	Fe (wt%)	Se (wt%)	Cu (wt%)	Cr (wt%)	Ni (wt%)	Co (wt%)
Post cauldron	Deldona	DELDF-339-987 SP-2	33.04	0	64.11	0.14	2.09	0.04	0.11	0	0.01	0.01
		DELDF-339-987 SP-20	32.86	0	64.37	0.15	2.02	0.02	0.1	0	0	0
		DELDF-339-987 SP-21	32.86	0.03	64.29	0.11	2.1	0.03	0.05	0	0	0.02
		DELDF-339-987 SP-22	32.76	0.01	64.1	0.17	2.09	0.03	0.01	0	0	0.02
		DELDF-339-987 SP-23	33.02	0	64.13	0.12	2.07	0	0.03	0	0.02	0
		DELDF-339-987 SP-24	32.67	0	64.41	0.15	2.1	0.03	0.03	0	0.01	0
		DELDF-339-987 SP-26	32.9	0.01	64.21	0.14	2.12	0.03	0.07	0	0	0.01
		DELDF-339-987 SP-27	33.33	0	64.07	0.11	2.09	0.03	0.07	0	0	0.02
		DELDF-339-987 SP-3	32.91	0.01	62.05	0.1	3.13	0.01	1.47	0	0	0
		DELDF-339-987 SP-30	32.87	0.01	64.45	0.11	2.07	0	0.01	0.01	0	0.01
Deldona	Deldona	DELDF-339-987 SP-4	32.79	0.01	64.15	0.14	2.01	0	0.06	0	0	0.01
		DELDF-339-987 SP-5	32.87	0.03	64.2	0.14	2.04	0.01	0.07	0	0	0.01
		DELDF-339-987 SP-6	32.43	0.04	64.38	0.14	2.09	0.03	0.07	0	0	0
		DELDF-339-987 SP-7	32.49	0	64.56	0.12	2.14	0.02	0.06	0	0	0.01
		DELDF-339-987 SP-8	32.96	0.01	64.3	0.14	2.03	0.01	0.01	0	0	0
		DELDF-339-987 SP-9	32.83	0.05	64.11	0.11	2.08	0.01	0.06	0	0	0.01
		DELDF-339-986 SP-1	32.91	0	64.31	0.13	2.12	0.01	0.04	0	0.01	0
		DELDF-339-986 SP-10	32.7	0	64.79	0.13	2.16	0.03	0.05	0	0	0.01
		DELDF-339-986 SP-11	32.64	0.01	64.26	0.15	2.42	0	0.04	0	0	0.01
		DELDF-339-986 SP-12	32.79	0	64.95	0.17	2.15	0	0.05	0	0.01	0
		DELDF-339-986 SP-13	32.62	0.08	64.93	0.14	2.12	0.01	0.04	0	0	0
		DELDF-339-986 SP-14	32.82	0	64.83	0.12	1.86	0.02	0.09	0	0	0
		DELDF-339-986 SP-15	32.61	0.03	64.55	0.15	2.15	0.02	0.06	0.01	0	0.01
		DELDF-339-986 SP-16	32.76	0	64.46	0.12	2.17	0	0.08	0	0	0
		DELDF-339-986 SP-17	32.79	0	64.42	0.09	2.26	0	0.29	0	0	0
		DELDF-339-986 SP-18	32.32	0.03	64.98	0.12	2.24	0	0.03	0	0.02	0
		DELDF-339-986 SP-19	32.7	0.09	64.28	0.11	2.08	0	0.07	0	0	0
		DELDF-339-986 SP-2	32.64	0	64.46	0.16	2.06	0.01	0.05	0	0	0
		DELDF-339-986 SP-20	32.77	0	64.81	0.16	2.14	0.02	0.03	0	0	0
		DELDF-339-986 SP-21	32.54	0	64.97	0.14	2.13	0.01	0.03	0	0.01	0
		DELDF-339-986 SP-22	32.83	0	64.68	0.11	2.17	0.01	0.04	0	0	0.03
		DELDF-339-986 SP-23	32.73	0	64.76	0.15	2.13	0	0.09	0	0	0
		DELDF-339-986 SP-24	32.86	0	65.06	0.16	2.25	0	0.06	0	0	0
		DELDF-339-986 SP-25	32.76	0	64.68	0.13	2.24	0	0.24	0	0.01	0
		DELDF-339-986 SP-26	33.09	0	64.98	0.12	2.33	0.01	0.04	0.01	0	0
		DELDF-339-986 SP-27	32.77	0.02	64.65	0.13	2.23	0.02	0.04	0	0	0.01
		DELDF-339-986 SP-28	32.7	0	64.2	0.12	2.14	0.03	0.05	0	0	0
		DELDF-339-986 SP-29	32.67	0	64.82	0.11	2.11	0	0.03	0	0	0
		DELDF-339-986 SP-3	32.73	0	64.83	0.1	2.08	0	0.03	0	0	0.02
		DELDF-339-986 SP-30	32.86	0	64.86	0.14	2.14	0.02	0.07	0	0.01	0
		DELDF-339-986 SP-4	32.84	0	64.87	0.13	2.17	0	0.04	0	0	0
		DELDF-339-986 SP-5	32.72	0	65.03	0.1	1.95	0	0.06	0	0	0
		DELDF-339-986 SP-6	32.77	0.04	64.95	0.09	2.22	0	0.12	0	0.01	0.01
		DELDF-339-986 SP-7	32.7	0.03	64.9	0.15	2.2	0.05	0.06	0	0	0.01
		DELDF-339-986 SP-8	32.85	0	64.54	0.14	2.18	0	0.05	0	0.01	0
		DELDF-339-986 SP-9	32.79	0.04	64.97	0.11	2.1	0.01	0.03	0	0	0.01
		DELDF-339-985 SP-1	32.73	0	63.95	0.18	2.1	0.03	0.03	0	0	0
		DELDF-339-985 SP-10	32.89	0	64.78	0.14	2.1	0.03	0.03	0	0.01	0.01
		DELDF-339-985 SP-11	32.72	0.02	64.51	0.17	2.15	0.01	0.05	0	0	0
		DELDF-339-985 SP-12	32.77	0.03	64.6	0.15	2.16	0.02	0.07	0	0	0
		DELDF-339-985 SP-13	32.66	0.01	64.32	0.17	2.13	0	0.06	0	0	0
		DELDF-339-985 SP-14	32.64	0	64.94	0.14	2.17	0.04	0.05	0	0.01	0.03
		DELDF-339-985 SP-15	32.88	0	64.53	0.14	2.17	0.03	0.04	0	0.01	0.01
		DELDF-339-985 SP-16	32.66	0	64.35	0.15	2.13	0.05	0.04	0	0.01	0.01
		DELDF-339-985 SP-17	32.76	0.01	64.7	0.18	2.14	0	0.07	0	0	0.02
		DELDF-339-985 SP-18	32.94	0.02	64.7	0.18	2.16	0.04	0.05	0	0	0
		DELDF-339-985 SP-19	32.79	0	64.61	0.18	2.1	0.01	0.07	0	0	0
		DELDF-339-985 SP-2	32.69	0	64.76	0.13	2.12	0.04	0.06	0	0	0.02
		DELDF-339-985 SP-20	32.89	0	64.5	0.16	2.11	0.03	0.07	0	0	0.03
		DELDF-339-985 SP-21	32.68	0	64.17	0.16	2.11	0.05	0.09	0	0	0
		DELDF-339-985 SP-22	32.64	0	64.59	0.12	2.11	0.03	0.06	0	0.01	0.02
		DELDF-339-985 SP-23	32.86	0	64.54	0.15	2.13	0.01	0.07	0.01	0	0.02
		DELDF-339-985 SP-24	32.79	0	64.36	0.16	2.13	0.04	0.07	0	0	0.01
		DELDF-339-985 SP-25	32.87	0	64.42	0.17	2.24	0.02	0.13	0	0	0.01
		DELDF-339-985 SP-26	32.89	0	64.5	0.17	2.12	0.01	0.07	0	0	0
		DELDF-339-985 SP-27	32.7	0.12	64.39	0.11	2.13	0.01	0.04	0	0	0.02
		DELDF-339-985 SP-28	32.67	0.05	64.63	0.17	2.17	0.03	0.06	0	0.01	0.02
		DELDF-339-985 SP-29	32.66	0	63.73	0.17	2.11	0.01	0.08	0	0	0
		DELDF-339-985 SP-3	32.56	0	64.71	0.13	2.17	0.01	0.06	0	0	0
		DELDF-339-985 SP-30	32.77	0	64.53	0.15	2.13	0.03	0.08	0	0.01	0.01
		DELDF-339-985 SP-4	32.42	0.09	64.94	0.14	2.13	0.01	0.02	0	0	0.01
		DELDF-339-985 SP-5	32.66	0	64.69	0.15	2.22	0.04	0.07	0	0.01	0.01
		DELDF-339-985 SP-6	32.59	0	64.37	0.15	2.15	0	0.04	0	0	0.02
		DELDF-339-985 SP-8	32.74	0.02	64.5	0.15	2.14	0.03	0.06	0	0	0.03
		DELDF-339-985 SP-9	32.91	0.04	64.68	0.15	2.25	0	0.08	0	0	0
		DELDF-339-1004 PY-1	33.37	0	64.68	0.06	1.85	0	0.07	0	0.01	0
		DELDF-339-1004 PY-2	33.26	0.03	64.99	0.12	1.84	0	0.05	0	0.01	0.02
		DELDF-339-985 PY/GN-1	33.17	0	63.41	0.15	2.65	0	0.07	0	0.01	0
		DELDF-339-987 GN/SP-10	33.14	0	64.11	0.1	2.25	0.02	0.08	0	0	0.02
		DELDF-339-987 GN/SP-13	33.1	0	63.86	0.12	2.07	0.02	0.05	0	0.01	0
		DELDF-339-987 GN/SP-14	33.19	0.03	64.26	0.1	2.18	0.03	0.1	0	0	0.01
		DELDF-339-987 GN/SP-15	33.6	0	64.16	0.14	2.2	0	0.06	0	0.01	0.01
		DELDF-339-987 GN/SP-2	33.15	0.03	63.65	0.13	2.28	0	0.28	0	0	0
		DELDF-339-987 GN/SP-3	33.64	0.06	63.91	0.06	2.17	0	0.06	0	0	0
		DELDF-339-987 GN/SP-4	33.33	0.02	63.85	0.13	2.12	0.03	0.09	0	0	0.01
		DELDF-339-987 GN/SP-5	32.89	0.04	61.09	0.1	3.41	0.01	2.06	0	0.01	0.01
		DELDF-339-987 GN/SP-6	33.09	0.06	64.02	0.13	1.97	0.01	0.09	0	0.01	0
		DELDF-339-987 GN/SP-7	33.09	0	63.82	0.12	2.33	0	0.07	0	0.01	0.01
		DELDF-339-987 GN/SP-9	33	0	59.01	0.1	4.16	0.04	2.95	0	0	0
Delbridge												

Table A1.3 Sphalerite (cont.)

Stratigraphic position	Deposit	Sample	S (wt%)	As (wt%)	Zn (wt%)	Cd (wt%)	Fe (wt%)	Se (wt%)	Cu (wt%)	Cr (wt%)	Ni (wt%)	Co (wt%)
Post cauldron	Delbridge	98DEB-2-1 PO(SP)-16	33.14	0.06	64.54	0.12	2.39	0.01	0.11	0	0.01	0
		98DEB-2-1 PO(SP)-17	33.06	0.03	64.35	0.12	2.54	0.01	0.09	0	0	0.01
		98DEB-2-1 PO(SP)-18	33.06	0	63.73	0.1	2.74	0	0.05	0	0.01	0
		98DEB-2-1 PO(SP)-19	33.1	0	63.75	0.13	2.85	0.03	0.16	0	0	0.02
		98DEB-2-1 PO(SP)-2	33.01	0	63.62	0.11	2.77	0	0.21	0	0.01	0.01
		98DEB-2-1 PO(SP)-20	33.22	0	64.06	0.11	2.39	0.04	0.13	0	0.01	0
		98DEB-2-1 PO(SP)-4	33.09	0.01	63.97	0.14	2.47	0.01	0.2	0	0	0
		98DEB-2-1 PO(SP)-5	33.13	0.05	63.68	0.12	2.76	0.02	0.3	0	0.01	0.01
		98DEB-2-1 PO(SP)-6	33.11	0	64.92	0.15	2	0.02	0.11	0	0	0
		98DEB-2-1 PO(SP)-7	32.86	0	64.02	0.12	2.36	0	0.13	0	0	0
		98DEB-2-1 PO(SP)-8	32.97	0	63.32	0.14	2.52	0.02	0.19	0	0	0.01
		98DEB-2-1 PO(SP)-9	33	0	63.34	0.14	2.5	0.04	0.11	0	0	0
		98DEB-4 SP-1	32.87	0	64.31	0.16	1.93	0	0.06	0	0	0
		98DEB-4 SP-10	32.97	0.01	64.96	0.15	1.78	0	0.08	0	0	0.01
		98DEB-4 SP-11	33.15	0.01	64.75	0.14	1.91	0.03	0.05	0	0	0.01
		98DEB-4 SP-12	32.96	0	64.85	0.12	1.81	0	0.05	0	0	0
		98DEB-4 SP-2	32.87	0	64.61	0.12	1.7	0.03	0.05	0	0	0
		98DEB-4 SP-3	32.82	0	64.77	0.1	1.67	0	0.07	0	0	0
		98DEB-4 SP-4	33.09	0	64.7	0.1	1.75	0.02	0.03	0	0	0
		98DEB-4 SP-5	33.14	0	64.16	0.14	1.94	0	0.04	0	0	0
		98DEB-4 SP-6	32.75	0.01	64.37	0.13	1.94	0.02	0.06	0	0	0
		98DEB-4 SP-7	33.2	0	63.95	0.13	1.82	0.04	0.06	0	0	0
		98DEB-4 SP-8	32.87	0	64.82	0.14	1.73	0.01	0.05	0	0	0
		98DEB-4 SP-9	33.02	0	64.67	0.12	1.86	0.01	0.07	0	0	0
		98DEB-4 PY-1	32.78	0.02	63.92	0.09	2.52	0	0.03	0	0.01	0
		98DEB-4 PY-11	32.71	0.08	64.24	0.12	2.03	0	0.07	0	0	0.01
		98DEB-4 PY-12	32.73	0	63.7	0.12	2.95	0	0.06	0	0.01	0
		98DEB-4 PY-13	32.92	0	63.9	0.12	2.51	0.01	0.07	0	0.01	0
		98DEB-4 PY-14	32.96	0	64.32	0.1	2.03	0	0.03	0	0	0.01
		98DEB-4 PY-16	32.62	0.04	64.03	0.15	2.54	0	0.07	0	0.01	0
		98DEB-4 PY-17	32.98	0.04	64.81	0.12	2.14	0	0.03	0	0.01	0
		98DEB-4 PY-19	32.97	0	64.75	0.13	1.95	0.02	0.04	0	0	0.01
		98DEB-4 PY-2	32.91	0.06	65.2	0.11	2.18	0.02	0.06	0	0	0
		98DEB-4 PY-20	33.01	0	64.86	0.12	2.2	0	0.04	0	0	0
		98DEB-4 PY-3	32.73	0	64.09	0.12	2.15	0.02	0.04	0	0	0
		98DEB-4 PY-4	32.74	0	64.86	0.11	2.17	0	0.05	0	0	0
		98DEB-4 PY-5	32.58	0	64.51	0.15	2.45	0	0.05	0	0	0
		98DEB-4 PY-6	32.85	0	64.83	0.15	2.07	0.01	0.06	0	0	0
		98DEB-4 PY-7	33.12	0	64.7	0.12	1.94	0.02	0.07	0	0	0
		98DEB-4 PY-8	32.83	0	64.81	0.15	2.16	0.01	0.04	0	0	0.01
		98DEB-4 PY-9	32.94	0	64.26	0.08	2.15	0.01	0.05	0	0	0
		98DEB-6 PY(GN)-1	33.21	0.06	63.19	0.13	2.38	0	0.59	0	0	0
		98DEB-6 PY(GN)-2	33.01	0.01	64.99	0.08	1.64	0	0.09	0	0	0
Gallen	JH98GLLN-2MS1	JH98GLLN-2MS1 SP-1	33.07	0	62.62	0.24	3.8	0	0.02	0	0	0
		JH98GLLN-2MS1 SP-2	33.25	0.04	61.94	0.22	4.2	0	0.08	0	0	0
		JH98GLLN-2MS1 SP-3	33.18	0	62.77	0.19	3.69	0.04	0.04	0	0	0
		JH98GLLN-2MS1 SP-4	33.03	0	62.21	0.22	3.76	0	0.06	0	0	0
		JH98GLLN-2MS1 SP-5	33.05	0	62.51	0.2	3.7	0	0.06	0	0	0
		JH98GLLN-2MS1 SP-6	33.25	0	61.87	0.23	3.68	0	0.08	0	0	0
		JH98GLLN-2MS1 SP-8	33.26	0.08	62.66	0.21	3.54	0	0.09	0	0	0
		JH98GLLN-2MS1-1 SP-1	33.31	0.03	62.66	0.19	3.91	0	0.04	0	0.01	0
		JH98GLLN-2MS1-1 SP-10	33.07	0	62.81	0.22	3.9	0.02	0.05	0	0.03	0
		JH98GLLN-2MS1-1 SP-11	33.22	0	62.7	0.21	4.07	0	0.04	0	0.03	0
		JH98GLLN-2MS1-1 SP-12	33.22	0.01	62.68	0.22	3.88	0	0.06	0	0.02	0.03
		JH98GLLN-2MS1-1 SP-13	33.6	0	62.44	0.19	3.81	0	0.07	0	0.02	0.01
		JH98GLLN-2MS1-1 SP-14	33.3	0	62.39	0.19	3.56	0.03	0.03	0	0.03	0
		JH98GLLN-2MS1-1 SP-15	33.45	0	62.42	0.24	3.83	0	0.04	0	0.04	0
		JH98GLLN-2MS1-1 SP-17	33.35	0	61.82	0.21	3.83	0.01	0.04	0	0.01	0.01
		JH98GLLN-2MS1-1 SP-18	33.22	0.04	62.22	0.27	3.72	0	0.05	0	0.01	0.01
		JH98GLLN-2MS1-1 SP-19	33.18	0	62.45	0.25	3.65	0	0.07	0	0	0.01
		JH98GLLN-2MS1-1 SP-2	33.56	0	62.82	0.25	3.74	0.01	0.03	0	0.03	0.01
		JH98GLLN-2MS1-1 SP-20	33.02	0	62.68	0.21	3.64	0	0.04	0	0	0.02
		JH98GLLN-2MS1-1 SP-3	33.18	0.03	62.83	0.19	3.71	0	0.04	0	0.01	0
		JH98GLLN-2MS1-1 SP-4	33.17	0	62.33	0.23	4.14	0.01	0.03	0	0.02	0.02
		JH98GLLN-2MS1-1 SP-6	33.05	0	62.49	0.24	3.92	0	0.07	0	0.03	0
		JH98GLLN-2MS1-1 SP-7	33.35	0	62.51	0.22	3.82	0	0.07	0	0.04	0.01
		JH98GLLN-2MS1-1 SP-8	33.41	0.03	62.56	0.25	3.78	0.02	0.02	0	0.02	0
		JH98GLLN-2MS1-1 SP-9	33.21	0.05	62.6	0.19	3.73	0.01	0.05	0	0.04	0
		JH98GLLN-2MS1-1 PY-1	33.27	0.06	62.13	0.19	3.72	0	0.06	0	0	0
		JH98GLLN-2MS1-1 PY-4	33.08	0	61.26	0.26	4.55	0.02	0.05	0	0.01	0
		JH98GLLN-2MS1-1 PY-5	33.3	0.02	61.98	0.19	4.44	0.02	0.07	0	0	0.01
		JH98GLLN-2MS2 PY-1	33	0	64.64	0.2	2.14	0	0.06	0	0	0.02
		JH98GLLN-2MS2 PY-3	33.04	0.04	64.78	0.21	1.62	0	0.04	0	0	0
		JH98GLLN-2MS2 PY-4	32.99	0	65.28	0.25	1.76	0.02	0.05	0	0	0
		JH98GLLN-2MS2 PY-5	33.22	0	65.22	0.27	1.65	0	0.03	0	0.03	0.01
		JH98GLLN-2MS2-1 SP-1	33.15	0.01	65.35	0.16	1.46	0	0.06	0	0.01	0
		JH98GLLN-2MS2-1 SP-10	33.29	0	64.77	0.24	1.99	0	0.08	0	0.02	0
		JH98GLLN-2MS2-1 SP-11	33.31	0.01	64.39	0.19	2.08	0	0.03	0	0.01	0.01
		JH98GLLN-2MS2-1 SP-12	33.15	0	64.29	0.24	1.94	0.01	0.04	0	0	0
		JH98GLLN-2MS2-1 SP-13	33.4	0.01	65.11	0.27	1.76	0	0.05	0	0.01	0.01
		JH98GLLN-2MS2-1 SP-14	33.2	0.04	65.3	0.26	1.5	0	0.04	0	0	0.01
		JH98GLLN-2MS2-1 SP-15	33.15	0	64.09	0.2	2.22	0	0.07	0	0	0.01
		JH98GLLN-2MS2-1 SP-16	33.08	0.02	65.16	0.23	1.56	0	0.02	0	0.01	0
		JH98GLLN-2MS2-1 SP-17	33.22	0	65.22	0.25	1.82	0	0.05	0	0.01	0
		JH98GLLN-2MS2-1 SP-18	33.24	0.05	65.26	0.22	1.66	0	0.05	0	0	0
		JH98GLLN-2MS2-1 SP-19	33.07	0	64.84	0.18	1.9	0	0.1	0	0	0
		JH98GLLN-2MS2-1 SP-20	33.43	0.01	65.11	0.27	1.76	0	0.05	0	0.01	0.01
		JH98GLLN-2MS2-1 SP-3	33.51	0	59.03	0.17	7.12	0.01	0.07	0	0	0
		JH98GLLN-2MS2-1 SP-4	33.39	0.07	58.85	0.18	7.17	0.04	0.2	0	0.01	0
		JH98GLLN-2MS2-1 SP-5	33.52	0.03	58.78	0.19	7.25	0.01	0.05	0	0.02	0
		JH98GLLN-2MS2-1 SP-6	33.58	0	58.91	0.14	7.09	0.04	0.12	0	0	0
		JH98GLLN-2MS2-1 SP-7										

Table A1.3 Sphalerite (cont.)

Stratigraphic position	Deposit	Sample	S (wt%)	As (wt%)	Zn (wt%)	Cd (wt%)	Fe (wt%)	Se (wt%)	Cu (wt%)	Cr (wt%)	Ni (wt%)	Co (wt%)
Post cauldrom	Mobrun	86MOBR2 PY-3	33.14	0	64.27	0.47	2.26	0.01	0.08	0	0	0
		86MOBR2 PY-5	33.09	0.02	65.65	0.3	1.32	0.01	0.11	0	0	0
		86MOBR06 SP-1	33.42	0.02	64.7	0.39	2.19	0	0.19	0	0	0
		86MOBR06 SP-11	33.3	0.01	64.6	0.4	2.3	0.03	0.05	0	0.01	0.01
		86MOBR06 SP-12	32.76	0	64.18	0.39	2.34	0	0.12	0	0	0
		86MOBR06 SP-13	33.38	0.03	64.84	0.26	1.78	0.01	0.07	0	0.02	0
		86MOBR06 SP-14	33.17	0	64.53	0.39	2.18	0	0.07	0	0	0
		86MOBR06 SP-15	33.23	0.07	64.8	0.39	2	0	0.05	0	0	0
		86MOBR06 SP-16	33.39	0	64.12	0.43	2.26	0	0.07	0	0.01	0
		86MOBR06 SP-17	34.21	0.02	64.01	0.28	2.26	0	0.16	0	0	0
		86MOBR06 SP-18	33.59	0	64.26	0.39	2.19	0.01	0.06	0	0	0
		86MOBR06 SP-2	33.09	0	64.99	0.28	1.52	0.01	0.07	0	0	0.01
		86MOBR06 SP-3	33.6	0.04	64.66	0.35	2.19	0.04	0.06	0	0	0.01
		86MOBR06 SP-4	33.33	0	65	0.36	2.08	0.01	0.08	0	0.02	0.02
		86MOBR06 SP-5	33.33	0	64.7	0.34	1.87	0.01	0.11	0	0	0
		86MOBR06 SP-7	33.39	0.01	65.66	0.26	1.42	0	0.09	0	0	0
		86MOBR06 SP-8	33.43	0.01	65.17	0.26	1.73	0	0.12	0	0	0.01
		86MOBR06 SP-9	33.14	0	65.15	0.32	1.75	0.03	0.1	0	0	0

Note: Those data shown as 0 are below detection limit

Table A1.3 Chalcopyrite: EPMA analyses for chalcopyrite seperated by sample for sulfide grains from Noranda VMS deposits.

Stratigraphic Position	Deposit	Sample	S (wt%)	As (wt%)	Cu (wt%)	Cd (wt%)	Fe (wt%)	Se (wt%)	Zn (wt%)	Cr (wt%)	Ni (wt%)	Co (wt%)
Pre-Cauldron	Robb-Montbray	A95.16A-CP-G1-1	34.98	0	34.63	0	30.1	0.18	0	0	0	0
		A95.16A-CP-G1-2	35.12	0	34.8	0	30.02	0.15	0.02	0	0.03	0
		A95.16A-CP-G1-3	35.09	0	34.79	0	29.9	0.16	0.01	0	0	0.02
		A95.16A-CP-G2-1	35.1	0	34.87	0.03	29.86	0.16	0.04	0	0	0
		A95.16A-CP-G2-2	34.96	0	34.45	0.03	29.83	0.17	0.07	0	0.01	0
		A95.16A-CP-G2-3	35.03	0.06	34.87	0.01	30.02	0.18	0	0	0	0
		A95.16A-CP-G3-1	35.23	0.03	34.92	0	29.78	0.15	0.06	0	0	0.01
		A95.16A-CP-G3-2	35.09	0	34.69	0	29.86	0.18	0	0	0.02	0
		A95.16A-CP-G3-3	35.09	0.03	34.19	0	29.68	0.16	0.04	0	0	0
		A95.16A-CP-G4-1	35.12	0.06	34.71	0.03	29.76	0.18	0	0	0	0
		A95.16A-CP-G4-2	34.98	0	34.81	0	29.94	0.14	0.02	0	0	0
		A95.16A-CP-G4-3	35.13	0.01	34.65	0	29.84	0.15	0.04	0	0.01	0
		A95.16A-CP-G4-4	34.93	0	34.45	0.03	30.12	0.15	0.03	0	0.01	0
		A95.16A-CP-G4-5	34.99	0	34.49	0.05	29.83	0.14	0.02	0	0	0
		A95.16A-CP-G5-1	34.81	0	34.66	0	30.03	0.18	0	0	0	0
		A95.16A-CP-G5-2	34.98	0	34.54	0	29.88	0.19	0	0	0	0
		A95.16A-CP-G5-3	35.09	0	34.16	0	29.83	0.17	0.02	0	0	0.02
		A95.16A-CP-G6-1	34.95	0.04	34.57	0	29.91	0.18	0.02	0	0	0
		A95.16A-CP-G6-2	35	0	34.52	0	29.79	0.18	0.06	0	0.01	0
		A95.16A-CP-G7-1	35.11	0	34.48	0	29.71	0.14	0	0	0	0
		A95.16A-CP-G7-2	35.1	0.01	34.46	0.04	30.18	0.17	0.03	0	0	0
		A95.16A-CP-G7-3	35.06	0	34.6	0	29.85	0.14	0	0	0	0
		A95.16A-CP-G8-1	34.92	0.03	34.88	0	30.1	0.15	0	0	0.01	0
		A95.16A-CP-G8-2	35.08	0	34.45	0.01	30.08	0.19	0	0	0.01	0
		A95.16A-CP-G8-3	35.26	0	34.9	0.04	30.2	0.16	0.12	0	0.02	0
		A95.16A-CP-G9-1	35.01	0	34.46	0.02	29.91	0.17	0.03	0	0	0.01
		A95.16A-CP-G9-2	34.95	0.03	34.61	0	29.95	0.15	0	0	0.01	0.01
		A95.16A-CP-G9-3	35.1	0	34.87	0	29.86	0.17	0	0	0.02	0.01
		A95.16A-CP-G10-1	34.94	0	34.38	0.05	30.03	0.16	0.03	0	0	0.01
		A95.16A-CP-G10-2	34.85	0	34.42	0.03	29.97	0.17	0.01	0	0	0
		A95.16A-CP-G10-3	35.03	0	34.41	0	29.72	0.17	0.03	0	0	0.01
		A95.16A-PY-G11-1	35.1	0.03	34.21	0.01	30.33	0.23	0	0	0	0.01
		A95.16A-PY-G11-2	35.06	0.04	34.37	0	30.2	0.23	0.01	0	0	0
		A95.16B-CP-G1-1	34.94	0	34.63	0	29.71	0.25	0.03	0	0.01	0
		A95.16B-CP-G1-2	35.03	0	34.27	0.02	30.09	0.27	0	0	0	0.01
		A95.16B-CP-G1-3	35	0.07	34.38	0	29.82	0.23	0	0	0	0
		A95.16B-CP-G1-4	34.95	0	34.53	0	29.51	0.28	0.04	0	0	0
		A95.16B-CP-G2-1	35.22	0	34.83	0	30.01	0.33	0	0	0	0
		A95.16B-CP-G2-2	35.03	0	35.13	0	30.04	0.29	0.03	0	0.02	0
		A95.16B-CP-G2-3	35.14	0	34.77	0.01	30.04	0.28	0	0	0.02	0
		A95.16B-CP-G3-1	34.94	0	34.58	0	30	0.31	0.06	0	0	0
		A95.16B-CP-G3-2	35.06	0	34.8	0.01	30.2	0.27	0	0	0	0
		A95.16B-CP-G3-3	35.03	0	34.53	0.02	29.8	0.31	0.06	0	0.05	0.02
		A95.16B-CP-G4-1	35.01	0.01	34.56	0	30.02	0.26	0	0	0.01	0
		A95.16B-CP-G4-3	35.1	0	34.69	0.04	30.03	0.26	0.06	0	0.01	0.03
		A95.16B-CP-G5-1	34.92	0.01	34.69	0.03	29.95	0.27	0.01	0	0	0
		A95.16B-CP-G5-2	35.17	0	34.2	0	30.03	0.25	0	0	0	0
		A95.16B-CP-G6-1	35.08	0.04	34.65	0	30.09	0.27	0.01	0	0	0
		A95.16B-CP-G6-2	35.05	0	34.86	0.01	30.05	0.29	0	0	0	0
		A95.16B-CP-G6-3	35.15	0	34.53	0	30.02	0.26	0.05	0	0	0.02
		A95.16B-CP-G7-1	35.06	0.05	34.29	0	30.1	0.12	0.04	0	0	0.01
		A95.16B-CP-G7-2	35.27	0.02	34.76	0.03	30.15	0.09	0	0	0	0
		A95.16B-CP-G7-3	35.24	0.02	34.49	0.02	30.34	0.08	0	0	0.01	0
		A95.16B-CP-G8-1	35.13	0.03	34.68	0.03	30.18	0.23	0.01	0	0.01	0
		A95.16B-CP-G8-2	35.36	0.05	35.1	0.01	30.2	0.24	0.02	0	0	0
		A95.16B-CP-G8-3	35.19	0	34.3	0	29.89	0.24	0.02	0	0.02	0.02
		A95.16B-CP-G8-4	35.3	0.02	34.56	0.03	30.02	0.24	0.05	0	0	0
		A95.16B-CP-G8-5	35.18	0.01	34.4	0	29.97	0.21	0.01	0	0	0
		A95.16B-CP-G9-1	35.05	0	34.52	0.02	30.08	0.1	0	0	0	0
		A95.16B-CP-G9-2	35.37	0.04	34.44	0.03	30.05	0.12	0.02	0	0	0
		A95.16B-CP-G9-3	35.14	0.03	34.78	0.05	30.18	0.12	0.03	0	0.01	0
		A95.16B-CP-G9-4	35.28	0.01	34.65	0.01	29.98	0.12	0	0	0	0
		A95.16B-CP-G9-5	35.12	0	34.11	0.03	29.75	0.12	1.36	0	0	0.03
		A95.16B-CP-G10-1	35.11	0	34.2	0	29.66	0.31	0	0	0	0
		A95.16B-CP-G10-2	35.02	0.05	34.67	0.02	30.02	0.29	0	0	0	0.01
		A95.16B-CP-G10-3	35.08	0	33.9	0.06	29.55	0.22	0.81	0	0.03	0
		A95.16B-CP-G10-4	35.16	0	34.72	0.01	30.02	0.29	0.02	0	0.01	0
		A95.16B-CP-G11-1	35.11	0	34.35	0.02	29.83	0.23	0.03	0	0	0.01
		A95.16B-CP-G11-2	34.99	0.02	34.45	0	29.94	0.25	0.05	0	0	0.01
		A95.16B-CP-G11-3	35.07	0	34.45	0.06	29.71	0.23	0.03	0	0	0
		A95.16A-CP-1	34.98	0.03	34.65	0	30.52	0.19	0	0	0	0
		A95.16A-CP-2	35.17	0	34.81	0	30.59	0.18	0	0	0.01	0
		A95.16C-PY-G11-1	34.96	0.03	34.75	0.01	30.37	0.16	0	0	0	0.01
		A95.16C-PY-G11-2	35.08	0	34.65	0	30.46	0.14	0.02	0	0.03	0
		A95.16C-PY-G11-3	35.1	0	34.67	0.02	30.35	0.13	0.02	0	0	0
		A95.16C-PY-G12-1	35.14	0.06	34.41	0	30.3	0.15	0.02	0	0	0.02
		A95.16C-PY-G12-2	35.3	0	34.53	0.03	30.43	0.13	0	0.02	0	0
		A95.16C-PY-G12-3	35.22	0.02	34.69	0.01	30.38	0.08	0	0	0	0
		A95.16B-PY-1	35	0	34.44	0.03	30.69	0.15	0	0	0.01	0.01
		A95.16B-PY-2	34.98	0	34.42	0.02	30.88	0.16	0	0	0	0
		A95.16B-PY-3	34.78	0	34.65	0	30.88	0.16	0	0	0	0
		A95.16B-PY-4	34.9	0	34.32	0	30.71	0.19	0	0	0	0
		A95.16B-PY-5	34.94	0	34.55	0.04	30.6	0.12	0	0	0.01	0
		A95.16B-PY-6	34.47	0.01	34.54	0	30.57	0.19	0	0	0.03	0
		A95.16B-PY-7	34.92	0.01	34.45	0	30.58	0.13	0.03	0	0	0
		A95.16B-PY-8	34.74	0.03	34.65	0	30.59	0.17	0	0	0	0.01
		A95.16B-PY-9	34.75	0	34.53	0	30.49	0.15	0	0	0	0.02
		A95.16B-PY-10	35	0.03	34.38	0	30.45	0.15	0	0	0	0
		A95.16D-SP-G3-1	35.27	0.01	33.69	0.02	29.42	0.04	1	0	0	0.02
Horne No. 5	63RF33	63RF33 SP-1	35.08	0	34.6	0	30.53	0.02	0.03	0	0	0
		63RF33 SP-2	35.1	0.02	34.67	0.07	30.42	0.02	0.27	0	0	0
		63RF33 SP-3	35.09	0.04	34.67	0.01	30.65	0.02	0.37			

Table A1.3 Chalcopyrite (cont.)

Stratigraphic Position	Deposit	Sample	S (wt%)	As (wt%)	Cu (wt%)	Cd (wt%)	Fe (wt%)	Se (wt%)	Zn (wt%)	Cr (wt%)	Ni (wt%)	Co (wt%)
Pre-Cauldron	Horne No. 8	H63H20 PY-1	35.04	0	34.21	0	30.87	0.12	0	0	0	0
		H63H20 PY-2	34.97	0	34.44	0	30.78	0.08	0	0	0	0
		H63H20 PY-3	35.17	0.03	34.3	0	30.48	0.13	0	0	0	0
		H63H20 PY-5	35.03	0	34.33	0	30.78	0.1	0	0	0	0
		H63H20 PY-6	34.99	0	34.26	0	30.92	0.09	0	0	0.02	0
		H63H22 PY-1	35.01	0.03	34.57	0.02	30.73	0.07	0	0	0	0
		H63H22 PY-2	35.03	0	34.53	0	30.64	0.08	0	0	0	0.01
		H63H10 PO-1	34.97	0	34.4	0.01	30.85	0.03	0	0	0.01	0
		H63H10 PO-2	35.05	0.01	34.62	0	30.78	0.06	0.01	0	0	0.01
		H63H10 PO-3	35.08	0.02	34.5	0	30.74	0.02	0	0	0	0
		H63H10 PO-4	34.93	0.01	34.7	0	30.77	0.03	0	0	0	0.01
		H63H10 PO-5	34.97	0	34.62	0	30.61	0.04	0	0	0	0.01
		H63H14 PO-1	35.06	0.01	34.59	0	30.69	0.03	0	0	0.01	0.01
		G3RF36 CP-1	35.72	0.02	34.37	0	30.43	0.16	0	0	0	0
		G3RF36 CP-10	35.02	0	34.72	0	30.49	0.21	0	0	0	0
		G3RF36 CP-11	34.91	0	34.6	0.01	30.54	0.2	0	0	0	0.01
		G3RF36 CP-12	35.17	0	34.48	0.03	30.65	0.14	0.03	0	0	0
		G3RF36 CP-13	35.09	0	34.78	0	30.6	0.16	0	0	0.01	0
		G3RF36 CP-14	35.24	0	34.61	0	30.58	0.26	0	0	0	0
		G3RF36 CP-2	35.44	0	34.53	0	30.59	0.24	0	0	0.01	0
		G3RF36 CP-3	35.01	0	34.37	0.02	30.68	0.27	0.03	0	0.01	0.01
		G3RF36 CP-4	35.22	0.01	34.51	0.01	30.64	0.17	0	0	0	0
		G3RF36 CP-6	34.92	0.02	34.58	0	30.6	0.32	0	0	0.01	0
		G3RF36 CP-7	35.18	0	34.47	0.02	30.53	0.1	0	0	0	0
		G3RF36 CP-8	35.09	0	34.49	0	30.4	0.2	0	0	0	0
		G3RF36 CP-9	35.13	0	34.77	0	30.6	0.15	0.03	0	0	0
Cauldron Margin	Aldermac	A95-14A PY-1	34.47	0	34.02	0.01	30.07	0	0.97	0	0	0.01
		A95-14B SP-1	34.92	0	34.64	0	30.34	0.01	0.24	0	0	0
		A95-14B SP-2	34.94	0	34.71	0	30.38	0.05	0.11	0	0	0
		A95-14B SP-3	34.94	0.02	34.58	0.01	30.42	0	0.07	0	0.01	0
		A95-14C CP-1	35.23	0.01	34.33	0	30.8	0.01	0	0	0	0
		A95-14C CP-10	35.19	0	34.5	0	30.73	0.03	0	0	0.01	0
		A95-14C CP-11	35.06	0.01	34.63	0	30.72	0.01	0	0	0	0
		A95-14C CP-12	35.04	0.04	34.56	0	30.67	0.01	0	0	0	0
		A95-14C CP-14	35.38	0	34.69	0	30.85	0.01	0	0	0	0
		A95-14C CP-15	35.33	0	34.55	0	30.71	0.01	0	0	0	0.01
		A95-14C CP-3	35.4	0.07	34.57	0.05	30.68	0.02	0	0	0.01	0
		A95-14C CP-4	35.13	0.01	34.58	0	30.85	0	0	0	0.02	0
		A95-14C CP-5	35.06	0.04	34.6	0.02	30.6	0.01	0	0	0	0
		A95-14C CP-6	35.36	0	34.57	0	30.81	0.02	0	0	0	0
		A95-14C CP-7	35.15	0.02	34.57	0.01	30.74	0.03	0	0	0.01	0
		A95-14C CP-8	35.05	0.01	34.34	0.01	30.39	0.01	0	0	0	0
		A95-14C CP-9	35.12	0	34.58	0	30.68	0.02	0	0	0	0
		A95-14D CP-1	35.19	0.02	34.7	0	30.75	0	0	0	0	0.02
		A95-14D CP-10	35.56	0.03	34.56	0.03	30.69	0	0	0	0	0
		A95-14D CP-11	35.31	0	34.69	0.01	30.7	0.04	0	0	0	0.01
		A95-14D CP-12	35.32	0	34.61	0	30.78	0	0	0	0	0
		A95-14D CP-14	35.3	0	34.52	0	30.78	0.03	0	0	0	0
		A95-14D CP-15	34.97	0	34.8	0.03	30.69	0.02	0	0	0.01	0
		A95-14D CP-2	35.22	0	34.25	0	30.28	0.02	0	0	0	0
		A95-14D CP-3	35.22	0	34.3	0.01	30.38	0	0.03	0	0.01	0
		A95-14D CP-4	35.13	0	34.37	0	30.46	0.02	0	0	0	0
		A95-14D CP-5	35.17	0	34.65	0.01	30.41	0	0	0	0.01	0
		A95-14D CP-6	35.25	0.02	34.32	0	30.72	0.01	0	0	0.02	0
		A95-14D CP-7	35.35	0	34.57	0	30.59	0.01	0.02	0	0	0
		A95-14D CP-8	35.05	0.01	34.62	0	30.69	0	0	0	0	0
		A95-14D CP-9	35.08	0	34.41	0.03	30.52	0.01	0	0	0.01	0
New Inso		A95-12A CP1-1	35.05	0.02	34.72	0.01	30.68	0.04	0	0	0.01	0
		A95-12A CP1-10	35.06	0	34.56	0	30.77	0.05	0	0	0	0
		A95-12A CP1-11	35.28	0	34.48	0	30.66	0.05	0	0	0	0.01
		A95-12A CP1-12	35.17	0.03	34.74	0	30.64	0.05	0	0	0	0
		A95-12A CP1-13	35.27	0	34.7	0.01	30.67	0.04	0	0	0.01	0
		A95-12A CP1-14	35.22	0.02	34.6	0.01	30.65	0.02	0	0	0	0
		A95-12A CP1-15	35.3	0.03	34.61	0	30.72	0.03	0	0	0	0
		A95-12A CP1-2	35.28	0	34.57	0	30.53	0.01	0	0	0.01	0
		A95-12A CP1-3	35.13	0.01	34.65	0.06	30.68	0.03	0	0	0.01	0
		A95-12A CP1-4	35.23	0	34.4	0	30.5	0.02	0	0	0	0
		A95-12A CP1-5	35.17	0	34.59	0	30.54	0.04	0	0	0	0
		A95-12A CP1-6	35.11	0	34.49	0	30.42	0.04	0.01	0	0	0.02
		A95-12A CP1-7	35.59	0.01	34.59	0	30.67	0.05	0	0	0	0
		A95-12A CP1-8	35.29	0	34.53	0	30.73	0.04	0	0	0	0
		A95-12A CP1-9	35.18	0	34.52	0.02	30.51	0.04	0.02	0	0	0
		A95-12A CP2-1	35.18	0.02	34.42	0	30.84	0.04	0	0	0	0
		A95-12A CP2-10	35.28	0.01	34.42	0	30.85	0.01	0	0	0	0
		A95-12A CP2-11	35.04	0.01	34.49	0	30.47	0.03	0	0	0	0
		A95-12A CP2-12	35.13	0	34.66	0	30.87	0.03	0	0	0.01	0
		A95-12A CP2-13	35.22	0	34.38	0	30.7	0.06	0	0	0.01	0
		A95-12A CP2-15	35.29	0	34.65	0.02	30.77	0.03	0	0	0.01	0
		A95-12A CP2-2	35.29	0.02	34.5	0	30.72	0.05	0	0	0	0
		A95-12A CP2-3	35.03	0.01	34.61	0.04	30.6	0.03	0	0	0	0
		A95-12A CP2-4	35.22	0	34.7	0.03	30.94	0.02	0	0	0	0
		A95-12A CP2-5	35.13	0	34.8	0.01	30.77	0.02	0	0	0	0
		A95-12A CP2-6	34.83	0	34.37	0.04	30.69	0.04	0	0	0.01	0
		A95-12A CP2-7	34.9	0.01	34.71	0.02	30.65	0.04	0	0	0	0
		A95-12A CP2-8	35.18	0	34.46	0	30.62	0.03	0	0	0	0
		A95-12A CP2-9	35.08	0	34.65	0	30.65	0.03	0	0	0	0
Cauldron	Corbet	CRBT3.800N-SP-G2-1	34.9	0	33.35	0	28.71	0.02	2.62	0	0	0
		CRBT3.800N-SP-G2-2	34.65	0.01	33.62	0	29.01	0	1.95	0	0	0
		CRBT3.800N-SP-G4-1	34.48	0	34.24	0	30.21	0	0.28	0	0	0
		CRBT3.800N-SP-G4-2	34.74	0	34.22	0.03	30.05	0.02	0.37	0	0.01	0
		CRBT3.800N-SP-G4-3	34.97	0.04	34.35	0	30.03	0	0.53	0	0	0
		CRBT3.800N-SP-G5-1	34.82	0	34.46	0	30.22	0.02	0.16	0	0	0
		CRBT3.800N-SP-G5-3	34.63	0.01	34.38	0	30.11	0.03	0.13	0	0	0
		CRBT3.800N-SP-G2-1	34.9	0	33.35	0	28.71	0.02	2.62	0	0	0
		CRBT3.800N-SP-G2-2	34.65	0.01	33.62	0	29.01	0	1.95	0	0	0
Bedford Hill		A95-10A PY-1	35.42	0.05	33.84	0	30.26	0	1.15	0	0.01	0.01
		A95-10A PY-2	35.02	0	34.32	0	30.53	0.01	0.23	0	0	0
		A95-10C CP-1	34.92	0	34.51	0	30.27	0.04	0	0	0	0
		A95-10C CP-5	34.88	0	34.27	0	30.19	0.06	0	0	0	0
		A95-10C CP-6	35.06	0	34.5	0.03	30.26	0.07	0	0	0	0.02
		A95-10C CP-7	34.54	0	34.73	0	30.17	0.05	0.03	0	0	0
		A95-10C CP-8	34.95	0.02	34.49	0	30.29	0.05	0	0	0	0
		A95-10C CP-9	35.03	0	34.44	0	30.08	0.06	0	0	0	0
		A95-10C CP-10</td										

Table A1.3 Chalcopyrite (cont.)

Stratigraphic Position	Deposit	Sample	S (wt%)	As (wt%)	Cu (wt%)	Cd (wt%)	Fe (wt%)	Se (wt%)	Zn (wt%)	Cr (wt%)	Ni (wt%)	Co (wt%)
Cauldron	Bedford Hill	A95-10B-CP-3	34.95	0	34.48	0	30.26	0.06	0	0	0	0
		A95-10B-CP-4	34.9	0.02	34.63	0.02	30.22	0.07	0	0	0	0
		A95-10B-CP-5	34.95	0	34.66	0.06	30.16	0.06	0	0	0	0
		A95-10B-CP-6	34.85	0	34.56	0	30.2	0.09	0.02	0	0	0
		A95-10B-CP-7	34.84	0.03	34.31	0	30.22	0.08	0	0	0	0
		A95-10B-CP-8	34.97	0	34.58	0	30.33	0.08	0	0	0.01	0
		A95-10B-CP-9	34.96	0	34.54	0.01	30.29	0.04	0	0	0.02	0
		A95-10B-CP-10	34.75	0	34.52	0.01	30.3	0.05	0.03	0	0	0
		A95-10B-CP-11	34.74	0.03	34.6	0	30.29	0.07	0.02	0	0	0
		A95-10B-CP-12	35.03	0.03	34.47	0	30.24	0.05	0	0	0.01	0.01
		A95-10B-CP-13	34.89	0	34.43	0	30.34	0.06	0.01	0	0	0
		A95-10B-CP-14	34.89	0	34.46	0	30.04	0.05	0	0	0.01	0
		A95-10B-CP-15	34.75	0	34.51	0	30.17	0.1	0	0	0	0
		ANSL 98-MTMS PY-1	35.05	0.01	34.14	0.01	30.75	0.05	0	0	0	0.01
Ansil	Ansill	ANSL 98-MTMS PY-2	35.04	0	34.47	0.01	30.75	0.06	0	0	0	0
		ANSL 98-MTMS PY-3	34.83	0.02	34.32	0	30.65	0.04	0.04	0	0	0
		ANSL 98-MTMS PY-4	35.01	0.02	34.6	0.04	30.9	0.08	0	0	0.01	0
		ANSL 98-MTMS PY-5	35.05	0	34.52	0	30.67	0.06	0	0	0	0.01
		ANSL 98-MTMS PY-6	34.9	0	34.34	0	30.69	0.07	0	0	0	0
		ANSL 98-MTMS PY-7	35.04	0.06	34.55	0	30.75	0.06	0.01	0	0	0
		ANSL 98-MTMS PY-8	35	0.01	34.33	0	30.62	0.05	0.03	0	0.01	0
		ANSL 98-MTMS PY-9	34.75	0.01	34.49	0.01	30.68	0.09	0	0	0.01	0
		ANSL 98-MTMS PY-10	34.86	0	34.7	0	30.72	0.09	0	0	0	0
		ANSL 98-MTMS PY-11	34.73	0	34.58	0.01	30.5	0.06	0	0	0	0
		ANSL 98-MTMS PY-12	34.96	0.01	34.35	0.01	30.79	0.07	0	0	0	0
		ANSL 98-MTMS PY-13	35.17	0.03	34.59	0.01	30.66	0.09	0	0	0.01	0
		ANSL 98-MTMS PY-14	35.12	0.02	34.8	0.01	30.72	0.07	0	0	0	0
		ANSL 98-MTMS PY-15	34.94	0.05	34.44	0	30.5	0.07	0.01	0	0.01	0
Ansil	Ansill	ANSL 6C-HW-CP-1	34.99	0.04	34.55	0.02	30.36	0.07	0	0	0	0
		ANSL 6C-HW-CP-2	34.78	0	34.51	0	30.26	0.03	0.1	0	0	0
		ANSL 6C-HW-CP-3	35.18	0.01	34.36	0	30.25	0.04	0	0	0	0
		ANSL 6C-HW-CP-4	34.82	0	34.33	0.01	30.29	0.05	0	0	0	0
		ANSL 6C-HW-CP-5	35.32	0	34.49	0	30.21	0.07	0.02	0	0.01	0.01
		ANSL 6C-HW-CP-6	34.91	0	34.44	0	30.39	0.06	0	0	0	0
		ANSL 6C-HW-CP-7	34.96	0.02	34.45	0	30.34	0.07	0	0	0	0
		ANSL 6C-HW-CP-8	34.76	0.02	34.23	0	29.73	0.07	0	0	0	0
		ANSL 6C-HW-CP-9	34.78	0	34.49	0	30.34	0.08	0	0	0	0
		ANSL 6C-HW-CP-10	34.93	0	34.58	0	30.33	0.06	0	0	0	0
		ANSL 6C-HW-CP-11	34.7	0.01	34.39	0	30.42	0.06	0	0	0.01	0
		ANSL 6C-HW-CP-12	34.85	0	34.35	0	30.27	0.05	0.01	0	0.01	0
		ANSL 6C-HW-CP-13	35.01	0.03	34.61	0	30.31	0.04	0	0	0.01	0
		ANSL 6C-HW-CP-14	34.85	0.02	34.64	0	30.39	0.05	0	0	0.01	0
		ANSL 6C-HW-CP-15	34.62	0	34.49	0.01	30.33	0.04	0	0	0	0
Lac Dufault	Lac Dufault	ANSL 6A-4140-CP-1	34.78	0.01	34.5	0.01	30.31	0.1	0	0	0	0
		ANSL 6A-4140-CP-2	34.76	0	34.43	0.01	30.36	0.09	0	0	0	0.01
		ANSL 6A-4140-CP-3	35.18	0.01	34.54	0	30.35	0.11	0	0	0	0
		ANSL 6A-4140-CP-4	34.85	0.01	34.49	0	30.17	0.06	0	0	0	0
		ANSL 6A-4140-CP-5	34.88	0	34.49	0	30.26	0.1	0	0	0.01	0
		ANSL 6A-4140-CP-6	35.12	0	34.32	0.02	30.35	0.08	0	0	0.01	0
		ANSL 6A-4140-CP-7	34.94	0	34.4	0	30.3	0.06	0	0	0	0.01
		ANSL 6A-4140-CP-8	34.92	0.03	34.4	0	30.31	0.08	0	0	0	0
		ANSL 6A-4140-CP-14	35.33	0	34.53	0	30.42	0.04	0	0	0	0
		ANSL 6A-4140-CP-15	34.83	0	34.6	0	30.36	0.08	0	0	0.01	0
		JH70-04-CP-2	34.89	0.01	34.15	0	30.34	0.03	0	0	0.02	0
		JH70-04-CP-5	34.51	0	34.07	0	30.5	0.01	0	0	0	0
		JH70-04-CP-7	35.02	0.05	34.51	0	30.59	0.01	0	0	0	0
		JH70-04-CP-8	35.44	0	34.11	0	29.96	0.01	0	0	0.01	0
		JH70-04-CP-10	34.98	0.01	34.45	0.01	30.45	0	0	0.01	0.02	0
		JH70-04-CP-11	34.62	0	34.25	0	30.38	0	0.01	0	0.01	0
		JH70-04-CP-13	34.81	0	34.74	0	30.39	0.02	0	0	0	0
Lac Dufault	Lac Dufault	LDF-N-127-CP-1	36.44	0.02	34.12	0	30.3	0.04	0.01	0.01	0.01	0
		LDF-N-127-CP-2	35.34	0	34.26	0	30.49	0.01	0	0	0	0
		LDF-N-127-CP-3	35.27	0	34.41	0	30.39	0.01	0	0.01	0	0
		LDF-N-127-CP-4	35.24	0	34.23	0	30.47	0.01	0	0	0	0
		LDF-N-127-CP-5	35.03	0	34.12	0.01	30.24	0.01	0.01	0	0	0.01
		LDF-N-127-CP-6	35.5	0.01	34.34	0	30.41	0.04	0	0	0	0.01
		LDF-N-127-CP-7	35.29	0.03	34.43	0	30.27	0.03	0.03	0.01	0.01	0.01
		LDF-N-127-CP-8	35.32	0.01	34.33	0	30.52	0.02	0	0	0.02	0.01
		LDF-N-127-CP-9	35.28	0	33.96	0	30.34	0.02	0	0	0.01	0.01
		LDF-N-127-CP-10	34.43	0.03	34.35	0.01	30.49	0.02	0.01	0	0	0.02
		LDF-N-127-CP-11	34.91	0.02	34.17	0	30.26	0.03	0.13	0.01	0	0.01
		LDF-N-127-CP-12	35.19	0.01	34.51	0	30.51	0.02	0	0	0	0
		LDF-N-127-CP-14	35.03	0	34.54	0	30.55	0.02	0	0.01	0.02	0
		LDF-N-127-CP-15	35.38	0	34.36	0.01	30.51	0.01	0	0	0	0
		LDF-N-127-CP-16	35.82	0	34.18	0	30.55	0.01	0	0	0	0
		LDF-N-127-CP-17	35.19	0	34.37	0	30.54	0.02	0	0.01	0	0
		LDF-N-127-CP-18	35.23	0.04	34.23	0	30.49	0.02	0	0.01	0	0
		LDF-N-127-CP-19	35.11	0.04	34.3	0	30.48	0	0.15	0	0.02	0
		LDF-N-127-CP-20	35.6	0	34.32	0	30.62	0.02	0	0	0	0.02
		LDF-N-127-CP-21	35.1	0	34.28	0.01	30.66	0.03	0	0	0	0
Moosehead	Moosehead	LDF-N-127-CP-22	35.16	0.02	34.39	0.02	30.61	0.01	0.02	0	0	0.01
		LDF-N-127-CP-23	35.18	0	33.76	0	30.04	0	0.55	0	0.01	0
		LDF-N-127-CP-24	35.36	0	34.23	0	30.31	0	0	0	0	0.01
		LDF-N-127-CP-25	35.26	0.04	34.22	0	30.34	0.03	0	0	0	0.01
		LDF-N-127-CP-26	35.11	0	34.69	0	30.6	0.02	0	0	0.01	0
		LDF-N-127-CP-27	34.96	0	34.22	0.02	30.47	0.02	0	0	0	0.01
		LDF-N-127-CP-28	35.15	0.07	34.77	0.01	30.37	0.03	0	0	0	0
		LDF-N-127-CP-29	35.4	0	34.09	0	30.55	0	0	0	0	0
		LDF-N-127-CP-30	35.11	0.02	34.3	0	30.58	0	0.05	0.01	0	0
		A95-09A-SP-1	35.19	0	34.25	0	30.42	0	0.09	0	0	0.01
		A95-09A-SP-2	34.88	0.04	34.34	0	30.67	0	0.07	0	0.02	0
		A95-09A-SP-3	35.18	0.02	34.41	0						

Table A1.3 Chalcopyrite (cont.)

Stratigraphic Position	Deposit	Sample	S (wt%)	As (wt%)	Cu (wt%)	Cd (wt%)	Fe (wt%)	Se (wt%)	Zn (wt%)	Cr (wt%)	Ni (wt%)	Co (wt%)
Cauldron	Amulet F-Shaft	AMF28001-CP-16	34.8	0.01	34.6	0	30.35	0.06	0.01	0	0	0.01
		AMF28001-CP-17	35.65	0	34.36	0	30.49	0.1	0.01	0	0.01	0.01
		AMF28001-CP-18	34.25	0	35.11	0	30.16	0.09	0	0	0.01	0
		AMF28001-CP-19	34.72	0.03	34.6	0	30.37	0.07	0	0	0.01	0
		AMF28001-CP-20	34.78	0	34.51	0	30.29	0.1	0	0	0	0
		AMF28001-CP-21	34.7	0.03	34.45	0	30.19	0.09	0.01	0	0.01	0
		AMF28001-CP-22	34.75	0.02	34.73	0	30.3	0.1	0	0	0.01	0
		AMF28001-CP-23	34.98	0.01	34.44	0.03	30.44	0.1	0	0	0.02	0
		AMF28001-CP-24	34.76	0	34.56	0.04	30.3	0.07	0	0	0	0
		AMF28001-CP-25	34.64	0	34.8	0.01	30.45	0.08	0	0	0	0
		AMF28001-CP-26	34.27	0	34.88	0.02	30.09	0.08	0	0	0	0
		AMF28001-CP-27	34.32	0.02	34.96	0	30.42	0.09	0	0	0	0
		AMF28001-CP-28	34.86	0	34.33	0	30.48	0.08	0	0	0.02	0
		AMF28001-CP-29	34.77	0	34.55	0	30.5	0.08	0	0	0	0
		AMF28001-CP-30	34.85	0.02	34.44	0.02	30.47	0.07	0	0	0.01	0
		AMLF8601-CP-1	35.01	0	34.06	0	30.47	0.02	0	0	0	0
		AMLF8601-CP-2	34.84	0	34.22	0.01	30.47	0.04	0.03	0	0.01	0.01
		AMLF8601-CP-3	35	0	34.66	0	30.32	0.04	0	0	0.01	0.01
		AMLF8601-CP-4	34.87	0	34.22	0	30.23	0.01	0.51	0	0	0
		AMLF8601-CP-5	34.89	0	34.43	0	30.49	0.01	0.11	0	0	0
		AMLF8601-CP-6	35.16	0	33.82	0	30.22	0.02	0.14	0.01	0	0.02
		AMLF8601-CP-7	35.16	0	33.65	0.02	30	0.01	0.65	0.01	0.02	0
		AMLF8601-CP-8	34.69	0.02	33.9	0	30.44	0	0.02	0	0.01	0
		AMLF8601-CP-9	34.54	0.07	34.13	0	30.49	0.01	0.04	0.01	0	0
		AMLF8601-CP-10	34.88	0	34.12	0	30.46	0.02	0.04	0	0	0
		AMLF8601-CP-11	35.71	0	34.21	0.04	30.42	0	0.05	0.02	0	0
		AMLF8601-CP-12	34.98	0	34.2	0	30.43	0	0.06	0	0.02	0
		AMLF8601-CP-13	35.99	0	34.04	0	30.41	0.01	0.07	0	0	0
		AMLF8601-CP-14	34.83	0	34.01	0.01	30.22	0.02	0.39	0	0.01	0.01
		AMLF8601-CP-16	35.03	0.01	34.13	0	30.6	0	0.09	0	0	0.01
		AMLF8601-CP-17	35.7	0	33.79	0	29.75	0.01	0.24	0	0	0
		AMLF8601-CP-18	35.75	0	34.03	0	30.39	0	0.05	0.01	0	0.01
		AMLF8601-CP-19	35.39	0.01	34.24	0	30.55	0	0.08	0.01	0	0
		AMLF8601-CP-20	36.06	0.05	34.13	0.01	30.37	0.02	0.23	0	0	0
		AMLF8601-CP-21	34.69	0	34.7	0.02	30.34	0.02	0	0	0	0
		AMLF8601-CP-22	34.74	0.01	34.75	0.02	30.39	0.03	0	0	0.01	0
		AMLF8601-CP-23	35.01	0	34.23	0	30.4	0.02	0	0	0	0
		AMLF8601-CP-24	35.07	0.02	34.48	0	30.44	0	0	0	0	0
		AMLF8601-CP-25	35.17	0	34.32	0.01	30.48	0.04	0.03	0	0	0
		AMLF8601-CP-26	35.17	0	34.08	0.02	30.48	0.02	0.14	0.01	0.01	0
		AMLF8601-CP-27	35.4	0.03	34.31	0	30.52	0	0.09	0	0	0.01
		AMLF8601-CP-28	35.17	0.02	34.44	0.03	30.43	0.01	0.07	0	0	0
		AMLF8601-CP-29	35.28	0.01	33.8	0.01	30.27	0	0.36	0	0	0
		AMLF8601-CP-30	35.27	0.01	34.24	0.03	30.3	0	0.18	0	0.01	0.02
		AMFZ80-PO-17	34.97	0.01	34.38	0	30.27	0.1	0	0	0	0.01
		AMFZ80-PO-18	34.84	0	34.23	0.02	30.21	0.08	0.02	0	0	0
		AMFZ80-PO-19	35.27	0	33.94	0.02	30.38	0.09	0	0	0	0
		AMFZ80-PO-20	35.3	0.02	34.11	0.01	30.16	0.06	0	0	0.01	0
		AMFZ80-PO-21	35.2	0	34.21	0	30.41	0.06	0	0	0	0.01
		AMFZ80-PO-22	34.94	0	34.04	0	30.52	0.07	0	0	0	0
	Amulet A Upper	A95-07D-PY-1	34.61	0	34.36	0.01	30.6	0	0	0	0	0
		A95-07E-CP-1	34.95	0	34.72	0	30.48	0.02	0.03	0	0	0
		A95-07E-CP-10	34.52	0	34.69	0.02	30.61	0.04	0	0	0.01	0
		A95-07E-CP-11	34.42	0	34.75	0.01	30.59	0.06	0.04	0	0	0
		A95-07E-CP-12	34.63	0.01	34.6	0.01	30.33	0.05	0.02	0	0	0
		A95-07E-CP-13	34.38	0	34.83	0	30.5	0.07	0	0	0.01	0
		A95-07E-CP-14	34.61	0.02	34.84	0	30.49	0.07	0	0	0	0
		A95-07E-CP-15	34.55	0	34.63	0.03	30.49	0.01	0	0	0	0
		A95-07E-CP-2	34.49	0	34.84	0	30.62	0.06	0.01	0	0	0
		A95-07E-CP-3	34.49	0.02	34.67	0	30.49	0.02	0.01	0	0	0
		A95-07E-CP-4	34.22	0	34.51	0	30.35	0.06	0.07	0	0.01	0
		A95-07E-CP-5	34.58	0	34.84	0	30.61	0.03	0.01	0	0	0
		A95-07E-CP-6	35.09	0	34.49	0	30.25	0.08	0.03	0	0	0
		A95-07E-CP-7	34.7	0	34.73	0.01	30.52	0	0	0	0	0.01
		A95-07E-CP-8	34.91	0	34.56	0.03	30.65	0.03	0	0	0	0
		A95-07F-CP-1	35.16	0.03	34.33	0	30.31	0.07	0.67	0	0	0
		A95-07F-CP-10	34.1	0	32.9	0	29.51	0.07	0	0	0	0
		A95-07F-CP-11	35.03	0.01	34.71	0.02	30.56	0.03	0.01	0	0.01	0
		A95-07F-CP-12	34.62	0	34.86	0	30.33	0.05	0	0	0	0
		A95-07F-CP-13	34.92	0	34.61	0	30.42	0.04	0	0	0.01	0
		A95-07F-CP-14	34.77	0.02	34.65	0	30.67	0.04	0	0	0	0
		A95-07F-CP-15	34.63	0	34.8	0.02	30.61	0.05	0	0	0.01	0
		A95-07F-CP-2	34.66	0	34.54	0.02	30.61	0.07	0	0	0	0
		A95-07F-CP-3	34.84	0.01	34.82	0	30.56	0.02	0	0	0	0
		A95-07F-CP-4	34.71	0	34.76	0	30.52	0.04	0	0	0	0.01
		A95-07F-CP-5	34.88	0	34.93	0.04	30.47	0.04	0	0	0	0.01
		A95-07F-CP-6	34.72	0	34.68	0.01	30.58	0.04	0	0	0	0.02
		A95-07F-CP-7	35.07	0	34.77	0	30.55	0.03	0.01	0	0	0.02
		A95-07F-CP-8	34.65	0	34.87	0.01	30.5	0.03	0	0	0	0
		A95-07F-CP-9	34.63	0	34.94	0.04	30.35	0.02	0	0	0	0
	Amulet C	A95-08B-SP-1	33.8	0.02	33.29	0	29.72	0.01	0.12	0	0	0
		A95-08B-SP-1	34.91	0.04	34.17	0	30.42	0.01	0.2	0	0	0
		A95-08A-PY-1	34.91	0.01	34.76	0	30.49	0.04	0	0	0	0.02
		A95-08F-CP-1	34.87	0.02	34.92	0	30.48	0.1	0	0	0	0.02
		A95-08F-CP-2	34.95	0.02	34.58	0.01	30.39	0.07	0	0	0	0
		A95-08F-CP-3	34.78	0	34.73	0	30.42	0.06	0	0	0.01	0
		A95-08F-PO-1	34.98	0.01	34.5	0	30.59	0.05	0	0	0.01	0
		A95-08F-PO-2	35.14	0	34.41	0	30.76	0.1	0	0	0.01	0.01
		A95-08F-PO-3	34.93	0.02	34.5	0	30.64	0.11	0.04	0	0	0
		A95-08F-PO-4	35.07	0	34.54	0	30.84	0.1	0	0	0	0
		A95-08F-PO-5	35.19	0	34.45	0	30.73	0.06	0	0	0	0
		A95-18B-CP-1	35.17	0	34.79	0	30.69	0.01	0	0	0	0.01
	Old Waite	A95-18B-CP-10	34.73	0.03	34.53	0	30.64</td					

Table A1.3 Chalcopyrite (cont.)

Stratigraphic Position	Deposit	Sample	S (wt%)	As (wt%)	Cu (wt%)	Cd (wt%)	Fe (wt%)	Se (wt%)	Zn (wt%)	Cr (wt%)	Ni (wt%)	Co (wt%)
Cauldron	East Waite	A95-17D CP-1	35.52	0	34.06	0	30.63	0.07	0	0	0	0
		A95-17D CP-10	35.03	0.03	34.46	0	30.4	0.09	0	0	0.02	0.01
		A95-17D CP-11	35.12	0.02	34.15	0	30.61	0.09	0.02	0	0	0
		A95-17D CP-12	35.11	0	33.91	0	30.56	0.05	0	0	0	0
		A95-17D CP-13	35.23	0	33.96	0	30.37	0.07	0	0	0.01	0
		A95-17D CP-14	35.21	0.03	34.58	0	30.42	0.11	0	0.01	0	0
		A95-17D CP-15	34.94	0	34.18	0.03	30.43	0.08	0.02	0	0.01	0
		A95-17D CP-16	35.1	0	33.98	0	30.43	0.07	0	0	0	0
		A95-17D CP-17	34.97	0.02	34.22	0.03	30.56	0.07	0	0	0	0.01
		A95-17D CP-18	35.14	0	34.23	0.01	30.54	0.06	0	0	0	0
		A95-17D CP-19	35.07	0	34.16	0	30.33	0.09	0	0	0.01	0
		A95-17D CP-2	35.46	0	33.93	0	30.64	0.08	0	0	0.01	0.01
		A95-17D CP-20	35.01	0.02	34.2	0	30.59	0.05	0	0	0	0
		A95-17D CP-21	35.22	0	34.31	0	30.65	0.06	0	0	0	0
		A95-17D CP-22	35.06	0.01	34.03	0	30.42	0.07	0	0	0	0
		A95-17D CP-23	34.77	0.01	34.13	0	30.51	0.05	0	0	0	0
		A95-17D CP-24	35.27	0	34.27	0	30.42	0.08	0.03	0.01	0	0
		A95-17D CP-25	35.01	0.04	34	0	30.16	0.08	0	0	0	0.01
		A95-17D CP-26	34.72	0.01	34.58	0	30.5	0.07	0	0	0	0
		A95-17D CP-27	35.02	0.04	34.92	0.02	30.45	0.06	0	0	0	0
		A95-17D CP-29	35.1	0	34.37	0	30.21	0.04	0.01	0	0	0
		A95-17D CP-3	35.9	0	33.76	0	30.6	0.08	0.01	0	0	0
		A95-17D CP-30	34.96	0.02	34.16	0.01	30.69	0.07	0	0	0.01	0
		A95-17D CP-4	34.93	0	33.8	0.02	30.46	0.07	0.01	0	0	0
		A95-17D CP-5	34.63	0	34.72	0	30.37	0.06	0	0	0	0
		A95-17D CP-6	35	0	34.34	0	30.57	0.08	0	0	0.01	0
		A95-17D CP-7	35.15	0	33.98	0.02	30.43	0.07	0	0	0	0
		A95-17D CP-8	35.13	0	33.9	0	30.31	0.04	0	0	0	0
		A95-17D CP-9	35.02	0	34	0.01	30.6	0.05	0.01	0	0.01	0
		A95-17D PO-1	35.22	0	34.59	0	30.7	0.06	0	0	0	0
		A95-17D PO-3	34.87	0	34.5	0	30.69	0.1	0.01	0	0	0
		A95-17D PO-4	35.15	0	34.56	0	30.76	0.07	0	0	0.01	0
		A95-17D PO-5	35.01	0.01	34.65	0	30.61	0.08	0.02	0	0.01	0
Vauze	Vauze	A95-11E CP-1	35.09	0.02	34.81	0.01	30.65	0.05	0.03	0	0.01	0
		A95-11E CP-11	34.96	0.02	34.73	0	30.43	0.1	0	0	0	0
		A95-11E CP-12	35.1	0	34.55	0	30.7	0.1	0	0	0	0
		A95-11E CP-13	34.89	0	34.66	0	30.61	0.02	0	0	0	0
		A95-11E CP-14	35.02	0	34.48	0	30.6	0.07	0	0	0.01	0
		A95-11E CP-15	34.95	0	34.62	0	30.45	0.04	0	0	0	0
		A95-11E CP-2	35.03	0	34.91	0	30.62	0.07	0	0	0.01	0
		A95-11E CP-3	35.12	0	34.47	0.05	30.51	0.04	0	0	0	0
		A95-11E CP-4	35.18	0	34.72	0.03	30.6	0.03	0	0	0	0
		A95-11E CP-5	35.09	0.02	34.7	0	30.46	0.02	0	0	0	0.01
		A95-11E CP-6	34.89	0	34.88	0.02	30.56	0.12	0	0	0	0.01
		A95-11E CP-7	35.09	0.01	34.92	0.01	30.49	0.09	0.01	0	0	0
		A95-11E CP-8	35.07	0	34.68	0.02	30.54	0.03	0	0	0	0
		A95-11F CP-1	35.04	0	34.37	0	30.69	0.02	0	0	0	0
		A95-11F CP-10	34.89	0.03	34.63	0.04	30.51	0.07	0.02	0	0	0
		A95-11F CP-11	34.95	0.03	34.55	0.01	30.63	0.05	0	0	0	0
		A95-11F CP-12	35.04	0.05	34.51	0.01	30.28	0.04	0	0	0	0
		A95-11F CP-14	34.98	0.02	34.5	0.01	30.43	0.02	0	0	0	0
		A95-11F CP-15	35.03	0	34.5	0.01	30.52	0.03	0	0	0	0.02
		A95-11F CP-2	35.05	0.03	34.55	0	30.61	0.03	0.05	0	0	0
		A95-11F CP-3	35.25	0.03	34.37	0	30.6	0.02	0	0	0	0.02
		A95-11F CP-4	34.89	0	34.59	0	30.59	0.04	0	0	0	0
		A95-11F CP-5	35.02	0	34.63	0	30.72	0.05	0	0	0	0.01
		A95-11F CP-6	35.11	0	34.6	0	30.46	0.06	0.01	0	0	0
		A95-11F CP-7	35.27	0	34.62	0	30.5	0.04	0	0	0	0
		A95-11F CP-8	35.12	0	34.63	0	30.52	0.07	0	0	0	0
		A95-11F CP-9	34.91	0	34.56	0	30.59	0.04	0.18	0	0	0
		A95-11F PO-1	34.89	0.03	34.42	0	30.5	0.06	0.07	0	0	0.03
		A95-11F PO-10	35.05	0	34.5	0.01	30.63	0.03	0.18	0	0	0.01
		A95-11F PO-11	34.98	0	34.79	0.01	30.72	0.05	0.04	0	0	0.01
		A95-11F PO-12	34.97	0	34.48	0	30.52	0.07	0.08	0	0	0
		A95-11F PO-13	34.82	0	34.76	0	30.7	0.04	0.1	0	0.01	0.01
		A95-11F PO-14	34.81	0	34.34	0	30.51	0.04	0.27	0	0	0
		A95-11F PO-15	35.19	0	34.54	0.01	30.64	0.03	0.15	0	0	0
		A95-11F PO-2	35	0.02	34.61	0	30.17	0.05	0.21	0	0.01	0
		A95-11F PO-3	34.99	0.03	34.47	0.02	30.56	0.06	0.03	0	0.01	0.03
		A95-11F PO-4	35.18	0.04	34.51	0	30.6	0.02	0.14	0	0	0
		A95-11F PO-5	34.96	0	34.47	0	30.73	0.05	0.11	0	0.02	0
		A95-11F PO-6	35.02	0	34.37	0	30.56	0.01	0.32	0	0	0
		A95-11F PO-7	34.91	0.02	34.54	0	30.51	0.08	0.14	0	0	0
		A95-11F PO-9	35.14	0.03	34.43	0	30.29	0.06	0.59	0	0	0
Newbec	Newbec	NEWB44 CP-2	35.57	0.03	34.1	0	29.96	0	0	0	0.01	0.02
		NEWB44 CP-3	35.07	0	34.69	0	30.65	0.01	0	0	0	0
		QT4-2 SP-30	34.99	0	33.86	0.01	29.83	0.06	0.55	0	0	0
		QT4-2 SP-31	35.63	0.07	34.03	0	29.46	0.06	1.13	0	0.01	0
		QT4-2 SP-33	34.92	0	33.77	0	29.88	0.06	0.86	0	0	0
		QT4-2 SP-34	35.45	0.01	34	0	29.9	0.05	0.73	0	0	0
		QT4-2 PY(SP)-41	35.01	0	33.57	0.01	30.09	0.06	0.3	0	0.01	0
		QT17-5 SP(CP2)-21	35.16	0	34.03	0	30.21	0	0.17	0	0	0
		QT17-5 SP(CP2)-24	35.08	0	34.28	0	30.11	0.01	0.09	0.01	0.02	0
		QT17-5 SP(CP2)-25	35.14	0.03	34.62	0.02	30.45	0	0.01	0	0.02	0.01
		QT17-5 SP(CP2)-26	35.02	0	34.38	0	30.37	0.01	0.17	0	0	0
		QT17-5 SP(CP2)-27	35.31	0	34.39	0	30.03	0.01	0.11	0	0.01	0
		QT17-5 SP(CP2)-28	35.12	0.04	34.26	0	30.45	0	0.23	0	0	0.01
		QT17-5 SP(CP2)-29	35.17	0	34.46	0	30.24	0	0.29	0	0	0
		QT17-5 SP(CP2)-30	35.11	0	34.32	0.02	30.29	0.01	0.06	0	0	0
		QT17-5 SP(CP2)-31	35.45	0.01	34.42	0	30.39	0.02	0.07	0	0	0
		QT17-5 SP(CP2)-32	34.91	0.04	34.54	0	30.05	0	0.01	0	0	0
		QT17-5 SP(CP2)-33	35.06	0	34.43	0.01	30.29	0	0.06	0.01	0	0.01
		QT17-5 SP(CP2)-34	35.16	0	34.19	0	30.37	0	0.21	0	0	0
		QT17-5 SP(CP2)-35	35.3	0.03	34.51	0	30.51	0.03	0.12	0	0	0
		QT17-5 SP(CP2)-36	35.57	0.01	34.5	0	30.45	0</td				

Table A1.3 Chalcopyrite (cont.)

Stratigraphic Position	Deposit	Sample	S (wt%)	As (wt%)	Cu (wt%)	Cd (wt%)	Fe (wt%)	Se (wt%)	Zn (wt%)	Cr (wt%)	Ni (wt%)	Co (wt%)
Cauldron	Quemont	QT8-6 CP-5	35.38	0	34.58	0.02	30.67	0.01	0	0	0.01	0.01
		QT8-6 CP-7	35.13	0.03	34.41	0.01	30.6	0.03	0	0	0	0.02
		QT8-6 CP-8	34.96	0.07	34.4	0	30.66	0.02	0	0	0.01	0
		QT8-6 CP-9	35.16	0.01	34.88	0	30.49	0	0.01	0	0	0
		QT9-4 PY(SP)-1	34.77	0	34.69	0	30.23	0.09	0.01	0	0	0
		QT9-4 PY(SP)-2	35.03	0.01	34.4	0	30.22	0.04	0	0	0	0
		QT9-4 PY(SP)-3	34.76	0.02	34.61	0.03	30.28	0.06	0	0	0	0
		QT9-4 PY(SP)-4	34.87	0.01	34.4	0	30.43	0.01	0	0	0	0
		QT9-4 PY(SP)-5	34.99	0.01	34.67	0	30.08	0.05	0	0	0	0.01
		QT14-4 PO-1	35.06	0	34.29	0	30.58	0.06	0	0	0	0
		QT14-4 PO-2	34.95	0.04	34.06	0.01	30.72	0.03	0.01	0	0	0
		QT14-4 PO-3	34.96	0	34.52	0	30.3	0.05	0	0	0	0
		QT14-4 PY(CP2)-1	35.24	0.01	34.66	0.01	30.59	0.05	0	0	0.01	0
		QT14-4 PY(CP2)-2	35.37	0	34.81	0	30.71	0.06	0	0	0	0
		QT14-4 PY(CP2)-3	35.11	0.02	34.13	0	30.84	0.05	0	0	0.01	0
		QT14-4 PY(CP2)-4	35.08	0.04	34.4	0.02	30.59	0.04	0	0	0	0
		QT14-4 PY(CP2)-5	35.19	0	34.62	0	30.55	0.05	0	0	0	0
Post-cauldron	Deldona	DELD-F339-985 SP-1	34.49	0.01	34.6	0.01	30.15	0	0.26	0	0.01	0.01
		DELD-F339-985 SP-2	34.35	0.01	34.37	0	30.29	0.01	0.21	0	0	0
Delbridge		98DELB-2 SP-1	35.51	0	34.21	0.03	30.39	0.01	0.28	0	0	0
		98DELB-2 SP-2	34.81	0.02	34.31	0	30.36	0.01	0.38	0	0	0
		98DELB-2 SP-3	34.9	0	34.21	0.01	30.46	0.02	0.26	0	0	0
		98DELB-2-1 PO(SP)-10	34.77	0	34.58	0	30.46	0	0.14	0	0	0
		98DELB-2-1 PO(SP)-11	35	0.02	34.7	0	30.36	0	0.22	0	0	0
		98DELB-2-1 PO(SP)-12	34.78	0.04	34.38	0.01	30.28	0.03	0.34	0	0	0
		98DELB-2-1 PO(SP)-14	34.76	0	34.63	0.01	30.44	0	0.17	0	0	0
		98DELB-2-1 PO(SP)-15	34.83	0	34.21	0	30.39	0.01	0.27	0	0	0
		98DELB-2-1 PO(SP)-16	35.24	0.02	34.26	0.01	30.23	0.02	0.32	0	0.01	0
		98DELB-2-1 PO(SP)-17	35.12	0	34.33	0	30.5	0.02	0.24	0	0	0
		98DELB-2-1 PO(SP)-18	34.95	0.02	34.26	0	30.3	0.01	0.05	0	0.01	0
		98DELB-2-1 PO(SP)-19	34.73	0	34.39	0	30.43	0	0.39	0	0	0
		98DELB-2-1 PO(SP)-2	34.97	0	34.53	0.01	30.4	0.01	0.14	0	0	0
		98DELB-2-1 PO(SP)-20	34.77	0	34.44	0.01	30.25	0	0.41	0	0.01	0
		98DELB-2-1 PO(SP)-3	34.92	0	34.48	0.01	30.42	0.02	0.11	0	0	0.01
		98DELB-2-1 PO(SP)-4	35.05	0	34.34	0.01	30.2	0.01	0.37	0	0.01	0
		98DELB-2-1 PO(SP)-5	35.17	0.01	34.33	0	30.18	0.03	0.29	0	0.01	0
		98DELB-2-1 PO(SP)-6	34.88	0	34.43	0	30.47	0.01	0.06	0	0	0
		98DELB-2-1 PO(SP)-7	35.02	0	33.97	0	30.73	0	0.2	0	0	0.01
		98DELB-2-1 PO(SP)-8	34.86	0	34.39	0.01	30.34	0.02	0.17	0	0	0.02
		98DELB-2-1 PO(SP)-9	35.15	0.03	34.6	0.01	30.52	0.01	0.1	0	0.02	0
Gallen		JH98GLLN-3EFP CP-1	35.18	0	34.46	0	30.5	0.04	0	0	0	0.01
		JH98GLLN-3EFP CP-10	34.95	0.03	34.37	0.01	30.49	0.02	0	0	0	0
		JH98GLLN-3EFP CP-11	35.42	0.04	33.83	0	29.87	0	0.03	0	0	0
		JH98GLLN-3EFP CP-12	34.98	0	34.46	0.01	30.4	0	0.04	0	0.01	0.01
		JH98GLLN-3EFP CP-13	34.93	0.01	34.67	0.01	30.48	0.01	0	0	0.01	0
		JH98GLLN-3EFP CP-15	35.62	0.03	34.56	0	30.37	0	0	0	0	0
		JH98GLLN-3EFP CP-2	34.97	0.02	34.72	0	30.37	0.01	0	0	0	0
		JH98GLLN-3EFP CP-4	35.07	0	34.56	0.01	30.47	0.02	0	0	0	0
		JH98GLLN-3EFP CP-5	34.97	0	34.65	0	30.4	0	0	0	0	0
		JH98GLLN-3EFP CP-6	35.3	0.04	34.64	0	30.37	0.01	0	0	0.01	0
		JH98GLLN-3EFP CP-7	35.04	0	34.73	0	30.35	0.02	0	0	0.01	0
		JH98GLLN-3EFP CP-8	35.11	0	34.49	0.02	30.54	0	0	0	0.03	0
Mohrun		86M0RR12 SP-2	35.32	0	34.1	0	30.66	0.02	0.21	0	0.01	0

Note: Those data shown as 0 are below detection limit

Table A1.3 Pyrrhotite: EPMA analyses for pyrrhotite separated by sample for sulfide grains from Noranda VMS deposits.

Stratigraphic Position	Deposit	Sample	S (wt%)	As (wt%)	Cu (wt%)	Cd (wt%)	Fe (wt%)	Se (wt%)	Zn (wt%)	Cr (wt%)	Ni (wt%)	Co (wt%)
Pre-cauldron	Horne No. 8	H63H10 PO-10	39.12	0	0	0.01	61.66	0.03	0.02	0	0.04	0.05
		H63H10 PO-11	39.29	0	0.03	0	61.18	0.01	0	0	0.01	0.04
		H63H10 PO-12	39.02	0	0	0	61.18	0.04	0.02	0	0.03	0.04
		H63H10 PO-13	39.23	0	0.04	0	61.3	0.03	0	0	0.01	0.04
		H63H10 PO-14	39.01	0	0	0	61.15	0.02	0.03	0	0.02	0.03
		H63H10 PO-15	39.12	0	0.04	0.01	61.31	0.05	0	0	0.02	0.07
		H63H10 PO-2	38.82	0.01	0.02	0.01	61.28	0.03	0	0	0.01	0.05
		H63H10 PO-3	39.03	0.01	0.03	0	61.09	0.03	0	0	0.04	0.04
		H63H10 PO-4	39.25	0	0.05	0	61.28	0.03	0	0	0.01	0.04
		H63H10 PO-5	39.16	0.02	0.02	0.01	61.25	0.04	0	0	0.02	0.01
		H63H10 PO-6	39.8	0.04	0.09	0.01	60.58	0.03	0	0	0.01	0.03
		H63H10 PO-7	38.89	0.02	0.04	0.01	61.34	0.04	0	0	0.02	0.04
		H63H10 PO-8	39.08	0.03	0.04	0.02	61.2	0.02	0.01	0	0	0.03
		H63H10 PO-9	39.26	0.09	0.02	0	61.12	0.04	0.04	0	0.03	0.04
		H63H14 PO-1	39.14	0	0	0	61.08	0.01	0	0	0	0.03
		H63H14 PO-10	39.21	0	0	0	61.51	0.02	0	0	0	0.03
		H63H14 PO-11	38.94	0	0	0	61.3	0.02	0	0	0	0.01
		H63H14 PO-12	39.16	0	0	0	61.34	0.03	0	0	0.01	0
		H63H14 PO-13	39.08	0.01	0	0	61.49	0.02	0.02	0	0	0
		H63H14 PO-14	39.02	0.04	0.02	0	61.27	0.02	0.01	0	0	0
		H63H14 PO-15	39.14	0.04	0	0	61.32	0.04	0	0	0	0
		H63H14 PO-2	39.08	0.02	0	0	61.04	0.02	0.04	0	0	0.01
		H63H14 PO-3	39.07	0	0.02	0	61.25	0.02	0	0	0.01	0.02
		H63H14 PO-4	39.3	0.02	0	0	61.39	0.04	0	0	0	0
		H63H14 PO-5	39.11	0.01	0	0	61.26	0.02	0	0	0.01	0
		H63H14 PO-6	39.03	0	0	0	61.23	0.02	0	0	0	0
		H63H14 PO-7	39.3	0.01	0	0.01	61.3	0.03	0.03	0	0.01	0.02
		H63H14 PO-8	38.99	0.01	0	0	61.4	0.05	0.01	0	0	0.04
		H63H14 PO-9	38.95	0	0.01	0.01	61.43	0.04	0.03	0	0.01	0.01
Cauldron Margin	Aldermac	A95-14B SP-1	38.76	0	0	0	61.11	0.01	0.89	0	0	0
Cauldron	Decouer-Garon	A95.13D-G-PO-po-G1-1	39.2	0.05	0.1	0	59.81	0	0	0	0.1	0.05
		A95.13D-G-PO-po-G1-2	39.05	0.03	0.08	0	59.95	0	0	0	0.06	0.05
		A95.13D-G-PO-po-G1-3	39.01	0	0.06	0	60.08	0.01	0	0	0.07	0.05
		A95.13D-G-PO-po-G1-4	39.07	0.02	0.12	0.01	60.05	0	0	0	0.09	0.04
		A95.13D-G-PO-po-G2-1	39.22	0	0.07	0	59.88	0	0	0	0.05	0.12
		A95.13D-G-PO-po-G2-2	39.38	0	0.08	0	59.72	0.01	0.02	0	0.03	0.15
		A95.13D-G-PO-po-G3-1	39.38	0.03	0.05	0	59.83	0	0	0	0.1	0.1
		A95.13D-G-PO-po-G3-2	39.1	0	0.04	0	59.87	0.01	0	0.01	0.08	0.1
		A95.13D-G-PO-po-G3-3	39.11	0.01	0.07	0	59.83	0	0	0	0.06	0.11
		A95.13D-G-PO-po-G3-4	39.18	0.04	0.11	0.02	59.66	0.02	0	0	0.11	0.13
		A95.13D-G-PO-po-G4-1	38.92	0.03	0.06	0	60.19	0	0	0	0.07	0.02
		A95.13D-G-PO-po-G4-2	38.99	0.03	0.08	0	60.02	0	0.02	0	0.05	0.05
		A95.13D-G-PO-po-G5-1	39.18	0	0.09	0.03	59.9	0	0.05	0	0.02	0.16
		A95.13D-G-PO-po-G5-2	39.03	0.01	0.03	0	60	0.01	0.03	0	0.04	0.14
		A95.13D-G-PO-po-G5-3	39.43	0	0.08	0	59.78	0	0	0	0.05	0.11
		A95.13D-G-PO-po-G6-1	39.5	0	0.04	0	59.9	0	0.01	0	0.07	0.09
		A95.13D-G-PO-po-G6-2	39.18	0.02	0.02	0	59.96	0	0.01	0.01	0.09	0.12
		A95.13D-G-PO-po-G6-3	38.92	0	0.03	0	60.02	0.01	0	0	0.04	0.12
		A95.13D-G-PO-po-G7-1	39.02	0	0.04	0	59.97	0.01	0	0	0.09	0.08
		A95.13D-G-PO-po-G7-2	39.05	0	0.03	0	60.03	0.01	0	0	0.12	0.05
		A95.13D-G-PO-po-G7-3	38.96	0.02	0.03	0	59.99	0	0	0	0.09	0.06
		A95.13D-G-PO-po-G8-1	38.55	0	0.04	0	60.76	0.01	0	0	0.08	0.01
		A95.13D-G-PO-po-G8-2	38.95	0	0.03	0	60.06	0	0	0	0.05	0
		A95.13D-G-PO-po-G8-3	38.78	0	0.03	0	60.37	0.01	0.04	0	0.04	0
		A95.13D-G-PO-po-G9-1	38.98	0.04	0.05	0	59.55	0.01	0.01	0	0.21	0.08
		A95.13D-G-PO-po-G9-2	39.1	0	0.05	0	59.87	0.01	0	0	0.19	0.07
		A95.13D-G-PO-po-G9-3	39.37	0	0.05	0.02	59.58	0	0	0	0.14	0.05
		A95.13D-G-PO-po-G9-4	39.19	0	0.06	0.01	59.56	0	0.02	0	0.16	0.04
		A95.13D-G-PO-po-G10-1	38.91	0.02	0.05	0	59.92	0.01	0	0	0.03	0.11
		A95.13D-G-PO-po-G10-2	39.18	0	0.02	0.02	60.19	0.01	0	0	0	0.12
		A95.13D-G-PO-po-G10-3	39.23	0	0.04	0	59.92	0	0	0	0.04	0.1
Ansil		ANSL 98-MTMS PY-1	38.72	0	0	0	61.56	0.03	0.01	0	0.01	0.01
		ANSL 98-MTMS PY-2	38.98	0	0.04	0	61.49	0.04	0	0	0	0.05
		ANSL 98-MTMS PY-3	38.39	0.01	0	0	61.72	0.07	0.01	0	0	0.05
		ANSL 98-MTMS PY-4	39	0	0.02	0.01	61.44	0.06	0	0	0.01	0.09
		ANSL 98-MTMS PY-5	38.52	0	0.03	0	61.65	0.06	0.01	0	0.02	0.12
		ANSL 98-MTMS PY-6	38.61	0	0	0	61.46	0.03	0.03	0	0	0.05
		ANSL 98-MTMS PY-7	38.51	0.01	0.01	0.01	61.61	0.03	0.02	0	0	0.04
		ANSL 98-MTMS PY-8	38.53	0.03	0	0.01	61.56	0.04	0	0	0	0.09
		ANSL 98-MTMS PY-9	38.68	0.04	0	0	61.67	0.03	0	0	0.01	0.06
		ANSL 98-MTMS PY-10	38.83	0	0	0	61.61	0.04	0	0	0	0.07
		ANSL 98-MTMS PY-11	38.75	0	0.01	0.01	61.72	0.07	0	0	0.01	0.02
		ANSL 98-MTMS PY-12	38.65	0.03	0.01	0	61.62	0.03	0	0	0.01	0.03
		ANSL 98-MTMS PY-13	38.98	0.03	0.03	0	61.53	0.05	0	0	0.01	0.06
		ANSL 98-MTMS PY-14	38.57	0.03	0	0.01	61.7	0.05	0.05	0	0	0.03
		ANSL 98-MTMS PY-15	38.75	0	0.02	0	61.85	0.05	0	0	0.01	0.06
		ANSL 6A-4140-CP-1	38.47	0.03	0.07	0	61.52	0.04	0	0	0	0.09
		ANSL 6A-4140-CP-2	38.67	0	0.05	0.04	61.3	0.07	0.01	0	0.01	0.06
		ANSL 6A-4140-CP-3	38.61	0.04	0.04	0	61.61	0.06	0.03	0	0	0.03
		ANSL 6A-4140-CP-4	38.48	0	0.06	0	61.65	0.03	0	0	0	0.02
		ANSL 6A-4140-CP-5	38.72	0.01	0.08	0	61.38	0.07	0	0	0.01	0.08
		ANSL 6A-4140-CP-6	38.42	0.03	0.03	0	61.6	0.04	0	0	0.01	0.08
		ANSL 6A-4140-CP-7	38.48	0	0.04	0.01	61.71	0.05	0	0	0	0.09
		ANSL 6A-4140-CP-8	38.53	0	0.07	0	61.71	0.05	0	0	0	0.09
		ANSL 6A-4140-CP-9	38.38	0.02	0.13	0	61.76	0.04	0.01	0	0	0.04
		ANSL 6A-4140-CP-10	38.42	0	0.04	0	61.45	0.06	0	0	0.01	0.03
		ANSL 6A-4140-CP-11	38.44	0	0.02	0	61.55	0.06	0.03	0	0.01	0
		ANSL 6A-4140-CP-12	38.87	0	0.06	0	61.71	0.06	0	0	0	0.02
		ANSL 6A-4140-CP-13	38.45	0.01	0.03	0	61.78	0.05	0.01	0	0	0.03
		ANSL 6A-4140-CP-14	38.39	0.02	0.01	0	61.61	0.05	0.01	0	0	0.02
		ANSL 6A-4140-CP-15	38.45	0	0.01	0	61.72	0.05	0.02	0	0	0
		ANSL 11A247-SP-1	39.1	0	0.07	0	60.89	0	0.83	0	0	0
		ANSL 11A247-SP-2	39.09	0.03	0.03	0.01	61.05	0	0.43	0	0.01	0.01
Amulet F-Shaft		AMF280-PO-1	39.19	0	0.07	0	60.77	0.05	0.01	0.01	0.01	0.1
		AMF280-PO-2	39.07	0	0.06	0	60.98	0.06	0.04	0	0.01	0.1
		AMF280-PO-3	39.26	0.02	0.1	0.02	60.99	0.1	0	0	0	0.09
		AMF280-PO-4	39.91	0	0.27	0.01	59.82	0.04	0.03	0	0	0.01
		AMF280-PO-5	39.03	0	0.1	0.03	60.76	0.07	0	0	0.01	0.13
		AMF280-PO-6	39.13	0.02	0.06	0.03	60.82	0.07	0.02	0	0	0.07</td

Table A1.3 Pyrrhotite (cont.)

Stratigraphic Position	Deposit	Sample	S (wt%)	As (wt%)	Cu (wt%)	Cd (wt%)	Fe (wt%)	Se (wt%)	Zn (wt%)	Cr (wt%)	Ni (wt%)	Co (wt%)
Cauldron	Amulet C	A95-08F-PO-12	38.91	0	0.02	0	61.17	0.07	0.03	0	0	0.07
		A95-08F-PO-13	39.07	0	0.06	0	61.33	0.07	0	0	0	0.04
		A95-08F-PO-15	38.9	0.03	0.04	0.01	61.21	0.06	0	0	0	0.04
		A95-08F-PO-2	39.17	0	0.01	0	61.24	0.07	0	0	0	0.07
		A95-08F-PO-3	39.39	0	0.02	0	61.28	0.08	0.02	0	0.01	0.06
		A95-08F-PO-4	39.31	0.04	0.02	0	60.95	0.07	0.03	0	0	0.06
		A95-08F-PO-5	39.24	0	0.05	0	61.17	0.08	0.01	0	0	0.06
		A95-08F-PO-6	39.22	0.01	0.03	0.01	61.21	0.06	0.01	0	0	0.07
		A95-08F-PO-7	39.3	0.04	0.04	0	60.89	0.07	0.01	0	0.01	0.06
		A95-08F-PO-8	39.08	0.04	0.02	0	61.13	0.06	0	0	0	0.05
		A95-08F-PO-9	39.06	0.01	0.1	0	61.2	0.09	0.02	0	0	0.01
Old Waite		A95-18B-PO-1	39.35	0	0.06	0	61.08	0.03	0	0	0	0.05
		A95-18B-PO-10	39.02	0.04	0	0	61.48	0.01	0	0	0	0.08
		A95-18B-PO-2	39.32	0.01	0.04	0	61.21	0.02	0.03	0	0	0.07
		A95-18B-PO-3	39.14	0.01	0.06	0	61.28	0.02	0.03	0	0.01	0.05
		A95-18B-PO-4	39.16	0.01	0.02	0	61.22	0.03	0.01	0	0	0.05
		A95-18B-PO-5	38.98	0	0.07	0	61.31	0.01	0	0	0	0.05
		A95-18B-PO-6	38.93	0	0.06	0	60.96	0.01	0	0	0.01	0.07
		A95-18B-PO-7	39.08	0	0.05	0.02	61.24	0.01	0.04	0	0	0.08
		A95-18B-PO-8	39.19	0.02	0.07	0	61.1	0.02	0	0	0.02	0.06
		A95-18B-PO-9	39.09	0.02	0.05	0	61.2	0	0	0	0	0.06
East Waite		A95-17A-PO-1	39.38	0	0.03	0	61.47	0.01	0	0	0.02	0
		A95-17A-PO-10	39.02	0	0.04	0.01	61.48	0	0	0	0.02	0
		A95-17A-PO-2	38.97	0	0.03	0.01	60.97	0.02	0.03	0	0.01	0
		A95-17A-PO-3	39.15	0.03	0.02	0	61.29	0.01	0	0	0.01	0.01
		A95-17A-PO-4	39.14	0.01	0.03	0	61.16	0	0	0	0	0.01
		A95-17A-PO-5	39.11	0.01	0.03	0	61.33	0.02	0.01	0	0.01	0
		A95-17A-PO-6	39.54	0.01	0.03	0.02	60.91	0	0	0	0.01	0
		A95-17A-PO-7	39.02	0	0.02	0	61.19	0.01	0	0	0.01	0
		A95-17A-PO-8	39.39	0	0.01	0	61.22	0	0	0	0	0
		A95-17A-PO-9	39.28	0.01	0	0.01	61.14	0.02	0.03	0	0.01	0
		A95-17D-PO-1	39.24	0.01	0.06	0	61.29	0.06	0	0	0.01	0.03
		A95-17D-PO-2	38.98	0	0.02	0	61.09	0.05	0	0	0	0.04
		A95-17D-PO-3	39.25	0	0.04	0	61.12	0.06	0	0	0	0.03
		A95-17D-PO-4	39.14	0.02	0.05	0.02	61.28	0.04	0	0	0.02	0
		A95-17D-PO-5	39.79	0	0.07	0.02	60.62	0.05	0	0	0	0.04
		A95-17B-PY-1	38.6	0.06	0.04	0.01	61.57	0.03	0.17	0	0.01	0
		A95-17B-PY-2	38.91	0.03	0.03	0.01	61.14	0.02	0.38	0	0	0
Quemont		QT18-1 PO(CP)-1	40.15	0	0.12	0	60.32	0	0.04	0	0	0
		QT18-1 PO(CP)-10	39.78	0	0.08	0	60.6	0	0.05	0	0.01	0
		QT18-1 PO(CP)-11	39.55	0.04	0.09	0	61.15	0.01	0.07	0	0.01	0
		QT18-1 PO(CP)-12	40.05	0	0.08	0	60.45	0.01	0.03	0	0	0.02
		QT18-1 PO(CP)-14	40.28	0	0.08	0	60.44	0	0.02	0	0	0
		QT18-1 PO(CP)-15	39.85	0.01	0.1	0	60.81	0	0.02	0	0	0
		QT18-1 PO(CP)-16	40	0.03	0.05	0	60.82	0.02	0.01	0	0	0
		QT18-1 PO(CP)-17	40.15	0.01	0.09	0.01	60.25	0	0.04	0	0.01	0
		QT18-1 PO(CP)-2	39.83	0	0.1	0	60.7	0	0	0	0	0
		QT18-1 PO(CP)-21	39.23	0	0.09	0	61.13	0	0	0.01	0	0
		QT18-1 PO(CP)-22	40.55	0.01	0.08	0	60.04	0.02	0.04	0	0	0.02
		QT18-1 PO(CP)-24	41.68	0.03	0.07	0	58.9	0.01	0	0	0	0
		QT18-1 PO(CP)-25	40.05	0.01	0.09	0.01	60.22	0	0	0	0.01	0
		QT18-1 PO(CP)-26	40.2	0	0.15	0.02	60.22	0	0	0	0	0
		QT18-1 PO(CP)-28	39.9	0	0.11	0	60.35	0	0.06	0	0	0.01
		QT18-1 PO(CP)-29	39.78	0	0.05	0.01	60.42	0	0.01	0	0.01	0
		QT18-1 PO(CP)-4	38.85	0.01	0.05	0	60.01	0	0.1	0	0	0
		QT18-1 PO(CP)-5	39.53	0	0.07	0.01	60.26	0	0	0	0	0
		QT18-1 PO(CP)-6	40.11	0	0.09	0	60.39	0	0.04	0	0	0
		QT18-1 PO(CP)-7	40.7	0.03	0.06	0	60.2	0	0.06	0	0	0
		QT18-1 PO(CP)-8	39.73	0	0.09	0	60	0	0.09	0.01	0.01	0
		QT7-7 SP(PD)-1	38.93	0.01	0.07	0.02	60.74	0.01	0.04	0.01	0	0
		QT7-7 SP(PD)-2	38.41	0	0.06	0.01	60.63	0.02	0.18	0	0	0.01
		QT7-7 SP(PD)-3	38.3	0.01	0.06	0	61.12	0.01	0.34	0	0	0
		QT7-7 SP(PD)-4	38.31	0	0.03	0	60.93	0.03	0.28	0	0.01	0
		QT7-7 SP(PD)-5	38.5	0	0.06	0.01	60.9	0.04	0.24	0	0	0
		QT27-2 PO-1	39.15	0	0.04	0	60.27	0.09	0	0	0	0
		QT27-2 PO-2	38.82	0.02	0.02	0.01	61.1	0.1	0	0	0	0
		QT27-2 PO-3	38.74	0.02	0.02	0	61.18	0.1	0	0	0	0
		QT27-2 PO-4	39.2	0.02	0.04	0.03	60.26	0.08	0.01	0	0.01	0
		QT27-2 PO-5	39.16	0.03	0.04	0	60.32	0.08	0	0	0	0
		QT7-7 PO(SP)-1	39.01	0.04	0.1	0	61.15	0.05	0.04	0	0	0.02
		QT7-7 PO(SP)-10	39.06	0	0.11	0	60.93	0.01	0	0	0	0.01
		QT7-7 PO(SP)-11	38.99	0	0.1	0	61.62	0.03	0.02	0	0	0
		QT7-7 PO(SP)-13	39.35	0.02	0.07	0.01	61.04	0.04	0.03	0	0	0
		QT7-7 PO(SP)-14	39.8	0.03	0.04	0.05	60.44	0.01	0.4	0	0	0.01
		QT7-7 PO(SP)-15	39.23	0	0.09	0	61.19	0.01	0	0	0	0
		QT7-7 PO(SP)-17	39.93	0	0.07	0	60.68	0.01	0.01	0	0	0.02
		QT7-7 PO(SP)-18	39.78	0	0.12	0	60.61	0.03	0.05	0	0	0
		QT7-7 PO(SP)-19	39.85	0	0.07	0	60.46	0.01	0.03	0	0	0
		QT7-7 PO(SP)-20	39.79	0.02	0.05	0	60.61	0.02	0.06	0	0.02	0
		QT7-7 PO(SP)-3	39.77	0	0.07	0	60.41	0.04	0.58	0	0	0
		QT7-7 PO(SP)-4	39.76	0	0.1	0	60.43	0.02	0.1	0	0	0
		QT7-7 PO(SP)-5	39.32	0	0.07	0	61.26	0.01	0.15	0	0	0.01
		QT7-7 PO(SP)-6	39.82	0	0.07	0.04	60.74	0.02	0.03	0	0	0
		QT7-7 PO(SP)-7	39.17	0	0.07	0	61.17	0.02	0.21	0	0.01	0
		QT7-7 PO(SP)-8	39.12	0	0.07	0	61.59	0.03	0.03	0	0	0.01
		QT7-7 PO(SP)-9	39.76	0.02	0.09	0	60.66	0.04	0.06	0	0	0
		QT7-7 PO(SP)-10	39.83	0.02	0.15	0	60.49	0.01	0	0	0	0.01
		QT7-7 PO(SP)-11	39.84	0	0.11	0	60.52	0.01	0	0	0	0.02
		QT7-7 PO(SP)-13	39.73	0	0.1	0	60.76	0.01	0	0	0	0
		QT7-7 PO(SP)-14	39.84	0.02	0.12	0	60.49	0	0	0	0.01	0
		QT7-7 PO(SP)-15	39.73	0	0.11	0	60.38	0.02	0	0	0	0
		QT7-7 PO(SP)-16	39.73	0	0.11	0	60.75	0.02	0	0	0.01	0
		QT7-7 PO(SP)-17	39.88	0	0.13	0	60.6	0	0	0	0	0
		QT7-7 PO(CP)-3	39.81	0	0.14	0.02	60.56	0	0.04	0	0	0.01
		QT7-7 PO(CP)-4	39.7	0.04	0.1	0	60.65	0.01	0	0	0.01	0
		QT7-7 PO(CP)-5	39.02	0	0.12	0	61.24	0.01	0.02	0	0	0
		QT7-7 PO(CP)-6	39.65	0.01	0.11	0	60.73	0	0	0	0	0.01
		QT7-7 PO(CP)-7	39.79	0	0.1	0	60.69	0.02	0.01	0	0	0
		QT7-7 PO(CP)-8	39.81	0	0.09	0.02	60.49	0.01	0	0	0.01	0
		QT7-7 PO(CP)-9	39.69	0	0.08	0.01	60.36	0	0	0	0	0
		QT7-7 PO(CP)-10	39.61	0.01	0.4	0	59.89	0	0.01	0	0	0
		QT7-7 PO(CP)-11	39.87	0.03	0.17	0	60.47	0.03	0.02	0	0.01	0
		QT7-7 PO(CP)-15	40.01	0	0.11	0.04	60.					

Table A1.3 Galena: EPMA analyses for galena separated by sample for sulfide grains from Noranda VMS deposits.

Stratigraphic Position	Deposit	Sample	S (wt%)	As (wt%)	Zn (wt%)	Pb (wt%)	Fe (wt%)	Se (wt%)	Cu (wt%)	Cd (wt%)	Ni (wt%)	Co (wt%)	Cr (wt%)
Pre-cauldron	Horne No. 8	63RF10 GN-1	12.19	0.04	0.02	85.47	0.03	2.19	0.04	0.15	0	0	0
		63RF10 GN-10	13.11	0.01	0	86.47	0	0.58	0	0.1	0	0.02	0
		63RF10 GN-11	13.07	0	0.01	86.28	0.02	0.61	0.01	0.07	0	0.03	0
		63RF10 GN-13	12.98	0	0	85.31	0.01	1.46	0	0.04	0.01	0	0
		63RF10 GN-14	12.04	0	0.02	85.35	0.02	2.73	0	0.12	0.01	0	0
		63RF10 GN-15	12.31	0	0.01	85.55	0	2.18	0.02	0.06	0	0.02	0
		63RF10 GN-2	12.95	0	0.02	86.51	0.01	0.65	0	0.07	0.01	0	0
		63RF10 GN-6	13.01	0.02	0.01	86.23	0.02	0.89	0	0.06	0.01	0	0
		63RF10 GN-8	13.01	0	0	86.39	0.01	0.68	0.03	0.06	0	0.03	0
		63RF10 GN-9	13.14	0	0	86.61	0.03	0.6	0	0.07	0.01	0.03	0
Cauldron	Moosehead	A95-09A-PY-1	13.38	0.01	0.04	86.9	0.03	0.01	0.06	0.08	0.01	0.01	0
		A95-09A-PY-2	12.95	0	0.53	85.58	0.15	0	0.08	0.07	0	0	0
		A95-09A-PY-3	13.25	0.04	0.04	86.6	0.43	0	0.05	0.08	0.03	0.01	0
		A95-09A-PY-4	13.03	0	0.23	86.08	0.23	0.15	0.04	0.06	0	0.02	0
		A95-09B-PY-1	13.15	0	0.01	86.63	0.16	0.03	0.02	0.13	0	0	0
		A95-09B-PY-2	13.12	0.04	0	86.87	0.16	0.02	0.01	0.02	0.01	0.02	0
		A95-09B-PY-3	13.34	0	0.01	87.1	0.06	0.02	0.01	0.04	0.01	0	0
		A95-09B-PY-4	13.09	0.02	0	86.63	0.08	0.08	0.02	0.08	0.01	0	0
		A95-09B-PY-5	13.41	0	0	87.14	0.12	0	0.02	0.03	0	0.02	0
Quemont	Quemont	QT18-1 SP(GN)-41	13.48	0	0.24	85.34	0.13	0	0.04	0.04	0.01	0	0
		QT18-1 SP(GN)-42	13.49	0	0.58	86.21	0.11	0.15	0.08	0.05	0	0.01	0
		QT18-1 SP(GN)-43	13.3	0	0.84	85.75	0.1	0.11	0.07	0.14	0	0.02	0
		QT18-1 SP(GN)-45	13.5	0	0.85	85.9	0.03	0.01	0.05	0.09	0	0.01	0
		QT18-1 SP(GN)-46	13.44	0.04	0.06	86.16	0.04	0.01	0.05	0.1	0	0	0
		QT18-1 SP(GN)-47	13.42	0.02	0.24	86.38	0.06	0	0.04	0.04	0	0.01	0
		QT18-1 SP(GN)-48	13.47	0	0.05	86	0.03	0.01	0.09	0.09	0	0.01	0
		QT18-1 SP(GN)-49	13.5	0.02	0.14	86.01	0.02	0	0.06	0.05	0	0	0
		QT18-1 SP(GN)-50	13.52	0	0.1	86.32	0.14	0	0.03	0.12	0	0	0
		63RFS3GN-1	13.41	0.03	0.02	85.14	0.01	0	0.05	0.09	0	0	0
		63RFS3GN-10	12.82	0	0	86.56	0.03	0	0.13	0.08	0	0.01	0
		63RFS3GN-11	13.14	0	0	85.35	0.01	0.02	0.14	0.05	0	0	0
		63RFS3GN-13	13.21	0	0	85.2	0.02	0	0.08	0.03	0.01	0	0
		63RFS3GN-14	13.12	0.02	0	85.74	0.01	0.04	0.03	0.07	0.01	0	0
		63RFS3GN-15	13.09	0.01	0	85.62	0.01	0	0.06	0.08	0	0.02	0
		63RFS3GN-16	13.12	0.01	0	85.46	0.01	0.01	0.06	0.09	0.01	0	0
		63RFS3GN-17	13.12	0	0	85.79	0.01	0.01	0.06	0.04	0	0.01	0
		63RFS3GN-19	13.15	0	0	85.46	0.02	0	0.05	0.04	0	0	0
		63RFS3GN-2	13.47	0	0	84.74	0.02	0	0.09	0.15	0.01	0	0
		63RFS3GN-20	13.27	0	0.01	84.97	0	0.01	0.09	0.04	0	0.03	0
		63RFS3GN-21	13.44	0	0	84.77	0.01	0	0.02	0.01	0	0	0.01
		63RFS3GN-22	13.44	0.01	0.01	85.61	0.03	0	0.06	0.08	0.01	0	0
		63RFS3GN-23	13.01	0.01	0	85.58	0.01	0	0.04	0.07	0.02	0	0
		63RFS3GN-24	13.15	0	0.02	84.89	0.02	0	0.03	0	0.01	0.02	0
		63RFS3GN-25	13.03	0	0.02	84.89	0.02	0	0.03	0	0	0	0
		63RFS3GN-26	13.11	0.03	0	85.35	0.03	0.01	0.01	0	0	0	0
		63RFS3GN-27	13.06	0	0	85.5	0.01	0	0.13	0.04	0	0	0
		63RFS3GN-28	13.03	0.05	0	85.51	0	0	0.01	0.06	0.01	0	0
		63RFS3GN-29	13.1	0.03	0	85.09	0.03	0	0.11	0	0	0.01	0
		63RFS3GN-4	13.2	0	0	85.07	0.02	0	0.08	0.06	0.01	0.01	0
		63RFS3GN-7	13.15	0	0	85.83	0.01	0.01	0.05	0.02	0	0	0
		63RFS3GN-8	13.14	0	0.03	85.67	0	0	0.04	0.06	0	0	0
Post-cauldron	Deldona	DELD-F339-985 SP-1	12.61	0	2.43	83.93	0.15	1.79	0.01	0.02	0	0	0
		DELD-F339-985 SP-2	12.49	0.01	1.58	83.16	0.04	1.84	0.02	0.07	0	0	0
		DELD-F339-1004 PY-3	13.6	0	0.02	85.95	0.7	0.17	0.01	0.1	0	0.01	0
		DELD-F339-985 PY/GN-3	12.54	0	0.07	85.84	0.08	1.77	0.01	0.09	0	0	0
		DELD-F339-985 PY/GN-4	12.54	0	0.04	85.46	0.17	1.75	0.03	0.08	0	0.02	0
		DELD-F339-985 PY/GN-5	12.6	0.01	0	84.63	0.16	1.75	0.05	0.04	0.01	0	0
		DELD-F339-985 PY/GN-6	12.46	0	0.39	85.12	0.26	2.01	0.05	0.06	0	0	0
		DELD-F339-987 GN/SP-1	12.92	0	0.03	85.76	0.02	0.92	0.03	0.06	0	0	0
		DELD-F339-987 GN/SP-10	12.99	0	0	85.61	0.05	0.89	0.04	0.03	0	0	0
		DELD-F339-987 GN/SP-11	12.98	0	0	86.1	0.03	0.9	0.03	0.05	0	0	0
		DELD-F339-987 GN/SP-12	12.98	0	0	86.32	0.03	0.86	0.02	0.05	0.01	0	0
		DELD-F339-987 GN/SP-13	13.11	0	0.06	85.83	0.01	0.85	0.03	0.07	0.02	0.01	0
		DELD-F339-987 GN/SP-14	13.12	0.01	0.04	86.14	0	0.81	0.05	0.09	0	0	0
		DELD-F339-987 GN/SP-15	12.97	0	0	86.42	0.01	0.86	0.06	0.07	0.01	0	0
		DELD-F339-987 GN/SP-16	13.02	0	0	85.57	0.03	0.88	0.04	0.04	0.01	0	0
		DELD-F339-987 GN/SP-17	13.07	0	0.01	85.3	0.04	0.89	0.05	0.07	0	0.03	0
		DELD-F339-987 GN/SP-18	12.91	0	0.01	85.74	0.03	0.89	0.04	0.08	0	0.01	0
		DELD-F339-987 GN/SP-19	13.09	0.03	0.15	86.1	0.03	0.78	0.08	0.1	0.01	0	0
		DELD-F339-987 GN/SP-20	13.03	0	0.04	86.04	0.01	0.72	0.04	0.05	0.01	0	0
		DELD-F339-987 GN/SP-21	12.87	0	0.16	86.06	0.03	0.95	0.03	0.09	0.01	0	0
		DELD-F339-987 GN/SP-5	13.12	0.01	0.08	86.32	0.03	0.87	0.01	0.08	0	0.01	0
		DELD-F339-987 GN/SP-6	13.17	0	0.07	85.55	0.03	0.9	0.04	0.05	0.01	0	0
		DELD-F339-987 GN/SP-7	13.05	0.02	0.23	85.96	0.06	0.78	0.04	0.07	0	0	0
		DELD-F339-987 GN/SP-8	12.99	0.02	0.06	85.98	0.14	0.88	0.09	0.02	0	0	0
		DELD-F339-987 GN/SP-9	12.99	0.03	0.1	86.22	0.04	0.86	0.05	0.04	0.02	0	0

Note: Those data shown as 0 are below detection limit

Table A1.4: Investigation of equilibrium of sulfide mineral pairs and temperature of formation. bold denotes samples that fit both requirements.

Deposit	Sample	Mineralogy	$\delta^{34}\text{S}$ (% V-CDT)	$\delta^{34}\text{S}$ (% V-CDT)	$\Delta^{34}\text{S}$ (%o V-CDT)	$\Delta\delta = \delta^{34}\text{S}_\text{a} - \delta^{34}\text{S}_\text{b}$	Temperature (K) ¹	Temperature (C) ¹	Viable temperature ²	Isotopic Equilibrium ³
Robb-Montbray (Inmont)	A95-16A CP	Cp	-0.078	-0.03	-0.045				No	Yes
	A95-16A PY	PY	0.10	0.22	-0.166	0.37	1108	835	No	Yes
	A95-16B CP	Cp	-0.327	-0.50	-0.67			N/A ⁴	N/A	Yes
	A95-16B PY	PY	-0.222	-1.28	-0.064	-0.77				
Horne No.5	63RF31 CP	Cp	-0.537	-0.93	-0.056			N/A ⁴	N/A	Yes
	63RF31 PY	PY	0.374	0.81	-0.045	1.75	507	234	Yes	Yes
Aldermac	A95-14A PY	PY	-0.047	0.23	-0.163					
	A95-14A SP	Sp	-0.791	-1.12	-0.212	1.35	473	200	Yes	No
	A95-14B PO	PY (Sp)	-0.510	-0.68	-0.160					
	A95-14B SP	Sp	-0.536	-0.76	-0.143	0.08	1895	1622	No	Yes
	A95-14C CP	Cp	-0.390	-0.51	-0.125					
	A95-14C PY	PY	0.382	-0.49	-0.132	0.03	3928	3655	No	Yes
A95-14A CP	A95-14A CP	Cp	-0.041	0.10	-0.091					
	A95-14A CP	Cp	-0.027	-0.08	-0.067			N/A ⁴	N/A	No
	A95-14A CP	Cp	-0.027	-0.08	-0.067					
Moosehead	A95-09A PY	PY	0.285	0.88	-0.170					
	A95-09A SP	Sp	0.114	0.55	-0.169	0.33	954	681	No	Yes
	A95-09B PY	PY	0.021	0.29	-0.129					
Amulet A Upper	A95-07B PY	PY	0.575	1.47	-0.183					
	A95-07B SP	Sp	0.145	0.59	-0.161	0.88	588	315	Yes	Yes
	A95-08F CP	Cp	-0.074	0.08	-0.116					
Amulet C	A95-08F PO	Po	0.069	0.37	-0.122	N/A ⁵	N/A	N/A	Yes	
	A95-18A PY	PY	0.429	1.20	-0.190					
	A95-18A SP	Sp	-0.050	0.30	-0.202	0.480	794	521	No	Yes
Old Waite (Waite-Montoornerv)	A95-18B PY	PY	0.429	1.20	-0.190					
	A95-18B CP	Cp	-0.140	0.49	-0.392	-0.09	N/A ⁴	N/A	No	
	A95-18B PO	Po	-0.140	0.49	-0.394					
A95-18B PY	A95-18B PY	PY	-0.267	0.40	-0.471	2.30	363	90	No	No
	A95-17A PO	Po	-0.140	0.23	-0.259	0.081	1927	1654	No	Yes
	A95-17A PY	PY	-0.059	0.39	-0.262					
A95-17A SP	A95-17A SP	Sp	0.019	0.54	-0.260	-0.15	N/A ⁴	N/A	Yes	
	A95-17D CP	Cp	-0.960	-1.54	-0.168					
	A95-17D PO	Po	-0.603	-0.84	-0.170	N/A ⁵	N/A	N/A	Yes	
Vauze	A95-11A PY	PY	0.201	0.84	-0.234					
	A95-11A SP	Sp	-0.282	-0.02	-0.272	0.86	592	319	Yes	Yes
	A95-11B PY	PY	0.121	0.65	-0.216					
A95-11B SP	A95-11B SP	Sp	0.127	0.67	-0.217	-0.01	N/A ⁴	N/A	Yes	
	A95-11F CP	Cp	-0.353	-0.21	-0.246					
	A95-11F PO	Po	-0.363	-0.22	-0.256	N/A ⁴	N/A	N/A	Yes	
Ouemont	Q14-2 PY(SP)	PY (Sp)	0.579	1.34	-0.110					
	Q14-2 SP	Sp	0.008	0.23	-0.112	1.10	523	250	Yes	Yes
	Q17-7 PO(SP)	Po(Sp)	0.091	0.43	-0.130					
	Q17-7 SP	Sp	0.328	0.87	-0.118					
	Q17-7 SP(Po)	Sp(Po)	0.347	0.93	-0.131	N/A ⁵	N/A	N/A	Yes	
	OT8-6 CP	Cp	0.085	0.34	-0.088					
	OT8-6 PO(CP)	Po(CP)	0.195	0.55	-0.088	N/A ⁵	N/A	N/A	Yes	
	OT9-4 PY	PY	-0.015	0.29	-0.164					
	OT9-4 PY(SP)	PY (Sp)	-0.280	-0.19	-0.185	N/A ⁴	N/A	N/A	No	
	OT14-1 PO	PY	0.567	1.32	-0.112					
OT14-1 PY	OT14-1 PY	PY	0.531	1.27	-0.101					
	OT14-1 PY(CP2)	PY (Cp)	0.651	1.09	-0.099	N/A ⁴	N/A	N/A	Yes	
	OT15-4 PY	PY	0.458	1.19	-0.156					
OT15-4 SP	OT15-4 SP	Sp	0.042	0.34	-0.132	0.85	595	322	Yes	Yes
	OT17-5 PO(MT)	Po (Mt)	0.137	0.53	-0.138					
	OT17-5 PY	PY (Cp)	0.617	1.46	-0.134					
OT17-5 SP(CP2)	OT17-5 SP(CP2)	Sp (Cp)	0.254	0.76	-0.137	N/A ⁵	N/A	N/A	Yes	
	OT18-1 PO(SP)	PY	0.676	1.76	-0.228	N/A ⁴	N/A	N/A	No	
	OT18-1 PY(GN)	PY (Gn)	0.952	2.25	-0.204					
OT18-1 SP(GN)	OT18-1 SP(GN)	Sp (Gn)	0.815	1.99	-0.210	-0.24	N/A ⁶	N/A	Yes	
	DELD F339-985 PY(GN)	PY (Gn)	0.804	1.96	-0.204					
	DELD F339-985 SP	Sp	0.427	1.34	-0.264	0.62	701	428	Yes	No
DELD F339-987 GN(SP)	DELD F339-987 GN(SP)	Po	0.216	0.94	-0.266					
	DELD F339-987 SP	Sp	0.447	1.36	-0.253	0.42	1305	1032	No	Yes
	DELD F339-989 PY(SP)	PY (Sp)	0.044	2.04	-0.248					
DELD F339-989 SP	DELD F339-989 SP	Sp	0.497	1.42	-0.236	0.90	581	308	Yes	Yes
	98DEL B2 PY	PY	1.011	2.49	-0.270					
	98DEL B2 SP	Sp	0.476	1.44	-0.266	1.05	538	265	Yes	Yes
98DEL B4 PY	98DEL B4 PY	PY	0.757	2.01	-0.275					
	98DEL B4 SP	Sp	0.376	1.33	-0.310	0.67	671	398	Yes	No
	98DEL B5 PO	PY	0.799	2.00	-0.231					
98DEL B5 PY	98DEL B5 PY	PY	0.575	1.60	-0.249	N/A ⁴	N/A	N/A	Yes	
	JH98GLN-2MS1-1 PY	PY	0.539	1.51	-0.239					
	JH98GLN-2MS1-1 SP	Sp	0.512	1.43	-0.224	0.08	1918	1645	No	Yes
JH98GLN-2MS2-1 SP	JH98GLN-2MS2-1 SP	Sp	-0.082	0.05	-0.109					
	JH98GLN-2MS2-1 PY	PY	0.561	1.03	-0.272	0.98	555	282	Yes	Yes
	Mobrun	86MOBR12 PY	PY	0.057	0.67	-0.286				
Mobrun	86MOBR12 SP	Sp	-0.191	0.00	-0.191	0.67	674	401	Yes	No

¹ Temperatures are calculated using measured $\delta^{34}\text{S}$ values and fractionation factors from Ohmoto and Rye (1979)² Based on a temperature of 200 - 400°C from modern hydrothermal systems (Petersen et al., 1998)³ Mineral pairs with $\Delta\delta$'s values that overlap within the 2σ reproducibility of the measurements ($\pm 0.02\%$) are consistent with isotopic equilibrium (Jamieson et al., 2006)⁴ Mineral pair has the same dominant mineralogy, therefore temperature cannot be calculated⁵ Equilibrium fractionation between sphalerite and pyrrhotite and chalcopyrite and pyrrhotite is negligible, therefore temperatures cannot be calculated⁶ $\Delta\delta < 0$ therefore temperatures cannot be calculated

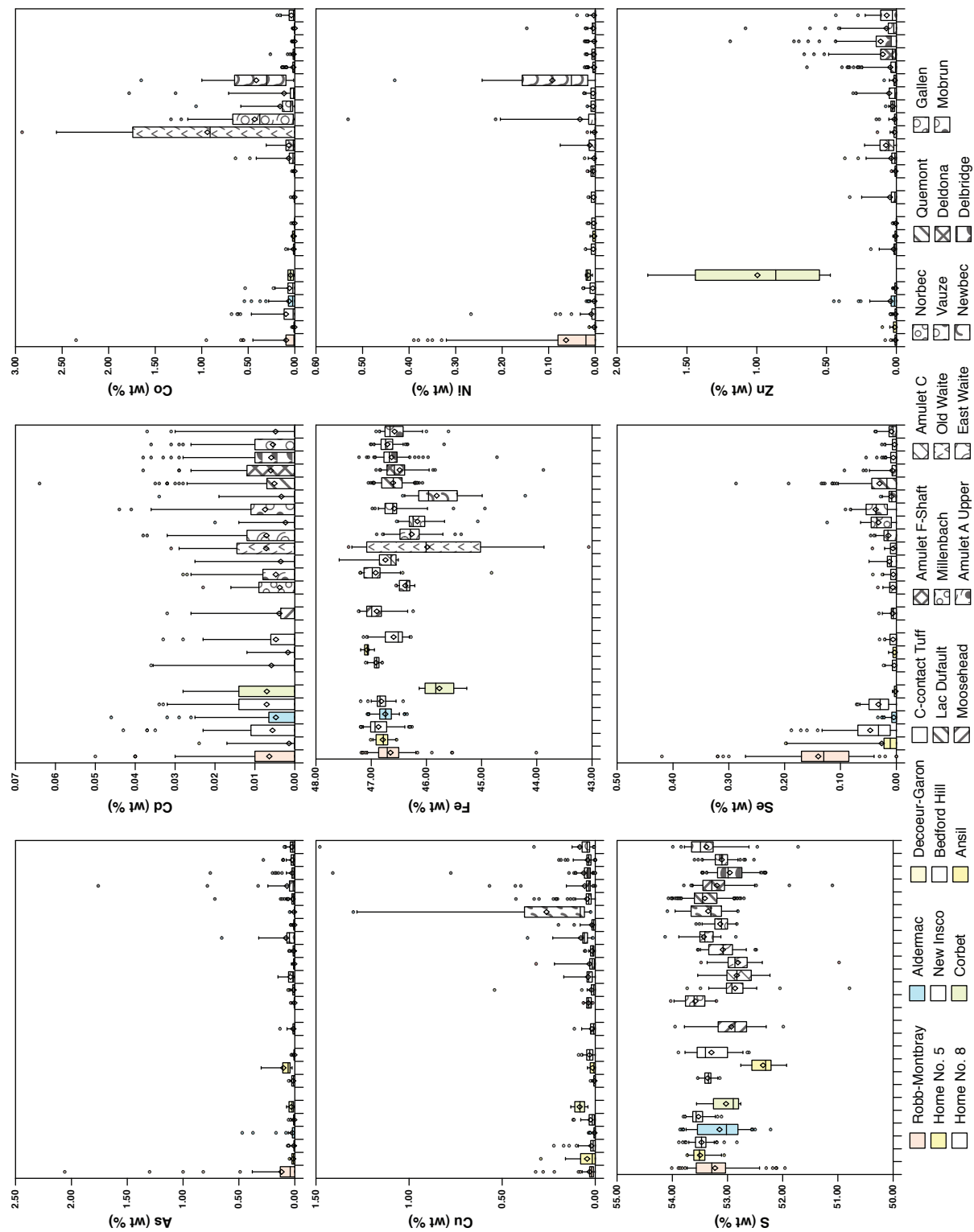


Fig. A1.1: Box and Whisker diagrams of trace element concentrations for pyrite from EPMA data separated by deposit showing 5th percentile and outliers (diamond indicates mean). 95th percentile and outliers (diamond indicates mean).

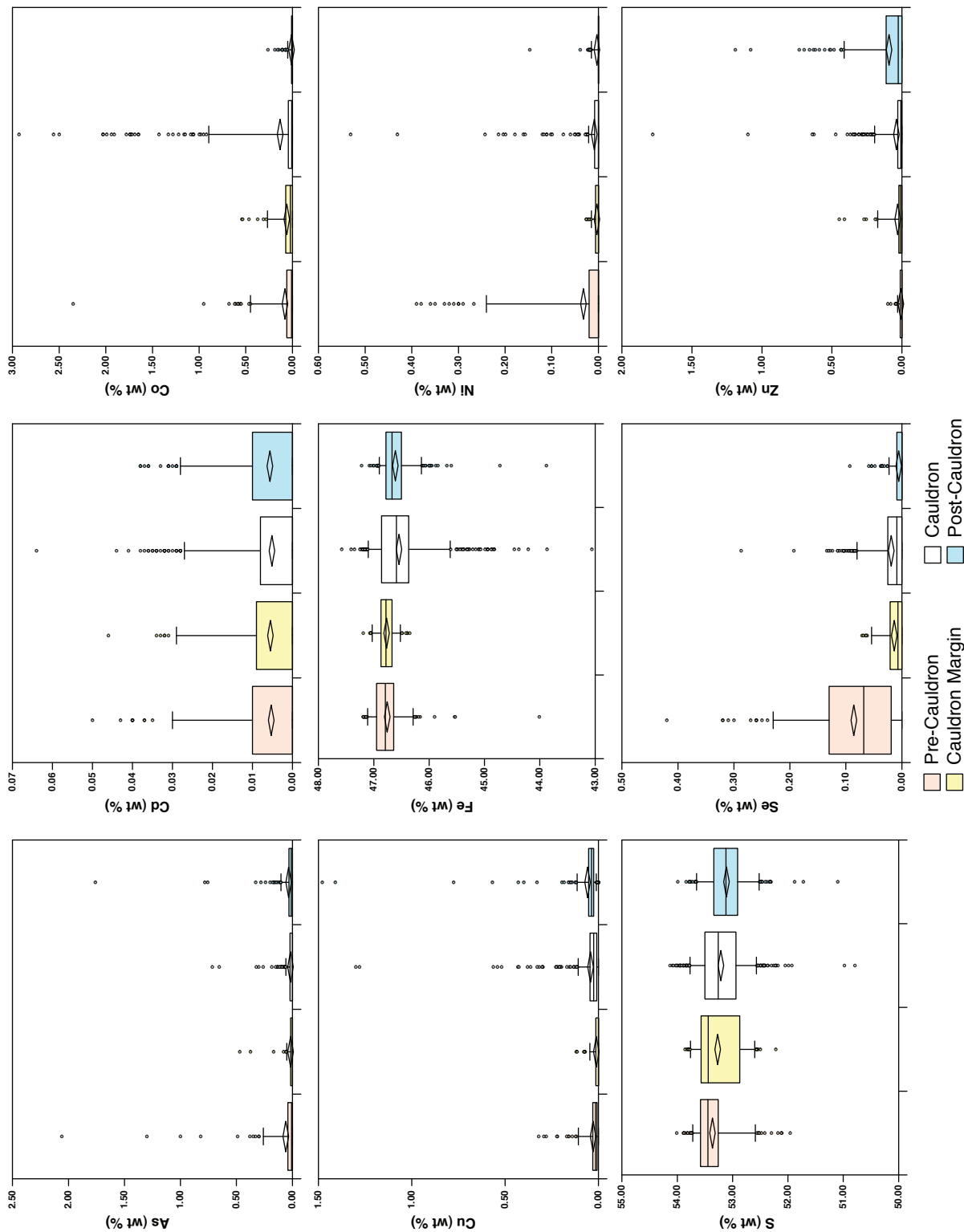


Fig. A1.2: Box and Whisker diagrams of trace element concentrations for pyrite from EPMA data separated by stratigraphic position showing 5th percentile, 95th percentile and outliers (diamond indicates mean).

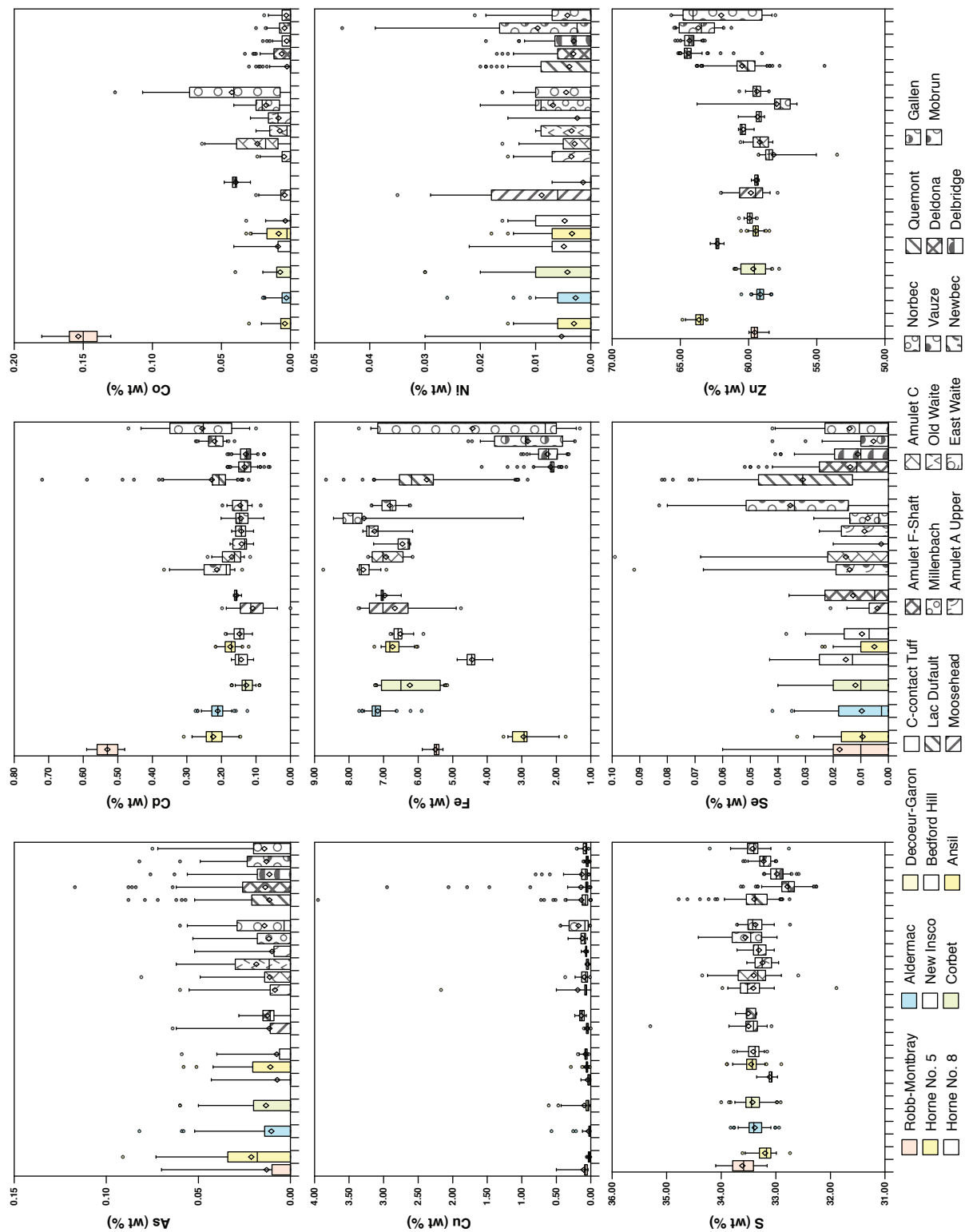


Fig. A1.3: Box and Whisker diagrams of trace element concentrations for sphalerite from EPMA data separated by deposit showing 5th percentile, 95th percentile and outliers (diamond indicates mean).

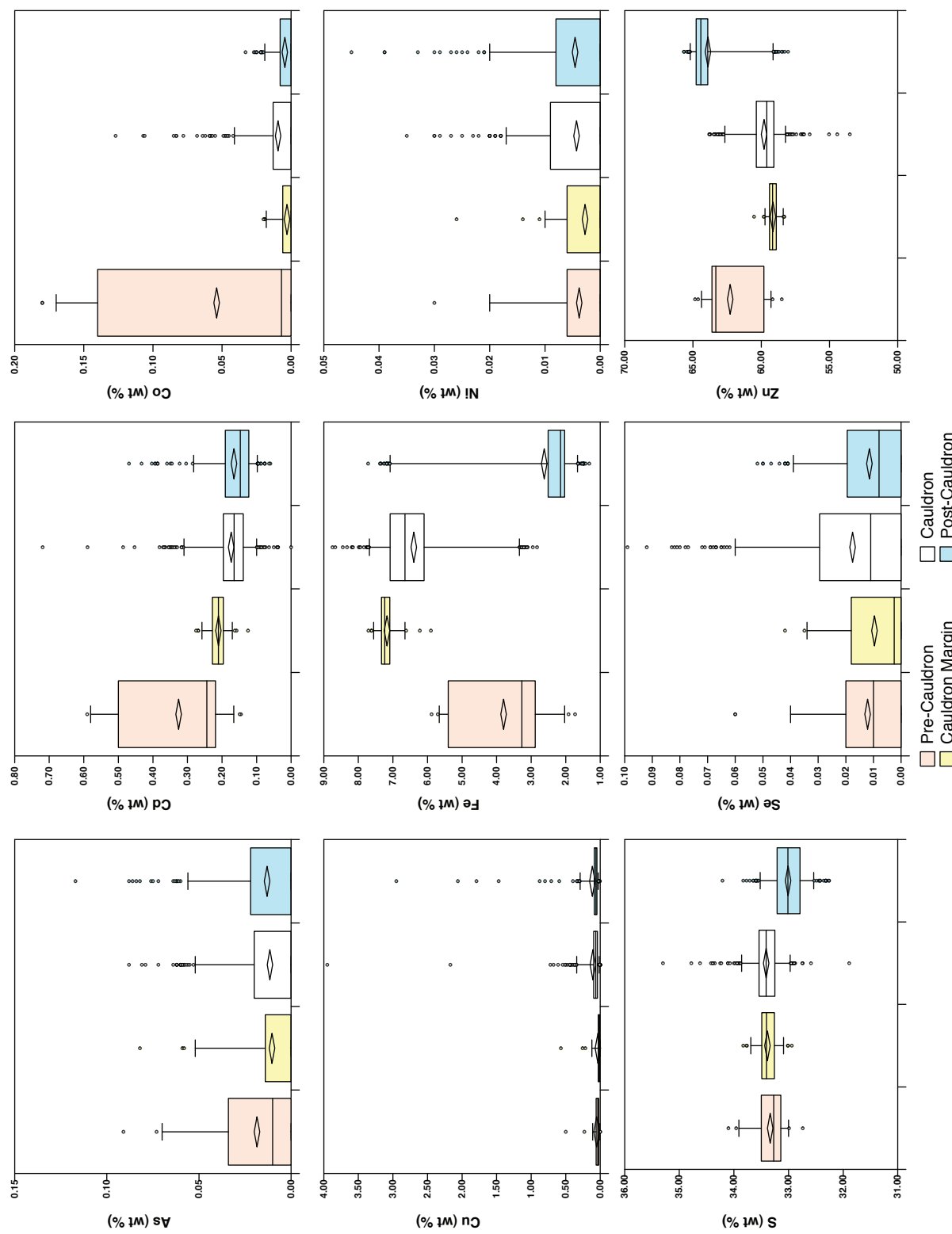


Fig.A.1.4: Box and Whisker diagrams of trace element concentrations for sphalerite from EPMA data separated by stratigraphic position showing 5th percentile, 95th percentile and outliers (diamond indicates mean).

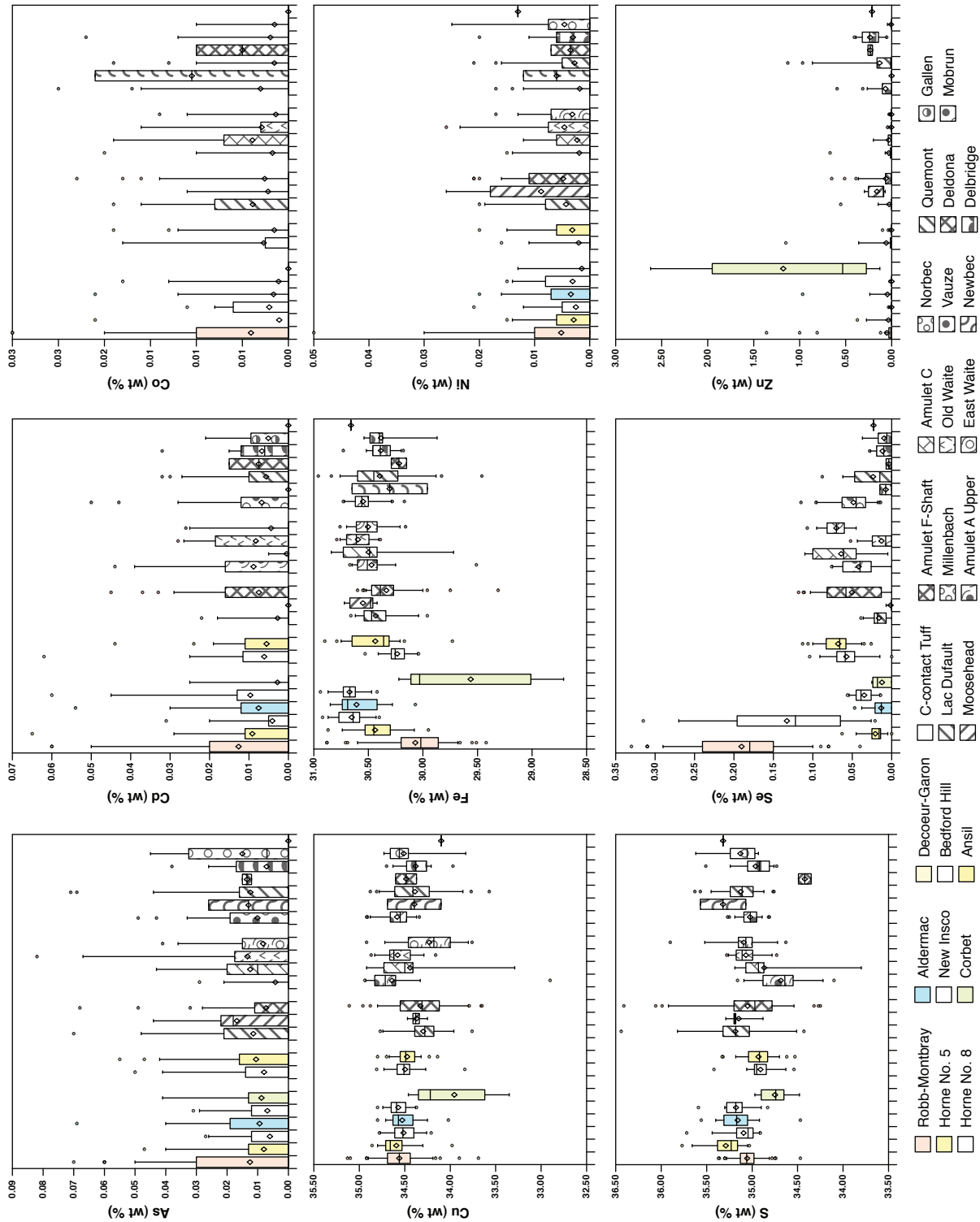


Fig. A1.5: Box and Whisker diagrams of trace element concentrations for chalcopyrite from EPMA data separated by deposit showing 5th percentile, 95th percentile and outliers (diamond indicates mean).

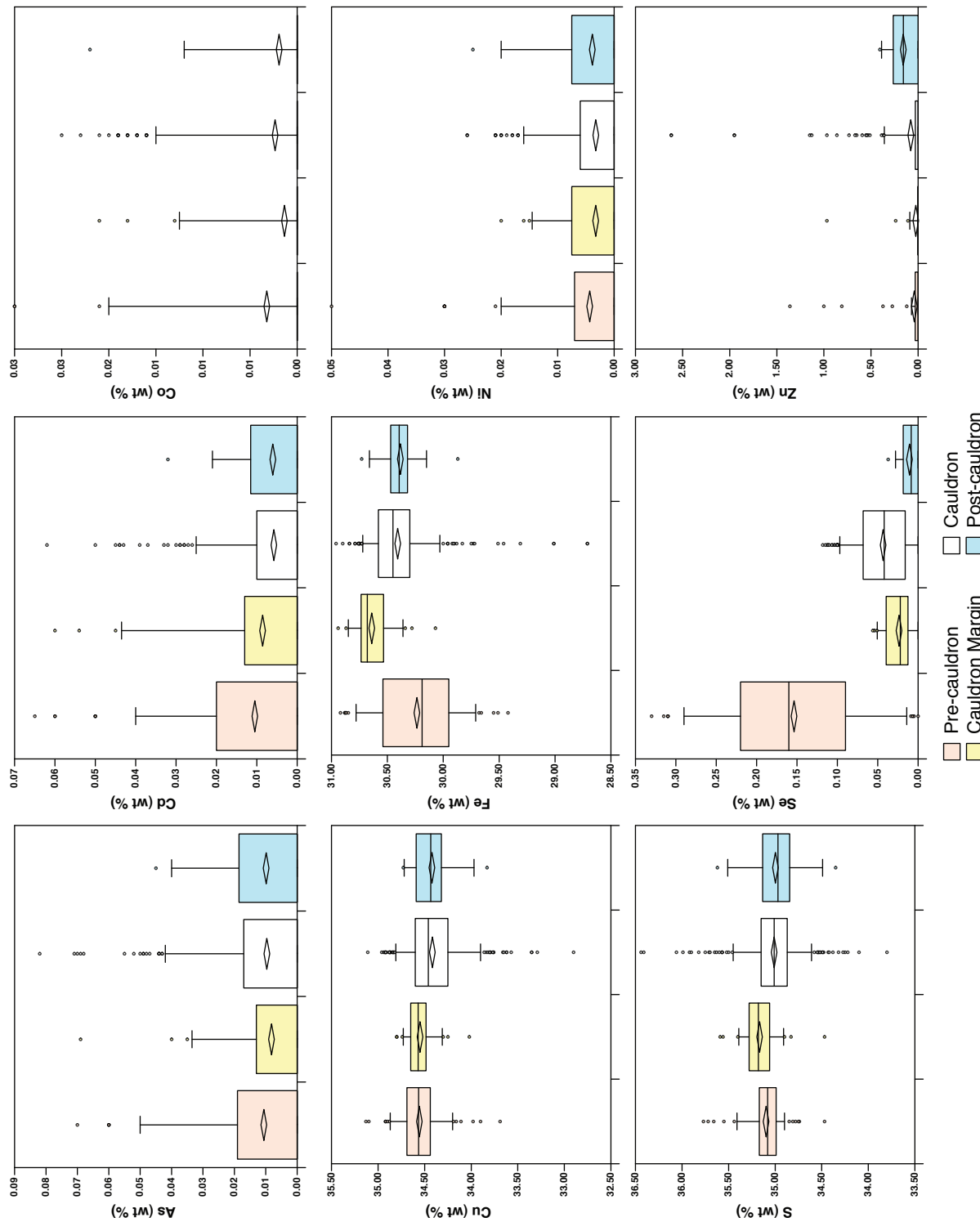


Fig. A1.6: Box and Whisker diagrams of trace element concentrations for chalcopyrite from EPMA data separated by stratigraphic position showing 5th percentile, 95th percentile and outliers (diamond indicates mean).

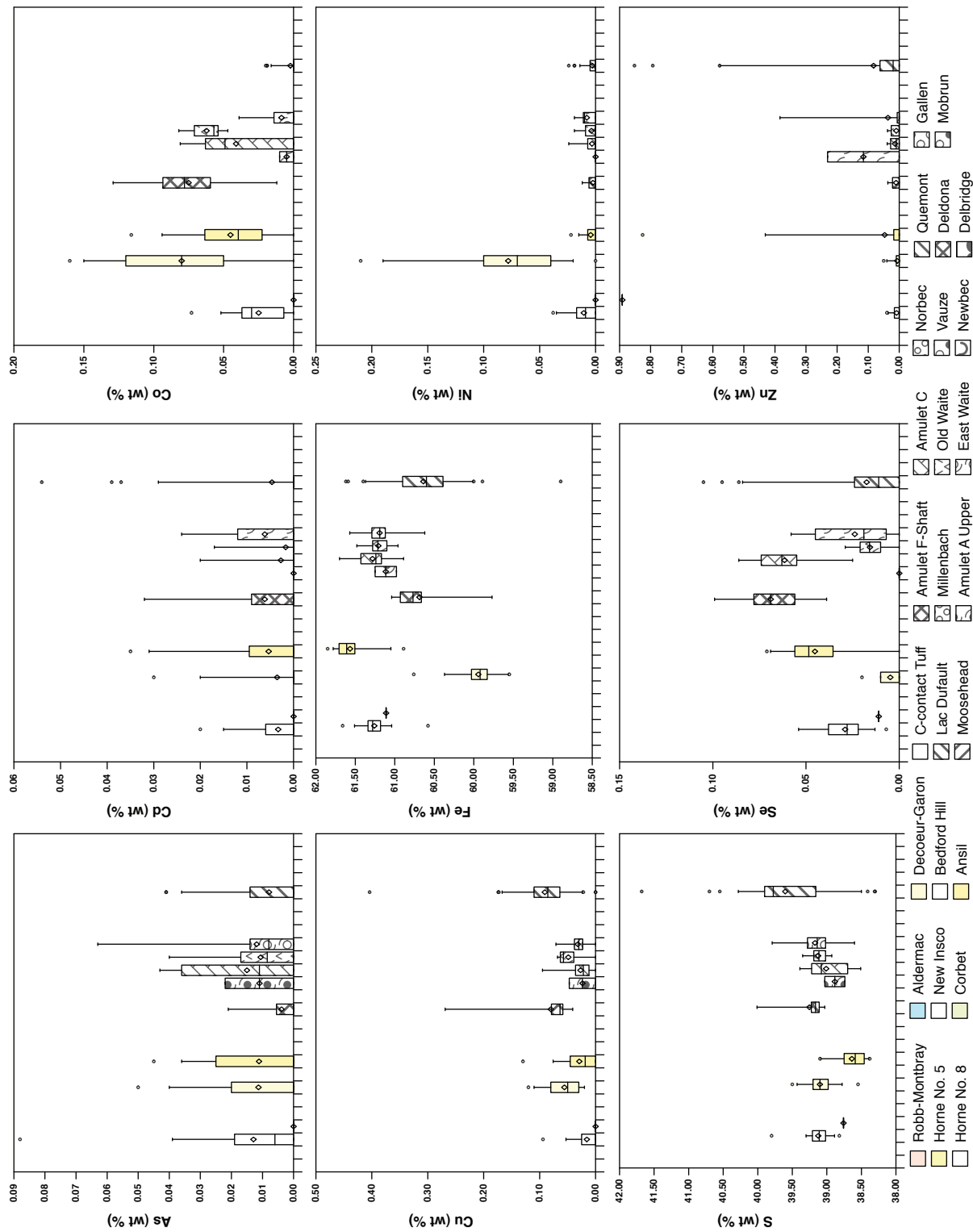


Fig. A1.7: Box and Whisker diagrams of trace element concentrations for pyrrhotite from EPMA data separated by deposit showing 5th percentile, 95th percentile and outliers (diamond indicates mean).

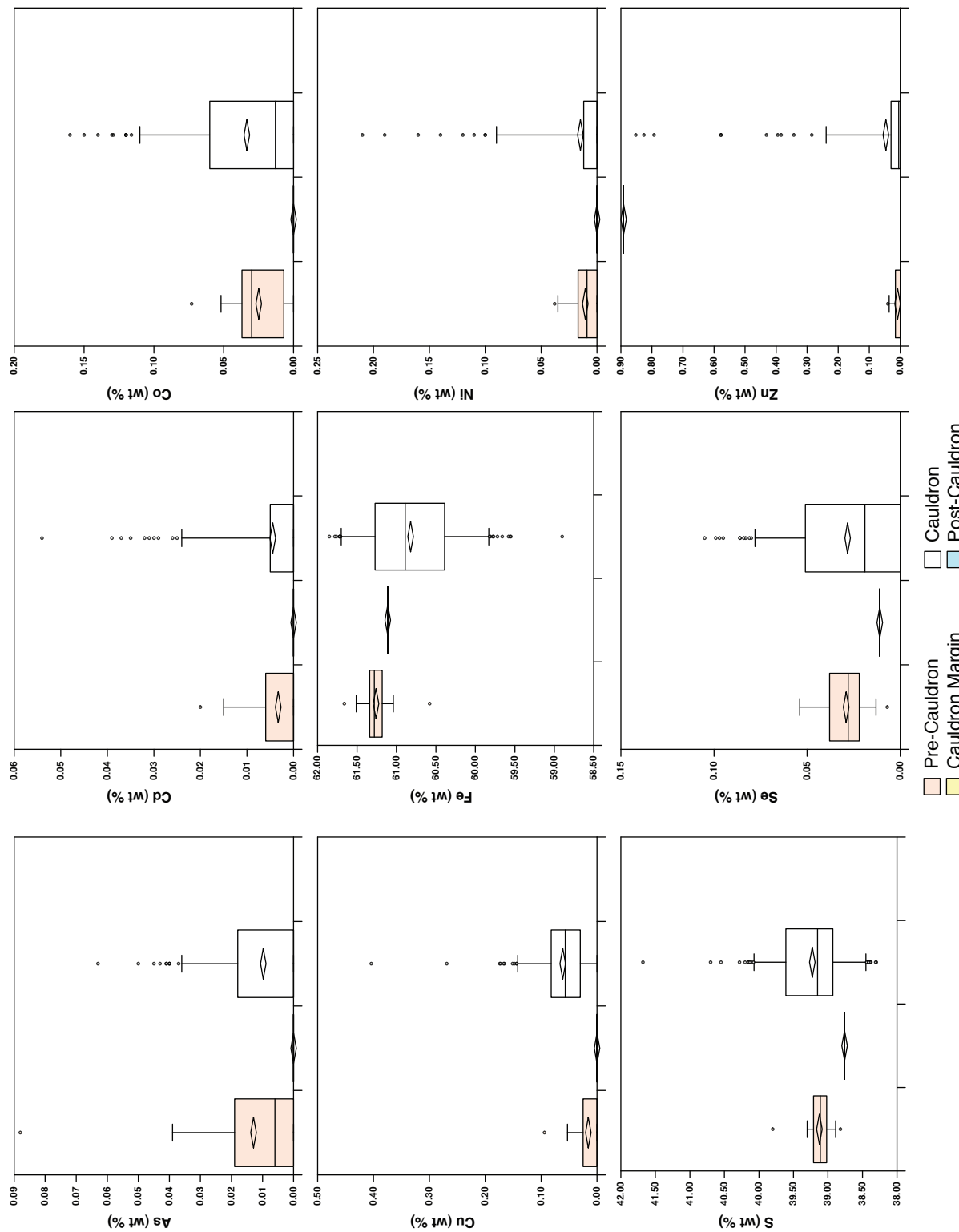


Fig. A1.8: Box and diamond diagrams of trace element concentrations for pyrrhotite from EPMA data separated by stratigraphic position showing 5th percentile, 95th percentile and outliers (diamond indicates mean).

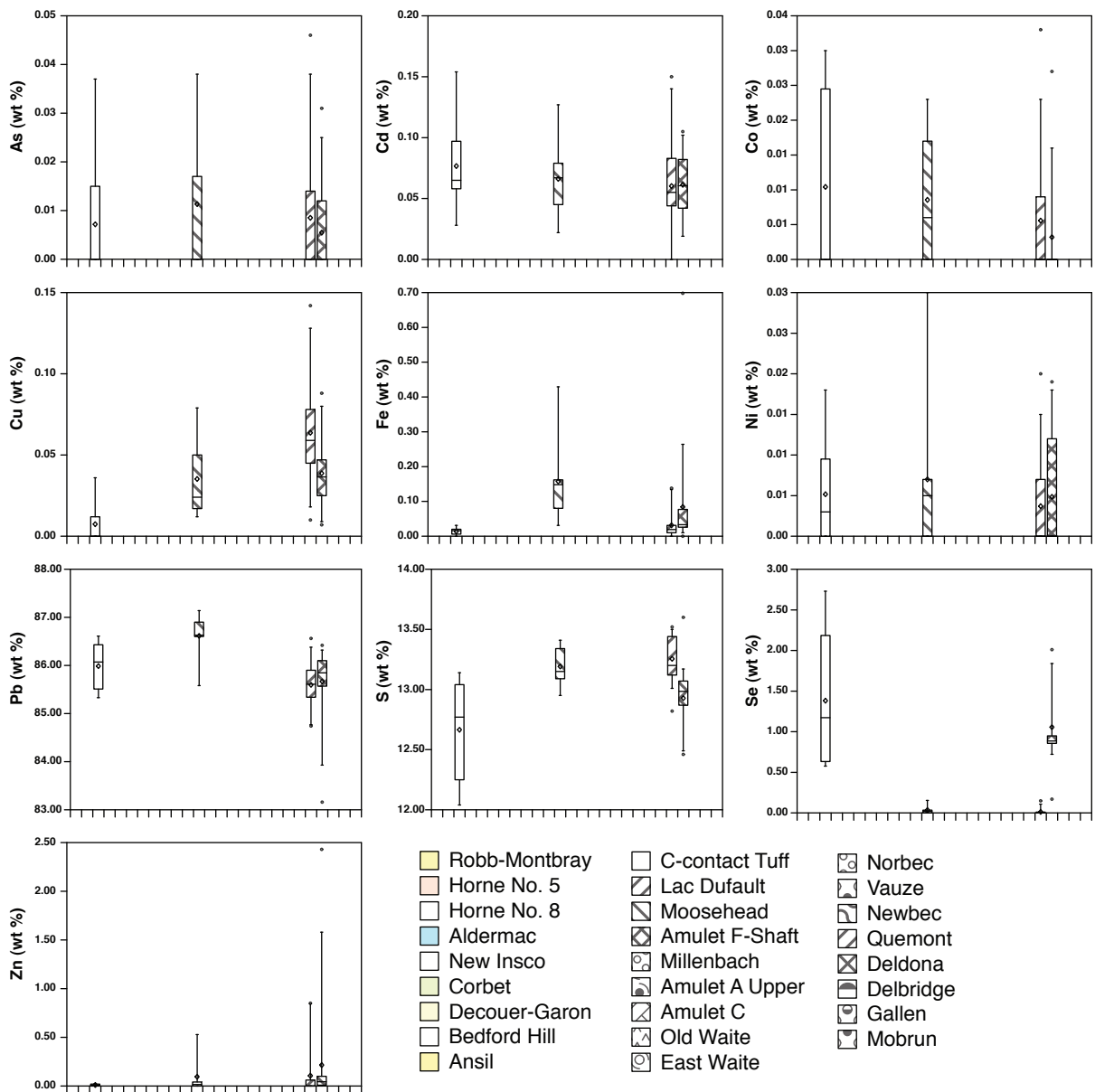


Fig. A1.9: Box and Whisker diagrams of trace element concentrations for galena from EPMA data separated by deposit showing 5th percentile, 95th percentile and outliers (— indicates mean).

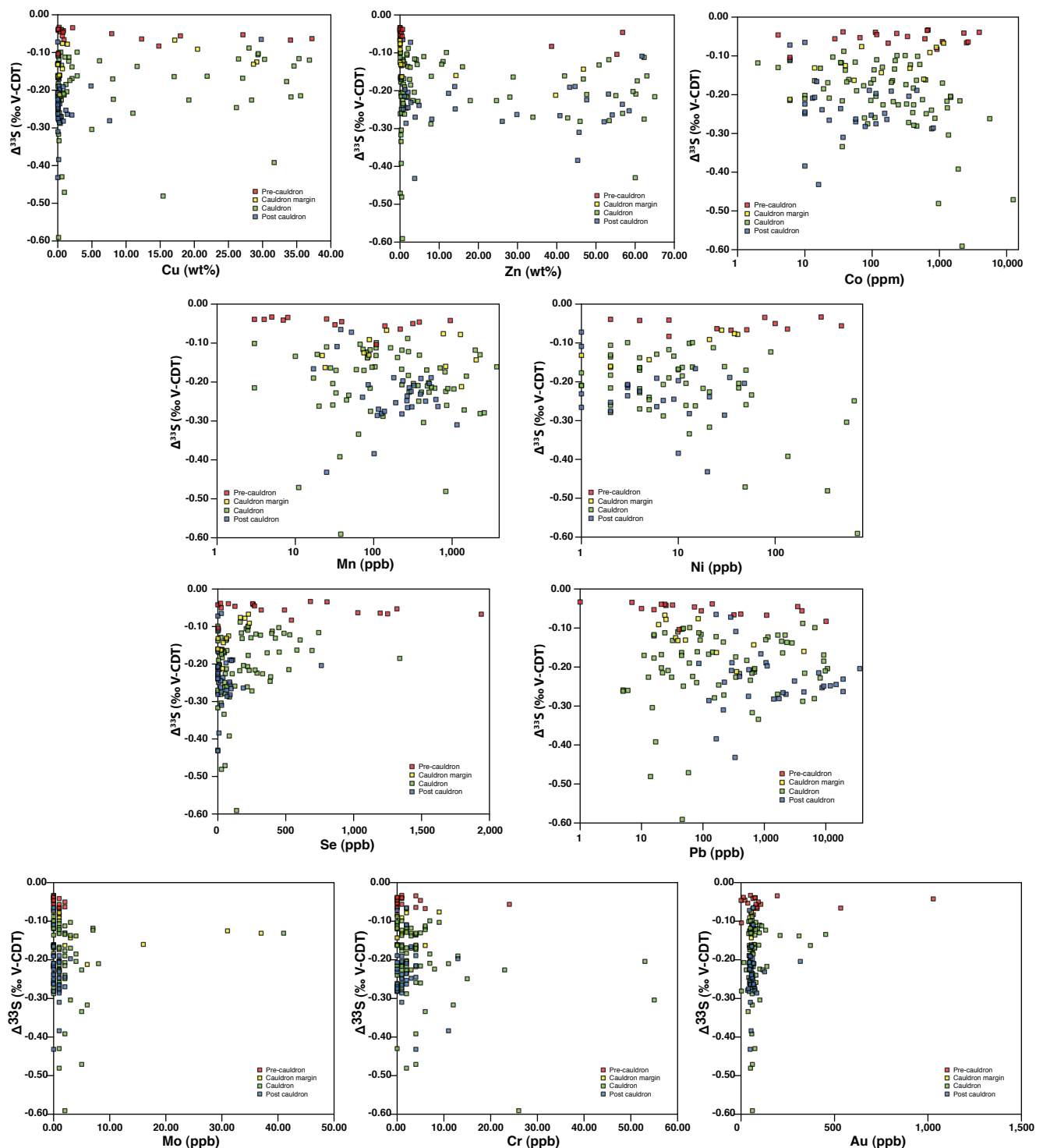


Fig. A1.10: Binary diagrams of trace elements vs. $\Delta^{33}\text{S}$ for Noranda sulfides from ICP-MS analyses divided by stratigraphic position.

APPENDIX 2

Table A2.1: Detailed descriptions of the ore deposits of the Doyon-Bousquet-LaRonde (Mercier-Langevin et al., 2007c) and accompanying samples for each deposit.

Mineralisation type	Characteristics	Deposit	Subdivision	Stratigraphic position	Mineralisation style	Sulphide mineralogy	Other notes
Au-rich VMS	Stacked ore lenses at different stratigraphic intervals in the Bousquet Fm. Characterised by semi-massive to massive sulphide lenses and thin zones of (commonly associated with variable amounts of disseminated sulphides). Lenses are located higher in the stratigraphy in the east. All lenses have a steeply dipping plunge to the west (primary elongation along inferred primary synvolcanic faults). Mimicked at smaller scale by distribution of volcanic units at depth, hydrothermal alteration zonation and metal zonation within lenses.	Lake Ronde Penna	20 South	Uppermost lens in the camp and close to the contact with the Cadillac Group (sediments).	Economic mineralisation is concentrated in two zones, and the lens is up to 10m thick in upper levels and thins with depth. Mineralisation also occurs as centimetre- to metre-wide Au- and Zn-rich massive sulphides.	Py, po, sph, cp and gn with minor tellurides and electrum.	Highest Au grades are associated with massive sulphide part of lens. Sp and gn concentrated in upper part of the lens. Lens is slightly discordant to host lithologies implying may have formed in part by replacement. Contact of Bousquet Fm - Bousquet Fm.
		20 North Zn	Occurs in upper member of Bousquet Fm.	Massive sulphide which becomes more sph rich in upper part of the lens as centimetre- to decimetre-re-scaled massive bands parallel to regional foliation alternating with massive py. Gn occurs with sph as localized narrow veins and veinlets at top of lens.	Py, sph, cp with minor gn	This zone also contains pyrite-bearing dismembered graphitic argillite beds.	D167174, D167175, D167176, D167177, Upper contact of Bousquet Fm - Bousquet Fm.
		20 North Au	Occurs below the 20 North Zn lens but also within the upper member of the Bousquet Fm.	Comprises auriferous sulphide veins and veinlets forming a dense stockwork with local semimassive centimetre- to metre-thick lenses which have been strongly flattened and transposed in main foliation.	Py and cp	Thought to be subsurface replacement and represent a feeder zone to 20 North Zn lens. At depth this zone gradually changes in zone of disseminated to semimassive to locally massive sulphides (auriferous py, cp hosted in qtz-Kv+and+staur+muscovite schist) formed the aluminium zone.	D167165, D167166, D167167, D167168, D167169, D167170, D167171, D167172, D167173, D181001
Bousquet 2-Dumagami		Zone 6	Located near base of upper member of Bousquet Fm.	Semimassive to massive sulphides which form as numerous isolated economic lenses.	Py, ch, sph + minor po, mg, tellurides, Au	Au-rich massive sulphide-bearing talus breccia also identified at margins of zone 6.	D167185
		Zone 7	Occurs at same stratigraphic position as 20 North lens	Single Au- and Cu-rich ore body with Zn and Pb enrichment towards its top. Comprises three principal sulphide facies: 1) Stringer veins composed 15-35 vol % partially transposed a hastenising veins and 2) Massive py and sulphide ore breccia occurring in the central part of the one body and comprising discontinuous massive py lenses of up to 5m thick interfingered with py stringers supporting wall-rock fragments. Elevated Cu and Au associated with bi-Interstitial to granoblastic py. 3) Banded and brecciated sulphide facies comprises narrow, strongly transposed, and discontinuous semimassive to massive sulphide veins and lenses.	Py with minor sph and sph with ch, bn, tennantite, trace digenite and sph. 2) Py with variable amounts of bn, cp, sph, po, tennantite, and cc. 3) Py and/or sph with variable amounts cp, bn, po and gn	Au-rich sulphide zones are characterised by late north-south fractures locally filled with sulfides and coated by Au.	D181003A, D181003B
Bousquet 1	Zone 1 and 2			Characterised by foliation-oblique veins which are folded, transposed, and discontinuous stringers that form in zones, hundreds of metres long. Composed predominantly of py and qtz in felsic host rocks.	Py, with accessory minerals which include sph, gn, apy, po, bn, mg, rutile, gedrite, stannite, Au.	Hosts 80% of the ore in this deposit. Au occurs as auriferous disseminations in disseminated py.	D181011, D181012, D181013, D181014, D181015
	Zone 3	Located between lower and upper members of Bousquet Fm.		Mostly comprises foliation parallel veins which form centimetre- to meter-thick east-west pinch-and-swell structures. Consist of sulphide with lesser amounts of qtz and musc.	Py+cp+sph, po, gn, bn, rutile, tellurides	Au occurs as auriferous disseminations in disseminated py in Zone 5.	
	Zone 4			Characterised by foliation-oblique veins which are folded, transposed, and discontinuous stringers that form in zones, hundreds of metres long. Composed predominantly of py and carbonate (with local concentrations of cp) in mafic host rocks.	Py, ch, accessory minerals include sph, gn, apy, po, bn, mg, rutile, gedrite, stannite		
Westwood	North Corridor	Located in upper part of lower member, or base of the upper member of the Bousquet Fm. and same stratigraphic position as Bousquet 1 zones 3, 4, and 5 Ellison A, B, C.	Comprises metre-wide auriferous disseminated sulphide zones cut by centimetre- to decimetre-thick semimassive to massive sulphide veins which form transposed stringers on schistose rocks.	Sulphides are dominated by granoblastic py + trace po and interstitial cp, also trace sph, gn, tellurides and Au.	Characterized by Au-Cu association.		
Ellison	Zone A, B			Forms narrow transposed stringers of semimassive to massive sulphide	Py+cp+sph, trace po, gn, electrum, Au	Similar to Bousquet 1.	D181008, D181009, D181010
Warrenmac		Located near interface between lower and upper members of the Bousquet Fm.	Comprise semimassive to massive sulphides	Py+sph+cp+po with trace gn, electrum, Au	Characterized by a Au-Zn association		

Table A2.1 (cont.)

Mineralisation type	Characteristics	Deposit	Stratigraphic position	Mineralisation style	Sulphide mineralogy	Other notes	Samples
Epicontactal intrusion-related Au-Cu veins	Comprise sulfide-rich veins and veinlets, porphyry and py-cp disseminations and quartz-sulfide veins. Inferred link between the hydrothermal activity that led to the formation of sulfide-rich Au-Cu veins and emplacement of late intrusive phases of the Moosha synvolcanic pluton at shallow depth.	Doyon	Zone 1 Along southward margin of Moosha intrusion.	Comprises numerous py and quartz veinlets (few millimetres to centimetres wide) or laminations. Represent sulfide-rich vein networks transposed into discrete east-west deformation zones.	Cp, sph, gn, apy, cc all occur as trace minerals associated with py.	Au finely disseminated and interstitial to py grains.	DOPL-2007-001A, DOPL-2007-002
		Zone 2		Venks discordant to stratigraphy and regional foliation. Characterized by breciated texture and vary in thickness from a few centimetres to a few decimetres. Py forms coarse-grained, semimassive to massive aggregates within veins commonly cut by irregular cp veins and veinlets which are restricted to the quartz and sulfide veins.	Comprise mainly py with cp locally abundant and associated with tellurides.	Au locally abundant and associated with tellurides.	DOPL-2007-003, DOPL-2007-006A, DOPL-2007-006B, DOPL-2007-008
		West zone					DOPL-2007-005, DOPL-2007-009
Shear zone-hosted (orogenic) Au-Cu veins	Three main types of mineralisation 1) stringer zones comprising sulfide cp, po, py veins and veinlets in a quartz-dominated matrix and dissemination 2) Orz/crystalline quartz (po, cp) veins which resemble epizonal intrusion-related Au-Cu veins at Doyon. 3) Quartz-sulfides (cp, po, py) ± tourmaline-carbonate-chalcocite veins characterized by laminated crack-and-seal or banded textures and containing much less sulfide than other vein types. These veins typically follow the margins of dykes that transect the Moosha intrusion. Veins of all types typically vary from a few centimetres to a few decimetres in thickness. Au occurs micro-inclusions in sulfides, free grains or filling late microfractures in quartz and/or sulfides.	Mouska	Zones 07, 08, 22, 40, 50, 50 south, 60	Series of subparallel, subvertical east-west to northwest-southeast trending sulfides and quartz-sulfides vein systems and associated narrow high-angle reverse ductile and brittle ductile shear zones superimposed on regional foliation. Veins hosted in high-strain zones.	Type 1 veins - zone 22; type 2 veins - zones 07, 08, 40, 50, type 3 veins - zone 40, 50, 08A, MM-08B, (MM-09), Type 2, MM-03, MM-06, MM-07A, Type 3, MM-01, MM-02, MM-04, MM-10, MM-12		
		Mac Mac		Hosted in Hebecourt Fm.			
		Moosha A		Hosted in northern part of Moosha intrusion			
		Moosha B		Hosted in northern part of Moosha intrusion.	Type 3 veins dominate.		

Note: py - pyrite; cp - chalcopyrite; sph - sphalerite; po - pyrrhotite; gn - galena; apy - arsenopyrite; bn - bornite; cc - chalcocite; mag - magnetite

Table A2.2: Detailed description of all samples collected from the Doyon-Bousquet-LaRonde mining camp including polished block descriptions.

Sample Number	Deposit	Location	Field Description	Hand Sample Description	Polished Block Description	Microdrilling notes
D167165	LaRonde-Penna	Core 3215-99 (1080.20 - 1080.30m), 20N Zone	Fine grained disseminated sulfides (py) in schistose host rock	Fine grained sulfides dominated by py (near euhedral to subhedral) with minor associated cp, sph and po. Sulfides seem to be controlled by fabric of rock and may have been metamorphically recrystallised in places	Potentially low S% in sample	Potentially low S% in sample
D167169	LaRonde-Penna	Core 3215-99 (1099.50 - 1099.60m), 20N Zone	Alternating layers of sphalerite-rich and py-rich sulfide. Py comprises 1-3 mm blebs, sphalerite is more massive	A - Sample dominated by sulfide which comprises py grains surrounded by sph (don't know if they formed together or if the sph post-dates the py). B - Sample is dominated by sulfides, typically py surrounded by sph, but percentage of py:sph changes through sample	A - Pyrite rich, B - Sphalerite rich	A - Pyrite rich, B - Sphalerite rich
D167171	LaRonde-Penna	Core 3220-04 (719.90 - 720.00m), 20N Zone	Sample from middle of py-rich zone	Sample comprises two parts - one part is layered, with py occurring as stringers zones parallel to foliation. Second part is more massive py with possible assoc. cp. - different zones more clearly seen on back of sample	A - Bands of semi-massive sulfides interchanged with bands of groundmass with fine-grained disseminated sulfide (euhedral to subhedral py). In some places the groundmass also has very very fine-grained sulfide. Semi-massive sulfides have veins of cp with occasional mo B - Sample dominantly fine-grained euhedral py in groundmass with occasional very fine-grained sph. Occasional clusters of py grains C - Mostly groundmass with fine grained euhedral to subhedral py ± very fine-grained sph, also occasional py clump	A - Bands of semi-massive sulfides interchanged with bands of groundmass with fine-grained disseminated sulfide (euhedral to subhedral py). In some places the groundmass also has very very fine-grained sulfide. Semi-massive sulfides have veins of cp with occasional mo B - Sample dominantly fine-grained euhedral py in groundmass with occasional very fine-grained sph. Occasional clusters of py grains C - Mostly groundmass with fine grained euhedral to subhedral py ± very fine-grained sph, also occasional py clump
D167173	LaRonde-Penna	Core 3220-04 (736.50 - 7736.60m), 20N Zone	In Zn-rich zone (sphalerite rich)	Sample comprises ~70% sph (salmon pink to dark pink) with very fine-grained disseminated py	Sample comprises ~50% sph which varies in % across sample. Also get euhedral py in varying % (more py often associated with less sph)	Sphalerite + minor pyrite (low S% possible)
D167174	LaRonde-Penna	Core 1062180-1 (23.00 - 23.05m), 20S Zone	Very very rich zone (Zn, Cu, Ag, Au - no zoning). This sample - pyrite, chalcopyrite, sphalerite.	Massive sulfide. Dominated by py, with minor sph and cp. May be two generations of py.	Sample comprises ~50% sph which varies in % across sample. Also get euhedral py in varying % (more py often associated with less sph)	Sphalerite + minor pyrite
D167175	LaRonde-Penna	Core 1062180-1 (24.10 - 24.15m), 20S Zone	Argillite with deformed/re-crystallised pyrite nodules.	Argillite with very fine-grained disseminated sulfides. At one end a series of fractured, altered, re-crystallised py nodules - interior of largest nodule is po.	Sample comprises ~50% sph which varies in % across sample. Also get euhedral py in varying % (more py often associated with less sph)	A- Groundmass with fine-grained sulfide (low S% in sample) B - Pyrite from nodule C - Po from nodule Mainly pyrrhotite sampled
D167176	LaRonde-Penna	Core 1182178-2 (13.50 - 13.60m), 20S Zone	Pyrrhotite stringer in footwall andesite (stringer connects 20S and 20N lenses)	Interstitial sulfides (po) comprising ~30% of sample	Sample comprises ~50% sph which varies in % across sample. Also get euhedral py in varying % (more py often associated with less sph)	A- Groundmass with fine-grained sulfide (low S% in sample) B - Pyrite from nodule C - Po from nodule Mainly pyrrhotite sampled
D167177	LaRonde-Penna	Core 1182178-2 (23.65 - 23.75m), 20S Zone	Sphalerite and pyrite within ore body	Massive sulfide - py dominated (mostly fine-grained and subhedral) with associated sphalerite	Sample comprises ~50% sph which varies in % across sample. Also get euhedral py in varying % (more py often associated with less sph)	A - Sphalerite rich band B - Pyrite rich band

Table A2.2 (cont.)

Sample Number	Deposit	Location	Field Description	Hand Sample Description	Polished Block Description	Microdrilling notes
D167179	LaRonde-Penna	Core 31122-01 (305.00 - 305.10m), 20N Zone	Pyrite bearing sample in Au-Cu zone	Extensive fine grained disseminated py, may be crudely strata-bound.	Sample varying from 30-50% euhedral to subhedral py. Varies in size from ~10 - 100 µm and seem to be heidite. Very rarely get cp associated with py	
D167181	LaRonde-Penna	Core 31122-01 (311.70 - 311.75m), 20N Zone	Pyrite bearing graphitic argillite.	Argillite / tuff layer with fine-grained sulfide zones (py)	Sample comprises ~50% sulfide (mostly py) varying in size from 10 s - 110 s µm. Very jumbled and combination of crystalline and dirty py	
D167182	LaRonde-Penna	Core 31122-01 (313.80 - 313.90m), 20N Zone	Sphalerite bearing sample towards top of Zn-rich zone.	Sample comprises two parts, one part seems to be a stack of altered nodules which have been deformed, grading into fine-grained (~1mm) subhedral py with interstitial sphal.	A - Sample comprises py (mostly subhedral) varying in size from ~10 - 1000 µm. Varies in % from 10 - 70%. Surrounded by ~90 sph and ~10% gn (which is focused in small areas) B - Massive sulfide, dominantly py (50-90%) surrounded by sph. Py has been recrystallised (see triple junctions). Remnant nodule visible to naked eye, but no major difference in nodule to rest of py (maybe a bit more massive) C - Sample comprises >95% py (euhedral to subhedral) usually 100 to a few 100 µm. Often annealed, and between py get sph and gn	A - Sphalerite rich, B - Pyrite rich
D167184	LaRonde-Penna	Core 31122-03 (443.60 - 443.65m)	Pyrrhotite and chalcocite bearing sample. Contact between Bosquet & Cadillac group - sulfides present	Disseminated blebby po + cp	Mix of pyrrhotite and chalcocite sampled	
D167185	LaRonde-Penna	Core 3146-05 (163.10 - 163.15m), Zone 7	Fine-grained disseminated sulfides	Qtz rich sample with fine grained disseminated sulfides (py and sph?)	Mainly sphalerite sampled with some pyrite, probably low sulfide in drilled sample	
D167199	LaRonde-Penna	Core 31194-08 (1331.10 - 1331.20m), 20N Zone	Disseminated sulfides. From further down in package, less homogenous therefore 2 samples taken.	Fine grained (1-2mm) disseminated subhedral py. Also have Al-alteration (white mineral). Seems to have remnant bedding.	Similar to D167198, slightly higher % of py but fewer large clots of py. Also have large silicate grains (Al - alteration mineral) which have very fine grained (<10µm) sph inclusions, and seems to be rimmed by recrystallised py. As with D167198 also see areas with disseminated fine grained (10 - 100 µm) euhedral to subhedral py in groundmass. Very minor cp present	Blebs sampled
D181001	LaRonde-Penna	Core 31170-11B (1753.05 - 1753.15m), 20N Zone	More stringy. Al-alteration zone (acid leaching very strong, mostly silica) - most magmatic signature - acidic fluid is thought to have magmatic signature	Sample is shot through with disseminated sulfide stringers (<1-2mm). Py dominated, sub- to anhedral. Seems to generally follow remnant bedding.	Fine-grained (10 - 100µm) disseminated py (~10%), mostly euhedral almost to subhedral sometimes. Also minor associated sph (usually 10 - 20µm). Occasionally get blebs of recrystallised py, but not many, and not too big	Sulfide in pale band

Table A2.2 (cont.)

Sample Number	Deposit	Location	Field Description	Hand Sample Description	Polished Block Description	Microdrilling notes
D181003	Bousquet 2 - Dumagami	Core D04-2777 (1948.90 - 1949.00m)	Massive sulfide. Deep extension of contact 2, massive sulfide at the contact between Bousquet Fm and Cadillac Group (volcanics & sediments)	Massive sulfide. Most of sample comprises fine-grained (<1mm), subhedral py with interstitial sphal (dark red/orange. One end of sample (3cm) comprises sooty py that looks like flattened bands.		A - Massive sulfide, B - Band at end of sample
D181009	'Ellison' Property	Core 121-06-16 (274.00 274.10m)	Zone A, more massive, silicified, in mafic rocks (andesite). Nodular ('sort-of') pyrite (Zone A)	Remnant rhyolite, heavily altered. Pyrite occurs throughout sample (~15%) as subhedral, near cubic, but near rounded blebs that in some cases look as if they have pressure tails. Vary in size from <1mm to almost 1cm. Maybe even two growth stages?		Drilled out one pyrite
D181010	'Ellison' Property	Core 121-06-16 (274.90 - 274.95m)	Main ore zone, massive sulfide (Zone A)	Sample is ~50% sulfide, dominated by py. Appears to be somewhat banded and comprising dominantly subhedral py crystals (1-3mm) surrounded by sooty py.		Pyrite sampled
D181011	Bousquet 1	Core D83 909 (32.90 - 33.10m)	Contact between Cadillac and Blake River Group (sulfide rich). Massive sulfide at boundary (mineralised horizon badly panned)	Near massive sulfide dominated by py with minor cp and sph (dark brown/orange). Py comprises subhedral py crystals (1-2 mm) surrounded by massive sooty py. Some even appears to be nodular.		A - Pyrite from middle of nodule B - Interstitial sphalerite and pyrite
D181013	Bousquet 1	Core D83 909 (97.80 - 97.90m)	Chalcopyrite rich	Fine grained (1-2mm) disseminated py+cp in felsic host rock. Potentially within shear zone.		Sample contains both pyrite and chalcopyrite (may be small pieces of drill bit in sample)
D181015	Bousquet 1	Core D83 909 (124.65 - 124.70m)	Darker lithology	Fine grained (~1 mm) disseminated py ± cp in felsic+mafic striped host rock. Potentially within shear zone.		Fine grained interstitial pyrite sampled
DPL-2007-001-A	Doyon	Level 11-2 (Zone 1)	Vein E-33, Zone 1, Stockwork veins with py+cp in a pink schist envelope à Sr (Alteration zone), sulfide stringers	Pyrite stringers in thin quartz veins.		Sulfide from vein
DPL-2007-003	Doyon		Vein K-2, zone 2, qtz ± carbonate vein with pyrite cubes, chalcopyrite, and free Au	Qtz-carbonate vein with py, possible cp and Au		Pyrite + chalcopyrite (and maybe Au) (slightly low S% in sample)
DPL-2007-005	Doyon	Level 9-0 (West Zone)	West zone, vein T-23/T-26	Disseminated py (fine grained) and zones of more massive sulfide (py+ cp) associated with qtz-carb vein		Pyrite + chalcopyrite in vein
MN-04	Mouska			Massive quartz + tourmaline vein with sulfides. sulfides appear to be cp, but in places have a cubic crystal structure (replacing py?)		Sulfide in tourmaline

Table A2.2 (cont.)

Sample Number	Deposit	Location	Field Description	Hand Sample Description	Polished Block Description	Microdrilling notes
MN-06	Mouska			Massive samples with quartz veins with pervasive massive sulfide (highly oxidised), probably pyrrhotite and chalcopyrite sampled.		
MN-07	Mouska			Sample with extensive sulfide mineralisation (mostly sphalerite + pyrrhotite), sulfides are oxidised. One end of sample has a quartz vein with visible gold and maybe silver.		A - Sulfide (cp) associated with quartz vein, B - Other vein
MN-10	Mouska			Quartz-tourmaline (probably) with zones of blebby disseminated sulfides (mostly sphalerite).		Sulfide in tourmaline

Note: py - pyrite; sph - sphalerite; cp - chalcopyrite; po - pyrrhotite